Application of Concentrated Solution Theory and Core Potential to Ion Exchange Media

Taeho Jung

Wolfson College

University of Oxford

Supervised by

Prof Charles Monroe & Prof David Howey

Submitted: Trinity Term, 2023

This thesis is submitted to the Department of Engineering Science, University of Oxford, in partial fulfilment of the requirements for the degree of Doctor of Philosophy.

To my mum and dad

Acknowledgement

I would like to express my gratitude to the Department of Engineering Science, University of Oxford, for partially funding this work through the research studentship. The remaining funding was generously provided by my parents, without whose financial and emotional support this endeavour would not have been possible, so thank you. I am also grateful to the Faraday Institution for travel and conference grants.

I have to admit that the course of my DPhil programme has been vastly different from what I had initially envisioned. My understanding of what it means to pursue a doctoral degree had been naive; the level of self-discipline required was beyond my imagination. Navigating through the fields of electrochemistry, thermodynamics, and transport phenomena often left me feeling lost, leading to many moments of self-doubt and frustration. Moving to a new country came with its own set of challenges, not to mention the British weather. On top of everything, the Covid-19 pandemic hit; all the changes and uncertainties it had brought exacerbated such feelings and changed me fundamentally. It seems miraculous that this thesis came together after all.

Needless to say, my DPhil journey was far from my endeavour alone and I would like to take this opportunity to thank everyone who has helped me along the way. First of all, I would like to thank my primary supervisor, Prof Charles Monroe, who instilled in me the importance of rigour in scientific investigations. The intellectual freedom he has fostered in the group has allowed me to grow as an independent researcher. Encouragement and support from my second supervisor, Prof David Howey, have been invaluable, especially in my times of low. Special thanks to Dr Andrew Wang for conducting the liquid-junction-potential measurements and guiding me through the

experiment, Prof Guanchen Li at the University of Glasgow for discussions on the single-solvent approximation, and Dr Nicola Courtier for helping me with membrane-model simulations and countless discussions.

I would also like to extend my thanks to other members and alumni of Monroe Group and Battery Intelligence Lab: Dr Howie Chu, Dr Kirk Smith, Mr Rohit Rungta, Ms Emmanuelle Hagopian, Prof Jie Lin, Dr Amangeldi Torayev, Dr Zeyang Geng, Ms Helen Crockford, Ms Malgorzata Wojtala, Mr Adam Lewis-Douglas, Ms Rebecca Perriment, Mr Zihao Zhou, Mr Masaki Adachi, Dr Antti Aitio, Dr Volkan Kumtepeli, and Mr Ralph Lane.

Declaration

I declare that this thesis is an original report of my research, which has been written by me and has not been submitted for any previous degree. The liquid-junction-potential measurements for the EMC:EC:$LiPF_6$ system were performed principally by Dr Andrew A. Wang; my contribution to the experiment was minimal and of assistant nature only. Parts of this thesis have resulted in conference posters and oral presentations, as well as the following publication.

Jung, T.; Wang, A. A.; Monroe, C. W. Overpotential from Cosolvent Imbalance in Battery Electrolytes: $LiPF_6$ in EMC:EC. *ACS Omega* **2023**, *8*, 21133–21144.

Taeho Jung

June 2023

Abstract

Simple electrolytic systems are studied under the framework of Newman's concentrated-solution theory without making an explicit assumption of electroneutrality. To ensure thermodynamic consistency in non-electroneutral systems, Goyal and Monroe's core-potential theory [1] is incorporated.

Three electrolytic solutions are investigated first in this thesis: (1) the binary electrolyte, (2) the three-ion ionic liquid, and (3) the binary salt in two neutral solvents. Corrections to electrochemical-potential differentials ($d\mu_i$) are derived by combining core-potential theory with the Boltzmann distribution, in accordance with Goyal and Monroe's treatment. The new $d\mu_i$'s —which satisfy the fundamental Gibbs–Duhem relation universally— can be directly employed to describe systems and situations in which diffusion takes place, regardless of the charge state of the system.

Using the new $d\mu_i$ expressions in practice requires knowing the functional forms of concentration-dependent thermodynamic factors. The liquid-junction potential accessed by the concentration-cell experiment is investigated as the main thermodynamic-factor characterisation technique in this thesis. Thus measured liquid-junction potential for the EMC:EC:$LiPF_6$ electrolyte —a commonly used cosolvent electrolyte in conventional lithium-ion batteries— is parameterised as an illustrative example. This exercise reveals that overpotentials arise from solvent polarisation; thus, it is important to distinguish the two solvents in high-fidelity battery models for an accurate description of long-term battery operation.

The theoretical endeavour so far is then extended to a charged membrane submerged in a binary electrolyte, which shares aspects of the three-ion ionic liquid (having two

neutral entities with a shared ion) and the binary salt in two neutral solvents (having four species). Corrections to $d\mu_i$'s, as well as thermodynamic-factor expressions, are derived. Furthermore, concentration dependences of two Stefan–Maxwell diffusivities associated with the charged membrane end-group are derived for Nafion 117 in aqueous sulfuric acid. This is done by revisiting Verbrugge and Hill's radio-tracing experiment and the ionic-conductivity measurement [2, 3]. The resulting Stefan–Maxwell diffusivities are then utilised to estimate the macroscopic transport properties, illustrating the usefulness of having access to the full suite of concentration-dependent Stefan–Maxwell diffusivities.

Contents

List of Figures

List of Tables

Chapter 1

Introduction

As the global demand for electricity increases, today's energy sector is faced with the conundrum of reducing its carbon footprint to mitigate global warming. Many governments are now committed to making a transition to clean energy production and phasing out fossil-fuel-based energy generation (e.g., the Paris Agreement was signed by 196 parties [10]). Due to the variable nature of renewable energy sources such as sunlight and wind, energy storage is a crucial component in realising complete independence from carbon-intense energy production. Furthermore, energy storage generally benefits electricity grids by improving their resilience and efficiency. Suitable grid-level electrochemical energy storage options include lithium-ion, sodium-ion, sodium-sulfur, and redox flow batteries, with vanadium commonly employed as a redox agent for the latter system [11–13].

Apart from electricity generation, transportation is another segment of the energy sector responsible for significant CO_2 emissions; in fact, it accounted for 16.2% of global greenhouse gas emissions in 2016 [14]. Relievedly, the transportation sector has actively engaged in decarbonisation efforts in recent years, thanks primarily to the success of the lithium-ion battery technology. Continuous research and development since the technology's commercialisation by Sony in 1991 has led to optimisation of the device itself, as well as the establishment of a manufacturing ecosystem, decreasing costs steadily and substantially [15, 16]. More efforts are still being directed to further

improve the energy density of the lithium-ion battery, e.g., introducing silicon in the anode [17]. Other novel systems incorporating metallic lithium as the anode —which can be paired with a sulfur cathode (lithium-sulfur battery) or a porous cathode that admits oxygen (lithium-oxygen battery) [18, 19]— have also been investigated.

To go beyond electrifying passenger vehicles, however, lithium-ion batteries are not enough. The current lithium-ion battery is at a disadvantage for heavy-duty and long-haul transport because a significant proportion of its stored energy would have to be expanded for carrying its own weight. In such applications, hydrogen fuel cells may be a more appropriate solution. Hydrogen fuel cells are electrochemical devices that admit hydrogen gas at the anode and oxygen at the cathode, mediated by an ionically conducting but electrically insulating layer (for automotive applications, proton-exchange membranes such as Nafion are commonly used). Hydrogen as a fuel is attractive because of its high volumetric energy density when pressurised (compared to batteries), no harmful waste-product generation, and no self-discharge upon long-term storage [20]. However, there are many hurdles to overcome before the technology becomes economically viable; low efficiency, difficulty storing hydrogen, as well as production of green hydrogen are among key obstacles [20, 21].

Whether it is battery or fuel cell one aims to improve, understanding the movement of charged species within the system is critical. This is particularly important when mathematical models are employed to guide decision-making processes for system performance improvements and optimisation; any inconsistencies in the models would undermine the reliability and credibility of the model output. In this regard, using concentrated-solution theory put forward by Newman as the basis for describing diffusion across charged membranes like Nafion may pose a problem. This is because electroneutrality —an assumption tightly incorporated in his theory [22]— is violated at the membrane-solution interface, due to the presence of fixed charged membrane end-groups, i.e., a Gibbs–Donnan potential arises. Although the electrical double layers in electrolytic solutions are known to be thin, this does not signify that the associated

overpotentials are small; in fact, the fact that Debye screening occurs in these layers implies high electric fields and is likely to have the opposite impact. Thus, the membrane boundary layers may meaningfully influence the flux of charged species in the system and a new framework that can consistently account for this is necessary.

Unfortunately, relaxing electroneutrality in a thermodynamically consistent manner is not as simple as one might think. For instance, an intuitive approach would be to write the electrochemical potential μ_i in the standard form —as a sum of a chemical part and an electrical part, such that $\mu_i = \mu_i^{\text{chem}} + Fz_i\Phi$, where μ_i^{chem} is the chemical potential, F is the Faraday constant, z_i is the equivalent charge of species i, and Φ is the electric potential, following Guggenheim's construction [23]— and derive the flux equations and macroscopic transport properties without setting the excess charge density to zero. However, Guggenheim's expression does not obey a fundamental thermodynamic relationship called the Gibbs–Duhem relation[1] as soon as the system deviates from electroneutrality [1]. This relation derives directly from the second law of thermodynamics and can be thought of as a microscopic force-balance relation among the species in the system, i.e., a form of Newton's thrid law. Hence, any model that fails to satisfy the relation bears a major flaw, jeopardising the trustworthiness of the model output.

The core-potential theory proposed by Goyal and Monroe [1] offers a rigorous treatment of system energetics under non-electroneutrality and forms an important theoretical pillar in this thesis. When combined with the Boltzmann distribution, it can produce a correction term to the electrical part of $d\mu_i$ to clarify the thermodynamic inconsistency, so that the Gibbs–Duhem relation is satisfied regardless of the charge state of the system. The resulting $d\mu_i$ expressions can then be fused with concentrated-solution theory to describe diffusion in moderately concentrated and concentrated so-

[1]The Gibbs–Duhem relation states that $\sum y_i d\mu_i = 0$ for isothermal and isobaric systems, where y_i is the particle fraction of species i. Using Guggenheim's μ_i to write the Gibbs–Duhem relation, one obtains $\sum y_i d\mu_i^{\text{chem}} = -\overline{\mathrm{P}} d\Phi$, where $\overline{\mathrm{P}}$ (capital ρ with an overbar) is the molar excess charge. In an ideal solution where $d\mu_i^{\text{chem}} = RTd\ln y_i$ holds (a common assumption in the Nernst–Planck flux formalism), $\sum y_i d\mu_i^{\text{chem}}$ disappears upon summation, while $\overline{\mathrm{P}} d\Phi$ remains unless the system is electroneutral ($\overline{\mathrm{P}} = 0$). Thus, Guggenheim's μ_i only guarantees thermodynamic consistency under electroneutrality.

lutions in which many electrochemical devices operate. Furthermore, the utility of core-potential theory is not limited to non-electroneutral systems. The theory reveals a relationship among thermodynamic factors, which is not immediately intuitive when applying concentrated-solution theory to multicomponent systems. This allows $d\mu_i$ to be written with a parsimonious set of thermodynamic factors, eliminating redundant characterisation experiments.

Although the initial aim of this thesis was to relax electroneutrality in charged membranes to simulate the crossover in the vanadium redox flow battery (VRFB), it was soon realised that this was too ambitious of a goal. Systems with more than four species immensely complicate the diffusion-model construction using the Onsager–Stefan–Maxwell (OSM) equations; furthermore, the core-potential theory can be difficult to parse and execute correctly in such systems. Therefore, the scope of the thesis was re-adjusted to study a more tractable yet relevant system for the VRFB, i.e., Nafion in aqueous sulfuric acid. Nafion and sulfuric acid are respectively a common membrane and supporting electrolyte of choice for the VRFB. To aid in achieving this goal, simpler electrolytic systems are investigated first, which also have practical applications of their own. This exercise also helps consolidate Goyal and Monroe's rather abstract core-potential theory.

The rest of this thesis is structured as follows. Chapter 2 sets the scene by summarising notable works leading to the core-potential theory. How the OSM equations develop and find their way to describe diffusion in electrolytic solutions is also touched on, followed by an overview of membrane models. In Chapter 3, core-potential gradients are directly employed to write transport and MacInnes (modified Ohm's law) equations for three simple systems: (1) the binary electrolyte, (2) the three-ion ionic liquid, and (3) the binary salt in two neutral solvents. The complexity of using core-potential gradients directly compels us to consider another route Goyal and Monroe [1] suggested, i.e., using the Boltzmann distribution to derive correction terms for $d\mu_i$, which can be directly substituted into the OSM equations. In Chapter 4, connection

to thermodynamic-factor measurement is established and a liquid-junction-potential ternary map for the EMC:EC:$LiPF_6$ system is presented as an illustrative example. In Chapter 5, Verbrugge and Hill's radio-tracing experiment and ionic-conductivity measurement for the Nafion-117 membrane (submerged in aqueous sulfuric acid of various concentrations) [2, 3] are re-evaluated to derive concentration-dependent Stefan–Maxwell diffusivities associated with the charged membrane end-group (i.e., sulfonate end-group). Finally, the thesis is summarised and future work is suggested in Chapter 6.

Chapter 2

Literature Review

This chapter briefly summarises important works leading to concentrated-solution theory, a framework for writing transport constitutive laws that accounts for all species-species interactions (through the Onsager–Stefan–Maxwell equations) and thermodynamic non-idealities in non-dilute solutions (through thermodynamic factors). As part of this journey, validation of symmetry relations among the Stefan–Maxwell diffusivities —a common assumption made when implementing the theory— is also discussed. This is followed by the delineation of difficulties associated with separating chemical and electrical effects when studying the movement of ions in electrolytic solutions. Practical workarounds, one of which is the core-potential theory, are also discussed. Then, membrane models are presented.

2.1 Concentrated-solution theory

2.1.1 Development of diffusion theories

Early works on diffusion

Diffusion is a process whereby individual particles such as atoms or molecules move and disperse from a region of high concentration to a region of low concentration, in order to redistribute themselves evenly across the entire system volume. The first attempt

at mathematically describing this phenomenon was made by Fick [24], who stated that the diffusional flux J_i is proportional to the concentration gradient ∇c_i of the diffusing component i, in analogy to the flow of heat.

$$J_i = -D_i \nabla c_i \tag{2.1}$$

Here, c_i is the molar concentration of species i and D_i is a proportionality constant, commonly referred to as the Fickian diffusivity. Fick seems to have been mainly concerned with diffusion in liquids — not only did he carry out experiments on sodium chloride diffusing in water himself [24], he also examined the results of Graham [25], whose work dealt with diffusivity measurement for various aqueous salt solutions [26] (see Patzek [27, 28] and especially Cussler [29] for summaries of early diffusion works).

At around the same time, in the field of thermodynamics, scientists had been making various attempts to explain the properties of gases based on the kinetic theory. This theory posits that individual gas molecules are in constant motion due to thermal excitation [30, 31] and their macroscopic behaviours can be predicted through statistical means. The kinetic theory of gases scrutinises both equilibrium and non-equilibrium conditions, so it is capable of calculating transport properties, such as viscosity, thermal conductivity, diffusivity, etc., in addition to equilibrium properties, such as pressure, temperature, kinetic energy, etc. A notable development in relation to gas diffusion is the work of Maxwell [30], who set out to determine the mean free path of gases *via* 'strict mechanical principles', i.e., molecules were assumed to be perfectly elastic spheres. Two thought experiments were conducted; two gases initially contained in separate chambers were allowed to interdiffuse by connecting them with (1) a hollow tube and (2) a tube fitted with a porous plug. In two-component systems like these, mechanical principles naturally demanded that (1) the force exerted on each gaseous species during diffusion is equal and opposite and (2) the magnitude of this force is proportional to the density of both species and their *relative* velocity. A more in-depth exposition was made in his later work [31], where the idea of using rigid elastic spheres

for gas molecules was replaced by using more generic asymmetrical small bodies (whose geometric centres do not necessarily coincide with their centres of gravity), addressing contributions from oscillations and other internal molecular motions to the total energy. Built upon this was a flexible framework that related the mean value of any property (of a given system) to its flux, capable of delivering the equations of continuity and motion coherently. The force-balance equation that manifested from this framework reaffirmed again the two statements that had arisen from mechanical principles in his previous work. Maxwell also derived an expression for diffusivity in terms of pressure (which is a gauge for density in the gas phase) and quantitatively evaluated it using experimental results. Even though only the simplest case involving two gases was studied, the novelty of his works was the demonstration that only relative motions are important in diffusion.

The Stefan–Maxwell formalism

Soon after, Maxwell's works were extended to multicomponent gaseous systems by Stefan [32], who specified a distinct diffusion coefficient for each pair of species. This set of multicomponent diffusion equations is called the Stefan–Maxwell transport equations[1] and takes the following form.

$$\vec{d}_i = \frac{RT}{c_\mathrm{T}} \sum_{j=1}^{n} \frac{c_j \vec{N}_i - c_i \vec{N}_j}{\mathscr{D}_{ij}} \tag{2.2}$$

Here, $\vec{d}_i$ is the thermodynamic driving force responsible for the flux of species i (note that Stefan [32] only considered gaseous systems, hence partial-pressure gradients comprised driving forces), $\vec{N}_i$ is its molar flux, R is the universal gas constant, T is the temperature, $c_\mathrm{T} = \sum c_i$ is the total molar concentration of all species in the system, and $\mathscr{D}_{ij}$ is the Stefan–Maxwell diffusivity of species i through j. Since $\vec{N}_i = c_i \vec{v}_i$, where $\vec{v}_i$ is the velocity of species i, the impacts of the constituent species' concentrations and

[1] Equation (2.2) will eventually acquire the name Onsager–Stefan–Maxwell transport equations, as more thermodynamic rigour is instilled. More details are given in the following subsection.

their relative velocities are clearly enunciated by eq.(2.2). The appearance of summation in this equation bestows flexibility to specify pairwise interactions individually, instead of collectively quantifying interactions of one species with the rest as in Fick's law. Nonetheless, Fick's law remained prevalent for liquid systems for decades to come, as evident in the Nernst–Planck flux equation developed in 1890 [33, 34]:

$$\vec{N}_i = c_i\vec{v} - z_i u_i F c_i \nabla\Phi - D_i \nabla c_i, \tag{2.3}$$

where z_i is the equivalent charge of species i, u_i is its mobility, F is the Faraday constant, and Φ is the electric potential. This equation illustrates that the movement of a charged species i is attributed to three mechanisms in this theory: convection (due to the bulk flow with velocity $\vec{v}$), migration (due to the electric potential gradient $\nabla\Phi$), and diffusion (determined based on Fick's formalism). The greatest forte of this approach is simplicity; one parameter is sufficient to describe the flux of a species with the use of the Nernst–Einstein relation, where mobility and diffusivity can be related to each other. However, one should be mindful of the theory's limitations when applying it; while the simplicity of the Nernst–Planck model still makes it the most practical and popular option for modelling diffusion in dilute solutions, inaccuracies proliferate as solutions become more concentrated.

Onsager's contributions

A more fundamental insight into diffusion came about a half-century after the introduction of the Nernst–Planck equation. Onsager [35] claimed that it was more convenient to describe diffusion by constructing a function called the dissipation function based on his previous works on irreversible processes [36, 37]. The dissipation function is of great importance because it is directly related to the rate of entropy generation and thus identifies thermodynamically consistent driving forces and fluxes [38]. Onsager made explicit that the diffusion flux must be solely dissipative, i.e., contributions from bulk flow should be excluded, and as a result, it is necessary to employ transport

constitutive frameworks in which the information about dissipation is invariant with respect to the choice of convective reference velocity.

Furthermore, a close examination of the dissipation function led Onsager to suggest the gradient of electrochemical potential as a more natural diffusion driving force, rather than the conventional concentration gradient. The electrochemical potential μ_i represents the amount of energy carried by a mole of a substance i at a given temperature and pressure. This can be mathematically described as

$$\mu_i = \left(\frac{\partial G}{\partial n_i}\right)_{T,p,n_{j\neq i}}, \tag{2.4}$$

where G is the Gibbs free energy, n_i is the molar number of particles of species i, and the subscripts T, p, and $n_{j\neq i}$ indicate that temperature, pressure, and the molar content of species other than i are constant (more detailed discussions on μ_i are provided in section 2.3). Representing the driving force $\vec{d_i}$ as $-c_i\nabla\mu_i$, eq.(2.2) provides a common theoretical ground for both gaseous and liquid systems. Hereafter, eq.(2.2) is referred to as the Onsager–Stefan–Maxwell (OSM) transport equation to acknowledge Onsager's contribution in realising the electrochemical-potential gradient as a more general driving force, as well as his identification of the reciprocal relations among phenomenological coefficients. A more complete form of the driving force, taking into account elastic and plastic deformation stresses, has been presented by Goyal and Monroe [39], which is of considerable importance for systems involving solid phases. But for isothermal, isobaric liquid-phase systems, $\vec{d_i} = -c_i\nabla\mu_i$ suffices.

Onsager's rather abstract exposition was elaborated more concretely by Hirschfelder et al. [40]. They coherently summarised statistical-mechanical theories of dilute and dense monatomic gases, as well as of liquids (see references [41–44] for more details on the statistical-mechanical theory of transport processes), along with quantum-mechanical treatment of dilute monatomic gases (which is of importance at extremely low-temperature and high-pressure environments; such conditions are out of scope of this thesis). It would seem that their greatest contribution to the development of dif-

fusion theories was explicitly writing out a general expression for the thermodynamic diffusion driving force $\vec{d}_i$ in a way that was more accessible to the wider engineering community while maintaining rigour; chemical-potential gradients ($\nabla\mu_i^{\text{chem}}$; they did not use *electro*chemical potential) were translated to concentration gradients (∇c_i) that are easier to work with experimentally, and temperature and pressure gradients were retained for broad applicability (quantum effects were assumed to be negligible, however).

Based upon the general treatment of Hirschfelder et al. [40], Lightfoot et al. [45] considered diffusion in isothermal, isobaric liquids and quantitatively confirmed that the force-explicit OSM equations are of merit for condensed multicomponent systems, too. They inferred Stefan–Maxwell diffusivities from existing experimental results for the water–glycine–potassium chloride system and found that they were (reasonably) concentration independent, unlike the phenomenological coefficients L_{ij} of the flux-explicit form used by Onsager [36, 37] and Fickian diffusivities[2]. This suggested that Stefan–Maxwell diffusivities are more reliable and fundamental in nature in relation to diffusion, imparting legitimacy, or at least preference for the OSM transport equations over their flux-explicit counterparts (as long as the full suite of Stefan–Maxwell diffusivities is available for a given system). Stefan–Maxwell diffusivities have an added advantage of carrying a clear, frame-independent microscopic meaning as the inverse species-species drag coefficient [46], in comparison to the rather ambiguous Onsager coefficients L_{ij}[3].

Because Lightfoot et al.'s system [45] involved ionic species, they attempted to extend the framework of Hirschfelder et al. [40] (which contended with chemical potentials only) to charged species. To do so, they employed a separate electrical part that was proportional to the electrostatic potential gradient, on top of the usual concentration gradient in the diffusion driving force. It should be noted that this approach

[2]Characteristics of Fickian diffusivities are well illustrated by Taylor and Krishna [46].

[3]But in performing molecular-dynamic simulations, L_{ij} can be interpreted as 'the extent of correlation between the motions of species i and j' and are sometimes favoured over Stefan–Maxwell diffusivities, because they can be obtained directly *via* statistical means, according to Fong et al. [47].

does not bear much physical meaning because any division of species' electrochemical potentials into chemical and electrical contributions is arbitrary and cannot be verified experimentally, as pointed out by Guggenheim [23]. Nonetheless, the calculations of Lightfoot et al. [45] did not incur any inconsistencies because their system boundary was assumed to be electroneutral, i.e., they set the boundary electric-potential gradient to zero, so their conclusions remain valid. Further discussions of the electric potential in electrolytic solutions are provided in section 2.3.

Newman's concentrated-solution theory

A more comprehensive treatment of diffusion in electrolytic solutions was given by Newman et al. [48] based on the OSM equations, which later became known as concentrated solution theory. In Newman's work, the chemical and electrical contributions that separately appeared in Lightfoot et al.'s [45] OSM equations were combined within a single electrochemical-potential gradient, adding thermodynamic rigour by circumventing Guggenheim's quandary [23]. An electric potential still appears in this theory as part of the McInnes equation (also called the modified Ohm's law because it takes into account diffusion potential) but in a more concrete sense. That is, the electric potential Newman uses is related to the electrochemical potential of electrons in a probing reference electrode in equilibrium with the charged species in solution. Therefore, it can be measured by a galvanostat and its meaning is unambiguous. The theory also contains experimentally accessible transport properties such as the salt diffusion coefficient, transference number, and ionic conductivity that can all be expressed using the microscopic Stefan–Maxwell diffusivities. As a result, these relations can be inverted to find the Stefan–Maxwell diffusivities in terms of measurable properties, which are more readily established experimentally.

Despite its rigour and clarity, Newman's concentrated-solution theory is not flawless; because electroneutrality is assumed from the outset, it cannot handle non-electroneutral regions. Electroneutrality is a valid assumption in many cases —especially when dealing with bulk electrolytic solutions— but in situations where the length scale

of the system is comparable to the Debye length and/or when the electric potential changes rapidly over a short distance (e.g., in porous media with embedded charges such as charged membranes), electrical interactions are expected to become more prominent. Monroe and Delacourt [49] elaborated on concentrated-solution theory to relax this assumption by employing the Smyrl–Newman potential [50]. By doing so, they attempted to gather all electrical effects into the electrochemical potential of a single reference species. However, later investigations revealed that it had not reached a satisfactory resolution; as Goyal and Monroe [1] illustrated, the Smyrl–Newman potential still fails to satisfy the Gibbs–Duhem relation under non-electroneutrality. A new notion of electrochemical potential called the core potential, suggested by Goyal and Monroe [1], is free from such inconsistency and is pursued in this thesis. More details about the core potential are provided in section 2.3.3.

Inversion to flux-explicit forms

Although the OSM equation encapsulates transport phenomena in fluids more coherently than the Nernst–Planck equation, its force-explicit nature makes it harder to incorporate it into material balances (continuity equations). To resolve this difficulty, some authors introduced the so-called effective diffusivity to attain easy utility and theoretical soundness. This involves rearranging OSM equations (under simplifying assumptions) to produce a single parameter that encompasses several Stefan–Maxwell diffusivities, which can then be easily substituted into the standard Nernst–Planck flux-explicit equations. However, effective diffusivities are not universally applicable in all situations. The necessary simplifying assumptions may turn off some crucial species-species interactions, eliminating the associated Stefan–Maxwell diffusivities in the effective-diffusivity expression, as a result. For example, Graham and Dranoff [51] and Pinto and Graham [52] had to make electroneutrality and zero-current assumptions to arrive at their effective diffusivities. Their assumptions might have been reasonable for some simple situations, such as diffusivity-measurement experiments, but are in general too restrictive for practical engineering applications, such as battery

models. Another example is found in Lightfoot and Scattergood [53], where a ratio of scaled fluxes was employed on a rather ad hoc basis to deliver an effective-diffusivity expression.

The restrictiveness of effective diffusivities points to a need for more concrete inversion approaches from the OSM equations to flux-explicit forms. To achieve this, it makes the most sense to utilise matrix-inversion processes from linear algebra, which are already well established. Once the OSM equations are written in a vector–matrix form, one can proceed with the inversion as prescribed by linear algebra, as long as the constituent equations are linearly independent. For multicomponent systems, however, redundancies exist because of the phase rule (i.e., particle fractions must always add up to 1). Therefore, a pseudo-inversion process is necessary, because the transport matrix is singular. A number of valid approaches have been presented in the literature. For instance, Bearman and Kirkwood [54] eliminated a redundant equation by using the fact that the sum of mass diffusion fluxes (relative to the mass-average velocity) is zero. Newman and Thomas-Alyea [22] and later Monroe and Delacourt [49] took a similar approach but used the Gibbs–Duhem relation instead, because the solvent velocity was chosen as the reference velocity[4] (it is noted that no constraints are imposed on diffusion fluxes when the solvent velocity sets the reference frame, unlike the mass-average velocity). Both methods result in reducing the dimension of the phenomenological-coefficient matrix by one. Helfand [55], on the other hand, demonstrated an inversion process that retains the original size of the coefficient matrix, with the diffusion fluxes defined using the mass-average velocity. This is advantageous because the original flux and force vectors are preserved, achieving inversion without incurring a loss of clarity from the reduction of order. Nonetheless, Monroe and Delacourt's method [49] is arguably the most detailed and consistent, as well as easy to interpret because its connection to the well-known concentrated-solution theory is clear. A more recent work of Van-Brunt et al. [56] is also available using a 'salt-charge basis', but this approach is restricted to electroneutral systems.

[4]The reference velocity indicates the velocity at which the diffusion reference frame moves.

This sums up the evolution of diffusion theories up to the present time. For more comprehensive reviews, readers are referred to references [57–59].

2.1.2 Reciprocal relations among Stefan–Maxwell diffusivities

In arriving at flux equations from the force-explicit OSM equations, a key underlying assumption was that there existed symmetric relations among the Stefan–Maxwell diffusivities, i.e., $\mathscr{D}_{ij} = \mathscr{D}_{ji}$. For many, an obvious starting point for justifying this assumption was Newton's third law of motion, that action equals reaction. Those who appealed to this idea include Maxwell [30], Stefan [32][5], Johnson [60], and Newman et al. [48]. As enunciated by Truesdell [61], however, this argument is not satisfactory for systems containing more than two species because diffusion forces are no longer guaranteed to be binary. That is, if an extra species C is added to a binary mixture of A and B, the presence of C may influence interactions between A and B such that the force exerted by A on B is not the same as the force exerted by B on A, although A, B, and C obey Newton's third law as a whole.

Others, such as Lamm [62], Miller [63], and Fong et al. [47], simply referred to Onsager's general reciprocal relations for irreversible processes [36, 37] to assert symmetry among the drag coefficients K_{ij}. However, Coleman and Truesdell [64] refuted this claim, showing Onsager's reciprocal relations do not have to hold for fluxes and driving forces commonly employed for describing diffusion.

Fortunately, symmetry among Stefan–Maxwell diffusivities has been proved by Monroe et al. [65] by looking at linearised transient responses away from equilibria with Onsager–Casimir fluctuation theory. It is rather surprising that a rigorous proof of the reciprocal relation for multicomponent mass transport was delivered only recently, despite the ostensibly trivial and intuitive nature of the symmetry relation. The rest of this section briefly addresses significant works leading to this proof.

[5]Note that Stefan–Maxwell diffusivities were not directly mentioned by Maxwell [30] and Stefan [32]. Instead, symmetry of what is now termed the drag coefficient in Newman's nomenclature, $K_{ij} \propto 1/\mathscr{D}_{ij}$, was asserted [22].

Onsager's treatment of irreversible processes

When a system evolves irreversibly from one state to another, fluxes arise and they are often brought about by multiple driving forces of seemingly disparate nature. Well-known examples of this phenomenon are thermoelectric effects that manifest when two dissimilar metals are brought together to form two junctions. For example, an interesting phenomenon called the Peltier effect is observed when an electric potential difference (i.e., voltage) is applied across the two junctions initially resting at the same temperature. Not only does it cause an electric current to flow through the system, but also a flow of heat is induced such that one junction heats up (heat flux in) and the other cools down (heat flux out). Conversely, the Seebeck effect is the appearance of a voltage difference (hence an electric current) when the two junctions are subjected to different temperatures.

While relationships among auxiliary fluxes and inconspicuous driving forces had been speculated based on experimental results, there had been no rigorous theoretical basis for these observations until Onsager's elucidation in 1931. Onsager published seminal papers establishing reciprocal relations for heat conduction in anisotropic crystals [36], as well as for any general transport process [37]. He explained that given two irreversible processes 1 and 2, associated fluxes J_1 and J_2 can be described by a linear combination of corresponding driving forces X_1 and X_2 (corresponding in the sense that in the absence of process 2, $J_1 \propto X_1$, and vice versa) as below when deviations from equilibrium are small.

$$\begin{aligned} J_1 &= L_{11}X_1 + L_{12}X_2 \\ J_2 &= L_{21}X_1 + L_{22}X_2 \end{aligned} \tag{2.5}$$

Employing the following four assumptions, Onsager proved a symmetric relation between the coefficients, i.e., $L_{12} = L_{21}$.

1. A flux is described by a linear combination of driving forces as in eq.(2.5) (or a driving force is described by a linear combination of fluxes).

2. A thermodynamic equilibrium is interpreted as a statistical equilibrium.

3. The principle of microscopic reversibility applies, i.e., given a time period τ, the probability of an event A, followed by an event B after τ, is equal to the probability of the event A, preceded by the event B before τ.

4. The regression hypothesis applies, i.e., microscopic fluctuations on average decay according to familiar macroscopic laws.

Note that the principle of microscopic reversibility derives from an assumption of time-reversal symmetry of equilibrium fluctuations, rather than from the second law of thermodynamics [66]. Onsager also demonstrated that the symmetry relation can be equivalently expressed using a variational principle, i.e.,

$$\dot{S}(\alpha, \dot{\alpha}) - \Phi(\dot{\alpha}, \dot{\alpha}) = \text{maximum},$$

where α is the magnitude of an equilibrium fluctuation and $\dot{\alpha}$ is its change with respect to time, $\dot{S}$ is the rate of entropy generation, and Φ is the dissipation function. The dissipation function is defined as the sum over the product of all flux–driving-force pairs in the system, i.e., $\Phi = \sum J_i X_i$, which is in fact equal to half the rate of entropy production [37].

The success and fallibility of Onsager's treatment

Onsager's works paved a pathway to analysing irreversible processes and became the fundamental basis upon which more complicated continuum theories of transport phenomena are built. For instance, the conduction of heat in crystals and conduction of electricity in solids were studied in more detail by Casimir [67]. He also confirmed that Onsager's reciprocal relations hold for both even and odd functions of the displacement variable α, extending the validity of the theory further (Onsager had assumed it to be an even function to achieve the time invariance). Onsager [35] himself applied his theory to study diffusion based on the dissipation function. Theories regarding galvanic cells with a liquid–liquid junction were revisited by Bearman [68] from Onsager's

thermodynamic perspectives.

Nonetheless, not all possible pairs of driving forces and fluxes obey symmetric Onsager reciprocal relations, even those that appear in the dissipation function. Onsager's theory demands that the flux be $\partial\alpha/\partial t$ and the driving force be $\partial G/\partial\alpha$ (where G is the Gibbs free energy) but these are not the fluxes and driving forces commonly deployed in the transport literature [69]. Unfortunately, the regression hypothesis does not guarantee that these typical fluxes and driving forces yield the reciprocal relations [70]. Coleman and Truesdell [64] realised this issue and recognised that it is meaningless to ask about symmetry among phenomenological coefficients (L_{ij}) when fluxes and driving forces are chosen merely based on the dissipation function. This is because any skew matrix ($W_{ij} = -W_{ji}$) can be added to L_{ij} (hence breaking the symmetry) without changing the dissipation, since linear transport laws imply that the dissipation function is a quadratic form in the forces (or fluxes)[6]. They went on to assert that the selection of fluxes and driving forces must be meticulous if the Onsager reciprocal relations were to be used, undermining the broad applicability of the relations. Despite this, the relations seemed to have been applied to various systems without much hesitance. This might have been due to many positive experimental affirmations for the relations (within experimental errors; Miller [71] summarises these experiments), including Stefan–Maxwell diffusivities in ternary systems [72].

Reconciliation

No significant reconciliation had been made between Onsager's reciprocal relations and the criticism of Coleman and Truesdell [64] for almost half a century until Monroe and Newman's work appeared [69]. They finally confirmed that as long as 'proper' fluxes and driving forces are used (i.e., in accordance with Onsager's definitions), a symmetric coefficient matrix is ensured for any generic irreversible processes participating in a

[6]Note that as a result of adding a skew matrix W_{ij}, an extra term of the form $\sum_i^n \sum_j^n W_{ij} X_j X_i$ appears in the dissipation function, where n is the total number of processes considered. Remembering that X_i and X_j represent vectors, $X_j X_i$ forms a symmetric matrix. Thus, the double summation adds up to zero due to the skewness of W_{ij}.

given system. In fact, they showed that Coleman and Truesdell's counter-example [64] violated Onsager's definitions.

Regarding diffusion processes, the works of Newman and colleagues are noteworthy. The symmetric reciprocity of Stefan–Maxwell diffusivities was first shown to hold by Wheeler and Newman [73] using Nyquist–Johnson linear-response theory and the principle of microscopic reversibility, and later by Monroe et al. [65] based on the regression hypothesis, a route more closely in line with Onsager's original approach. Therefore, these results assure the legitimacy of the transport equations and properties presented in concentrated-solution theory.

2.2 Thermodynamic factors

Despite the thermodynamic robustness instilled by the electrochemical-potential gradients in the OSM equations, they are more cumbersome to deal with than concentration gradients in practice. For example, given an electrolytic solution, measuring the change in energy as more salt is added is experimentally more involved than calculating the molarity/molality change of the solution. Therefore, a dimensionless parameter called the thermodynamic factor comes in handy, which helps convert electrochemical-potential gradients to concentration gradients. Originally employed by Darken [74] to study diffusion in binary alloys, thermodynamic factors χ_{ij} in multicomponent systems can be written as[7]

$$RT\chi_{ij} = y_i \left(\frac{\partial \mu_i}{\partial y_j} \right)_{T,p,y_{k\neq j,n}}, \tag{2.6}$$

where $y_i = c_i/c_\mathrm{T}$ is the particle fraction of species i, c_i is its molar concentraiton, $c_\mathrm{T} = \sum_{k=1}^{n} c_k$ is the total molar concentration, n is the total number of species in the

[7]Note that the Darken matrix $\overline{Q}_{ij}$ used by Goyal and Monroe [1] is defined as

$$\overline{Q}_{ij} = y_i \left(\frac{\partial \mu_i}{\partial y_j} \right)_{T,p,y_{k\neq j,n}}$$

and therefore has a unit of molar energy, whereas the thermodynamic factor matrix χ_{ij} is dimensionless.

system, and the subscripts T, p, and $y_{k\neq j,n}$ indicate that temperature, pressure, and the particle fraction of species other than j and n are held constant while evaluating the derivative. Particle fractions are used in this definition to clearly demonstrate that only $n-1$ species are independent; one particle fraction depends on the rest of the particle fractions due to the phase rule: $1 = \sum_{i=1}^{n} y_i$. The Gibbs–Duhem relation under isothermal, isobaric conditions is

$$\sum_{i=1}^{n} y_i d\mu_i = 0 \tag{2.7}$$

and it allows one electrochemical-potential gradient to be eliminated as well, making χ_{ij} a matrix of size $(n-1)\times(n-1)$. Electrochemical-potential gradients can then be expressed in terms of particle-fraction gradients as

$$d\mu_i = \frac{RT}{y_i} \sum_{j=1}^{n-1} \chi_{ij} dy_j. \tag{2.8}$$

In section 3.4, the process of systematically choosing the smallest set of independent thermodynamic factors will be demonstrated, based on the core-potential framework.

2.3 Potentials for electrochemical systems

Although concentrated-solution theory is well established, its intrinsic electroneutrality assumption renders it difficult to extend to non-electroneutral systems. In this section, the existing ideas on chemical and electrochemical potentials are briefly illuminated and the new notion called the core potential is introduced, which can successfully manage non-electroneutrality without thermodynamic inconsistencies.

2.3.1 Electrochemical potentials and Guggenheim's quandary

The definition of the electrochemical potential

Energy is intrinsic to matter and its contribution must appear in the first law of thermodynamics when the transfer of matter is allowed across the system boundary, i.e., when the system of interest is open. A quantity called the chemical potential, which encapsulates energy associated with each particle of matter, is thus used to fulfil this requirement. The chemical potential μ_i^{chem} of species i is defined as

$$\mu_i^{\text{chem}} = \left(\frac{\partial G}{\partial n_i}\right)_{T,p,n_{j\neq i}}, \tag{2.9}$$

where G is the Gibbs free energy, n_i is the molar number of particles of species i, and the subscripts T, p, and $n_{j\neq i}$ indicate that temperature, pressure, and the molar content of species other than i are constant. If the system contains charged species, its energy content should also vary when subjected to an electric field. Since this change in energy must be proportional to the number of charged species in the system, it is natural to extend the notion of chemical potential to include electrical information, as well. Thus, Guggenheim [23] proposed a new thermodynamic quantity called the *electro*chemical potential μ_i and expressed it as

$$\mu_i = \mu_i^{\text{chem}} + z_i F \Phi, \tag{2.10}$$

where z_i is the equivalent charge of species i, F is the Faraday constant, and Φ is the electric potential. It is noted that the electrochemical potential μ_i still obeys the definition in eq.(2.9) as a partial derivative of G, if Φ is seen as the intensive variable conjugate to the species charge $z_i n_i$. Using Guggenheim's form of electrochemical potential, and without presuming the charge state of the system, the Gibbs–Duhem relation becomes

$$0 = \sum_{i=1}^{n} y_i d\mu_i = \sum_{i=1}^{n} y_i d\mu_i^{\text{chem}} + \overline{\mathrm{P}} d\Phi. \tag{2.11}$$

If the ideal mixing behaviour is chosen such that $d\mu_i^{\text{chem}} = RTd\ln y_i$, as is typically done in Nernst–Planck models, then $y_i d\mu_i^{\text{chem}}$ terms add up to zero, while the $\overline{\text{P}}d\Phi$ term remains, unless the molar excess charge $\overline{\text{P}}$ is zero. Therefore, the fundamental Gibbs–Duhem relation is violated and thermodynamic consistency is compromised for non-electroneutral systems if Guggenheim's μ_i is employed. The relation must hold regardless of the charge state of the system because it essentially dictates the microscopic force balance in the system. Thus, the satisfaction of the the Gibbs–Duhem relation is the most important criterion against which alternative types of potentials will be evaluated.

Guggenheim's quandary

Although μ_i in eq.(2.10) is composed of distinct chemical and electrical parts, they are not in general separately measurable [75], as noted by Guggenheim himself when he first proposed this definition [23]. It is the electrochemical potential —not its decomposed parts— that is a thermodynamically meaningful quantity whose gradient is responsible for driving physical phenomena such as diffusion. Splitting the two parts is arbitrary because charge always resides on the matter; thus, observing purely electric effects without altering the chemical composition is not possible when μ_i is measured according to eq.(2.9). Decomposing μ_i is further complicated by the fact that, unlike temperature or pressure, there is no absolute reference point for the electric potential. This inevitably leads the chemical part of μ_i to be dependent on the choice of the electric reference state. As a result, solely measuring the electric-potential difference across two regions is futile, unless the measurement is taken between two points in the same material of uniform composition, where the chemical environments in which charged species reside are identical [76].

Nonetheless, this measurability problem has not precluded theorists from developing models that rely on the electrostatic potential[8] as an independent quantity. For

[8]The electrostatic potential is a type of electric potential conventionally used for metallic media. Practically, electrons are the only mobile species in the system (ignoring the slow diffusion of metallic atoms) and the chemical composition is hardly affected by the transfer of electrons. Therefore, the

example, Debye–Hückel theory, which predicts how dilute electrolytic solutions are expected to deviate from thermodynamically ideal mixing behaviour[9], uses the Poisson–Boltzmann equation to relate the electric potential to the excess charge in the solution phase [77]. The energy term in the Boltzmann distribution is chosen to originate entirely from the local electric potential rather than the electrochemical potential, so the theory is applicable to sufficiently dilute solutions only.

2.3.2 Quantifying the electrochemical potential

Even after accepting that μ_i cannot be split into chemical and electrical parts, there still remains a problem of quantifying it for charged species. According to eq.(2.9), the measurement process involves adding/removing an incremental amount of a charged species to/from the system to observe the corresponding change in the Gibbs free energy, while holding the rest of the species contents constant. This process is fundamentally prohibited, however, as only neutral salt-formula units can be added to or removed from a material due to electroneutrality. To circumvent this ambiguity and to clearly quantify μ_i for charged species, a number of strategies have been suggested. Three noteworthy approaches are discussed below.

Potential measured by a reference electrode

Guggenheim [23] realised that a reference electrode that undergoes a reversible electrochemical reaction involving at least one ionic species in the solution can provide a thermodynamically reversible voltage measurement. Because electrode half reactions involve the exchange of charge from one phase to another in a way that does not conserve the charge of a bulk electrolytic solution, properly defined reference electrodes can be used to represent μ_i's of solution-phase species without being constrained in the same way by electroneutrality. The voltage measured between two reference elec-

chemical part in the electrochemical potential of electrons can be disregarded.

[9] Ideal in the sense that the activity coefficients of ions are one. In electrolytic solutions, non-ideality partly arises because dissociated ions interact with each other electrically. Hence, their distributions are not completely random [22].

trodes immersed in an electrochemically reactive phase represents the difference in the electrochemical potential of the electrons within them. Because the sum of the species' μ_i's on both sides of the redox-reaction equation must equate at equilibrium, one can write μ_i of charged species in terms of clearly defined quantities, i.e., using the chemical potential of neutral species and the measured voltage. Based on this principle, Guggenheim [23] calculated the potential across cells with a liquid junction. Later, the same approach was adopted by Newman to underpin his concentrated-solution theory [22]. The resultant μ_i of the reversible charged species can be related to the electrostatic potential (representing purely electric effects) if necessary, according to Guggenheim [78].

The electric potential used in dilute-solution theory (also called the Nernst–Planck potential, understood as the electrostatic potential within the solution phase) can also be related to the reference-electrode potential, as shown by Garrido and Manzanares [79] and Bizeray et al. [80]. Many restrictive thermodynamic assumptions are needed to derive Nernst–Planck potential. Consequently, it cannot be applied to concentrated (or even moderately dilute) electrolytic solutions without inducing significant error.

One should be aware that the electrochemical potential is not an absolute quantity, so it is necessary to establish two reference states to compare its values under different conditions. Firstly, the primary reference state is commonly chosen such that the chemical potential of a given pure substance is set to zero at 25°C under 1 bar. In reference to this state, the chemical potential of the substance can be determined when subjected to conditions other than the standard condition. For a species in a mixture, its chemical potential also depends on its concentration. Therefore, the secondary reference state corresponds to the concentration at which the solution behaves ideally, i.e., its activity coefficient is one in this state. Because the activity coefficients of ions depend on the electrical state of the system, deciding on the secondary reference state inevitably fixes a reference state for the electric potential. See Newman and Thomas-Alyea [22] for more details.

The quasi-electrostatic potential

Another line of attack to define a thermodynamically rigorous, non-ideal electrochemical potential is to use the quasi-electrostatic potential Φ_{q}, employed by Smyrl and Newman [50]. Φ_{q} is defined by adopting a convention that a reference ionic species n has a thermodynamic ideal mixing entropy. Thus, if the molar concentration of n is c_n, then

$$\mu_n = RT \ln c_n + z_n F \Phi_{\mathrm{q}}. \tag{2.12}$$

This allows one to create neutral combinations of ions with measurable chemical potentials of the form

$$\mu_i^n = \mu_i - \frac{z_i}{z_n}\mu_n, \tag{2.13}$$

while electrical effects are accounted for by the reference ion alone. Therefore, μ_i of any ion can be expressed unambiguously by rearranging eq.(2.13), so long as local electroneutrality is maintained [22]. The Smyrl–Newman approach is particularly useful when there is no electrode reversible to species in the system or if one has no specific reference electrode in mind, i.e., for theoretical purposes. Although the quasi-electrostatic potential Φ_{q} cannot be measured directly, at least μ_n/z_nF behaves like the potential of a reference electrode reversible to the species n [50]. When there is no compositional variation, μ_n/z_nF and Φ_{q} behave like the electrostatic potential and obey the Laplace equation: $\nabla^2\Phi = 0$ [50].

The twin chemical potential

Another novel attempt at quantifying the electrochemical potential of charged species is the work of Kokotov [81]. Kokotov introduced a concept called the twin chemical potential based on a *pair* of ions that preserves electroneutrality, rather than a single reference ion, to establish the meaning of μ_i's for charged species.

The twin chemical potential presents itself naturally as a conjugate to the composition variable when equivalent expressions for the Gibbs free energy G are obtained

from different neutral pairs of ions. Kokotov's process is to redefine G as a function of $(n-1)$ composition variables (where n is the total number of species in the system), by assuming that the total charge content is constant (or zero if electroneutral). This allows one species to be freely added or subtracted without affecting G at all, resolving the contradiction imposed by the differential definition of μ_i for charged species in eq.(2.9). That is, the twin chemical potential of a charged species i is quantified by measuring the change in G when an incremental amount of i is added to the system, immediately followed by either an addition or removal of the species[10] on which G does not depend to satisfy electroneutrality. Because G is constructed in a way that is independent of this second step of the measurement process, it provides a means by which one can define μ_i of charged species clearly.

Although its definition seems rather convoluted, the twin chemical potential is thermodynamically clearer than the Smyrl–Newman chemical potential μ_i^n because it is directly related to G without requiring inaccessible quantities like the quasi-electrostatic potential Φ_{q}. It is more general than μ_i^n because it does not require choosing a particular charged species as a referent. It is also valid for non-electroneutral systems and can be used to define the mean activity coefficient of electrolytes. A drawback of Kokotov's approach is that the twin chemical potentials rely on a matrix of quantities, which is analytically cumbersome.

Inconsistencies in conventional electrochemical potential definitions

Unfortunately, the three approaches presented so far are not entirely satisfactory for several reasons. Guggenheim's reference-electrode method is the most concrete in that it is directly linked to measurement but one is faced with perplexity when there is no reliable electrode for the species of interest. Also, the Gibbs free energy written as the sum of μ_i's is not the most convenient, since the electrical information does not appear explicitly as an independent term. Furthermore, and perhaps most problematically, an assumption of local electroneutrality is necessary within Guggenheim's framework.

[10] Addition of this species if it is counter-charged to the species i and removal if like-charged.

The Smyrl–Newman chemical potential μ_i^n —which was designed to be free from the electric potential dependence— has been found to be insufficient for non-electroneutral systems, as well [1]; similar to Guggenheim's μ_i that divides the chemical and electrical parts, μ_i^n fails to satisfy the fundamental Gibbs–Duhem relation when the system attains excess charge. Actually, such inconsistency is a universal problem in any formalisms that deploy the electrochemical potential as an arbitrary sum of chemical and electrical parts, as illustrated by Goyal and Monroe [1].

Furthermore, Kokotov's twin chemical potential, despite its theoretical elegance and validity for non-electroneutral systems, comes in an unconventional matrix structure; this is due to its definition that involves every possible pair of species in the system. This makes integration with existing theories challenging, where the norm is to express electrochemical potentials in a vector form, not a matrix form.

2.3.3 The core-potential theory

The core potential and naive electric potential

The failure to meet the Gibbs–Duhem relation under non-electroneutrality and the structural complexity (matrix vs. vector) in the existing electrochemical-potential definitions call for a better one. Conveniently, Goyal and Monroe [1] have recently presented a new potential, called the core potential, to resolve both these issues. As shown in the first law of thermodynamics in eq.(2.14) (using the Gibbs free energy G as the main energy descriptor), the electrical information of the system is hidden in the last term, intertwined with the chemical information.

$$dG = -SdT + Vdp + \sum_{i=1}^{n} \mu_i dn_i \tag{2.14}$$

In this equation, S is the entropy, T is the temperature, V is the volume, p is the pressure, and n is the total number of species in the system. The key idea of Goyal and Monroe's core-potential theory [1] is to deconvolute this chemical–electrical en-

tanglement so that the electrical contribution stands alone in the Gibbs-free-energy expression, i.e., write $\Phi\overline{\mathrm{P}}$ separately, where $\overline{\mathrm{P}} = F\sum_{i=1}^{n} z_i y_i$ defines the molar excess charge, according to Faraday's law. This is achieved by a two-step process. Firstly, a new composition basis called the neutralizable composition x_i is adopted, in which $\overline{\mathrm{P}}$ explicitly appears as one of the independent variables in the basis set (note that x_i is a vector of length $n-1$).

$$x_i = \begin{cases} y_i & ; \quad i < n-1 \\ \\ \frac{\overline{\mathrm{P}}}{F(z_n - z_{n-1})} & ; \quad i = n-1 \end{cases} \tag{2.15}$$

Secondly, the electric potential is clearly defined as the partial derivative of molar Gibbs free energy $\overline{G}$ with respect to the molar excess charge.

$$\Phi = \left(\frac{\partial \overline{G}}{\partial \overline{\mathrm{P}}}\right)_{T,p,y_{i<n-1}} \tag{2.16}$$

This Φ —which is different from the potential measured by the reference electrode— is called the naive electric potential because it follows the most primitive definition of electric potential in physics, i.e., the electric potential is the thermodynamic conjugate of the excess charge. The naive electric potential can be shown to directly relate to the electrochemical potential of two ions of opposite charges (called the charging and reference ions and denoted by $n-1$ and n, respectively) as

$$\Phi = \frac{1}{F(z_n - z_{n-1})}\left(\frac{\partial \overline{G}}{\partial x_{n-1}}\right)_{T,p,x_{i<n-1}} = \frac{\mu_n - \mu_{n-1}}{F(z_n - z_{n-1})}. \tag{2.17}$$

Therefore, the electrical information is essentially measured relative to what Goyal and Monroe [1] called the two-ion secondary reference state, in resemblance to Kokotov's twin chemical potential [81].

Upon replacing the composition basis y_i with x_i in the first law in eq.(2.14), a new set of potentials M_i^n (where M denotes capital μ and the superscript n indicates the

reference ion) naturally arises as conjugate variables to x_i, which can be written as [1]

$$\mathrm{M}_i^n = \begin{cases} \mu_i - \frac{z_n - z_i}{z_n - z_{n-1}}\mu_{n-1} - \frac{z_i - z_{n-1}}{z_n - z_{n-1}}\mu_n & ; \quad i < n-1 \\ F\left(z_n - z_{n-1}\right)\Phi & ; \quad i = n-1 \\ \frac{z_n\mu_{n-1} - z_{n-1}\mu_n}{z_n - z_{n-1}} & ; \quad i = n \end{cases} . \tag{2.18}$$

M_i^n is called the core potential to convey its fundamentally and thermodynamically consistent nature (by satisfying the Gibbs–Duhem relation) regardless of the charge state, with a clear separation between the chemical and electrical contributions in the first law, as illustrated below.

$$\begin{aligned} dG &= -SdT + Vdp + \sum_{i=1}^{n-1} \mathrm{M}_i^n dx_i \\ &= -SdT + Vdp + \sum_{i=1}^{n-2} \mathrm{M}_i^n dy_i + \Phi d\overline{\mathrm{P}} \end{aligned} \tag{2.19}$$

Interestingly, the core potential is not discrete from other electrochemical-potential formalisms; it can be rearranged to resemble the Smyrl–Newman or twin chemical potentials [1]. Therefore, the core potential can be thought of as a subspace of the twin chemical potential with specific reference and charging ions. It is noted that having a reference ion is not a nuisance in practice, since comparison with measurement data will always mandate a choice of a secondary reference electrode.

By performing the inverse transformation of eq.(2.18), it is also possible to express the standard electrochemical potential in terms of core potentials.

$$\mu_i = \begin{cases} \mathrm{M}_i^n + \frac{z_i}{z_n - z_{n-1}}\mathrm{M}_{n-1}^n + \mathrm{M}_n^n & ; \quad i < n-1 \\ \frac{z_{n-1}}{z_n - z_{n-1}}\mathrm{M}_{n-1}^n + \mathrm{M}_n^n & ; \quad i = n-1 \\ \frac{z_n}{z_n - z_{n-1}}\mathrm{M}_{n-1}^n + \mathrm{M}_n^n & ; \quad i = n \end{cases} \tag{2.20}$$

In fact, conversion from one form to the other can be straightforwardly captured by

a matrix multiplication. For instance, the transformation eq.(2.21) (in which δ_{ij} represents the Kronecker delta) converts the core potentials to standard electrochemical potentials when multiplied by a list of core potentials from the right, according to Goyal and Monroe [1].

$$\left(\mathbf{T}_n^{\mu\leftarrow\mathrm{M}^n}\right)_{ij} = \delta_{ij} + \left(\frac{z_i}{z_n - z_{n-1}} - \delta_{i(n-1)}\right)\delta_{(n-1)j} + (1-\delta_{in})\,\delta_{nj} \tag{2.21}$$

Advantages of the core potential

In addition to the clear decoupling of the electrical information in the Gibbs-free-energy expression, the core-potential formalism carries other desirable characteristics, too. Because no arbitrary division of chemical and electrical parts is made in the core-potential theory, the Gibbs–Duhem equation invokes no contradiction even in non-electroneutral systems. This is a critical difference that sets the core potential apart from other preceding potentials.

Another major advantage is that the core-potential formalism gives obvious structures to thermodynamic factors. Goyal and Monroe [1] showed that the core-thermodynamic-factor matrix is the Hessian (second-order partial derivative) of the molar Gibbs free energy with respect to the independent composition variables in the two-ion reference state. Thermodynamic stability demands that the Gibbs free energy be convex and this puts constraints on the possible values of core thermodynamic factors, i.e., the core thermodynamic-factor matrix has to have a non-negative determinant, trace, etc. to guarantee a full complement of non-negative eigenvalues. In addition, the core-potential Maxwell relations dictate that the core thermodynamic-factor matrix be symmetric. This means that the lower triangular elements of the matrix are sufficient for modelling, reducing the number of independent thermodynamic factors by almost half (from $(n-1)^2$ if all entries were independent to $n(n-1)/2$). Hence, core-potential theory allows one to determine the most parsimonious set of thermodynamic factors naturally, based on thermodynamic reasoning. Such information can help one make an informed decision when assigning numerical values to thermodynamic factors,

especially when the system comprises more than two components and experimental data is available only in a limited composition space.

2.4 Membrane models

Membranes are an integral part of many engineering systems that incorporate fluxes of charged species, e.g., desalination through reverse osmosis, removal of impurities using electrodialysis, production of chemicals by electrolysis, fuel cells, redox flow batteries, etc. Since membranes are a key component that mediates the transport of species at the intersection of two different solutions, advanced mathematical modelling of such systems necessarily demands a proper treatment of the membrane. As a result, colossal efforts have been invested to understand and mathematically describe membrane performance. This section provides a brief overview of membrane models, focussing on ion-exchange membranes that are selectively permeable due to the presence of embedded charged groups in the material. Models that admit both liquid and gas phases, e.g., as in fuel-cell membranes, are out of the scope of this thesis. Before delving into the details, a principal concept called the Gibbs–Donnan effect is introduced to lay down a theoretical foundation first.

2.4.1 The Gibbs–Donnan effect

The ideal Gibbs–Donnan effect

The Gibbs–Donnan effect is a phenomenon whereby an uneven distribution of charged species is produced on either side of a selectively permeable material that divides two electrolytic solutions of different compositions or concentrations [82]. This effect is attributed to the competition between diffusion and migration among the ionic species in the system. Thus, the phenomenon is relevant for systems involving membranes in contact with electrolytic solutions, e.g., fuel cells, redox flow batteries, and electrodialysis and Donnan dialysis systems (which are used for the treatment of brackish water;

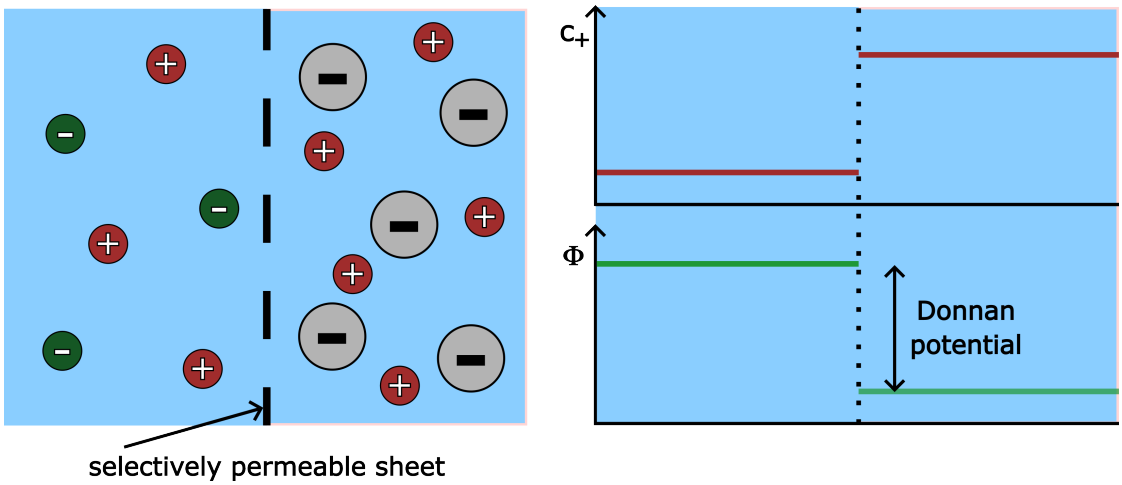

Figure 2.1: A selectively permeable sheet divides two electrolytic solutions. The reservoir on the left contains a cation and an anion, both of which are permeant to the sheet. The reservoir on the right contains the same permeant cation but a different anion that cannot penetrate the sheet.

the former uses an applied electric field for the separation of ions, while the latter only relies on the Gibbs–Donnan effect) [83–86].

To see the Gibbs–Donnan effect in play, imagine a situation where a thin sheet of permeable material is placed between two reservoirs, each containing a different simple binary salt dissolved in a common solvent, as illustrated in Figure 2.1. The salt in the first reservoir dissociates into a cation and an anion, both of which can move through the sheet (permeant). In contrast, the salt in the second reservoir is composed of an anion that is too bulky to cross the sheet (impermeant), while the dissociated cation is the same type of cation as the one in the first reservoir and hence permeant. If the salt concentration in the second reservoir were higher than the first reservoir, the permeant cation would diffuse down the concentration gradient through the dividing sheet. But this causes an electric-charge imbalance in the reservoirs because the impermeant anion is bound to one side of the sheet. Therefore, some cations that have travelled through the sheet to the other reservoir are pulled back against their concentration gradient, due to the Coulombic force emanating from the bound anions. Hence, a uniform distribution of the permeant cation across the two reservoirs is hindered and an electric potential difference is set up between them. This potential difference at equilibrium is

called the Donnan potential. Note that the reservoirs remain electroneutral overall and the potential distribution at the interface is treated as discontinuous in the classical Gibbs–Donnan theory [87].

Introducing the Gibbs–Donnan effect to membrane models

In reality, selectively permeable sheets typically used in electrochemical devices are not infinitely thin and contain charged ionic groups embedded in hydrophobic polymer-matrix structures [88]. For example, a common and reliable such material used for electrochemical energy storage systems (e.g., fuel cells and redox flow batteries) is an ion-exchange membrane called Nafion, which is a copolymer composed of side-chains with negatively charged sulfonate (SO_3^-) end-groups attached to an electrically neutral semicrystalline polymer backbone [89]. Because these negative sites are bound to the polymer structure while the counterions (cations in this case) are free to navigate through, the membrane can be treated as a separate phase of its own from the Gibbs–Donnan perspective [88]. Therefore, a system of two electrolytic solutions separated by an ion-exchange membrane would exhibit two Donnan potentials, one for each side of the membrane.

However, the discontinuous electric potential at the interface in the classical Gibbs–Donnan theory is rather non-physical. Near a charged surface submerged in an electrolytic solution, it is well known that there is an electrical double layer whose thickness is of the order of the Debye length, within which the potential changes continuously. Therefore, eliminating the discontinuity at the membrane–reservoir interfaces can lead to a more realistic representation of the membrane behaviours. In this regard, the work of Mauro [90] is of high relevance; a continuous electric-potential profile was obtained by assuming Boltzmann-distributed ions in the solution phase, in addition to the fixed charged end-groups in the background, resulting in a space-charge region (i.e., non-zero net charge) in the vicinity of the membrane–reservoir interface. Mauro's approach is elaborated in more detail in section 5.7. In the meantime, we return to the literature to survey different types of membrane models.

2.4.2 Considerations for the membrane-model length scales

In broad strokes, the field of membrane modelling can be divided into two categories: macro-homogeneous and microscopic models. The former treats the membrane as a single homogeneous phase without regard to its internal morphology and detailed microstructure, while the latter assumes that a percolation network of channels forms from simple (and often repeating) microstructures within the solid material, through which a second fluid phase freely flows. The most commonly implemented microstructure is parallel circular capillaries, but different geometries can also be used, e.g., see reference [91]. Given a membrane system, the appropriate resolution of its mathematical description depends on the physical processes one aims to incorporate, as well as the level of accuracy one desires to achieve. Therefore, it is useful to know of the approximate scale the two models deal with.

Quantitative values for membrane-model length scales

For macro-homogeneous models, the length scale of interest is simply of the order of the membrane width; e.g., Nafion 117, the membrane that will be studied in Chapter 5, is 230 μm thick [7]. By model construction, there is little use considering anything significantly smaller than this because the membrane is supposed to be uniform when magnified beyond this scale, although microstructural knowledge can inform the values of phenomenological parameters. By contrast, structural variations at the nanometer level play an important role in microscopic models. For example, the microscopic morphologies of Nafion can be inferred from small-angle scattering techniques such as SAXS (using X-rays) and SANS (using neutrons), e.g., see references [92–95]. Such investigations have revealed that the Nafion polymer chains are arranged such that the charged sulfonate end-groups wrap around aqueous flow channels, forming (hollow) cylindrical regions embedded in a matrix of hydrophobic polymer backbones (this structure is also referred to as cylindrical inverted micelles). Schmidt-Rohr and Chen's SAXS results [95] concluded that the cylinders have diameters of 1.8 – 3.5 nm, with an

average diameter of 2.4 nm, at the hydration level of 20% water by volume. Based on this result, they confirmed that treating Nafion as composed of cylindrical flow channels is sufficient to capture many important features of the membrane, as long as the membrane's hydration level is not too high. It should be noted that the ultimate application area of Schmidt-Rohr and Chen's investigation was fuel cells, so membranes that directly come in contact with aqueous solutions —as in the system in Chapter 5— are likely to be more hydrated.

For highly hydrated membranes, a model in which polymer chains form cylindrical bundles in the sea of solution was suggested [96–98] (schematics of such bundles and cross-sections of this Nafion model are illustrated in references [98] and [95], respectively). Using the SAXS and SANS techniques, Rubatat et al. [96, 98] revealed that the diameters of the bundles range between 3 and 6 nm, depending on the solvent used. This demonstrates how small a length scale microscopic models have to contend with. Such models are expected to be highly susceptible to the choice of membrane structure; how the flow path is constructed inside the membrane strongly affects the solutions to Poisson's equation (that sets the electric potential in non-electroneutral domains, usually solved with the Boltzmann distribution) and the material and momentum balances that govern multicomponent fluid flow through the polymer network.

In many applications involving energy transfer, however, the exact details of species movement inside the membrane are of secondary concern. It is often more important to understand the rates of mass exchange between the reservoirs mediated by the membrane. This aspect of membrane transport is the main concern of Chapter 5, where Verbrugge and Hill's experimental data [2, 3] are re-examined to derive the Stefan–Maxwell diffusivities between ions and Nafion's charged end-groups. In such cases, macro-homogeneous modelling generally suffices and is the approach pursued in this thesis, consequently. Important macro-homogeneous membrane models from the literature are addressed in the next section, followed by microscopic models.

2.4.3 Macro-homogeneous membrane models

Perhaps due to their analytical simplicity and the lack of experimental means to observe microstructures, early membrane models were macro-homogeneous. Initial models of membrane transport were basic; e.g., in the sieve theory proposed by Traube [99], membranes were treated as barriers that mechanically blocked ions. Nonetheless, the model was favourably received and this is perhaps not surprising, given Traube's authority in the field; he was responsible for synthesising the first artificial, uncharged membrane that "could completely distinguish between small solutes and water" in 1864 [100][11].

Following his success, many membranes with different properties and morphologies were made. This phase of increased interest and fast progression naturally sparked intellectual curiosity to better understand and characterise membranes. The celebrated Gibbs–Donnan effect was established in this era, too.

Charged-membrane models

With "the advance of the synthetic ion-exchange resins with cross-linked structures", ion-exchange membranes (with fixed charged end-groups) grew as an important class of membrane [101]. Their behaviours are more complex than uncharged membranes and this necessitated new modelling perspectives, which Teorell [102] provided. His work looked at non-mechanical mechanisms —on top of mere physical blockage— to describe the preferential accumulation of ions on one side of a dividing membrane. Treating the membrane as an ideal material with negligible thickness and permeable to *all* ions (in contrast to the Gibbs–Donnan effect where at least one impermeant ion has to be present), Teorell attributed the observed concentration difference across the two reservoirs in contact with the membrane to the difference in mobilities of the diffusing ions inside the membrane, e.g., anions in proton-exchange membranes were given lower mobility than protons. However, this theory failed to explain coherently why the ionic selectivity of membranes is affected by the membrane charge, an effect

[11] Note that the original publication of Traube [99] could not be found and therefore Kramer and Boyer [100] was quoted instead.

that was observed experimentally [103].

Soon, a more realistic model was conveyed by Teorell [104], and independently a year later by Meyer and Sievers [105][12], which captured the dependence of ion selectivity on the membrane charge. The Teorell–Meyer–Sievers (TMS) theory naturally considers the attraction and exclusion of ions due to the embedded membrane charges (which are impermeant species in the Gibbs–Donnan language) by enclosing the membrane in two ideal Gibbs–Donnan surfaces [106]. On top of the boundary Donnan potentials, a liquid-junction potential (associated with the two reservoirs on either side of the membrane and calculated by the Henderson equation[13]) is applied across the membrane as a constant voltage bias [101]. Note that the TMS theory is fundamentally different from Teorell's earlier model in that it was built upon the idea of absolute impermeability of fixed charged membrane end-groups —as stipulated in the Gibbs–Donnan equilibrium— rather than relative impermeability stemming from the differences in ionic mobilities [101].

Another macro-homogeneous model that appears fairly frequently in the literature (e.g., see references [108–111]) is the solution-diffusion model, developed by Merten [112]. What sets this theory apart from the TMS theory is that it takes into account the varying nature of the solvent chemical potential with respect to pressure. Therefore, Merten's theory is suitable for systems where pressure gradients participate significantly in transport phenomena, e.g., membranes used in brackish water desalination through reverse osmosis. The model is built upon Fick's law of diffusion for solutes whereas the solvent flux is proportional to the total pressure difference[14] across the membrane.

Macroscopic membrane models that stem from Newman and coworkers are also notable. Their approach is characterised by extending the framework of concentrated-solution theory to membranes, treating membrane-phase charged end-groups as an

[12]The original publication of Teorell [104], Meyer and Sievers [105] could not be found.

[13]The Henderson equation calculates a liquid-junction potential by assuming that "(a) concentrations of ions everywhere in the junction are equivalent to activities and (b) the concentration of each ion follows a linear transition between the two phases" [107].

[14]The total pressure difference is equal to the hydraulic pressure difference minus the osmotic pressure. The osmotic pressure encapsulates the solvent activity gradient.

immobile, dissolved species in the solution phase. Despite being constructed to model fuel cells [113] and electrolyzers [114], Newman's four-species membrane models (comprising membrane-bound anions, water, and two cations) do not distinguish the gas phase. Therefore, they are conceptually identical to the membrane model in Chapter 5 of this thesis.

2.4.4 Microscopic membrane models

Unfortunately, macroscopic models are not sufficient when membrane-property optimisation is required for a selected application. For example, predictions made by the TMS theory are not always in agreement with experimental findings [115, 116] and the solution-diffusion model is inherently limited due to its reliance on Fick's law. Stefan–Maxwell diffusivities in models inspired by concentrated-solution theory do not provide insight about how membrane structure should be changed to vary performance. Although some improvements can be made to these models, e.g., using a more accurate liquid-junction-potential expression for the TMS theory [117] or introducing the OSM equations for the solution-diffusion model [118], a need to capture structural information in models became more and more apparent, so that the effects of experimentally controllable structural parameters on membrane characteristics could be directly established.

A model that shows this shift in focus is the work of Lorenz [119]. On the surface, it resembles a typical macroscopic model based on the Onsager-form flux-explicit equations, but the phenomenological coefficients are expressed in terms of membrane pore dimensions, in this case, the radius of parallel circular capillaries[15] (all capillary radii equal). Of course, real membranes have a lot more complicated internal structures, but having this extra parameter provides experimentalists useful guidance during membrane-synthesis efforts.

[15]Treating a membrane as a collection of parallel capillaries seems to have originated from the already well-established studies of fluid flow through porous media, whose research interests were founded upon oil production, hydrology, irrigation, etc [120].

A route based on Eyring's theory of rate processes is another viable option, thoroughly investigated by Kobatake and coworkers. They treated membranes as a bundle of parallel circular capillaries and calculated the rate of ionic movement upon exposure to an electric field; the deviations of energy the applied electric field caused at the two ends of the capillaries were used as activation energies for ionic flows [121]. In implementing the model, however, some restrictions had to be placed for pragmatic reasons. For example, Nagasawa and Kobatake [121] (and later Kobatake [122] with more thermodynamic rigour) assumed that ionic concentrations in the membrane capillaries (having a range of radii) were small compared to the concentration of the charged membrane end-group to linearise the Poisson–Boltzmann equation. Furthermore, Kobatake [122] Kobatake and Fujita [123] only considered membranes with a large enough capillary radius compared to the Debye length to neglect electrical interactions originating from the charged membrane end-groups.

More accurate and flexible models free from restrictive assumptions were also quick to follow to investigate the electrokinetic effects in membranes. Studies on electro-osmosis (flow of fluid induced by an applied electric potential in capillaries) by Dresner [124] and Morrison and Osterle [125] are good examples, except diffusion across the membrane was not considered (this is because pressure and electric-potential gradients are the main driving forces in electro-osmosis, not concentration gradients). An improvement to this model was made by Gross and Osterle [126], permitting a small concentration difference across the membrane. This assumption was further relaxed by Fair and Osterle [127] and Anderson and Koh [91], thereby removing the limitation on the magnitude of the concentration difference altogether; to do so, Fair and Osterle [127] focused on the capillaries of circular cross-section only, whereas Anderson and Koh [91] considered elliptical and infinite slit shapes, as well. Furthermore, Verbrugge and Hill [8] suggested a more refined model that includes the solvation of ions and changes in the relative permittivity due to the varying electrostatic potential within the capillaries. This model was further improved by considering the adsorption of ions

onto the capillary surface [128] and was later incorporated with transport equations [129].

Microscopic details were introduced to models based on concentrated-solution theory, too [130, 131], and their model was used to simulate the vanadium redox flow battery [132].

It is noted again that a caveat to microscopic models is their dependence on the chosen microscopic structure. In cases where an accurate description of membrane microstructures is not available, it may be simpler and safer to opt for macroscopic models.

2.4.5 Flux laws for membranes

Regardless of the length scale membrane models deal with, there are three main ways to construct flux equations, namely, the Nernst–Planck equation, the OSM equation, and the Onsager-form flux-explicit equation (where fluxes are expressed as sums of diffusion driving forces, scaled by appropriate coefficients). Among macro-homogeneous models, those based on the Nernst–Planck equation are the most common [7, 102, 133–140]. Also, a solid volume of literature is devoted to the OSM approach [113, 114, 141–143] but the Onsager-form approach is less popular [119, 144].

Likewise, microscopic models can be classified as those employing the Nernst–Planck equation [91, 122, 123, 125–129, 145, 146], the OSM equation [147] and the Onsager-form approach [119, 124]. Approaches that do not readily fit in the three flux categories also exist, such as that of Nagasawa and Kobatake [121] (based on Eyring's theory of rate processes) and of Dresner and Kraus [148] (they dealt with equilibrium conditions, hence no discussion of fluxes). Both these works fall under the microscopic modelling realm with cylindrical capillaries.

2.5 How membrane models can benefit from the core-potential theory

The exisitng literature already suggests that the inclusion of the Donnan potential in vanadium-redox-flow-battery (VRFB) models improves their prediction capability. Notably, Knehr and Kumbur [84] showed that the omission of the Donnan potential produced a discrepancy of ∼35 mV between the predicted and experimentally measured open-circuit voltage (OCV) in their VRFB system. Because their OCV curve varied by ∼400 mV between the fully charged and fully discharged states of the battery (i.e., between the state of charge (SOC) of 1 and 0), the impact of this discrepancy is not negligible, i.e., without accounting for the Donnan potential, the SOC prediction could be off by ∼10%. The flat feature of the typical OCV curve in the intermediate OCV ranges exacerbates this issue. Knehr et al.'s [149] VRFB simulation using the improved OCV curve of Knehr and Kumbur [84] produced a satisfactory result for a single charge–discharge cycle; they found that the simulated and experimentally measured voltage responses differed only by 1.83 % on average when the Donnan potential was incorporated. However, the disagreement grew to 4.2 % over 45 cycles. The accumulation of errors can be attributed to multiple causes, such as failure to incorporate the crossover of species and side reactions accurately, as well as the fact that the non-electroneutral boundary regions at the membrane–reservoir interfaces were ignored in their model construction. Given real battery systems can undergo more than a thousand charge–discharge cycles during their lifetime, the accuracy of their model is not quite sufficient.

Accurate long-term predictions are particularly important for VRFB models because model outputs can assist in the sizing and maintenance scheduling of VRFB systems. Since VRFBs are usually paired with grid-scale renewable-energy generation, useful questions that models can quickly and economically answer include: (1) how will the battery behave given the intermittent nature of renewable energy sources?,

(2) how will the local climate (e.g., temperature and humidity) of the installation site affect the battery operation?, and (3) when should the electrolyte be regenerated?, etc. An overly conservative estimate of the battery-system performance will lead to chronic partial charging of the batteries, while an overestimation will lead to the underutilisation of renewable energy sources. Both scenarios are not ideal, since both directly lower the return on investment. Due to the high initial installation cost of such systems, imprecise predictions could inhibit funding bodies and investors from committing to financially reasonable projects that are essential in achieving carbon neutrality.

Because the Donnan potential —which is accompanied by a non-electroneutral interfacial region— is such a prominent feature of membrane systems, model performance is expected to improve with a more comprehensive treatment of the interfacial regions. A good example is the VRFB model of Lei et al. [150] that explicitly included interfacial space-charge regions. They concluded that the Gibbs–Donnan effect promoted vanadium crossover and led to a greater imbalance of vanadium species between the two reservoirs at the end of a charge–discharge cycle. However, the use of the Nernst–Planck flux equations in their model means that it is only strictly applicable to dilute solutions. VRFBs typically operate with 1 – 2 mol/L vanadium solutions and 3 – 6 mol/L supporting electrolyte (sulfuric acid) [151], which are far from the concentration range the dilute approximation can be safely made. To incorporate concentrated-solution theory to study the non-electroneutral effects near the membrane–reservoir interfaces, diffusion driving forces will need to be expressed as electrochemical-potential gradients. Only considering the vectorial form of electrochemical potentials (i.e., excluding Kokotov's electrochemical potential that comes in a matrix format), Goyal and Monroe's core potential is the only viable choice available in the literature for the given task; it satisfies the Gibbs–Duhem relation regardless of the charge state of the system, while Guggenheim's μ_i and Smyrl–Newman's μ_i^n do not.

Unfortunately, working with eight species in the VRFB makes the application of concentrated-solution theory and core-potential theory doubly challenging. The in-

version process from the force-explicit OSM equations to flux-explicit forms with 28 independent transport properties is going to be messy, as well as deriving corrected $d\mu_i$ expressions with 21 thermodynamic factors. An attempt to tackle a system of this level of complexity without prior studies is guaranteed to fail. Therefore, three simpler electrolytic systems are investigated first in chapters 3 and 4 as stepping stones, which also possess their own practical utility. This excerise additionally serves to solidify Goyal and Monroe's somewhat abstract core-potential theory. Then, the same type of excerise is carried out in Chapter 5 to study the simplest membrane system: a charged membrane immersed in a binary electrolyte.

Chapter 3

Transport equations in the core-potential space

In this chapter, the core-potential theory introduced in section 2.3.3 is developed further to study the following three simple electrolytic systems (note that the present study is only concerned with isothermal and isobaric conditions).

- The binary electrolyte; an electrolyte that dissociates into one type of cation and another type of anion in a neutral solvent
- The three-ion ionic liquid; an electrolytic solution that comprises three types of ions with no solvent
- The binary salt in two neutral solvents; an electrolyte that dissociates into one type of cation and another type of anion, dissolved in a cosolvent blend

Going down this list, the level of complexity increases and each system serves as a stepping stone to our end goal: to model a charged membrane imbued with a binary electrolyte. In particular, the fact that the three-ion ionic liquid is composed of two neutral salts with a common ion and the four-species nature of the binary salt in two neutral solvents will help us navigate the membrane system in Chapter 5. However, these intermediary systems do have importance in their own right. The binary electrolyte is the most basic system that essentially all electrolyte theorists and modellers

elect to study, e.g., Newman and Thomas-Alyea [22] and Monroe and Delacourt [49]. The binary electrolyte in two neutral solvents is commonly found in conventional Li-ion batteries; a blend of polar and non-polar carbonate solvents is used for optimum ionic conductivity and viscosity. Several three-ion ionic liquids are being investigated as potential candidates for electrolytes in a variety of battery chemistries, which offer advantages such as decreased flammability and increased electrochemical stability compared to traditional carbonate-based electrolytes [152–154].

This chapter is arranged in two main parts. Sections 3.1 and 3.2 lay out the transport equations (species flux equations) and a current-voltage relation called the MacInnes equation using the core-potential gradients directly. The level of complexity this approach brings promotes deriving correction terms for electrochemical-potential differential expressions, instead. This is done by employing the Boltzmann distribution for charged species and is covered in sections 3.3 and 3.4. The core-potential theory still forms the basis of this second approach, so the resulting expressions satisfy the Gibbs–Duhem relation in non-electroneutral regions, too. The outcomes of this chapter inform us to circumvent the direct use of core potentials for the more complicated membrane system in Chapter 5, saving us time and effort.

3.1 Core-potential gradients as diffusion driving forces

To arrive at the transport and MacInnes equations with core-potential gradients as diffusion driving forces, a convenient starting point of analysis is the work of Monroe and Delacourt [49], who laid out a general procedure for acquiring the desired equations for multicomponent, non-electroneutral systems. Their equations are expressed in terms of the Smyrl–Newman chemical-potential gradients $\nabla\mu_i^n$ and the reference-ion electrochemical-potential gradient $\nabla\mu_n$ (which is related to the quasi-electrostatic-potential gradient $\nabla\Phi_\mathrm{q}$). Because the core potentials and Smyrl–Newman chemical potentials are connected by a linear mapping, as illustrated by eq.(2.21), it is possible to take the equations of Monroe and Delacourt [49] to the core-potential space

by simple substitutions of the appropriate transformation matrices. In doing so, however, care should be given to ensure that the necessary transformations are performed on the force-explicit OSM equations, so that the conversion to the flux-explicit forms churns out correct transport properties in the core-potential domain. That is, mere substitutions of transformation matrices into the flux-explicit transport equations will leave the macroscopic transport properties in the Smyrl–Newman space, resulting in untidy and not entirely consistent transport equations. Therefore, some modifications are necessary to the inversion procedure presented by Monroe and Delacourt [49] if the transition to the core-potential formalism is to be done correctly. These modifications are summarised in the following two subsections.

In general, macroscopic transport properties defined in the Smyrl–Newman and core-potential formalisms are not expected to coincide exactly, since they correspond to differently defined electric potentials ($\nabla\mu_n$ and the naive potential Φ in eq.(2.16), respectively), albeit the difference might be subtle. Nevertheless, the Smyrl–Newman formalism under electroneutrality does correctly separate thermochemical and electrical effects, so transport properties related to an electrolyte's electrical response (i.e., the transference number and the ionic conductivity) in either formalism should produce the same expressions for electroneutral systems. On the other hand, macroscopic diffusivities in the two formalisms differ even in electroneutral systems; this is because the core potential is a linear combination of the Smyrl–Newman chemical potentials, so the entities that undergo diffusion as electrically neutral clusters are identified differently in the two formalisms.

3.1.1 The MacInnes equation and ionic conductivity

In systems where diffusion plays an important role, overpotentials associated with concentration gradients appear and their contributions must be taken into account when constructing a current-voltage relation. The MacInnes equation takes care of this by adding terms proportional to electrochemical-potential gradients (which can be con-

verted to concentration gradients) to the usual Ohm's law. The derivation of the equation starts with Faraday's law to relate the species fluxes —which are written in terms of the Stefan–Maxwell diffusivities through the OSM equations— to the current flowing through the system. Therefore, the equation is general and remains valid in concentrated solutions and in electroneutral and non-electroneutral regions, as long as the electrochemical-potential gradients are not further decomposed into chemical and electrical parts. The MacInnes equation is the standard current-voltage relation of choice in Newman's concentrated-solution theory [22], as well, and the author is not aware of any other alternative relations as flexibly applicable to electrolytic solutions as the MacInnes equation. It is noted that the versions of the equation in Newman's concentrated-solution theory [22] and Monroe and Delacourt [49] should only be used in electroneutral systems; they used the Smyrl–Newman potential μ_i^n and the quasi-electrostatic potential Φ_q to introduce the electric potential to the equation; as alluded to earlier, μ_i^n's do not satisfy the Gibbs–Duhem relation when electroneutrality is violated. A more consistent form of the equation can be obtained either by writing it entirely with core-potential gradients and the naive electric potential (see the rest of this subsection) or by updating the Smyrl–Newman μ_i^n's and the reference-ion electrochemical potential μ_n with the appropriate correction terms (see sections 3.3 and 3.4).

Given the MacInnes equation is essentially a modified Ohm's law, a logical starting point in obtaining the equation in the core-potential space is the excess-charge flux, relative to the velocity of species m: $\vec{i}-\rho_\mathrm{e}\vec{v}_m$. The solvent in excess is commonly chosen for the species that sets the reference velocity (since its velocity is usually negligible relative to the lab frame), but any choice of velocity is valid. The excess-charge flux is defined through Faraday's law as

$$\vec{i}-\rho_\mathrm{e}\vec{v}_m = F\sum_{i\neq m} z_i c_i(\vec{v}_i-\vec{v}_m), \tag{3.1}$$

where $\vec{i}$ is the current density, $\rho_\mathrm{e}=c_\mathrm{T}\overline{\mathrm{P}}$ is the excess-charge density, F is the Faraday

constant, c_i is the molar concentration of species i, z_i is its equivalent charge, $\vec{v}_i$ is its velocity, and $c_\mathrm{T} = \sum c_i$ is the total molar concentration of all species in the system. Monroe and Delacourt [49] showed that the OSM equations can be inverted to the flux-explicit form as below, which resembles the terms under summation in eq.(3.1).

$$c_i(\vec{v}_i - \vec{v}_m) = -\sum_{j \neq n} \frac{H_{ij}^{mn} c_\mathrm{T}}{RT} \nabla \mu_j \quad \text{for all } i \neq m \tag{3.2}$$

The index n denotes the (charge-state) reference ion and R is the universal gas constant. The matrix entry H_{ij}^{mn} encapsulates information about the rate of diffusion such that

$$(\mathbf{H}^{mn})_{ij}^{-1} = \begin{cases} -1/\mathscr{D}_{ij} & \text{if } i \neq j \\ \displaystyle\sum_{k \neq i} \frac{c_k}{c_i \mathscr{D}_{ik}} & \text{if } i = j \end{cases}, \tag{3.3}$$

where $\mathscr{D}_{ij}$ is the binary Stefan–Maxwell diffusivity. The superscripts mn on the matrix $\mathbf{H}$ indicate that the m-th row (that corresponds to the species that sets the reference frame for velocity) and n-th column (that corresponds to the reference ion) of $\mathbf{H}$ should be removed, a truncation necessary to make it non-singular.

Before substituting eq.(3.2) into eq.(3.1), however, a conversion that sends the flux equations to the core-potential space is required. That is, a linearly independent $(n-1) \times (n-1)$ transformation matrix that converts the Guggenheim electrochemical potentials $\nabla \mu_i$ to Goyal and Monroe's core potentials $\nabla \mathrm{M}_i^n$ is needed. Therefore, an $(n-1) \times (n-1)$ transformation matrix $\mathbf{T}_{n-1}^*$ that can implement an invertible map

$$\nabla \mu_i = \sum_{j=1}^{n-1} \left(\mathbf{T}_{n-1}^*\right)_{ij} \nabla \mathrm{M}_j^n \tag{3.4}$$

between the first $n-1$ Guggenheim potentials and the first $n-1$ core potentials is desired. Because an $n \times n$ matrix transformation between the Guggenheim and core-potential spaces is already provided by Goyal and Monroe [1] (see eq.(2.21)), the necessary reduction in order can be achieved by incorporating the Gibbs–Duhem

relation. For isothermal and isobaric systems, the Gibbs–Duhem relation in the core-potential space reduces to [1]

$$d\mathrm{M}_n^n = -\sum_{i=1}^{n-2} y_i d\mathrm{M}_i^n - \overline{\mathrm{P}} d\Phi, \tag{3.5}$$

where the summation is over all species, except the charging ($(n-1)$-th) and reference (n-th) ions. The sought after $\mathbf{T}_{n-1}^*$ can be obtained by incorporating eq.(3.5) into the transformation $\mathbf{T}_n^{\mu\leftarrow\mathrm{M}^n}$ in eq.(2.21), which yields

$$\left(\mathbf{T}_{n-1}^*\right)_{ij} = \left(\mathbf{T}_n^{\mu\leftarrow\mathrm{M}^n}\right)_{ij} - y_j + \left(y_{n-1} - \frac{\overline{\mathrm{P}}}{F(z_n - z_{n-1})}\right)\delta_{(n-1)j} \quad \text{for } i,j < n. \tag{3.6}$$

Substituting eq.(3.4) into eq.(3.2), the desired MacInnes equation finally results,

$$\vec{i} - \rho_\mathrm{e}\vec{v}_m = -\frac{c_\mathrm{T} z_n F}{RT}\sum_{i\neq m}\frac{z_i}{z_n}\sum_{l=1}^{n-2}\sum_{j\neq n} H_{ij}^{mn}\left(\mathbf{T}_{n-1}^*\right)_{jl}\nabla\mathrm{M}_l^n - \kappa_{(n-1)}^{*m}\nabla\Phi \tag{3.7}$$

with the ionic conductivity relative to the two-ion reference state defined as

$$\kappa_{(n-1)}^{*m} = \frac{c_\mathrm{T}(z_n - z_{n-1})F^2}{RT}\sum_{i\neq m} z_i \sum_{j\neq n} H_{ij}^{mn}\left(\mathbf{T}_{n-1}^*\right)_{j(n-1)}. \tag{3.8}$$

The superscript m on κ indicates that the velocity of the species m is used for the reference velocity, while the subscript $(n-1)$ indicates the choice of the charging ion, and the superscript $*$ denotes that it is in the core-potential space.

3.1.2 Flux-explicit transport equations and transference number

In order to acquire an expression for the transference number, one of the driving forces in the flux-explicit transport equations must be replaced by the excess-charge flux,

$\vec{i} - \rho_e \vec{v}_m$. We start with the OSM equations as in Monroe and Delacourt [49],

$$-c_i \nabla \mu_i^n = \frac{RT}{c_T} \sum_{j \neq m} c_i R_{ij}^{nm} c_j (\vec{v}_j - \vec{v}_m) \quad \text{for all } i \neq n \tag{3.9}$$

where the matrix R_{ij}^{nm} encapsulates appropriately scaled Stefan–Maxwell diffusivities similar to $(\mathbf{H}^{mn})_{ij}^{-1}$ (refer to reference [49] for the exact form). What is now demanded is a transformation that converts the Smyrl–Newman chemical potential to the core potential. This is again achieved by combining the transformation in eq.(2.21), the Gibbs–Duhem relation in eq.(3.5), as well as the fact that $\mu_i^n = \mu_i - z_i \mu_n / z_n$ by definition. This produces

$$\nabla \mu_i^n = \sum_{j=1}^{n-1} \left(\mathbf{T}_{n-1}^{**} \right)_{ij} \nabla \mathrm{M}_j^n, \tag{3.10}$$

where

$$\begin{aligned} \left(\mathbf{T}_{n-1}^{**} \right)_{ij} = & \left(\mathbf{T}_n^{\mu \leftrightarrow \mathrm{M}^n} \right)_{ij} - \left(\mathbf{T}_n^{\mu \leftrightarrow \mathrm{M}^n} \right)_{i(n-1)} \delta_{(n-1)j} \\ & - \left(1 - \frac{z_i}{z_n} \right) \left[y_j - \left(y_j - \frac{\overline{\mathrm{P}}}{F(z_n - z_{n-1})} \right) \delta_{(n-1)j} \right] \quad \text{for } i, j < n. \end{aligned} \tag{3.11}$$

The flux equation is then obtained by firstly substituting eq.(3.10) into eq.(3.9) and replacing one of the driving forces (i.e., $-c_{n-1} \nabla \mathrm{M}_{n-1}^n$) with the excess-charge flux in eq.(3.1), followed by a matrix inversion process.

$$c_i (\vec{v}_i - \vec{v}_m) = - \sum_{j < n-1} X_{ij}^{mn} c_j \nabla \mathrm{M}_j^n + \frac{c_T z_n F X_{i(n-1)}^{mn}}{\kappa_{(n-1)}^{*m}} (\vec{i} - \rho_e \vec{v}_m) \tag{3.12}$$

Here, the matrix $\mathbf{X}^{mn}$ is the inverse of matrix $\mathbf{S}^{nm}$, i.e., $\mathbf{X}^{mn} = (\mathbf{S}^{nm})^{-1}$, where

$$\mathrm{S}_{ij}^{nm} = \begin{cases} \dfrac{RT}{c_T} c_i \displaystyle\sum_{j \neq m} \sum_{l=1}^{n-1} \left(\mathbf{T}_{n-1}^{**} \right)_{il}^{-1} R_{lj}^{nm} & \text{if } i < n-1 \\ \dfrac{c_T z_n z_j F^2}{\kappa_{(n-1)}^{*m}} & \text{if } i = n-1 \end{cases}. \tag{3.13}$$

A group of terms that accompanies $(\vec{i} - \rho_e \vec{v}_m)$ in eq.(3.12) is associated with the transference number of species i. Given that the transference number is unitless, it is defined as

$$t_i^{*m} = \frac{c_T z_n z_i F^2 X_{i(n-1)}^{mn}}{\kappa_{(n-1)}^{*m}}, \tag{3.14}$$

where the superscript m identifies the species that sets the reference velocity and $*$ denotes that it is a core-potential quantity.

This completes the theoretical manipulations necessary to work in the core-potential space. It is now time to delve into the application of the core-potential theory through the three nominated simple systems: (1) the binary electrolyte, (2) the three-ion ionic liquid, and (3) the binary salt in two neutral solvents.

3.2 Flux and MacInnes equations for the three cases

3.2.1 Case I. The binary electrolyte

A binary electrolyte dissolved in a neutral solvent —the simplest and thus most popular electrolytic solution for theoretical treatment— is studied in this section without the electroneutrality assumption. The anion (denoted by $-$) is used as the reference ion and serves to define the Smyrl–Newman chemical potential $\mu_i^- = \mu_i - z_i \mu_- / z_-$, whose gradient constitutes one of the driving forces in Monroe and Delacourt's flux equations and MacInnes equation [49]. It is noted that using the anion as the reference ion was an arbitrary decision Monroe and Delacourt [49] made and the cation would have been an equally valid choice. Nonetheless, the anion is kept as the reference ion in this section to facilitate the comparison of the derived equations in the core-potential space and those in Monroe and Delacourt [49].

As for the reference velocity, the velocity of the solvent (denoted by 0) is used, i.e., the frame of reference moves at the same velocity as the average solvent velocity. This is a conventional choice in concentrated-solution theory [22] because the solvent is usually the species in excess and is thought to attain a negligible average velocity (in

which case simplifies the flux and MacInnes equations) relative to the lab frame. The same simplifications result in core-potential theory, so we adhere to the convention. Also note that because core-potential theory requires two ions to define the electrical reference state, the solvent is the only species remaining for the reference velocity. Therefore, following the ordering convention used by Monroe and Delacourt [49], the species indices in this system are ordered as $\{0, +, -\}$; the species that sets the reference velocity is placed at the beginning of the list, while the reference ion is placed at the end, with the penultimate species being the charging ion, whose charge must generally oppose the reference ion.

With the appropriately established references, one can go through the procedure in Monroe and Delacourt [49] and arrive at the following flux-explicit transport equations for the two ions (corresponding to equations (55) and (56) in [49]).

$$c_+(\vec{v}_+ - \vec{v}_0) = -\frac{c_\mathrm{T} z_- \mathscr{D}}{RT(z_+ - z_-)}\nabla\mu_0^- + \frac{t_+^0}{Fz_+}(\vec{i} - \rho_\mathrm{e}\vec{v}_0) \tag{3.15}$$

$$c_-(\vec{v}_- - \vec{v}_0) = \frac{c_\mathrm{T} z_+ \mathscr{D}}{RT(z_+ - z_-)}\nabla\mu_0^- + \frac{1 - t_+^0}{Fz_-}(\vec{i} - \rho_\mathrm{e}\vec{v}_0) \tag{3.16}$$

Note that $\nabla\mu_0^- = \nabla\mu_0 = -y\nabla\mu_\mathrm{e}/y_0$ through the Gibbs–Duhem relation when electroneutrality is assumed. The MacInnes equation can also be derived (corresponding to equations (45) and (57) in [49], respectively).

$$\vec{i} - \rho_\mathrm{e}\vec{v}_0 = -\frac{\kappa_+^0}{Fz_-}\nabla\mu_- + \frac{\mathscr{D}_{0+}(Fz_+c_0\mathscr{D}_{+-} + \rho_\mathrm{e}\mathscr{D}_{0-})c_\mathrm{T}}{(c_-\mathscr{D}_{0+} + c_+\mathscr{D}_{0-} + c_0\mathscr{D}_{+-})RT}\nabla\mu_0^- \tag{3.17}$$

$$\vec{i} - \rho_\mathrm{e}\vec{v}_0 = -\frac{\kappa_+^0}{Fz_-}\nabla\mu_- + \frac{\kappa_+^0 t_+^0 c_0}{Fz_+c_+ - \rho_\mathrm{e}t_+^0} \times \left[1 - \frac{Fz_+z_-\mathscr{D}c_\mathrm{T}}{RT(z_+ - z_-)\kappa_+^0 t_+^0 c_0}\rho_\mathrm{e}\right]\nabla\mu_0^- \tag{3.18}$$

In fact, the two equations are equivalent; eq.(3.17) is expressed in terms of Stefan–Maxwell diffusivities and eq.(3.18) is cast in terms of macroscopic transport properties. It is evident that the transport and MacInnes equations afford three transport properties: the thermodynamic diffusivity $\mathscr{D}$, the cation transference number t_+^0, and the ionic conductivity κ_+^0, which are all in agreement with those defined by Monroe and

Delacourt [49].

$$\begin{aligned}\mathscr{D} &= \frac{(z_+ - z_-)\mathscr{D}_{0+}\mathscr{D}_{0-}}{z_+\mathscr{D}_{0+} - z_-\mathscr{D}_{0-}} \qquad t_+^0 = \frac{z_+\mathscr{D}_{0+}}{z_+\mathscr{D}_{0+} - z_-\mathscr{D}_{0-}} \\ \kappa_+^0 &= -\frac{F^2 z_- c_- c_{\mathrm{T}} \mathscr{D}_{+-}}{RT} \frac{z_+\mathscr{D}_{0+} - z_-\mathscr{D}_{0-}}{c_-\mathscr{D}_{0+} + c_+\mathscr{D}_{0-} + c_0\mathscr{D}_{+-}}\end{aligned} \tag{3.19}$$

It is noted that the flux equations inverted from the OSM equations only naturally contain Stefan–Maxwell diffusivities as phenomenological coefficients and one has to identify manually what different groups of Stefan–Maxwell diffusivities (along with concentrations and equivalent charges) represent macroscopically. Dimensional analysis is central to this process.

The flux and MacInnes equations can also be written with core potentials, following the modified procedures outlined in the previous section.

$$c_+(\vec{v}_+ - \vec{v}_0) = -\frac{c_{\mathrm{T}} z_- \mathscr{D}^*}{RT(z_+ - z_-)}\nabla \mathrm{M}_0^- + \frac{t_+^{*0}}{F z_+}(\vec{i} - \rho_{\mathrm{e}}\vec{v}_0) \tag{3.20}$$

$$c_-(\vec{v}_- - \vec{v}_0) = \frac{c_{\mathrm{T}} z_+ \mathscr{D}^*}{RT(z_+ - z_-)}\nabla \mathrm{M}_0^- + \frac{1 - t_+^{*0}}{F z_-}(\vec{i} - \rho_{\mathrm{e}}\vec{v}_0) \tag{3.21}$$

$$\vec{i} - \rho_{\mathrm{e}}\vec{v}_0 = \frac{(c_+ + c_-)\mathscr{D}_{0+}\mathscr{D}_{0-}\rho_{\mathrm{e}} + c_0 F \mathscr{D}_{+-}(c_+ z_+ \mathscr{D}_{0+} + c_- z_- \mathscr{D}_{0-})}{RT(c_-\mathscr{D}_{0+} + c_+\mathscr{D}_{0-} + c_0\mathscr{D}_{+-})}\nabla \mathrm{M}_0^- - \kappa_+^{*0}\nabla\Phi \tag{3.22}$$

The new transport properties are defined as

$$\begin{aligned}\mathscr{D}^* &= \left(1 + \frac{c_0 z_- F}{\rho_{\mathrm{e}} - c_{\mathrm{T}} z_- F}\right) \frac{c_-(z_+ - z_-)F\mathscr{D}_{0+}\mathscr{D}_{0-}\mathscr{D}_{+-}}{\alpha_-^0\mathscr{D}_{0+}\mathscr{D}_{0-}\rho_{\mathrm{e}} - F\mathscr{D}_{+-}\left\{\alpha_-^+ c_+ z_+ \mathscr{D}_{0+} + c_- z_- \mathscr{D}_{0-}\right\}} \\ t_+^{*0} &= \frac{c_+ z_+ F \mathscr{D}_{0+}\left(\alpha_-^0\mathscr{D}_{0-} - \alpha_-^+\mathscr{D}_{+-}\right)}{\alpha_-^0\mathscr{D}_{0+}\mathscr{D}_{0-}\rho_{\mathrm{e}} - F\mathscr{D}_{+-}\left\{\alpha_-^+ c_+ z_+ \mathscr{D}_{0+} + c_- z_- \mathscr{D}_{0-}\right\}} \\ \kappa_+^{*0} &= \frac{\rho_{\mathrm{e}} - c_{\mathrm{T}} z_- F}{RT} \times \frac{\alpha_-^0\mathscr{D}_{0+}\mathscr{D}_{0-}\rho_{\mathrm{e}} - F\mathscr{D}_{+-}\left\{\alpha_-^+ c_+ z_+ \mathscr{D}_{0+} - (\alpha_-^0 c_0 + \alpha_-^+ c_+) z_- \mathscr{D}_{0-}\right\}}{c_-\mathscr{D}_{0+} + c_+\mathscr{D}_{0-} + c_0\mathscr{D}_{+-}}\end{aligned}, \tag{3.23}$$

where the superscript $*$ indicates the association with the core-potential space and

$$\alpha_-^0 = \frac{\rho_\mathrm{e}}{\rho_\mathrm{e} - c_\mathrm{T} z_- F} \qquad \text{and} \qquad \alpha_-^+ = \frac{\rho_\mathrm{e} - c_\mathrm{T} z_+ F}{\rho_\mathrm{e} - c_\mathrm{T} z_- F} \tag{3.24}$$

define two quantities dependent on the molar excess charge $\overline{\mathrm{P}} = \rho_\mathrm{e}/c_\mathrm{T}$. The full exposition of the ρ_e-dependence in the above expressions can be realised by making use of Faraday's law ($\rho_\mathrm{e} = F\sum c_i z_i$), but it is omitted here for notational compactness.

Although the relationships between the transport properties of the Smyrl–Newman and core-potential constructs are convoluted for non-electroneutral systems, electroneutrality simplifies them substantially. Firstly, using the notation $\Theta\big|_{\rho_\mathrm{e}=0}$ to mean the value of any parameter Θ evaluated under electroneutrality, it is found that $\mathscr{D}^*\big|_{\rho_\mathrm{e}=0} = (1-y_0)\mathscr{D}\big|_{\rho_\mathrm{e}=0}$, where $(1-y_0) = (c_\mathrm{T} - c_0)/c_\mathrm{T} = (c_+ + c_-)/c_\mathrm{T}$. The occurrence of this factor is natural, since $\nabla\mu_0^- = \nabla(\mathrm{M}_0^- + \mathrm{M}_-^-) = (1-y_0)\nabla\mathrm{M}_0^- - \overline{\mathrm{P}}\nabla\Phi$. In a way, it demonstrates a benefit of using the core potential, because the diffusion term in the flux equations is automatically made proportional to the concentration of the diffusing component, i.e., the salt as a whole. For the electrical transport properties, one obtains $t_+^{*0}\big|_{\rho_\mathrm{e}=0} = t_+^0\big|_{\rho_\mathrm{e}=0}$ and $\kappa_+^{*0}\big|_{\rho_\mathrm{e}=0} = \kappa_+^0\big|_{\rho_\mathrm{e}=0}$, as expected.

The Stefan–Maxwell diffusivities can be expressed in terms of the core-potential transport properties by simple rearrangement of expressions in eq.(3.23), such that

$$\begin{aligned}
\frac{1}{\mathscr{D}_{+-}} &= -\frac{c_0 z_- F(z_- - z_+)}{t_+^{*0}(z_- - z_+)\rho_\mathrm{e} + (\rho_\mathrm{e} - c_\mathrm{T} z_- F) z_+} \\
&\qquad \times \left[\frac{(z_- - z_+)(1 - t_+^{*0}) t_+^{*0}}{z_- \mathscr{D}^*} - \frac{z_+(\rho_\mathrm{e} - c_\mathrm{T} z_+ F)(\rho_\mathrm{e} - c_\mathrm{T} z_- F)}{c_0 RT(z_- - z_+)\kappa_+^{*0}}\right] \\
\frac{1}{\mathscr{D}_{0+}} &= -\frac{F(\beta^- t_+^{*0} c_0 + c_+)(z_- - z_+)^2}{(\rho_\mathrm{e} - c_\mathrm{T} z_- F) z_-} \times \frac{1 - t_+^{*0}}{\mathscr{D}^*} + \frac{F z_-(\rho_\mathrm{e} - c_\mathrm{T} z_+ F)}{RT\kappa_+^{*0}}\beta^+ \\
\frac{1}{\mathscr{D}_{0-}} &= -\frac{F(\beta^+(1 - t_+^{*0}) c_0 + c_-)(z_- - z_+)^2}{(\rho_\mathrm{e} - c_\mathrm{T} z_+ F) z_+} \times \frac{t_+^{*0}}{\mathscr{D}^*} + \frac{F z_+(\rho_\mathrm{e} - c_\mathrm{T} z_- F)}{RT\kappa_+^{*0}}\beta^-
\end{aligned} \tag{3.25}$$

where β^+ and β^- are proportional to the excess charge density and are defined as

$$\begin{aligned}\beta^+ &= \frac{\rho_e z_+}{t_+^{*0}(z_- - z_+)\rho_e + (\rho_e - c_T z_- F)z_+} \\ \beta^- &= \frac{\rho_e z_-}{t_+^{*0}(z_- - z_+)\rho_e + (\rho_e - c_T z_- F)z_+}\end{aligned} \quad . \tag{3.26}$$

These expressions can be inserted back into eq.(3.22) to write the MacInnes equation in terms of the measurable transport properties only.

3.2.2 Case II. The three-ion ionic liquid

Unlike the binary electrolyte, the three-ion ionic liquid comprises ions only and a neutral solvent in excess is absent from the system. Its negligibly low volatility and non-flammability, as well as a wide electrochemical stability window, have sparked interest in the scientific community as a potential electrolyte material in energy storage systems, but its high cost and viscosity (which induces poor transport properties) prevent a widespread commercial use at the moment [155]. For example, sodium bis(fluorosulfonyl)amide – potassium bis(fluorosulfonyl)amide (NaFSA–KFSA) eutectic mixture has been suggested for the sodium-battery electrolyte [152], potassium bis(flu-orosulfonyl)imide (KFSI) in *N*-butyl-*N*-methyl-pyrrolidinium FSI ($Pyr_{13}FSI$) for the potassium-ion battery [153], and lithium FSI (LiFSI) in $Pyr_{13}FSI$ for the next-generation Li-ion battery [154]. The aforementioned ionic liquids are all three-component systems containing two cations and a shared anion. Therefore, we look at the same type of ionic liquid in this section; the two cations are denoted by $+1$ and $+2$ and the anion by $-$.

Since the reference and charging ions must be of opposite charge, four distinct cases arise, namely $\{+1, +2, -\}$, $\{+1, -, +2\}$, $\{+2, +1, -\}$, and $\{+2, -, +1\}$, following the ordering convention adopted by Monroe and Delacourt [49]. For the illustrative purpose without repetition, only the first case $\{+1, +2, -\}$ is elaborated here, where the reference velocity is the average velocity of $+1$ and the reference ion is $-$ (but other

choices are valid, as enunciated previously). Repeating the procedure of Monroe and Delacourt [49] as before, the flux-explicit transport equations look identical to those in the binary-electrolyte case.

$$c_{+2}(\vec{v}_{+2} - \vec{v}_{+1}) = -\frac{c_{\mathrm{T}} z_- \mathscr{D}}{RT(z_{+2} - z_-)} \nabla \mu^-_{+1} + \frac{t^{+1}_{+2}}{F z_{+2}} (\vec{i} - \rho_{\mathrm{e}} \vec{v}_{+1}) \tag{3.27}$$

$$c_-(\vec{v}_- - \vec{v}_{+1}) = \frac{c_{\mathrm{T}} z_{+2} \mathscr{D}}{RT(z_{+2} - z_-)} \nabla \mu^-_{+1} + \frac{1 - t^{+1}_{+2}}{F z_-} (\vec{i} - \rho_{\mathrm{e}} \vec{v}_{+1}) \tag{3.28}$$

Defining Θ to represent a group of terms

$$\Theta = \frac{(c_- z_- + c_{+2} z_{+2}) z_{+1}}{\mathscr{D}_{+2-}} + \frac{(\rho_{\mathrm{e}}/F - c_{+2} z_{+2}) z_{+2}}{\mathscr{D}_{+1-}} - \frac{c_- z_-^2}{\mathscr{D}_{+1+2}}, \tag{3.29}$$

the three transport properties can be written more succinctly as

$$\begin{aligned} \mathscr{D} &= \frac{c_- z_- (z_{+2} - z_-)}{\Theta} \\ t^{+1}_{+2} &= \left\{ \frac{c_{+2} z_{+1}}{\mathscr{D}_{+2-}} + \frac{\rho_{\mathrm{e}}/F - c_{+2} z_{+2}}{\mathscr{D}_{+1-}} \right\} \frac{z_{+2}}{\Theta} \\ \frac{1}{\kappa^{+1}_{+2}} &= -\frac{RT}{c_{\mathrm{T}} F^2 \Theta} \times \left(\frac{c_-}{\mathscr{D}_{+1-}\mathscr{D}_{+2-}} + \frac{c_{+2}}{\mathscr{D}_{+1+2}\mathscr{D}_{+2-}} + \frac{c_{+1}}{\mathscr{D}_{+1+2}\mathscr{D}_{+1-}} \right) \end{aligned} \quad . \tag{3.30}$$

Note that $\mathscr{D}$ is interpreted as the diffusivity of the pair $(+2, -)$ through $+1$. The MacInnes equation in this case is

$$\vec{i} - \rho_{\mathrm{e}} \vec{v}_{+1} = \frac{c_{\mathrm{T}} F}{RT} \times \frac{\frac{c_{+2} z_{+2} + c_- z_-}{\mathscr{D}_{+2-}} + \frac{c_{+1} z_{+2}}{\mathscr{D}_{+1-}}}{\frac{c_-}{\mathscr{D}_{+1-}\mathscr{D}_{+2-}} + \frac{c_{+2}}{\mathscr{D}_{+1+2}\mathscr{D}_{+2-}} + \frac{c_{+1}}{\mathscr{D}_{+1+2}\mathscr{D}_{+1-}}} \nabla \mu^-_{+1} - \frac{\kappa^{+1}_{+2}}{F z_-} \nabla \mu_-. \tag{3.31}$$

The flux and MacInnes equations in the core-potential space become

$$c_{+2}(\vec{v}_{+2}-\vec{v}_{+1}) = -\frac{c_{\mathrm{T}} z_- \mathscr{D}^*}{RT(z_{+2}-z_-)}\nabla \mathrm{M}^-_{+1} + \frac{t^{*+1}_{+2}}{F z_{+2}}(\vec{i}-\rho_{\mathrm{e}}\vec{v}_{+1}) \tag{3.32}$$

$$c_-(\vec{v}_- - \vec{v}_{+1}) = \frac{c_{\mathrm{T}} z_{+2} \mathscr{D}^*}{RT(z_{+2}-z_-)}\nabla \mathrm{M}^-_{+1} + \frac{1-t^{*+1}_{+2}}{F z_-}(\vec{i}-\rho_{\mathrm{e}}\vec{v}_{+1}) \tag{3.33}$$

$$\vec{i}-\rho_{\mathrm{e}}\vec{v}_{+1} = \frac{F}{RT}\frac{\frac{(c_{+2}+c_-)(c_{+2}z_{+2}+c_-z_-)}{\mathscr{D}_{+2-}} + \frac{c_{+1}c_{+2}z_{+2}}{\mathscr{D}_{+1-}} + \frac{c_{+1}c_-z_-}{\mathscr{D}_{+1+2}}}{\frac{c_-}{\mathscr{D}_{+1-}\mathscr{D}_{+2-}} + \frac{c_{+2}}{\mathscr{D}_{+1+2}\mathscr{D}_{+2-}} + \frac{c_{+1}}{\mathscr{D}_{+1+2}\mathscr{D}_{+1-}}}\nabla \mathrm{M}^-_{+1} - \kappa^{*+1}_{+2}\nabla\Phi. \tag{3.34}$$

They involve the following three transport properties

$$\begin{gathered}
\mathscr{D}^* = \frac{c_{+2}(z_{+2}-z_-)F}{\rho_{\mathrm{e}}-c_{\mathrm{T}}z_-F} \times \frac{c_-(z_{+2}-z_-)}{\Theta^*} \\
t^{*+1}_{+2} = \left(\frac{\alpha^{+1}_-}{\mathscr{D}_{+2-}} - \frac{\alpha^{+2}_-}{\mathscr{D}_{+1-}}\right)\frac{c_{+2}z_{+2}}{\Theta^*} \qquad , \\
\frac{1}{\kappa^{*+1}_{+2}} = \frac{RT}{(\rho_{\mathrm{e}}-c_{\mathrm{T}}z_-F)\,\Theta^*} \times \left(\frac{c_-}{\mathscr{D}_{+1-}\mathscr{D}_{+2-}} + \frac{c_{+2}}{\mathscr{D}_{+1+2}\mathscr{D}_{+2-}} + \frac{c_{+1}}{\mathscr{D}_{+1+2}\mathscr{D}_{+1-}}\right)
\end{gathered} \tag{3.35}$$

where

$$\begin{gathered}
\alpha^{+1}_- = \frac{\rho_{\mathrm{e}}-c_{\mathrm{T}}z_{+1}F}{\rho_{\mathrm{e}}-c_{\mathrm{T}}z_-F} \qquad \alpha^{+2}_- = \frac{\rho_{\mathrm{e}}-c_{\mathrm{T}}z_{+2}F}{\rho_{\mathrm{e}}-c_{\mathrm{T}}z_-F} \\
\Theta^* = \frac{\alpha^{+1}_-(c_{+2}z_{+2}+c_-z_-)}{\mathscr{D}_{+2-}} - \frac{\alpha^{+2}_- c_{+2}z_{+2}}{\mathscr{D}_{+2-}} + \frac{c_-z_-}{\mathscr{D}_{+1+2}}
\end{gathered} \tag{3.36}$$

Again, $\rho_{\mathrm{e}} = F\sum c_i z_i$ can be used to eliminate one of the species concentrations, making the ρ_{e}-dependence explicit if need be.

Upon assuming electroneutrality, the relations $t^{*+1}_-\big|_{\rho_{\mathrm{e}}=0} = t^{+1}_-\big|_{\rho_{\mathrm{e}}=0}$ and $\kappa^{*+1}_{+2}\big|_{\rho_{\mathrm{e}}=0} = \kappa^{+1}_{+2}\big|_{\rho_{\mathrm{e}}=0}$ are observed for electrical properties, as expected. For the diffusivity, a prefactor complements the Smyrl–Newman diffusivity to produce the core-potential diffusivity, as shown below.

$$\mathscr{D}^*\big|_{\rho_{\mathrm{e}}=0} = \left[1-\left(1-\frac{z_{+1}}{z_-}\right)y_{+1}\right]\mathscr{D}\big|_{\rho_{\mathrm{e}}=0} \tag{3.37}$$

This makes sense because the same factor appears in the transformation between the two chemical-potential formalisms, i.e.,

$\nabla\mu^{-}_{+1} = \left[1-\left(1-\frac{z_{+1}}{z_{-}}\right)y_{+1}\right]\nabla \mathrm{M}^{-}_{+1} - \left(1-\frac{z_{+1}}{z_{-}}\right)\overline{\mathrm{P}}\nabla\Phi$. Rearranging expressions in eq.(3.35) allows one to write the binary Stefan–Maxwell diffusivities in terms of the core-potential transport properties

$$\begin{aligned}
\frac{1}{\mathscr{D}_{+2-}} &= -\frac{c_{+1}z_{-}F(z_{-}-z_{+2})}{t^{*+1}_{+2}(z_{-}-z_{+2})\rho_{\mathrm{e}}+(\rho_{\mathrm{e}}-c_{\mathrm{T}}z_{-}F)z_{+2}} \\
&\quad\times\left[\frac{(z_{-}-z_{+2})(1-t^{*+1}_{+2})t^{*+1}_{+2}}{z_{-}\mathscr{D}^{*}}-\frac{z_{+2}(\rho_{\mathrm{e}}-c_{\mathrm{T}}z_{+2}F)(\rho_{\mathrm{e}}-c_{\mathrm{T}}z_{-}F)}{c_{+1}(z_{-}-z_{+2})RT\kappa^{*+1}_{+2}}\right] \\
\frac{1}{\mathscr{D}_{+1+2}} &= -\frac{F(\beta^{-}t^{*+1}_{+2}c_{+1}+c_{+2})(z_{-}-z_{+2})^{2}}{(\rho_{\mathrm{e}}-c_{\mathrm{T}}z_{-}F)z_{-}}\times\frac{1-t^{*+1}_{+2}}{\mathscr{D}^{*}}+\frac{z_{-}F(\rho_{\mathrm{e}}-c_{\mathrm{T}}z_{+2}F)}{RT\kappa^{*+1}_{+2}}\beta^{+2} \\
\frac{1}{\mathscr{D}_{+1-}} &= -\frac{F(\beta^{+2}(1-t^{*+1}_{+2})c_{+1}+c_{-})(z_{-}-z_{+2})^{2}}{(\rho_{\mathrm{e}}-c_{\mathrm{T}}z_{+2}F)z_{+2}}\times\frac{t^{*+1}_{+2}}{\mathscr{D}^{*}}+\frac{z_{+2}F(\rho_{\mathrm{e}}-c_{\mathrm{T}}z_{-}F)}{RT\kappa^{*+1}_{+2}}\beta^{-}
\end{aligned} \tag{3.38}$$

where

$$\begin{aligned}
\beta^{+2} &= \frac{(\rho_{\mathrm{e}}-c_{\mathrm{T}}z_{+1}F)z_{+2}}{t^{*+1}_{+2}(z_{-}-z_{+2})\rho_{\mathrm{e}}+(\rho_{\mathrm{e}}-c_{\mathrm{T}}z_{-}F)z_{+2}} \\
\beta^{-} &= \frac{(\rho_{\mathrm{e}}-c_{\mathrm{T}}z_{+1}F)z_{-}}{t^{*+1}_{+2}(z_{-}-z_{+2})\rho_{\mathrm{e}}+(\rho_{\mathrm{e}}-c_{\mathrm{T}}z_{-}F)z_{+2}}
\end{aligned} \tag{3.39}$$

It should be noted that the assignment of the charging and reference ions is for theoretical convenience only; thus, macroscopic transport-property expressions must remain invariant when the designations for the two ions are swapped. This means that the ionic conductivities and transference numbers for the systems $\{+1,+2,-\}$ and $\{+1,-,+2\}$ must be equal because all of the current is carried by $+2$ and $-$ ions in both cases. This is indeed true in the core-potential theory, i.e., $\kappa^{*+1}_{+2}=\kappa^{*+1}_{-}$ and t^{*+1}_{-} in $\{+1,+2,-\}=t^{*+1}_{-}$ in $\{+1,-,+2\}$. Interestingly, the ionic conductivity defined using the quasi-electrostatic potential in the Smyrl–Newman formalism fails to satisfy this relationship. Instead, it embodies an invariance with respect to the reference species, i.e., $\kappa^{+1}_{+2}=\kappa^{+2}_{+1}$, which indicates that the two salts $\{+2,-\}$ and $\{+1,-\}$ must have the same propensity for conduction in the three-ion ionic liquid. It is easy to see that this statement does not have to hold in general. This counterintuitive characteristic is inherent to the Smyrl–Newman construct and was noticed by Smyrl and Newman [50], as well. By employing the core-potential formalism, the structural inconsistency

Smyrl and Newman [50] failed to rectify is naturally resolved.

One may question the applicability and relevance of the flux and MacInnes equations presented in this section because aggregates are expected to form as a result of strong electrostatic interactions between oppositely charged ionic species. That is, one may ask whether the three-species treatment of the system can describe species fluxes accurately, when in fact more than three species exist at the molecular level. Precisely because this thesis contends with macroscopic models, this question is not an impediment to the model construction and usage; the beauty of thermodynamics is that macroscopic observables suffice to describe a given system, without having to worry about microscopic details. For example, different solvation structures form even for salts in neutral solvents, (e.g., von Cresce and Xu [156] demonstrated this using lithium hexafluorophosphate ($LiPF_6$) in 1:0, 7:3, and 1:1 mixture of ethyl methyl carbonate (EMC) and ethylene carbonate (EC) by weight), but their individual contributions are not treated separately in standard models based on Newman's concentrated-solution theory. Not only is the concentration of individual microscopic entities difficult to ascertain, but one understands that their effects are collectively summed up in macroscopic properties such as thermodynamic diffusivity, transference number, ionic conductivity, and thermodynamic factor. The fact that species fluxes are driven by electrochemical-potential gradients and convection remains valid whether the system contains a neutral solvent or not. Therefore, there seems to be no logical basis on which to reject the macroscopic treatment provided in this section for delineating transport phenomena in the three-ion ionic liquid.

3.2.3 Case III. The binary salt in two neutral solvents

This section deals with a four-species system that contains a binary salt dissolved in two neutral solvents, denoted by 0 and o. While the reference velocity is still measured with respect to the species 0, the cation is taken to be the reference ion for easy comparison with the results of Monroe [157], i.e., the species are arranged

as $\{0, \mathrm{o}, -, +\}$ under the usual ordering convention. For convenience, notations for macroscopic transport properties in the binary electrolyte system are employed, as done by Monroe [157]. That is, $\mathscr{D}_{\mathrm{e}0}$, $t^0_{+\emptyset}$, and $\kappa_\emptyset$ respectively represent the diffusivity, the cation transference number, and the ionic conductivity for the three-species system $\{0, -, +\}$. This reduced system does not contain the second solvent o, so the transport properties are as defined in eq.(3.19) (note that c_T in the ionic conductivity expression must be replaced by $c_0 + c_+ + c_-$). Similarly, $\mathscr{D}_{\mathrm{eo}}$ and $t^{\mathrm{o}}_{+\emptyset}$ are for the system $\{\mathrm{o}, -, +\}$ that does not contain the first solvent 0. It is emphasised that introducing these binary-electrolyte macroscopic transport properties is for notational compactness only and does not impose any restrictions on the use of the equations that will be derived.

Applying the procedure of Monroe and Delacourt [49] as before, the following flux equations are obtained.

$$c_\mathrm{o}(\vec{v}_\mathrm{o} - \vec{v}_0) = \frac{c_\mathrm{o}}{RT}\left(\mathscr{X}_{0\mathrm{o}}\nabla\mu_0^+ - \mathscr{D}_\mathrm{o}\nabla\mu_\mathrm{o}^+\right) + \frac{(z_- - z_+)\Xi}{z_+ z_- F}(\vec{i} - \rho_\mathrm{e}\vec{v}_0) \tag{3.40}$$

$$c_-(\vec{v}_- - \vec{v}_0) = -\frac{c_\mathrm{T} z_+}{RT(z_- - z_+)}\left(\mathscr{D}_0\nabla\mu_0^+ + \frac{c_\mathrm{o}\mathscr{D}_{\mathrm{eo}}\mathscr{X}_{0\mathrm{o}}}{c_\mathrm{T}\mathscr{D}_{\mathrm{o}0}}\nabla\mu_\mathrm{o}^+\right) + \frac{1 - t^0_+}{F z_-}(\vec{i} - \rho_\mathrm{e}\vec{v}_0) \tag{3.41}$$

$$c_+(\vec{v}_+ - \vec{v}_0) = \frac{c_\mathrm{T} z_-}{RT(z_- - z_+)}\left(\mathscr{D}_0\nabla\mu_0^+ + \frac{c_\mathrm{o}\mathscr{D}_{\mathrm{eo}}\mathscr{X}_{0\mathrm{o}}}{c_\mathrm{T}\mathscr{D}_{\mathrm{o}0}}\nabla\mu_\mathrm{o}^+\right) + \frac{t^0_+}{F z_+}(\vec{i} - \rho_\mathrm{e}\vec{v}_0) \tag{3.42}$$

The MacInnes equation is

$$\vec{i} - \rho_\mathrm{e}\vec{v}_0 = -\frac{c_\mathrm{T} z_+ F\kappa^0_-}{RT}\left(A_0 c_0\nabla\mu_0^+ + A_\mathrm{o} c_\mathrm{o}\nabla\mu_\mathrm{o}^+\right) - \frac{\kappa^0_-}{z_+ F}\nabla\mu_+, \tag{3.43}$$

where

$$
\begin{aligned}
A_0 =& \frac{1}{\rho_\mathrm{e} t^0_{+\emptyset} - c_+ z_+ F}\left[\left(1-\frac{c_\mathrm{o}}{c_\mathrm{T}}\right)\left(1-\frac{\rho_\mathrm{e}}{c_+ z_+ F}\right)\frac{z_-}{z_- - z_+}\frac{\rho_\mathrm{e}\mathscr{D}_0}{c_0\kappa_\emptyset}\right.\\
&-\frac{RT}{c_\mathrm{T} z_+ F}\times\left\{\left(1-t^0_{+\emptyset}\right)\frac{\mathscr{D}_0}{\mathscr{D}_{\mathrm{e}0}}\right.\\
&\left.\left.-\left(1-t^\mathrm{o}_{+\emptyset}\right)\left(1-\frac{\rho_\mathrm{e}}{c_+ z_+ F}t^0_{+\emptyset}\right)\left(\frac{\rho_\mathrm{e}(z_- - z_+)}{c_0 z_+ z_- F}\frac{t^\mathrm{o}_{+\emptyset}}{\mathscr{D}_\mathrm{eo}}-\frac{1}{\mathscr{D}_{\mathrm{o}0}}\right)\frac{c_\mathrm{o}}{c_\mathrm{T}}\mathscr{X}_{0\mathrm{o}}\right\}\right]\\
A_\mathrm{o} =& \frac{1}{\rho_\mathrm{e} t^0_{+\emptyset} - c_+ z_+ F}\left[\left(1-\frac{c_\mathrm{o}}{c_\mathrm{T}}\right)\left(1-\frac{\rho_\mathrm{e}}{c_+ z_+ F}\right)\frac{z_-}{z_- - z_+}\frac{\mathscr{X}_{0\mathrm{o}}\mathscr{D}_\mathrm{eo}}{c_\mathrm{T}\mathscr{D}_{\mathrm{o}0}\kappa_\emptyset}\right.\\
&-\frac{RT}{c_\mathrm{T} z_+ F}\times\left\{\left(1-t^0_{+\emptyset}\right)\frac{c_0\mathscr{D}_\mathrm{o}}{c_\mathrm{T}\mathscr{D}_{\mathrm{o}0}}\right.\\
&\left.\left.+\left(1-t^\mathrm{o}_{+\emptyset}\right)\left(1-\frac{\rho_\mathrm{e}}{c_+ z_+ F}t^0_{+\emptyset}\right)\left(\frac{c_+(z_- - z_+)}{c_\mathrm{o} z_-}\frac{1}{\mathscr{D}_{\mathrm{e}0}}+\frac{1}{\mathscr{D}_{\mathrm{o}0}}\right)\frac{c_\mathrm{o}}{c_\mathrm{T}}\mathscr{X}_{0\mathrm{o}}\right\}\right]
\end{aligned}
\quad . \tag{3.44}
$$

From these equations, six macroscopic transport properties arise. As demonstrated before, each property can be expressed in terms of Stefan–Maxwell diffusivities (as well as concentrations and equivalent charges) with the help of dimensional analysis on the inverted OSM equations. Their functional forms are given below, along with the Taylor expanded expressions centred around $\rho_\mathrm{e} = 0$ for easy comparison with their electroneutral counterparts.

Thermodynamic diffusivity for the first solvent 0:

$$
\begin{aligned}
\mathscr{D}_0 =& \frac{\mathscr{D}_{\mathrm{e}0}\left[c_0\mathscr{D}_\mathrm{eo}+c_+\frac{z_- - z_+}{z_-}\left(1-\frac{\rho_\mathrm{e}}{c_+ z_+ F}t^\mathrm{o}_{+\emptyset}\right)\mathscr{D}_{\mathrm{o}0}\right]}{c_0\mathscr{D}_\mathrm{eo}+c_+\frac{z_- - z_+}{z_-}\left(1-\frac{\rho_\mathrm{e}}{c_+ z_+ F}t^\mathrm{o}_{+\emptyset}\right)\mathscr{D}_{\mathrm{o}0}+c_\mathrm{o}\mathscr{D}_{\mathrm{e}0}}\\
=& \frac{\mathscr{D}_{\mathrm{e}0}\left[c_0\mathscr{D}_\mathrm{eo}+c_+\frac{z_- - z_+}{z_-}\mathscr{D}_{\mathrm{o}0}\right]}{c_0\mathscr{D}_\mathrm{eo}+c_+\frac{z_- - z_+}{z_-}\mathscr{D}_{\mathrm{o}0}+c_\mathrm{o}\mathscr{D}_{\mathrm{e}0}} - \frac{(z_- - z_+)c_\mathrm{o}\mathscr{D}^2_{\mathrm{e}0}\mathscr{D}_{\mathrm{o}0}t^\mathrm{o}_{+\emptyset}\rho_\mathrm{e}}{z_+ z_- F\left(c_0\mathscr{D}_\mathrm{eo}+c_+\frac{z_- - z_+}{z_-}\mathscr{D}_{\mathrm{o}0}+c_\mathrm{o}\mathscr{D}_{\mathrm{e}0}\right)^2}\\
&+O(\rho^2_\mathrm{e})
\end{aligned}
\tag{3.45}
$$

Thermodynamic diffusivity for the second solvent o:

$$\begin{aligned}\mathscr{D}_{\mathrm{o}} =& \frac{c_{\mathrm{T}}\mathscr{D}_{\mathrm{eo}}\mathscr{D}_{\mathrm{o0}}}{c_0\mathscr{D}_{\mathrm{eo}} + c_+\frac{z_- - z_+}{z_-}\left(1 - \frac{\rho_{\mathrm{e}}}{c_+ z_+ F}t^{\mathrm{o}}_{+\not\emptyset}\right)\mathscr{D}_{\mathrm{o0}} + c_{\mathrm{o}}\mathscr{D}_{\mathrm{e0}}} \\ =& \frac{c_{\mathrm{T}}\mathscr{D}_{\mathrm{eo}}\mathscr{D}_{\mathrm{o0}}}{c_0\mathscr{D}_{\mathrm{eo}} + c_+\frac{z_- - z_+}{z_-}\mathscr{D}_{\mathrm{o0}} + c_{\mathrm{o}}\mathscr{D}_{\mathrm{e0}}}\left(1 + \frac{(z_- - z_+)t^{\mathrm{o}}_{+\not\emptyset}\mathscr{D}_{\mathrm{o0}}\rho_{\mathrm{e}}}{z_+ z_- F\left(c_0\mathscr{D}_{\mathrm{eo}} + c_+\frac{z_- - z_+}{z_-}\mathscr{D}_{\mathrm{o0}} + c_{\mathrm{o}}\mathscr{D}_{\mathrm{e0}}\right)}\right) \\ &+ O(\rho_{\mathrm{e}}^2)\end{aligned} \tag{3.46}$$

Cation transference number:

$$\begin{aligned}t^0_+ =& \frac{\left[c_0\mathscr{D}_{\mathrm{eo}} + c_+\frac{z_- - z_+}{z_-}\left(1 - \frac{\rho_{\mathrm{e}}}{c_+ z_+ F}t^{\mathrm{o}}_{+\not\emptyset}\right)\mathscr{D}_{\mathrm{o0}}\right]t^0_{+\not\emptyset} + c_{\mathrm{o}}\mathscr{D}_{\mathrm{e0}}t^{\mathrm{o}}_{+\not\emptyset}}{c_0\mathscr{D}_{\mathrm{eo}} + c_+\frac{z_- - z_+}{z_-}\left(1 - \frac{\rho_{\mathrm{e}}}{c_+ z_+ F}t^{\mathrm{o}}_{+\not\emptyset}\right)\mathscr{D}_{\mathrm{o0}} + c_{\mathrm{o}}\mathscr{D}_{\mathrm{e0}}} \\ =& \frac{\left[c_0\mathscr{D}_{\mathrm{eo}} + c_+\frac{z_- - z_+}{z_-}\mathscr{D}_{\mathrm{o0}}\right]t^0_{+\not\emptyset} + c_{\mathrm{o}}\mathscr{D}_{\mathrm{e0}}t^{\mathrm{o}}_{+\not\emptyset}}{c_0\mathscr{D}_{\mathrm{eo}} + c_+\frac{z_- - z_+}{z_-}\mathscr{D}_{\mathrm{o0}} + c_{\mathrm{o}}\mathscr{D}_{\mathrm{e0}}} \\ &+ \frac{(z_- - z_+)c_{\mathrm{o}}\mathscr{D}_{\mathrm{e0}}\mathscr{D}_{\mathrm{o0}}t^{\mathrm{o}}_{+\not\emptyset}\left(t^{\mathrm{o}}_{+\not\emptyset} - t^0_{+\not\emptyset}\right)\rho_{\mathrm{e}}}{z_+ z_- F\left(c_0\mathscr{D}_{\mathrm{eo}} + c_+\frac{z_- - z_+}{z_-}\mathscr{D}_{\mathrm{o0}} + c_{\mathrm{o}}\mathscr{D}_{\mathrm{e0}}\right)^2} + O(\rho_{\mathrm{e}}^2)\end{aligned} \tag{3.47}$$

Migration coefficient:

$$\begin{aligned}\Xi =& \frac{c_{\mathrm{o}}\left(t^0_{+\not\emptyset} - t^{\mathrm{o}}_{+\not\emptyset}\right)\mathscr{D}_{\mathrm{o0}}}{c_0\mathscr{D}_{\mathrm{eo}} + c_+\frac{z_- - z_+}{z_-}\left(1 - \frac{\rho_{\mathrm{e}}}{z_+ c_+ F}t^{\mathrm{o}}_{+\not\emptyset}\right)\mathscr{D}_{\mathrm{o0}} + c_{\mathrm{o}}\mathscr{D}_{\mathrm{e0}}} \\ =& \frac{c_{\mathrm{o}}\left(t^0_{+\not\emptyset} - t^{\mathrm{o}}_{+\not\emptyset}\right)\mathscr{D}_{\mathrm{o0}}}{c_0\mathscr{D}_{\mathrm{eo}} + c_+\frac{z_- - z_+}{z_-}\mathscr{D}_{\mathrm{o0}} + c_{\mathrm{o}}\mathscr{D}_{\mathrm{e0}}}\left(1 + \frac{(z_- - z_+)\mathscr{D}_{\mathrm{o0}}t^{\mathrm{o}}_{+\not\emptyset}\rho_{\mathrm{e}}}{z_+ z_- F\left(c_0\mathscr{D}_{\mathrm{eo}} + c_+\frac{z_- - z_+}{z_-}\mathscr{D}_{\mathrm{o0}} + c_{\mathrm{o}}\mathscr{D}_{\mathrm{e0}}\right)}\right) \\ &+ O(\rho_{\mathrm{e}}^2)\end{aligned} \tag{3.48}$$

Cross diffusivity:

$$\begin{aligned}\mathscr{X}_{0\mathrm{o}} =&\frac{c_{\mathrm{T}}\mathscr{D}_{\mathrm{e}0}\mathscr{D}_{\mathrm{o}0}}{c_0\mathscr{D}_{\mathrm{eo}}+c_+\frac{z_--z_+}{z_-}\left(1-\frac{\rho_{\mathrm{e}}}{z_+c_+F}t^{\mathrm{o}}_{+\emptyset}\right)\mathscr{D}_{\mathrm{o}0}+c_{\mathrm{o}}\mathscr{D}_{\mathrm{e}0}}\\ =&\frac{c_{\mathrm{T}}\mathscr{D}_{\mathrm{e}0}\mathscr{D}_{\mathrm{o}0}}{c_0\mathscr{D}_{\mathrm{eo}}+c_+\frac{z_--z_+}{z_-}\mathscr{D}_{\mathrm{o}0}+c_{\mathrm{o}}\mathscr{D}_{\mathrm{e}0}}\left(1+\frac{(z_--z_+)\mathscr{D}_{\mathrm{o}0}t^{\mathrm{o}}_{+\emptyset}\rho_{\mathrm{e}}}{z_+z_-F\left(c_0\mathscr{D}_{\mathrm{eo}}+c_+\frac{z_--z_+}{z_-}\mathscr{D}_{\mathrm{o}0}+c_{\mathrm{o}}\mathscr{D}_{\mathrm{e}0}\right)}\right)\\ &+O(\rho_{\mathrm{e}}^2)\end{aligned} \tag{3.49}$$

Ionic conductivity:

$$\begin{aligned}\frac{1}{\kappa^0_-} =&\frac{1}{\kappa_\emptyset}\left(1-\frac{c_{\mathrm{o}}}{c_{\mathrm{T}}}\right)\left(1-\frac{\rho_{\mathrm{e}}}{c_+z_+F}\right)\\ &\times\frac{c_0\mathscr{D}_{\mathrm{eo}}+c_+\frac{z_--z_+}{z_-}\left(1-\frac{\rho_{\mathrm{e}}}{c_+z_+F}t^{\mathrm{o}}_{+\emptyset}\right)\mathscr{D}_{\mathrm{o}0}+\frac{\rho_{\mathrm{e}}t^{\mathrm{o}}_{+\emptyset}-c_+z_+F}{\rho_{\mathrm{e}}t^{0}_{+\emptyset}-c_+z_+F}c_{\mathrm{o}}\mathscr{D}_{\mathrm{e}0}}{c_0\mathscr{D}_{\mathrm{eo}}+c_+\frac{z_--z_+}{z_-}\left(1-\frac{\rho_{\mathrm{e}}}{c_+z_+F}t^{\mathrm{o}}_{+\emptyset}\right)\mathscr{D}_{\mathrm{o}0}+c_{\mathrm{o}}\mathscr{D}_{\mathrm{e}0}}\\ &+\frac{c_{\mathrm{o}}(z_--z_+)RT}{c_+c_{\mathrm{T}}z_+^2z_-F^2\mathscr{D}_{\mathrm{eo}}}\times\frac{1}{c_0\mathscr{D}_{\mathrm{eo}}+c_+\frac{z_--z_+}{z_-}\left(1-\frac{\rho_{\mathrm{e}}}{c_+z_+F}t^{\mathrm{o}}_{+\emptyset}\right)\mathscr{D}_{\mathrm{o}0}+c_{\mathrm{o}}\mathscr{D}_{\mathrm{e}0}}\times\\ &\left[t^{\mathrm{o}}_{+\emptyset}(1-t^{\mathrm{o}}_{+\emptyset})\left\{-\frac{c_+z_+F}{\rho_{\mathrm{e}}t^0_{+\emptyset}-c_+z_+F}c_0\mathscr{D}_{\mathrm{eo}}+c_+\frac{z_--z_+}{z_-}\left(1-\frac{\rho_{\mathrm{e}}}{c_+z_+F}t^0_{+\emptyset}\right)\mathscr{D}_{\mathrm{o}0}+c_{\mathrm{o}}\mathscr{D}_{\mathrm{e}0}\right\}\right.\\ &\left.+\frac{c_+z_+F}{\rho_{\mathrm{e}}t^0_{+\emptyset}-c_+z_+F}\left\{\frac{\rho_{\mathrm{e}}}{c_+z_+F}\left(t^0_{+\emptyset}\right)^2\left(1-t^{\mathrm{o}}_{+\emptyset}\right)-\left(t^0_{+\emptyset}-t^{\mathrm{o}}_{+\emptyset}\right)^2\right\}c_0\mathscr{D}_{\mathrm{eo}}\right]\\ =&\left(1-\frac{c_{\mathrm{o}}}{c_{\mathrm{T}}}\right)\frac{1}{\kappa_\emptyset}\\ &+\frac{c_{\mathrm{o}}(z_--z_+)RT}{c_+c_{\mathrm{T}}z_+^2z_-F^2\mathscr{D}_{\mathrm{eo}}}\times\left\{t^{\mathrm{o}}_{+\emptyset}\left(1-t^{\mathrm{o}}_{+\emptyset}\right)+\frac{c_0\mathscr{D}_{\mathrm{eo}}\left(t^0_{+\emptyset}-t^{\mathrm{o}}_{+\emptyset}\right)^2}{c_0\mathscr{D}_{\mathrm{eo}}+c_+\frac{z_--z_+}{z_-}\mathscr{D}_{\mathrm{o}0}+c_{\mathrm{o}}\mathscr{D}_{\mathrm{e}0}}\right\}\\ &-\left[\left(1-\frac{c_{\mathrm{o}}}{c_{\mathrm{T}}}\right)\left\{1-\frac{c_{\mathrm{o}}\mathscr{D}_{\mathrm{e}0}\left(t^0_{+\emptyset}-t^{\mathrm{o}}_{+\emptyset}\right)}{c_0\mathscr{D}_{\mathrm{eo}}+c_+\frac{z_--z_+}{z_-}\mathscr{D}_{\mathrm{o}0}+c_{\mathrm{o}}\mathscr{D}_{\mathrm{e}0}}\right\}\frac{1}{\kappa_\emptyset}+\left\{t^0_{+\emptyset}\left(1-t^0_{+\emptyset}\right)c_0\mathscr{D}_{\mathrm{eo}}\right.\right.\\ &\left.+t^{\mathrm{o}}_{+\emptyset}\left(1-t^{\mathrm{o}}_{+\emptyset}-\frac{c_0\mathscr{D}_{\mathrm{eo}}\left(t^0_{+\emptyset}-t^{\mathrm{o}}_{+\emptyset}\right)}{c_0\mathscr{D}_{\mathrm{eo}}+\frac{z_--z_+}{z_-}c_+\mathscr{D}_{\mathrm{o}0}+c_{\mathrm{o}}\mathscr{D}_{\mathrm{e}0}}\right)c_+\frac{z_--z_+}{z_-}\mathscr{D}_{\mathrm{o}0}\right\}\\ &\left.\times\frac{c_{\mathrm{o}}(z_--z_+)RT}{c_+c_{\mathrm{T}}z_+^2z_-F^2\mathscr{D}_{\mathrm{eo}}}\times\frac{t^0_{+\emptyset}-t^{\mathrm{o}}_{+\emptyset}}{c_0\mathscr{D}_{\mathrm{eo}}+c_+\frac{z_--z_+}{z_-}\mathscr{D}_{\mathrm{o}0}+c_{\mathrm{o}}\mathscr{D}_{\mathrm{e}0}}\right]\frac{\rho_{\mathrm{e}}}{Fz_+c_+}+O(\rho_{\mathrm{e}}^2)\end{aligned} \tag{3.50}$$

When electroneutral, one obtains $\nabla\mu_0^+ = -(y_\mathrm{o}\nabla\mu_\mathrm{o}^+ + y\nabla\mu_\mathrm{e})/y_0$, so the flux and MacInnes equations can be rearranged to the exact forms given by Monroe [157]. Precisely because this substitution is not made here, $\mathscr{D}_\mathrm{o}$ looks different from the one defined by Monroe [157][1], but the remaining five macroscopic transport properties coincide.

Using the procedures in sections 3.1.1 and 3.1.2 as before, the core-potential flux and MacInnes equations can be obtained. Unfortunately, having one more solvent and relaxing electroneutrality mean that a high degree of complexity manifests in the equations; thus, the task of writing them in a reasonably concise and compact manner becomes a challenge. It is unlikely that one would use these highly complex equations in any practical situations, and therefore only the electroneutral forms are presented here. Again, binary-electrolyte transport properties in the core-potential space are used to simplify the results. $\mathscr{D}_\mathrm{e0}^*$, $t_{+\not\emptyset}^{*0}$, and $\kappa_{\not\emptyset}^*$ represent the properties for the electroneutral system $\{0,-,+\}$, as defined in equation (3.23). Similarly, $\mathscr{D}_\mathrm{eo}^*$ and $t_{+\not\emptyset}^{*\mathrm{o}}$ are the properties for the electronetural system $\{\mathrm{o},-,+\}$. With these, one arrives at the following electroneutral flux and MacInnes equations.

$$c_\mathrm{o}(\vec{v}_\mathrm{o}-\vec{v}_0) = \frac{c_\mathrm{o}}{RT}\left(\mathscr{X}_{0\mathrm{o}}^*\nabla\mathrm{M}_0^+ - \mathscr{D}_\mathrm{o}^*\nabla\mathrm{M}_\mathrm{o}^+\right) + \frac{(z_- - z_+)\Xi^*}{z_+z_-F}\vec{i} \tag{3.51}$$

$$\begin{aligned} c_-(\vec{v}_- - \vec{v}_0) =& \frac{1-t_+^{*0}}{Fz_-}\vec{i} - \frac{c_\mathrm{T}z_+}{RT(z_- - z_+)}\left[\mathscr{D}_0^*\nabla\mathrm{M}_0^+\right. \\ &\left. - \frac{c_\mathrm{o}(c_\mathrm{T}-c_\mathrm{o})}{c_\mathrm{T}(c_\mathrm{T}-c_0)}\frac{\mathscr{D}_\mathrm{e0}^*\left\{(c_+ + c_-)\mathscr{D}_{0\mathrm{o}} - (c_\mathrm{T}-c_0)\mathscr{D}_\mathrm{eo}^*\right\}\mathscr{X}_{0\mathrm{o}}^*}{\mathscr{D}_{0\mathrm{o}}\left\{(c_\mathrm{T}-c_\mathrm{o})\mathscr{D}_\mathrm{e0}^* + c_0\mathscr{D}_\mathrm{eo}^*\right\}}\nabla\mathrm{M}_\mathrm{o}^+\right] \end{aligned} \tag{3.52}$$

$$\begin{aligned} c_+(\vec{v}_+ - \vec{v}_0) =& \frac{t_+^{*0}}{Fz_+}\vec{i} + \frac{c_\mathrm{T}z_-}{RT(z_- - z_+)}\left[\mathscr{D}_0^*\nabla\mathrm{M}_0^+\right. \\ &\left. - \frac{c_\mathrm{o}(c_\mathrm{T}-c_\mathrm{o})}{c_\mathrm{T}(c_\mathrm{T}-c_0)}\frac{\mathscr{D}_\mathrm{e0}^*\left\{(c_+ + c_-)\mathscr{D}_{0\mathrm{o}} - (c_\mathrm{T}-c_0)\mathscr{D}_\mathrm{eo}^*\right\}\mathscr{X}_{0\mathrm{o}}^*}{\mathscr{D}_{0\mathrm{o}}\left\{(c_\mathrm{T}-c_\mathrm{o})\mathscr{D}_\mathrm{e0}^* + c_0\mathscr{D}_\mathrm{eo}^*\right\}}\nabla\mathrm{M}_\mathrm{o}^+\right] \end{aligned} \tag{3.53}$$

$$\begin{aligned} \vec{i} = \frac{\kappa_-^{*0}}{c_\mathrm{T}z_-F}&\left[\left\{1 + \frac{z_- - z_+}{z_+}\left(\Xi^* + t_+^{*0}\right)\right\}c_0\nabla\mathrm{M}_0^+\right. \\ &\left. + \left\{1 - \frac{z_- - z_+}{z_+}\left(\frac{c_\mathrm{T}-c_\mathrm{o}}{c_\mathrm{o}}\Xi^* - t_+^{*0}\right)\right\}c_\mathrm{o}\nabla\mathrm{M}_\mathrm{o}^+\right] - \kappa_-^{*0}\nabla\Phi \end{aligned} \tag{3.54}$$

[1] In fact, Monroe's $\mathscr{D}_\mathrm{o}$ is equal to $y_\mathrm{o}\mathscr{X}_{0\mathrm{o}} + y_0\mathscr{D}_\mathrm{o}$, using $\mathscr{X}_{0\mathrm{o}}$ and $\mathscr{D}_\mathrm{o}$ in equations (3.49) and (3.46), respectively [157].

The six core-potential transport properties that appear above are defined below under electroneutrality.

Thermodynamic diffusivity for the first solvent 0:

$$\mathscr{D}_0^* = \left(1-\frac{c_\mathrm{o}}{c_\mathrm{T}}\right)\left(1-\frac{c_0}{c_\mathrm{T}}\right)\left.\frac{\mathscr{D}_{\mathrm{e}0}^*\left[c_0\mathscr{D}_{\mathrm{eo}}^* + (c_+ + c_-)\mathscr{D}_{\mathrm{o}0}\right]}{\left(1-\frac{c_0}{c_\mathrm{T}}\right)c_0\mathscr{D}_{\mathrm{eo}}^* + \frac{(c_+ + c_-)^2}{c_\mathrm{T}}\mathscr{D}_{\mathrm{o}0} + \left(1-\frac{c_\mathrm{o}}{c_\mathrm{T}}\right)c_\mathrm{o}\mathscr{D}_{\mathrm{e}0}^*}\right|_{\rho_\mathrm{e}=0} \tag{3.55}$$

Thermodynamic diffusivity for the second solvent o:

$$\mathscr{D}_\mathrm{o}^* = \left(1-\frac{c_\mathrm{o}}{c_\mathrm{T}}\right)\left.\frac{\mathscr{D}_{\mathrm{o}0}\left[(c_\mathrm{T}-c_0)\mathscr{D}_{\mathrm{eo}}^* + c_\mathrm{o}\mathscr{D}_{\mathrm{e}0}^*\right]}{\left(1-\frac{c_0}{c_\mathrm{T}}\right)c_0\mathscr{D}_{\mathrm{eo}}^* + \frac{(c_+ + c_-)^2}{c_\mathrm{T}}\mathscr{D}_{\mathrm{o}0} + \left(1-\frac{c_\mathrm{o}}{c_\mathrm{T}}\right)c_\mathrm{o}\mathscr{D}_{\mathrm{e}0}^*}\right|_{\rho_\mathrm{e}=0} \tag{3.56}$$

Cation transference number:

$$t_+^{*0} = \left.\frac{\left[\left(1-\frac{c_0}{c_\mathrm{T}}\right)c_0\mathscr{D}_{\mathrm{eo}}^* + \frac{(c_+ + c_-)^2}{c_\mathrm{T}}\mathscr{D}_{\mathrm{o}0}\right]t_{+\not{o}}^{*0} + \left(1-\frac{c_\mathrm{o}}{c_\mathrm{T}}\right)c_\mathrm{o}\mathscr{D}_{\mathrm{e}0}^* t_{+\not{0}}^{*\mathrm{o}}}{\left(1-\frac{c_0}{c_\mathrm{T}}\right)c_0\mathscr{D}_{\mathrm{eo}}^* + \frac{(c_+ + c_-)^2}{c_\mathrm{T}}\mathscr{D}_{\mathrm{o}0} + \left(1-\frac{c_\mathrm{o}}{c_\mathrm{T}}\right)c_\mathrm{o}\mathscr{D}_{\mathrm{e}0}^*}\right|_{\rho_\mathrm{e}=0} \tag{3.57}$$

Migration coefficient:

$$\Xi^* = \left.\frac{\left(t_{+\not{o}}^{*0} - t_{+\not{0}}^{*\mathrm{o}}\right)\frac{c_+ + c_-}{c_\mathrm{T}}c_\mathrm{o}\mathscr{D}_{\mathrm{o}0}}{\left(1-\frac{c_0}{c_\mathrm{T}}\right)c_0\mathscr{D}_{\mathrm{eo}}^* + \frac{(c_+ + c_-)^2}{c_\mathrm{T}}\mathscr{D}_{\mathrm{o}0} + \left(1-\frac{c_\mathrm{o}}{c_\mathrm{T}}\right)c_\mathrm{o}\mathscr{D}_{\mathrm{e}0}^*}\right|_{\rho_\mathrm{e}=0} \tag{3.58}$$

Cross diffusivity:

$$\mathscr{X}_{0\mathrm{o}}^* = \left.\frac{\left(1-\frac{c_0}{c_\mathrm{T}}\right)\mathscr{D}_{\mathrm{o}0}\left\{c_0\mathscr{D}_{\mathrm{eo}}^* + (c_\mathrm{T}-c_\mathrm{o})\mathscr{D}_{\mathrm{e}0}^*\right\}}{\left(1-\frac{c_0}{c_\mathrm{T}}\right)c_0\mathscr{D}_{\mathrm{eo}}^* + \frac{(c_+ + c_-)^2}{c_\mathrm{T}}\mathscr{D}_{\mathrm{o}0} + \left(1-\frac{c_\mathrm{o}}{c_\mathrm{T}}\right)c_\mathrm{o}\mathscr{D}_{\mathrm{e}0}^*}\right|_{\rho_\mathrm{e}=0} \tag{3.59}$$

Ionic conductivity:

$$\frac{1}{\kappa_-^{*0}} = \left(1 - \frac{c_\mathrm{o}}{c_\mathrm{T}}\right) \frac{1}{\kappa_{\not\emptyset}^*} + \frac{c_\mathrm{o}(z_- - z_+)^2 RT}{c_\mathrm{T}(c_\mathrm{T} - c_0) z_+^2 z_-^2 F^2 \mathscr{D}_\mathrm{eo}^*} \times \left[t_{+\not\emptyset}^{*\mathrm{o}} \left(1 - t_{+\not\emptyset}^{*\mathrm{o}}\right) + \frac{\left(1 - \frac{c_0}{c_\mathrm{T}}\right) c_0 \mathscr{D}_\mathrm{eo}^* \left(t_{+\not\emptyset}^{*0} - t_{+\not\emptyset}^{*\mathrm{o}}\right)^2}{\left(1 - \frac{c_0}{c_\mathrm{T}}\right) c_0 \mathscr{D}_\mathrm{eo}^* + \frac{(c_+ + c_-)^2}{c_\mathrm{T}} \mathscr{D}_\mathrm{o0} + \left(1 - \frac{c_\mathrm{o}}{c_\mathrm{T}}\right) c_\mathrm{o} \mathscr{D}_\mathrm{e0}^*} \right] \Bigg|_{\rho_\mathrm{e}=0} \tag{3.60}$$

Bear in mind that when electroneutral, one obtains $t_{+\not\emptyset}^{*0} = t_{+\not\emptyset}^{0}\big|_{\rho_\mathrm{e}=0}$, $t_{+\not\emptyset}^{*\mathrm{o}} = t_{+\not\emptyset}^{\mathrm{o}}\big|_{\rho_\mathrm{e}=0}$, $\mathscr{D}_\mathrm{e0}^* = \frac{c_+ + c_-}{c_0 + c_+ + c_-} \mathscr{D}_\mathrm{e0}\big|_{\rho_\mathrm{e}=0}$, and $\mathscr{D}_\mathrm{eo}^* = \frac{c_+ + c_-}{c_\mathrm{o} + c_+ + c_-} \mathscr{D}_\mathrm{eo}\big|_{\rho_\mathrm{e}=0}$, so it is easy to show that the transference numbers, the ionic conductivities, and the migration coefficients of the Smyrl–Newman and the core-potential formalisms agree, i.e., $t_+^{*0} = t_+^0\big|_{\rho_\mathrm{e}=0}$, $\kappa_-^{*0} = \kappa_-^0\big|_{\rho_\mathrm{e}=0}$, and $\Xi^* = \Xi\big|_{\rho_\mathrm{e}=0}$. On the contrary, diffusivities relate in rather convoluted ways.

$$\mathscr{D}_0^* = \frac{c_+ + c_-}{c_\mathrm{T}} \left[1 + \frac{c_\mathrm{o} \mathscr{D}_\mathrm{o0}}{c_0 \mathscr{D}_\mathrm{eo} + (c_+ + c_-) \mathscr{D}_\mathrm{o0}}\right] \mathscr{D}_0 \Big|_{\rho_\mathrm{e}=0} = \frac{c_+ + c_-}{c_\mathrm{T}} \left[\mathscr{D}_0 + \frac{c_\mathrm{o}}{c_\mathrm{T}} \mathscr{X}_\mathrm{0o}\right] \Bigg|_{\rho_\mathrm{e}=0}$$

$$\mathscr{D}_\mathrm{o}^* = \left[1 - \frac{c_\mathrm{o}}{c_\mathrm{T}} \left(1 - \frac{\mathscr{D}_\mathrm{e0}}{\mathscr{D}_\mathrm{eo}}\right)\right] \mathscr{D}_\mathrm{o} \Big|_{\rho_\mathrm{e}=0}$$

$$\mathscr{X}_\mathrm{0o}^* = \left[1 - \frac{c_0}{c_\mathrm{T}} \left(1 - \frac{\mathscr{D}_\mathrm{eo}}{\mathscr{D}_\mathrm{e0}}\right)\right] \mathscr{X}_\mathrm{0o} \Big|_{\rho_\mathrm{e}=0} \tag{3.61}$$

3.3 The core-potential theory with Boltzmann-distributed charges

As demonstrated in the previous section —particularly for the binary salt in two neutral solvents—, directly working with core potentials as driving forces in the flux-explicit diffusion equations imparts undue complexity, especially if non-electroneutrality is to be enforced. Fortunately, there is an alternative route that is still enrooted in the core-potential framework. With an assumption that ions are Boltzmann-distributed,

Goyal and Monroe [1] illustrated a method by which thermodynamically consistent electrochemical potentials (in differential forms, $d\mu_i$) can be obtained for the symmetric binary electrolyte, regardless of the charge state of the system. They achieved this by introducing correction terms to the electrical parts of $d\mu_i$. A merit of the new $d\mu_i$ expressions is that they can simply be substituted into the existing theories —such as the flux equations inverted from the OSM equations— without incurring modifications[2]. Furthermore, the implementation of this new approach is simple; it involves just a few matrix multiplications, conveniently traversing the core-potential space without explicit engagement.

An underlying assumption of this approach is that the charged species in the system are arranged according to the Boltzmann distribution. To be more precise, the naive potential is apportioned into two parts [1],

$$\Phi = \Phi_0 - \Phi_\mathrm{P} \tag{3.62}$$

where Φ_0 is the electroneutral potential (represents the potential that arises when the system is electroneutral) and Φ_P is the Poisson–Boltzmann overpotential that embodies contribution from non-electroneutrality. The composition that generates $\Phi = \Phi_0$ is referred to as the electroneutral reference composition, which depends on the choice of the reference and charging ions. Since the effect of the electric potential becomes only relevant when the system deviates away from electroneutrality, Φ_0 is usually set to zero.

Although the theoretical exposition Goyal and Monroe [1] provided was comprehensive, the practical machinery of deriving electrical correction terms for actual systems (other than the binary electrolyte) can still be rather obscure. Therefore, a more

[2]The correction terms in $d\mu_i$ do change the magnitude of the electrical contributions in electrochemical potentials, but they do not affect the definition of transport properties because the OSM-equation inversion process deals with electrochemical potentials as a whole. On the contrary, standard electrochemical potentials are the weighted sum of core potentials, as shown in eq (2.20). Therefore, when core potentials are used to write the OSM equations, the reconstruction of the flux-explicit transport equations and the consequent redefinition of transport properties are unavoidable.

general procedure for obtaining the corrected electrochemical-potential differentials, extended from Goyal and Monroe's binary electrolyte example, is devised and outlined below.

1. Find the electroneutral reference composition y_i^0 (eq.86 in [1]).

$$y_i^0 = \begin{cases} y_i & ; \quad i < n-1 \\ \dfrac{z_n}{z_n - z_{n-1}} - \displaystyle\sum_{k=1}^{n-2} \dfrac{z_n - z_k}{z_n - z_{n-1}} y_k & ; \quad i = n-1 \\ -\dfrac{z_{n-1}}{z_n - z_{n-1}} - \displaystyle\sum_{k=1}^{n-2} \dfrac{z_k - z_{n-1}}{z_n - z_{n-1}} y_k & ; \quad i = n \end{cases} \tag{3.63}$$

2. Find the molar excess charge $\overline{\mathrm{P}}$, using the fact that the charged species are Boltzmann-distributed (eq.100 in [1]).

$$\overline{\mathrm{P}} = F \sum_{k=1}^{n} z_k y_k^0 \exp\left(-\frac{F z_k \Phi_{\mathrm{P}}}{RT}\right) \tag{3.64}$$

3. Find the neutralizable ionic strength $\overline{I}^{\mathrm{B}}$ (eq.101 in [1]).

$$\overline{I}^{\mathrm{B}} = \frac{1}{2} \sum_{k=1}^{n} z_k^2 y_k^0 \exp\left(-\frac{F z_k \Phi_{\mathrm{P}}}{RT}\right) \tag{3.65}$$

4. Find the $(n-1)$-th row of the $(n-1)\times(n-1)$ core-thermodynamic-factor matrix $\overline{\mathbf{X}}_{n-1}^{\mathrm{B}}$ (eq.103 in [1]; this is derived by partially differentiating $\overline{\mathrm{P}}$ with respect to composition variables).

$$\begin{aligned} \overline{\mathbf{X}}_{n-1}^{\mathrm{B}} = & \frac{RT}{2\overline{I}^{\mathrm{B}}} \left[(z_n - z_{n-1})^2 \delta_{(n-1)j} + z_j z_{n-1} \left(e^{-z_j \phi} - e^{-z_{n-1}\phi} \right) \right. \\ & \left. + z_{n-1} z_n \left(e^{-z_{n-1}\phi} - e^{-z_n \phi} \right) + z_n z_j \left(e^{-z_n \phi} - e^{-z_j \phi} \right) \right] \end{aligned} \tag{3.66}$$

The symmetry of $\overline{\mathbf{X}}_{n-1}^{\mathrm{B}}$ settles the entries in the $(n-1)$-th column, too. In the above expression, $\phi = F\Phi_{\mathrm{P}}/RT$ represents a dimensionless Poisson–Boltzmann overpotential.

5. Find Newman's electroneutral thermodynamic-factor matrix $\boldsymbol{\chi}_{n-1}$. To do so, write the diffusion driving forces under the isothermal, isobaric condition using the neutralizable composition gradients dx_i, accompanied by the (appropriately scaled) core-thermodynamic-factor matrix as below.

$$[y_i d\mu_i]_n = \left[\boldsymbol{\Gamma}_1 \mathbf{Y}_{n-1}^{-1} \left(\mathbf{T}_{n-1}^{dy \leftarrow\!\shortmid dx}\right)^{\mathrm{T}} \overline{\mathbf{X}}_{n-1}^{\mathrm{B}}\right] d[x_i]_{n-1} \tag{3.67}$$

Here, $[\alpha_i]_n$ indicates a vector of length n whose i-th entry is α_i and $\boldsymbol{\Gamma}_1 \mathbf{Y}_{n-1}^{-1} \left(\mathbf{T}_{n-1}^{dy \leftarrow\!\shortmid dx}\right)^{\mathrm{T}}$ captures the necessary transformations that can be calculated from equations 19, 27, and 66 in Goyal and Monroe [1] (these equations only depend on the particle fractions). Note that eq.(3.67) is a more general form of eq.110 in [1]. The scaled core-thermodynamic-factor matrix reduces to $\boldsymbol{\chi}_{n-1}$ (of size $n \times (n-2)$) under electroneutrality such that

$$\begin{aligned}[y_i d\mu_i]_n \big|_{\overline{\mathrm{P}}=0} &= \left[\boldsymbol{\Gamma}_1 \mathbf{Y}_{n-1}^{-1} \left(\mathbf{T}_{n-1}^{dy \leftarrow\!\shortmid dx}\right)^{\mathrm{T}} \overline{\mathbf{X}}_{n-1}^{\mathrm{B}}\right] \Big|_{\overline{\mathrm{P}}=0} d \begin{bmatrix} [y_i^0]_{n-2} \\ 0 \end{bmatrix} \\ &= RT \boldsymbol{\chi}_{n-1} d\left[y_i^0\right]_{n-2}\end{aligned} \tag{3.68}$$

because $x_{n-1} = \overline{\mathrm{P}}/F(z_n - z_{n-1}) = 0$. At this point, $\boldsymbol{\chi}_{n-1}$ contains unknown elements of $\overline{\mathbf{X}}_{n-1}^{\mathrm{B}}$ (i.e., those that do not belong to the $(n-1)$-th row and $(n-1)$-th column of the matrix). To determine them, connection to thermodynamic-factor measurements must be established.

6. A thermodynamic-factor measurement establishes an electroneutral relationship between $d\mu_i$ (or a combination of $d\mu_i$'s) and a measurable thermodynamic factor χ_{ij}^{m} (more details on thermodynamic factors in Chapter 4). Equate this relationship to the expression obtained in step 5 to verify how χ_{ij}^{m} is expressed as a linear combination of Newman's electroneutral thermodynamic factors (elements in $\boldsymbol{\chi}_{n-1}$). Now, append a non-electroneutral component χ_{ij}^{el} to χ_{ij}^{m} to form New-

man's non-electroneutral thermodynamic factor χ^*_{ij}, i.e., $\chi^*_{ij} = \chi^{\mathrm{m}}_{ij} + \chi^{\mathrm{el}}_{ij}$. Assume the relationship between χ^{m}_{ij} and $\boldsymbol{\chi}_{n-1} = \frac{1}{RT}\left[\boldsymbol{\Gamma}_1 \mathbf{Y}^{-1}_{n-1}\left(\mathbf{T}^{dy\leftarrow dx}_{n-1}\right)^{\mathrm{T}} \overline{\mathbf{X}}^{\mathrm{B}}_{n-1}\right]\Big|_{\overline{\mathrm{P}}=0}$ extends to non-electroneutral regions, so that the relationship between χ^*_{ij} and $\frac{1}{RT}\left[\boldsymbol{\Gamma}_1 \mathbf{Y}^{-1}_{n-1}\left(\mathbf{T}^{dy\leftarrow dx}_{n-1}\right)^{\mathrm{T}} \overline{\mathbf{X}}^{\mathrm{B}}_{n-1}\right]$ is governed in the same way, as well. This then reveals how the unknown elements of $\overline{\mathbf{X}}^{\mathrm{B}}_{n-1}$ are connected to χ^*_{ij}.

7. Construct expressions for non-electroneutral $d\mu_i$ using eq.(3.67) and $\overline{\mathbf{X}}^{\mathrm{B}}_{n-1}$, whose unknown entries are replaced with terms containing χ^*_{ij}, as per the previous step. At this point, the chemical parts in $d\mu_i$'s should contain terms involving χ^*_{ij} and Φ. χ^{el}_{ij} (the electrical part of χ^*_{ij}) can now be found by requiring $d\mu_i$ to display its expected electrical behaviour. How this step proceeds depends on the charge state of the species under investigation.

   (a) For an electrically neutral species i, $d\mu_i$ should have no dependence on Φ. Therefore, all χ^{el}_{ij}'s that appear in the chemical part must exactly cancel all Φ-dependent terms.

   (b) For a charged species, there must exist at least one oppositely charged species with whom it forms a neutral cluster. The electrochemical potential of this cluster must be independent of Φ and χ^{el}_{ij}'s can be chosen so as to annihilate all Φ-dependent terms in the chemical part.

8. Having chosen χ^{el}_{ij}'s, $\overline{\mathbf{X}}^{\mathrm{B}}_{n-1}$ can finally be constructed.

3.4 Corrections for electrochemical-potential differentials

The procedure in section 3.3 relies on the fact that there exist experimental methods that can characterise thermodynamic factors for a given system. With the knowledge of transport properties, e.g., transference numbers, migration coefficients, etc., the liquid-junction-potential measurement can be used to extract thermodynamic factors;

Chapter 4 explores this in more detail. Assuming the necessary thermodynamic factors are available, the above procedure is applied to (1) the binary electrolyte, (2) the three-ion ionic liquid, and (3) the binary salt in two neutral solvents in the rest of this section.

3.4.1 Case I. The binary electrolyte

The electroneutral reference composition (indicated by the superscript 0) for the system $\{0,+,-\}$ (so the reference ion is the anion) corresponds to

$$\left\{y_0^0, y_+^0, y_-^0\right\} = \left\{y_0, \frac{z_-(1-y_0)}{z_- - z_+}, -\frac{z_+(1-y_0)}{z_- - z_+}\right\}. \tag{3.69}$$

Assuming that the two ions are Boltzmann-distributed, one can set the electroneutral part of the electric potential to $\Phi_0 = 0$ and non-dimensionalise the remaining Poisson–Boltzmann overpotential by $\phi = F\Phi_\mathrm{P}/RT$. This leads to the molar excess charge

$$\overline{\mathrm{P}} = \frac{Fz_+z_-}{z_- - z_+}(1-y_0)\left(e^{-z_+\phi} - e^{-z_-\phi}\right) \tag{3.70}$$

and the ionic strength

$$\overline{I}^\mathrm{B} = \frac{z_+z_-}{2(z_- - z_+)}(1-y_0)\left(z_+e^{-z_+\phi} - z_-e^{-z_-\phi}\right). \tag{3.71}$$

The entries to the thermodynamic-factor matrix corresponding to the charging ion are

$$\overline{X}^\mathrm{B}_{+0} = \frac{RT(z_- - z_+)^2}{2\overline{I}^\mathrm{B}}\delta \qquad \overline{X}^\mathrm{B}_{++} = \frac{RT(z_- - z_+)^2}{2\overline{I}^\mathrm{B}}, \tag{3.72}$$

where δ below is chosen for notational compactness.

$$\delta = \frac{\left(e^{-z_+\phi} - e^{-z_-\phi}\right)z_+z_-}{(z_- - z_+)^2} = \frac{\overline{\mathrm{P}}}{F(1-y_0)(z_- - z_+)} \tag{3.73}$$

Then, the diffusion driving forces can be expressed with the neutralizable composition gradients dx_i, multiplied by the core thermodynamic factors as in eq.(3.67). This allows

us to identify Newman's electroneutral thermodynamic-factor matrix $\boldsymbol{\chi}_+$ by imposing $\overline{\mathrm{P}} = 0$, as per eq.(3.68).

$$\boldsymbol{\chi}_+ = \begin{bmatrix} \chi_{00} \\ \chi_{+0} \\ \chi_{-0} \end{bmatrix} = \frac{1}{RT} \begin{bmatrix} y_0(1-y_0)\overline{X}^{\mathrm{B}}_{00} \\ -y_0 y^0_+ \overline{X}^{\mathrm{B}}_{00} \\ -y_0 y^0_- \overline{X}^{\mathrm{B}}_{00} \end{bmatrix} \Bigg|_{\overline{\mathrm{P}}=0} \tag{3.74}$$

Comparing $d\mu_{\mathrm{e}}$ obtained from rearranging eq.(3.68) —which involves elements of $\boldsymbol{\chi}_+$— and $d\mu_{\mathrm{e}} = \nu RT \chi^{\mathrm{m}}_{\mathrm{ee}}\, d\ln y$ that contains the experimentally measurable thermodynamic factor $\chi^{\mathrm{m}}_{\mathrm{ee}}$ (hence the superscript m), cf., eq.(4.2), it is easy to see that the first entry of $\boldsymbol{\chi}_+$ corresponds to the measurable thermodynamic factor, i.e., $\chi_{00} = \chi^{\mathrm{m}}_{\mathrm{ee}}$. Supposing this relationship extends to non-electroneutral regions, one can write down the non-electroneutral Newman thermodynamic factor χ^* as below.

$$\chi^* = \frac{y_0(1-y_0)\overline{X}^{\mathrm{B}}_{00}}{RT} = \chi^{\mathrm{m}}_{\mathrm{ee}} + \chi^{\mathrm{el}} \tag{3.75}$$

Note that a simple addition of the term χ^{el} to $\chi^{\mathrm{m}}_{\mathrm{ee}}$ provides the necessary electrical dependence for the non-electroneutral Newman thermodynamic factor. Eq.(3.75) can be rearranged in favour of $\overline{X}^{\mathrm{B}}_{00}$ so as to allow the core-thermodynamic-factor matrix $\overline{\mathbf{X}}^{\mathrm{B}}_+$ to be written in terms of χ^*. When eq.(3.67) is evaluated with the updated $\overline{\mathbf{X}}^{\mathrm{B}}_+$, the electrochemical-potential differentials bear the following forms

$$\begin{aligned}
\frac{d\mu_0}{RT} &= \left[\chi^{\mathrm{m}}_{\mathrm{ee}} + \chi^{\mathrm{el}} + y_0\chi^{\mathrm{E}}\right] d\ln y_0 \\
\frac{d\mu_+}{RT} &= \left[\chi^{\mathrm{m}}_{\mathrm{ee}} + \chi^{\mathrm{el}} + y_0\chi^{\mathrm{E}}\right] d\ln(1-y_0) - \frac{z_+z_-}{z_- - z_+}\left[e^{-z_-\phi} - e^{-z_+\phi} + 1 - \frac{z_+}{z_-}\right] d\phi\,, \\
\frac{d\mu_-}{RT} &= \left[\chi^{\mathrm{m}}_{\mathrm{ee}} + \chi^{\mathrm{el}} + y_0\chi^{\mathrm{E}}\right] d\ln(1-y_0) + \frac{z_+z_-}{z_- - z_+}\left[e^{-z_+\phi} - e^{-z_-\phi} + 1 - \frac{z_-}{z_+}\right] d\phi
\end{aligned} \tag{3.76}$$

where

$$\chi^{\mathrm{E}} = -\frac{z_+ z_- \left(e^{-z_+\phi} - e^{-z_-\phi}\right)^2}{(z_- - z_+)\left(z_+ e^{-z_+\phi} - z_- e^{-z_-\phi}\right)} = -\frac{\overline{\mathrm{P}}^2}{2F^2(1-y_0)\overline{I}^{\mathrm{B}}}. \tag{3.77}$$

It is fair to expect the electrochemical potential of the neutral solvent to be independent of the Poisson–Boltzmann overpotential, so $\chi^{\mathrm{el}} = -y_0\chi^{\mathrm{E}}$ is chosen to annihilate the ϕ-dependence in $d\mu_0$. The electrochemical-potential differentials then reduce to

$$\begin{aligned} d\mu_0 &= RT\chi^{\mathrm{m}}_{\mathrm{ee}} d\ln y_0 \\ d\mu_+ &= RT\chi^{\mathrm{m}}_{\mathrm{ee}} d\ln(1-y_0) + \left(Fz_+ - \frac{\overline{\mathrm{P}}}{1-y_0}\right) d\Phi\,, \\ d\mu_- &= RT\chi^{\mathrm{m}}_{\mathrm{ee}} d\ln(1-y_0) + \left(Fz_- - \frac{\overline{\mathrm{P}}}{1-y_0}\right) d\Phi \end{aligned} \tag{3.78}$$

after converting ϕ to the naive potential Φ. One can observe that the electrical part now contains a correction term proportional to the excess charge density $\overline{\mathrm{P}}$, which disappears under electroneutrality; thus, $d\mu_+$ and $d\mu_-$ reduce to the usual forms Guggenheim constructed when electroneutral. Bringing together equations (3.72) and (3.75), the full core-thermodynamic-factor matrix $\overline{\mathbf{X}}^{\mathrm{B}}_+$ can be written as

$$\overline{\mathbf{X}}^{\mathrm{B}}_+ = \begin{bmatrix} \overline{X}^{\mathrm{B}}_{00} & \overline{X}^{\mathrm{B}}_{+0} \\ \overline{X}^{\mathrm{B}}_{+0} & \overline{X}^{\mathrm{B}}_{++} \end{bmatrix} = \frac{RT}{1-y_0} \begin{bmatrix} \frac{\chi^{\mathrm{m}}_{\mathrm{ee}}}{y_0} + \frac{\overline{\mathrm{P}}^2}{2F^2(1-y_0)\overline{I}^{\mathrm{B}}} & \frac{(z_- - z_+)\overline{\mathrm{P}}}{2F\overline{I}^{\mathrm{B}}} \\ \frac{(z_- - z_+)\overline{\mathrm{P}}}{2F\overline{I}^{\mathrm{B}}} & \frac{(1-y_0)(z_- - z_+)^2}{2\overline{I}^{\mathrm{B}}} \end{bmatrix}. \tag{3.79}$$

It is noted that its determinant —which should be non-negative due to the positive semi-definite nature of $\overline{\mathbf{X}}^{\mathrm{B}}_+$— is directly proportional to $\chi^{\mathrm{m}}_{\mathrm{ee}}$. Hence, thermodynamic stability is retained as long as $\chi^{\mathrm{m}}_{\mathrm{ee}} \geqslant 0$.

3.4.2 Case II. The three-ion ionic liquid

The electroneutral reference composition for the system $\{+1, +2, -\}$ is

$$\left\{y^0_{+1}, y^0_{+2}, y^0_-\right\} = \left\{y_{+1}, \frac{z_- + y_{+1}(z_{+1} - z_-)}{z_- - z_{+2}}, -\frac{z_{+2} + y_{+1}(z_{+1} - z_{+2})}{z_- - z_{+2}}\right\}. \tag{3.80}$$

If the system deviates away from this composition, it attains an excess charge and its density is

$$\begin{aligned}\overline{\mathrm{P}} =& \frac{F}{z_- - z_{+2}} \left[y_{+1} z_{+1} (z_- - z_{+2}) e^{-z_{+1}\phi} \right. \\ & \left. + z_{+2} (y_{+1}(z_{+1} - z_-) + z_-) e^{-z_{+2}\phi} - z_- (y_{+1}(z_{+1} - z_{+2}) + z_{+2}) e^{-z_-\phi} \right],\end{aligned} \tag{3.81}$$

using $\phi = F\Phi_{\mathrm{P}}/RT$ as a dimensionless Poisson–Boltzmann overpotential. The ionic strength is

$$\begin{aligned}\overline{I}^{\mathrm{B}} =& \frac{1}{2(z_- - z_{+2})} \left[y_{+1} z_{+1}^2 (z_- - z_{+2}) e^{-z_{+1}\phi} \right. \\ & \left. + z_{+2}^2 (y_{+1}(z_{+1} - z_-) + z_-) e^{-z_{+2}\phi} - z_-^2 (y_{+1}(z_{+1} - z_{+2}) + z_{+2}) e^{-z_-\phi} \right].\end{aligned} \tag{3.82}$$

The entries to the thermodynamic-factor matrix that correspond to the charging ion are

$$\overline{X}^{\mathrm{B}}_{+2+1} = \frac{RT(z_- - z_{+2})^2}{2\overline{I}^{\mathrm{B}}} \delta, \qquad \overline{X}^{\mathrm{B}}_{+2+2} = \frac{RT(z_- - z_{+2})^2}{2\overline{I}^{\mathrm{B}}}, \tag{3.83}$$

where

$$\delta = \frac{z_{+1}(z_{+2} - z_-) e^{-z_{+1}\phi} + z_{+2}(z_- - z_{+1}) e^{-z_{+2}\phi} + z_-(z_{+1} - z_{+2}) e^{-z_-\phi}}{(z_- - z_{+2})^2}. \tag{3.84}$$

δ in this case cannot be succinctly expressed in terms of the molar excess charge $\overline{\mathrm{P}}$ as in the binary-electrolyte case. Like before, one can obtain Newman's electroneutral thermodynamic-factor matrix $\boldsymbol{\chi}_{+2}$ by enforcing electroneutrality.

$$\boldsymbol{\chi}_{+2} = \begin{bmatrix} \chi_{+1+1} \\ \chi_{+2+1} \\ \chi_{-+1} \end{bmatrix} = \frac{1}{RT} \begin{bmatrix} y_{+1}(1 - y_{+1}) \overline{X}^{\mathrm{B}}_{+1+1} \\ -y_{+1} y^0_{+2} \overline{X}^{\mathrm{B}}_{+1+1} \\ -y_{+1} y^0_{-} \overline{X}^{\mathrm{B}}_{+1+1} \end{bmatrix} \Bigg|_{\overline{\mathrm{P}}=0} \tag{3.85}$$

Again, comparing $d\mu_{\mathrm{e}2}$ constructed using the elements of $\boldsymbol{\chi}_{+2}$ in eq.(3.85) (by rearranging eq.(3.68)) and $d\mu_{\mathrm{e}2} = \nu_{\mathrm{e}2} RT \chi^{\mathrm{m}}_{\mathrm{ee}} d\ln y_{\mathrm{e}2}$ involving the measurable thermody-

namic factor $\chi_{\mathrm{ee}}^{\mathrm{m}}$, cf. eq.(4.13), one attains

$$\chi_{\mathrm{ee}}^{\mathrm{m}} = -\frac{\nu_{+1}}{\nu_{\mathrm{e}1}}\left[\frac{\nu_{+2}}{y_{+2}^{0}}\chi_{+2+1} + \frac{\nu_{-}^{\mathrm{e}2}}{y_{-}^{0}}\chi_{-+1}\right] y_{\mathrm{e}2}, \tag{3.86}$$

where the thermodynamic-factor measurement is conducted by adding the binary salt $(+2,-)$ to the system composed of two binary salts $(+1,-)$ and $(+2,-)$. Note that $\nu_{\mathrm{e}1} = \nu_{+1} + \nu_{-}^{\mathrm{e}1}$ and $\nu_{\mathrm{e}2} = \nu_{+2} + \nu_{-}^{\mathrm{e}2}$ indicate the total number of ions in salts $(+1,-)$ and $(+2,-)$, repectively, and $y_{\mathrm{e}1} = y_{+1}/\nu_{+1} = y_{-}^{\mathrm{e}1}/\nu_{-}^{\mathrm{e}1}$ and $y_{\mathrm{e}2} = y_{+2}/\nu_{+2} = y_{-}^{\mathrm{e}2}/\nu_{-}^{\mathrm{e}2}$ indicate the particle fraction of each salt. $y_{-}^{\mathrm{e}1}$ and $y_{-}^{\mathrm{e}2}$ are the particle fractions of the anion released from each salt, which add up to the total anion particle fraction, i.e., $y_{-} = y_{-}^{\mathrm{e}1} + y_{-}^{\mathrm{e}2}$. Then, the non-electroneutral Newman thermodynamic factor χ^{*}, with χ^{el} encapsulating any electrical dependence, can be written by expanding eq.(3.86).

$$\begin{aligned}\chi^{*} = \chi_{\mathrm{ee}}^{\mathrm{m}} + \chi^{\mathrm{el}} =& \frac{\nu_{\mathrm{e}2}\nu_{+1}}{RT\nu_{\mathrm{e}1}} y_{+1}y_{\mathrm{e}2}\,\overline{X}_{+1+1}^{\mathrm{B}}\Big|_{\overline{\mathrm{P}}=0} + \chi^{\mathrm{el}} \\ =& \frac{\nu_{+1} - \nu_{\mathrm{e}1}y_{+1}}{RT\nu_{\mathrm{e}1}} y_{+1}\overline{X}_{+1+1}^{\mathrm{B}}\end{aligned} \tag{3.87}$$

There is no constraint placed on χ^{el}, so we have chosen to give χ^{*} the same functional dependence as in the electroneutral case, arriving at the second line of eq.(3.87) (note that a substitution $\nu_{\mathrm{e}2}y_{\mathrm{e}2} \to 1 - \nu_{\mathrm{e}1}y_{+1}/\nu_{+1}$ was made). The differential expressions for the three electrochemical potentials can now be written as

$$\begin{aligned}\frac{d\mu_{+1}}{RT} =& \left[\frac{\nu_{\mathrm{e}1}(1-y_{+1})}{\nu_{+1} - \nu_{\mathrm{e}1}y_{+1}}\left(\chi_{\mathrm{ee}}^{\mathrm{m}} + \chi^{\mathrm{el}}\right) + y_{+1}\chi^{\mathrm{E}}\right] d\ln y_{+1} \\ &- \frac{z_{+1}}{z_{-} - z_{+2}}\left[\left(1 + e^{-z_{-}\phi} - e^{-z_{+1}\phi}\right) z_{-} - \left(1 + e^{-z_{+2}\phi} - e^{-z_{+1}\phi}\right) z_{+2}\right] d\phi \\ \frac{d\mu_{+2}}{RT} =& \left[\frac{\nu_{\mathrm{e}1}(1-y_{+1})}{\nu_{+1} - \nu_{\mathrm{e}1}y_{+1}}\left(\chi_{\mathrm{ee}}^{\mathrm{m}} + \chi^{\mathrm{el}}\right) + y_{+1}\chi^{\mathrm{E}}\right] d\ln\left(1 - y_{+1}\right) \\ &- \frac{z_{+2}z_{-}}{z_{-} - z_{+2}}\left[e^{-z_{-}\phi} - e^{-z_{+2}\phi} + 1 - \frac{z_{+2}}{z_{-}}\right] d\phi \\ \frac{d\mu_{-}}{RT} =& \left[\frac{\nu_{\mathrm{e}1}(1-y_{+1})}{\nu_{+1} - \nu_{\mathrm{e}1}y_{+1}}\left(\chi_{\mathrm{ee}}^{\mathrm{m}} + \chi^{\mathrm{el}}\right) + y_{+1}\chi^{\mathrm{E}}\right] d\ln\left(1 - y_{+1}\right) \\ &+ \frac{z_{+2}z_{-}}{z_{-} - z_{+2}}\left[e^{-z_{+2}\phi} - e^{-z_{-}\phi} + 1 - \frac{z_{-}}{z_{+2}}\right] d\phi\end{aligned} \quad , \tag{3.88}$$

where

$$\chi^{\mathrm{E}} = -\frac{(1-y_{+1})(z_- - z_{+2})^2}{2\overline{I}^{\mathrm{B}}}\delta^2. \tag{3.89}$$

To determine χ^{el}, the electrochemical potential of the salt $(+2,-)$ is investigated, which is $d\mu_{\mathrm{e}2} = \nu_{+2}d\mu_{+2} + \nu_-^{\mathrm{e}2}d\mu_-$. After converting its composition dependence to be on a neutral species, i.e., from dy_{+1} to $dy_{\mathrm{e}2}$ *via* the phase rule, it follows that the chemical part of $d\mu_{\mathrm{e}2}$ must be independent of the electric potential. This is achieved when

$$\chi^{\mathrm{el}} = -y_{+1}\chi^{\mathrm{E}} \times \frac{\nu_{+1} - \nu_{\mathrm{e}1}y_{+1}}{\nu_{\mathrm{e}1}(1-y_{+1})}. \tag{3.90}$$

This result is corroborated by looking at the definiteness of $\overline{\mathbf{X}}^{\mathrm{B}}_{+2}$. All entries of the matrix are known from eq.(3.83) except $\overline{X}^{\mathrm{B}}_{+1+1}$. In order for the system to remain thermodynamically stable across all compositions, the Gibbs free energy must be concave upward. The core-thermodynamic-factor matrix is the Hessian (second-order partial derivative) of the Gibbs free energy, and linear algebra dictates that convexity is guaranteed when the Hessian is non-negative definite. This means that the determinant of $\overline{\mathbf{X}}^{\mathrm{B}}_{+2}$ must be non-negative, giving rise to a constraint

$$\overline{X}^{\mathrm{B}}_{+1+1} \geqslant \frac{RT(z_- - z_{+2})^2}{2\overline{I}^{\mathrm{B}}}\delta^2,$$

or equivalently,

$$\chi^{\mathrm{m}}_{\mathrm{ee}} \geqslant -y_{+1}\chi^{\mathrm{E}} \times \frac{\nu_{+1} - \nu_{\mathrm{e}1}y_{+1}}{\nu_{\mathrm{e}1}(1-y_{+1})} - \chi^{\mathrm{el}}. \tag{3.91}$$

A species' free energy is expected to increase as more of it is added to the system, so it is likely that the thermodynamic factor of the added salt is non-negative, i.e., $\chi^{\mathrm{m}}_{\mathrm{ee}} \geqslant 0$. This is supported experimentally, at least for binary electrolytes [4, 158–162]. $\chi^{\mathrm{m}}_{\mathrm{ee}} \geqslant 0$ is guaranteed when eq.(3.90) holds true, indicating the validity of this choice. Also, this choice of χ^{el} conveniently cancels out the electrical dependence in the chemical

part of the electrochemical-potential differentials. Thus, $d\mu_i$'s finally come down to

$$\begin{aligned}
d\mu_{+1} &= \frac{RT\nu_{\mathrm{e}1}(1-y_{+1})}{\nu_{+1}-\nu_{\mathrm{e}1}y_{+1}}\chi_{\mathrm{ee}}^{\mathrm{m}}\,d\ln y_{+1} \\
&\quad + Fz_{+1}\left[1-\exp\left(\frac{Fz_{+1}\Phi}{RT}\right)+\frac{z_{+2}\exp\left(\frac{Fz_{+2}\Phi}{RT}\right)-z_{-}\exp\left(\frac{Fz_{-}\Phi}{RT}\right)}{z_{+2}-z_{-}}\right]d\Phi \\
&= \frac{RT\nu_{\mathrm{e}1}(1-y_{+1})}{\nu_{+1}-\nu_{\mathrm{e}1}y_{+1}}\chi_{\mathrm{ee}}^{\mathrm{m}}\,d\ln y_{+1}+Fz_{+1}\left[1-\frac{\overline{\mathrm{P}}}{Fz_{+1}y_{+1}}\right. \\
&\quad \left.+\frac{z_{-}z_{+2}}{(z_{-}-z_{+2})z_{+1}}\times\frac{1-y_{+1}}{y_{+1}}\left\{\exp\left(\frac{Fz_{+2}\Phi}{RT}\right)-\exp\left(\frac{Fz_{-}\Phi}{RT}\right)\right\}\right]d\Phi \\
d\mu_{+2} &= \frac{RT\nu_{\mathrm{e}1}(1-y_{+1})}{\nu_{+1}-\nu_{\mathrm{e}1}y_{+1}}\chi_{\mathrm{ee}}^{\mathrm{m}}\,d\ln(1-y_{+1}) \\
&\quad + Fz_{+2}\left[1-\frac{z_{-}}{z_{-}-z_{+2}}\left\{\exp\left(\frac{Fz_{+2}\Phi}{RT}\right)-\exp\left(\frac{Fz_{-}\Phi}{RT}\right)\right\}\right]d\Phi \\
d\mu_{-} &= \frac{RT\nu_{\mathrm{e}1}(1-y_{+1})}{\nu_{+1}-\nu_{\mathrm{e}1}y_{+1}}\chi_{\mathrm{ee}}^{\mathrm{m}}\,d\ln(1-y_{+1}) \\
&\quad + Fz_{-}\left[1-\frac{z_{+2}}{z_{-}-z_{+2}}\left\{\exp\left(\frac{Fz_{+2}\Phi}{RT}\right)-\exp\left(\frac{Fz_{-}\Phi}{RT}\right)\right\}\right]d\Phi,
\end{aligned} \tag{3.92}$$

after converting ϕ to Φ. It is noted that the chemical parts simplify when y_{+1} is converted back to $y_{\mathrm{e}2}$ *via* $\nu_{\mathrm{e}2}y_{\mathrm{e}2}=1-\nu_{\mathrm{e}1}y_{+1}/\nu_{+1}$ under electroneutrality. On the other hand, the correction terms in the electrical parts do not simplify further down to be proportional to the excess charge density, as in the binary-electrolyte case. Finally, the core-thermodynamic-factor matrix can be written as

$$\overline{\mathbf{X}}_{+2}^{\mathrm{B}}=RT\begin{bmatrix}\frac{\nu_{\mathrm{e}1}}{y_{+1}(\nu_{+1}-\nu_{\mathrm{e}1}y_{+1})}\chi_{\mathrm{ee}}^{\mathrm{m}}+\frac{(z_{-}-z_{+2})^2}{2\overline{I}^{\mathrm{B}}}\delta^2 & \frac{(z_{-}-z_{+2})^2}{2\overline{I}^{\mathrm{B}}}\delta \\ \frac{(z_{-}-z_{+2})^2}{2\overline{I}^{\mathrm{B}}}\delta & \frac{(z_{-}-z_{+2})^2}{2\overline{I}^{\mathrm{B}}}\end{bmatrix}. \tag{3.93}$$

For the scenario where $(+2,-)$ is added to a ternary salt $(+1,+2,-)$, equations (3.86) – (3.93) are still valid, except ν_{+1} should be replaced with $\nu_{+1}^{\mathrm{e}1}$ and ν_{+2} with $\nu_{+2}^{\mathrm{e}2}$, where the superscripts e1 and e2 denote the salts $(+1,+2,-)$ and $(+2,-)$, respectively.

3.4.3 Case III. The binary salt in two neutral solvents

The electroneutral reference composition for $\{0, \mathrm{o}, -, +\}$ is

$$\left\{y_0^0, y_\mathrm{o}^0, y_-^0, y_+^0\right\} = \left\{y_0, y_\mathrm{o}, \frac{z_+(1-y_0-y_\mathrm{o})}{z_+-z_-}, -\frac{z_-(1-y_0-y_\mathrm{o})}{z_+-z_-}\right\}. \tag{3.94}$$

Given that ions in the system are Boltzmann-distributed, the excess charge density is

$$\overline{\mathrm{P}} = \frac{Fz_+z_-}{z_+-z_-}(1-y_0-y_\mathrm{o})\left(e^{-z_-\phi}-e^{-z_+\phi}\right) \tag{3.95}$$

and the ionic strength is

$$\overline{I}^\mathrm{B} = \frac{z_+z_-}{2(z_+-z_-)}(1-y_0-y_\mathrm{o})\left(z_-e^{-z_-\phi}-z_+e^{-z_+\phi}\right), \tag{3.96}$$

where $\phi = F\Phi_\mathrm{P}/RT$ is a dimensionless Poisson–Boltzmann overpotential, as usual. Three entries of the thermodynamic-factor matrix corresponding to the charging ion can be evaluated straight away,

$$\overline{X}^\mathrm{B}_{-0} = \overline{X}^\mathrm{B}_{-\mathrm{o}} = -\frac{RT(z_+-z_-)^2}{2\overline{I}^\mathrm{B}}\delta, \qquad \overline{X}^\mathrm{B}_{--} = \frac{RT(z_+-z_-)^2}{2\overline{I}^\mathrm{B}} \tag{3.97}$$

where

$$\delta = \frac{z_+z_-\left(e^{-z_+\phi}-e^{-z_-\phi}\right)}{(z_+-z_-)^2} = -\frac{\overline{\mathrm{P}}}{F(z_+-z_-)(1-y_0-y_\mathrm{o})}. \tag{3.98}$$

Due to the extra solvent o, Newman's electroneutral thermodynamic factors are now arranged in a 4×2 matrix, $\boldsymbol{\chi}_{-}$.

$$\begin{aligned}\boldsymbol{\chi}_{-} &= \begin{bmatrix} \chi_{00} & \chi_{0o} \\ \chi_{o0} & \chi_{oo} \\ \chi_{-0} & \chi_{-o} \\ \chi_{+0} & \chi_{+o} \end{bmatrix} \\ &= \frac{1}{RT} \begin{bmatrix} y_0\left((1-y_0)\overline{X}^{\mathrm{B}}_{00} - y_{\mathrm{o}}\overline{X}^{\mathrm{B}}_{\mathrm{o}0}\right) & y_0\left((1-y_0)\overline{X}^{\mathrm{B}}_{0\mathrm{o}} - y_{\mathrm{o}}\overline{X}^{\mathrm{B}}_{\mathrm{oo}}\right) \\ -y_{\mathrm{o}}\left(y_0\overline{X}^{\mathrm{B}}_{00} - (1-y_{\mathrm{o}})\overline{X}^{\mathrm{B}}_{\mathrm{o}0}\right) & -y_{\mathrm{o}}\left(y_0\overline{X}^{\mathrm{B}}_{0\mathrm{o}} - (1-y_{\mathrm{o}})\overline{X}^{\mathrm{B}}_{\mathrm{oo}}\right) \\ -y^0_{-}\left(y_0\overline{X}^{\mathrm{B}}_{00} + y_{\mathrm{o}}\overline{X}^{\mathrm{B}}_{\mathrm{o}0}\right) & -y^0_{-}\left(y_0\overline{X}^{\mathrm{B}}_{0\mathrm{o}} + y_{\mathrm{o}}\overline{X}^{\mathrm{B}}_{\mathrm{oo}}\right) \\ -y^0_{+}\left(y_0\overline{X}^{\mathrm{B}}_{00} + y_{\mathrm{o}}\overline{X}^{\mathrm{B}}_{\mathrm{o}0}\right) & -y^0_{+}\left(y_0\overline{X}^{\mathrm{B}}_{0\mathrm{o}} + y_{\mathrm{o}}\overline{X}^{\mathrm{B}}_{\mathrm{oo}}\right) \end{bmatrix}\Bigg|_{\overline{\mathrm{P}}=0} \end{aligned} \tag{3.99}$$

Comparison between $d\mu_{\mathrm{o}}$ and $d\mu_{\mathrm{e}}$ constructed using the elements of $\boldsymbol{\chi}_{-}$ in eq.(3.99) (by rearranging eq.(3.68)) and

$$d\mu_{\mathrm{o}} = \frac{RT}{y_{\mathrm{o}}}\left[\chi^{\mathrm{m}}_{\mathrm{oo}}\, dy_{\mathrm{o}} + \chi^{\mathrm{m}}_{\mathrm{oe}}\, dy\right] \quad \text{and} \quad d\mu_{\mathrm{e}} = \frac{\nu RT}{y}\left[\chi^{\mathrm{m}}_{\mathrm{eo}}\, dy_{\mathrm{o}} + \chi^{\mathrm{m}}_{\mathrm{ee}}\, dy\right] \tag{3.100}$$

cf., eq.(4.20) (where y_{o} and the salt particle fraction y are chosen as independent composition variables; note $dy_0 = -dy_{\mathrm{o}} - \nu dy$ *via* the phase rule) enables parameterisation of the (measurable) thermodynamic factors in terms of the electroneutral Newman thermodynamic factors. Assuming the same parameterisation holds for non-electroneutral regions, non-electroneutral Newman thermodynamic factors (indicated by asterisks)

can be written as

$$\begin{aligned}
\chi^*_{\mathrm{eo}} &= (\chi_{+\mathrm{o}} + \chi_{-\mathrm{o}} - \chi_{+0} - \chi_{-0})/\nu = \chi^{\mathrm{m}}_{\mathrm{eo}} + \chi^{\mathrm{el}}_{\mathrm{eo}} \\
\chi^*_{\mathrm{ee}} &= -\chi_{+0} - \chi_{-0} = \chi^{\mathrm{m}}_{\mathrm{ee}} + \chi^{\mathrm{el}}_{\mathrm{ee}} \\
\chi^*_{\mathrm{oe}} &= -\nu\chi_{\mathrm{o}0} = \chi^{\mathrm{m}}_{\mathrm{oe}} + \chi^{\mathrm{el}}_{\mathrm{oe}} \\
\chi^*_{\mathrm{oo}} &= \chi_{\mathrm{oo}} - \chi_{\mathrm{o}0} = \chi^{\mathrm{m}}_{\mathrm{oo}} + \chi^{\mathrm{el}}_{\mathrm{oo}}
\end{aligned} \quad . \tag{3.101}$$

As shown in the second set of equalities, χ^*_{ij} are partitioned into a measurable part (superscript m) under electroneutrality and an electrical part (superscript el). Denoting

$$\chi^{\mathrm{E}} = \frac{z_+ z_- \left(e^{-z_+\phi} - e^{-z_-\phi}\right)^2}{(z_+ - z_-)\left(z_+ e^{-z_+\phi} - z_- e^{-z_-\phi}\right)} = -\frac{\overline{\mathrm{P}}^2}{2F^2(1 - y_0 - y_{\mathrm{o}})\overline{I}^{\mathrm{B}}}, \tag{3.102}$$

the electrochemical-potential differentials can be written as

$$\begin{aligned}
d\mu_0 =& \frac{RT}{y_0}\left[\left\{\chi^*_{\mathrm{ee}} + \frac{\chi^*_{\mathrm{oe}}}{\nu} + y_0\chi^{\mathrm{E}}\right\} dy_{\mathrm{o}} + \left\{\chi^*_{\mathrm{ee}} - \chi^*_{\mathrm{oo}} - \nu\chi^*_{\mathrm{eo}} + \frac{\chi^*_{\mathrm{oe}}}{\nu} + y_0\chi^{\mathrm{E}}\right\} dy_{\mathrm{o}}\right] \\
d\mu_{\mathrm{o}} =& \frac{RT}{y_{\mathrm{o}}}\left[\left\{-\frac{\chi^*_{\mathrm{oe}}}{\nu} + y_{\mathrm{o}}\chi^{\mathrm{E}}\right\} dy_0 + \left\{\chi^*_{\mathrm{oo}} - \frac{\chi^*_{\mathrm{oe}}}{\nu} + y_{\mathrm{o}}\chi^{\mathrm{E}}\right\} dy_{\mathrm{o}}\right] \\
d\mu_- =& \frac{RT}{1 - y_0 - y_{\mathrm{o}}}\left[-\left\{\chi^*_{\mathrm{ee}} + (y_0 + y_{\mathrm{o}})\chi^{\mathrm{E}}\right\} dy_0 \left\{\nu\chi^*_{\mathrm{eo}} - \chi^*_{\mathrm{ee}} - (y_0 + y_{\mathrm{o}})\chi^{\mathrm{E}}\right\} dy_{\mathrm{o}}\right] \\
&+ RT\frac{z_+ z_-}{z_- - z_+}\left[e^{-z_+\phi} - e^{-z_-\phi} + 1 - \frac{z_-}{z_+}\right] d\phi \\
d\mu_+ =& \frac{RT}{1 - y_0 - y_{\mathrm{o}}}\left[-\left\{\chi^*_{\mathrm{ee}} + (y_0 + y_{\mathrm{o}})\chi^{\mathrm{E}}\right\} dy_0 \left\{\nu\chi^*_{\mathrm{eo}} - \chi^*_{\mathrm{ee}} - (y_0 + y_{\mathrm{o}})\chi^{\mathrm{E}}\right\} dy_{\mathrm{o}}\right] \\
&+ RT\frac{z_+ z_-}{z_- - z_+}\left[e^{-z_+\phi} - e^{-z_-\phi} - 1 + \frac{z_+}{z_-}\right] d\phi
\end{aligned} \quad . \tag{3.103}$$

Since both solvents are neutral, the electric-potential dependence in $d\mu_0$ and $d\mu_{\mathrm{o}}$ must be nullified, generating two equations to be solved simultaneously. Evaluating them using Mathematica, the desired result is achieved if

$$\chi^{\mathrm{el}}_{\mathrm{oo}} = \chi^{\mathrm{el}}_{\mathrm{eo}} = 0, \quad \chi^{\mathrm{el}}_{\mathrm{ee}} = -(y_0 + y_{\mathrm{o}})\chi^{\mathrm{E}}, \quad \text{and} \quad \chi^{\mathrm{el}}_{\mathrm{oe}} = \nu y_{\mathrm{o}}\chi^{\mathrm{E}}. \tag{3.104}$$

Incorporating these and converting ϕ back to the naive electric potential Φ produces

the following differential expressions.

$$\begin{aligned}
d\mu_0 &= -\frac{RT}{y_0}\left[\{\chi^{\mathrm{m}}_{\mathrm{oo}}+\nu\chi^{\mathrm{m}}_{\mathrm{eo}}\}\,dy_{\mathrm{o}}+\{\chi^{\mathrm{m}}_{\mathrm{oe}}+\nu\chi^{\mathrm{m}}_{\mathrm{ee}}\}\,\frac{d(1-y_0-y_{\mathrm{o}})}{\nu}\right]\\
d\mu_{\mathrm{o}} &= \frac{RT}{y_{\mathrm{o}}}\left[\chi^{\mathrm{m}}_{\mathrm{oo}}\,dy_{\mathrm{o}}+\chi^{\mathrm{m}}_{\mathrm{oe}}\frac{d(1-y_0-y_{\mathrm{o}})}{\nu}\right]\\
d\mu_- &= \frac{\nu RT}{1-y_0-y_{\mathrm{o}}}\left[\chi^{\mathrm{m}}_{\mathrm{eo}}\,dy_{\mathrm{o}}+\chi^{\mathrm{m}}_{\mathrm{ee}}\frac{d(1-y_0-y_{\mathrm{o}})}{\nu}\right]+\left[Fz_- -\frac{\overline{\mathrm{P}}}{1-y_0-y_{\mathrm{o}}}\right]d\Phi\\
d\mu_+ &= \frac{\nu RT}{1-y_0-y_{\mathrm{o}}}\left[\chi^{\mathrm{m}}_{\mathrm{eo}}\,dy_{\mathrm{o}}+\chi^{\mathrm{m}}_{\mathrm{ee}}\frac{d(1-y_0-y_{\mathrm{o}})}{\nu}\right]+\left[Fz_+ -\frac{\overline{\mathrm{P}}}{1-y_0-y_{\mathrm{o}}}\right]d\Phi
\end{aligned} \tag{3.105}$$

If the system is electroneutral, the above differentials can be simplified further by recognising $1-y_0-y_{\mathrm{o}}=y_++y_-=\nu y$. As in the binary-electrolyte case, the electrical part is corrected by a term proportional to the excess charge density.

To establish the core-thermodynamic-factor matrix, rearrange eq.(3.101) in terms of $\overline{X}^{\mathrm{B}}_{ij}$ and substitute the electrical parts obtained in eq.(3.104). $\overline{\mathbf{X}}^{\mathrm{B}}_-$ is a 3×3 matrix of the form

$$\overline{\mathbf{X}}^{\mathrm{B}}_- = \begin{bmatrix}
\overline{X}^{\mathrm{B}}_{00} & \overline{X}^{\mathrm{B}}_{0\mathrm{o}} & \overline{X}^{\mathrm{B}}_{0-}\\
\overline{X}^{\mathrm{B}}_{\mathrm{o}0} & \overline{X}^{\mathrm{B}}_{\mathrm{oo}} & \overline{X}^{\mathrm{B}}_{\mathrm{o}-}\\
\overline{X}^{\mathrm{B}}_{-0} & \overline{X}^{\mathrm{B}}_{-\mathrm{o}} & \overline{X}^{\mathrm{B}}_{--}
\end{bmatrix} \tag{3.106}$$

with each column expressed as

$$\begin{bmatrix} \overline{X}^{\mathrm{B}}_{00} \\ \overline{X}^{\mathrm{B}}_{\mathrm{o}0} \\ \overline{X}^{\mathrm{B}}_{-0} \end{bmatrix} = \frac{RT}{1-y_0-y_{\mathrm{o}}} \begin{bmatrix} \frac{1-y_{\mathrm{o}}}{y_0}\chi^{\mathrm{m}}_{\mathrm{ee}} + \frac{1-y_0-y_{\mathrm{o}}}{\nu y_0}\chi^{\mathrm{m}}_{\mathrm{oe}} - \chi^{\mathrm{E}} \\ \chi^{\mathrm{m}}_{\mathrm{ee}} - \frac{1-y_0-y_{\mathrm{o}}}{\nu y_{\mathrm{o}}}\chi^{\mathrm{m}}_{\mathrm{oe}} - \chi^{\mathrm{E}} \\ \frac{(z_+-z_-)\overline{\mathrm{P}}}{2F\overline{I}^{\mathrm{B}}} \end{bmatrix}$$

$$\begin{bmatrix} \overline{X}^{\mathrm{B}}_{0\mathrm{o}} \\ \overline{X}^{\mathrm{B}}_{\mathrm{oo}} \\ \overline{X}^{\mathrm{B}}_{-\mathrm{o}} \end{bmatrix} = \frac{RT}{1-y_0-y_{\mathrm{o}}} \begin{bmatrix} \frac{1-y_{\mathrm{o}}}{y_0}\left(\chi^{\mathrm{m}}_{\mathrm{ee}} - \nu\chi^{\mathrm{m}}_{\mathrm{eo}}\right) + \frac{1-y_0-y_{\mathrm{o}}}{\nu y_0}\left(\chi^{\mathrm{m}}_{\mathrm{oe}} - \nu\chi^{\mathrm{m}}_{\mathrm{oo}}\right) - \chi^{\mathrm{E}} \\ \chi^{\mathrm{m}}_{\mathrm{ee}} - \nu\chi^{\mathrm{m}}_{\mathrm{eo}} - \frac{1-y_0-y_{\mathrm{o}}}{\nu y_{\mathrm{o}}}\left(\chi^{\mathrm{m}}_{\mathrm{oe}} - \nu\chi^{\mathrm{m}}_{\mathrm{oo}}\right) - \chi^{\mathrm{E}} \\ \frac{(z_+-z_-)\overline{\mathrm{P}}}{2F\overline{I}^{\mathrm{B}}} \end{bmatrix}. \tag{3.107}$$

$$\begin{bmatrix} \overline{X}^{\mathrm{B}}_{0-} \\ \overline{X}^{\mathrm{B}}_{\mathrm{o}-} \\ \overline{X}^{\mathrm{B}}_{--} \end{bmatrix} = \frac{RT}{1-y_0-y_{\mathrm{o}}} \begin{bmatrix} \frac{(z_+-z_-)\overline{\mathrm{P}}}{2F\overline{I}^{\mathrm{B}}} \\ \frac{(z_+-z_-)\overline{\mathrm{P}}}{2F\overline{I}^{\mathrm{B}}} \\ \frac{(1-y_0-y_{\mathrm{o}})(z_+-z_-)^2}{2\overline{I}^{\mathrm{B}}} \end{bmatrix}$$

It is reminded that the last row and column of the matrix have already been evaluated in eq.(3.97). $\overline{\mathbf{X}}^{\mathrm{B}}_{-}$ is expected to be symmetric, so equating $\overline{X}^{\mathrm{B}}_{0\mathrm{o}}$ and $\overline{X}^{\mathrm{B}}_{\mathrm{o}0}$ produces a constraint such that

$$\chi^{\mathrm{m}}_{\mathrm{eo}} = \frac{1-y_0-y_{\mathrm{o}}}{\nu(1-y_{\mathrm{o}})}\left[\chi^{\mathrm{m}}_{\mathrm{ee}} - \chi^{\mathrm{m}}_{\mathrm{oo}} + \left(1+\frac{y_0}{y_{\mathrm{o}}}\right)\frac{\chi^{\mathrm{m}}_{\mathrm{oe}}}{\nu}\right]. \tag{3.108}$$

Thus, three thermodynamic factors suffice to parameterise thermodynamic non-idealities in this four-species system. Substituting this in, $\overline{X}^{\mathrm{B}}_{\mathrm{oo}}$ becomes

$$\overline{X}^{\mathrm{B}}_{\mathrm{oo}} = \frac{RT}{1-y_0-y_{\mathrm{o}}}\left[\frac{y_0}{1-y_{\mathrm{o}}}\chi^{\mathrm{m}}_{\mathrm{ee}} + \frac{1-y_0-y_{\mathrm{o}}}{y_{\mathrm{o}}\,(1-y_{\mathrm{o}})}\left\{\chi^{\mathrm{m}}_{\mathrm{oo}} - (1+y_0)\frac{\chi^{\mathrm{m}}_{\mathrm{oe}}}{\nu}\right\} - \chi^{\mathrm{E}}\right], \tag{3.109}$$

and the determinant of $\overline{\mathbf{X}}_{-}^{\mathrm{B}}$ is

$$|\overline{\mathbf{X}}_{-}^{\mathrm{B}}| = \frac{(RT)^3(z_- - z_+)^2}{2y_0y_\mathrm{o}(1-y_\mathrm{o})\overline{I}^{\mathrm{B}}}\left[-\frac{y_0+y_\mathrm{o}}{y_\mathrm{o}}\left(\frac{\chi_{\mathrm{oe}}^{\mathrm{m}}}{\nu}\right)^2 + (\chi_{\mathrm{oo}}^{\mathrm{m}} - \chi_{\mathrm{ee}}^{\mathrm{m}})\frac{\chi_{\mathrm{oe}}^{\mathrm{m}}}{\nu} + \frac{1-y_\mathrm{o}}{1-y_0-y_\mathrm{o}}\chi_{\mathrm{oo}}^{\mathrm{m}}\chi_{\mathrm{ee}}^{\mathrm{m}}\right]. \tag{3.110}$$

Remembering that $\overline{I}^{\mathrm{B}}$ is positive, the non-negative definiteness of $\overline{\mathbf{X}}_{-}^{\mathrm{B}}$ is guaranteed when $\chi_{\mathrm{oe}}^{\mathrm{m}}$ lies within the interval,

$$\frac{\nu y_\mathrm{o}}{2(y_0+y_\mathrm{o})}\left(\chi_{\mathrm{oo}}^{\mathrm{m}} - \chi_{\mathrm{ee}}^{\mathrm{m}} - \sqrt{\Delta}\right) \leqslant \chi_{\mathrm{oe}}^{\mathrm{m}} \leqslant \frac{\nu y_\mathrm{o}}{2(y_0+y_\mathrm{o})}\left(\chi_{\mathrm{oo}}^{\mathrm{m}} - \chi_{\mathrm{ee}}^{\mathrm{m}} + \sqrt{\Delta}\right) \tag{3.111}$$

where Δ is the discriminant defined as

$$\Delta = (\chi_{\mathrm{oo}}^{\mathrm{m}} - \chi_{\mathrm{ee}}^{\mathrm{m}})^2 + \frac{4(1-y_\mathrm{o})(y_0+y_\mathrm{o})}{y_\mathrm{o}(1-y_0-y_\mathrm{o})}\chi_{\mathrm{oo}}^{\mathrm{m}}\chi_{\mathrm{ee}}^{\mathrm{m}}. \tag{3.112}$$

Many papers report positive values for various salt thermodynamic factors $\chi_{\mathrm{ee}}^{\mathrm{m}}$ across a range of concentrations [4, 158–162]. It seems reasonable to assume that $\chi_{\mathrm{oo}}^{\mathrm{m}}$ will take a similar trend, too, because the electrochemical potential of a species should increase as more of it is added to the system. In this case, $\sqrt{\Delta}$ would always be real and both positive and negative values of $\chi_{\mathrm{oe}}^{\mathrm{m}}$ would be thermodynamically feasible. Negative thermodynamic factors have been observed experimentally; Nyman et al. [161] presented the thermodynamic factor for the EMC:EC cosolvent (with the single-solvent approximation) as a function of the salt concentration (i.e., essentially $\chi_{\mathrm{oe}}^{\mathrm{m}}$ at a fixed solvent ratio), which was negative across the concentration range studied and its absolute value was always smaller than the salt thermodynamic factor at the corresponding salt concentration. Eq.(3.111) becomes useful in situations where $\chi_{\mathrm{oe}}^{\mathrm{m}}$ is difficult to measure; a reasonable value can be ascribed to it based on the knowledge of the salt and solvent thermodynamic factors.

3.5 Summary and outlook

We set out to apply the core-potential theory to three simple electrolytic solutions in preparation for the more challenging system of charged membrane immersed in a binary electrolyte. Nonetheless, the utility of this chapter is not just limited to exemplar intermediary purposes. Many real electrochemical systems rely on these electrolytic solutions (e.g., ionic-liquid electrolytes for the next-generation batteries and cosolvent blends for the conventional Li-ion batteries, etc.), so the findings in this chapter have practical implications, especially in modelling.

The main outcomes of this chapter are summarised as follows.

1. The transport and MacInnes equations, as well as the accompanying transport properties for the three elected systems were derived using the core-potential gradients in sections 3.1 and 3.2. However, this approach was found to be not practical for systems with more than three species, especially if electroneutrality is to be relaxed.

2. As an alternative, correction terms for $d\mu_i$'s under non-electroneutrality were derived for the three cases in sections 3.3 and 3.4, by incorporating the Boltzmann distribution for charged species. These $d\mu_i$ expressions can be incorporated with the existing transport and continuity equations straightaway, making the core-potential theory more accessible to modellers working with the three simple electrolytic systems.

3. For the binary salt in two neutral solvents, symmetry in the Gibbs-free-energy Hessian was used to express a redundant thermodynamic factor in terms of three independent thermodynamic factors. This eliminates unnecessary thermodynamic-factor characterisation efforts.

4. The procedure in section 3.3 —which allows measurable thermodynamic factors and electrical correction terms to be introduced to the $d\mu_i$ expressions coherently— is more general than what Goyal and Monroe [1] provided. Thus,

the section is of benefit to those who aim to model more complicated systems, too.

Now, a barrier to using the derived $d\mu_i$ expressions is that the thermodynamic factors that appear in these expressions are unknown. Methods to parameterise them are investigated in the next chapter.

Chapter 4

Thermodynamic-factor characterisation

As illustrated in the previous chapter, thermodynamic factors are essential parameters if $d\mu_i$'s are to be expressed in terms of concentration gradients. One standard way of quantifying thermodynamic factors is to measure the composition dependence of the liquid-junction potential. The liquid-junction potential is a non-equilibrium property[1] that arises when two different concentrations of the same type of electrolytic solution come in contact, which can be measured easily and reliably using a concentration cell and a galvanostat [4, 158, 161–165]. In the standard concentration-cell experiment, two reservoirs containing solutions with different electrolyte concentrations are connected *via* a porous frit, which allows an electrochemical contact, while impeding interdiffusion, as illustrated in Figure 4.1. The concentration difference in the concentration cell induces a potential difference across the frit, which can be registered between reference electrodes immersed in the two reservoirs. If the dynamical losses due to mass transport are negligible, the diffusion potential so-measured is a state property,

[1] The voltage difference across the two solutions appears static, even though the system is not fully relaxed. This is because the increasing charge separation (due to different ions diffusing at different rates) and the decreasing charge density occur such that their rates of change oppose each other exactly, concealing dynamics in the system [166].

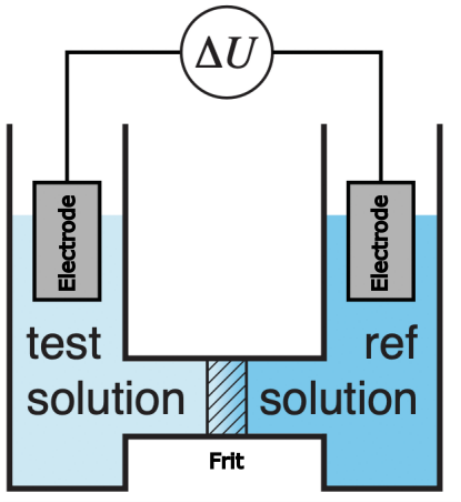

Figure 4.1: A schematic of the experimental setup to measure the liquid-junction potential using the concentration cell.

dependent only on the electrolyte compositions at either end of the cell[2]. Protocols for concentration-cell experiments have been described by Nyman et al. [161], Hou and Monroe [162], among others. A more precise measurement method called the 'shifting-reference concentration-cell' method, where multiple reference compositions are used to probe the liquid-junction potential differentially, was recently reported by Wang et al. [4].

This chapter employs the concentration-cell experiment as the main tool of analysis to extract thermodynamic information from the three electrolytic solutions of interest: (1) the binary electrolyte, (2) the three-ion ionic liquid, and (3) the binary salt in two neutral solvents. Section 4.1 establishes relationships between thermodynamic factors and concentration-cell voltage measurements for the three systems; the derivations closely trace the work of Newman and Thomas-Alyea [22] and Liu and Monroe [167]. In section 4.2, the theoretical investigation in the previous section is consolidated through a liquid-junction-potential parameterisation exercise for an actual binary salt in two neutral solvents. Specifically, lithium hexafluorophosphate ($LiPF_6$) in an ethyl-

[2]This can be checked by performing a series of concentration-cell experiments traversing different paths from one concentration to the other, e.g., A–B–C and A–B'–C, where each letter represents a specific solution composition. If the two paths generate the same voltage difference between A and C, i.e., if $\Delta U_{AB} + \Delta U_{BC} = \Delta U_{AB'} + \Delta U_{B'C}$, where ΔU_{IJ} refers to the liquid-junction potential between solutions I and J, then the liquid-junction potential qualifies as a state property.

methyl carbonate (EMC) – ethylene carbonate (EC) blend is chosen for its wide use in conventional Li-ion batteries. Contents in sections 4.1.3 and 4.2 have resulted in a peer-reviewed publication — see reference [5]. The use of cosolvent blends in Li-ion batteries is commonplace; hence, the impact of this publication is expected to be far-reaching, especially throughout the battery-modelling community. It is pointed out that section 4.2 was a collaborative effort. While all data processing was performed by the author, the liquid-junction-potential measurement data was provided by Dr A. Wang, an experimentalist who had been a student in the Monroe Group at the University of Oxford. The chapter then closes by exploring partial-pressure measurement as an alternative thermodynamic-factor characterisation method for cosolvent electrolytic solutions in section 4.3.

4.1 Measurable thermodynamic factors

4.1.1 Case I. The binary electrolyte

The system under investigation in this section is composed of an electrically neutral solvent (0) and a binary salt that dissociates into one type of cation (+) and one type of anion (−) upon coming in contact with the solvent. Since only the formula-unit salt can be introduced to the system when conducting experiments (as opposed to one of the ions discretely), it is more convenient to deal with the salt content as a whole. The electrochemical potential of the neutral salt can be written as

$$\mu_{\mathrm{e}} = \nu_+\mu_+ + \nu_-\mu_- = \mu_{\mathrm{e}}^{\theta} + \nu RT \ln\left(\lambda_{+-} y\right) + RT \ln\left(\nu_+^{\nu_+}\nu_-^{\nu_-}\right), \tag{4.1}$$

where $\mu_{\mathrm{e}}^{\theta}$ is the electrochemical potential of the salt in the standard state, ν_i is the number of ionic species i the electrolyte dissociates into, $\nu = \nu_+ + \nu_-$ is the total number of ions that are released upon dissociation, λ_{+-} is the particle-fraction activity coefficient of the salt, and $y = y_+/\nu_+ = y_-/\nu_-$ is the particle fraction of the salt. Due to the phase rule ($1 = y_0 + \nu y$), one particle fraction is sufficient to describe the

composition dependence of the system. Salt content, rather than solvent content, is typically controlled in experiments involving electrolytes, so Newman elects to write $\mu_e = \mu_e(y)$ [22]; the same convention is adopted here. With this functionality in mind, the differential form of the electrochemical potential of the salt can be expressed as

$$d\mu_e = \nu RT \chi_{ee}^{m} \, d\ln y, \tag{4.2}$$

where

$$\chi_{ee}^{m} = 1 + \left(\frac{\partial \ln \lambda_{+-}}{\partial \ln y} \right)_{T,p} \tag{4.3}$$

is the measurable (indicated by the superscript m) thermodynamic factor relating to the salt; it is the only independent thermodynamic factor in this system[3].

In a concentration-cell experiment, an electrode reaction takes place to equalise the salt concentration across the two reservoirs. A general electrode reaction for a binary electrolyte system can be written as

$$\sum_i A_i^{(\alpha)} + \sum_i B_i^{(\beta)} + s_+ M_+^{z+(\delta)} + s_- M_-^{z-(\delta)} + s_0 M_0^{(\delta)} \rightleftharpoons n_{e^-} e^{-(\alpha)}, \tag{4.4}$$

where A_i, B_i and M_i represent the species involved in the reaction, s_i is the corresponding stoichiometric coefficients, and n_{e^-} is the number of electrons involved in the reaction. Superscripts (α) and (δ) denote the electrode and solution phases, respectively, while (β) indicates any other phases that might be involved in the reaction. A charge balance for the reaction requires that the stoichiometric coefficients satisfy

[3]Starting with a 3×3 thermodynamic-factor matrix, the following reductions are made.

- Electroneutrality removes a column: knowing the particle fraction of one of the two ions immediately fixes the particle fraction of the other.
- Electroneutrality removes a row: the electrochemical potential of the salt is the weighted sum of the electrochemical potentials of the constituent ions. The weighting factors are the stoichiometric coefficients of the salt-dissociation reaction.
- The phase rule removes a column: knowing the particle fraction of the salt automatically determines the particle fraction of the solvent.
- The Gibbs–Duhem relation removes a row: it relates the electrochemical potentials of the solvent and the salt, so it is sufficient to know one of them to settle the other.

Thus, it shrinks to a 1×1 matrix.

$s_+z_+ + s_-z_- = n_{e^-}z_{e^-}$, where z_i is the equivalent charge of species i. When studying battery electrolytes, it is typical to use a reference electrode reversible only to cations, so that $s_0 = s_- = 0$, but we will retain the stoichiometric coefficients here to keep the analysis general. Reaction scheme in eq.(4.4) implies a relationship among the electrochemical potentials involved, namely,

$$\sum_i \mu_i^{(\alpha)} + \sum_i \mu_i^{(\beta)} + s_+\mu_+^{(\delta)} + s_-\mu_-^{(\delta)} + s_0\mu_0^{(\delta)} = n_{e^-}\mu_{e^-}^{(\alpha)}. \tag{4.5}$$

The liquid-junction potential ΔU quantifies the electrochemical-potential difference between electrons in the two electrodes that are immersed in the solutions on either side of the concentration cell; by definition $d\mu_{e^-} = Fz_{e^-}d\Phi$ at fixed T and p, where Φ is the electrical potential in the electrode. Presuming that the concentration cell in question uses symmetric half cells (i.e., the same electrode reactions occur at the two electrodes), μ_i in (α) and (β) phases cancel. Through eq.(4.5), the liquid-junction potential ΔU satisfies

$$Fz_{e^-}n_{e^-}\Delta U = s_+\int_\delta^{\delta'} d\mu_+ + s_-\int_\delta^{\delta'} d\mu_- + s_0\int_\delta^{\delta'} d\mu_0, \tag{4.6}$$

in which δ and δ' respectively designate the solutions residing in the reference chamber and test chamber of the concentration cell, and the integral is taken along a thermodynamic path that passes through the composition gradient in the frit.

One useful relationship between the electrochemical potentials and the current density $\vec{i}$ through the cell is [22],

$$\frac{1}{z_n}\nabla\mu_n = -\frac{F}{\kappa}\vec{i} - \sum_i \frac{t_i^0}{z_i}\left(\nabla\mu_i - \frac{z_i}{z_n}\nabla\mu_n\right) \tag{4.7}$$

where F is the Faraday constant, κ is the ionic conductivity, and t_i^0 is the transference number of species i (with respect to the reference frame moving at the same velocity as the solvent 0 on average). Incorporating the phase rule, the isothermal, isobaric Gibbs-

Duhem relation, $d\mu_{\mathrm{e}}(y)$ in eq.(4.2), as well as the fact that $\vec{i} = 0$ in concentration-cell experiments, ΔU can be written as

$$-\frac{F z_{\mathrm{e}^-} n_{\mathrm{e}^-} \Delta U}{\nu RT} = \int_{y^{(\delta)}}^{y^{(\delta')}} \left\{ \frac{s_0 y}{1-\nu y} - \frac{s_+}{\nu_+} + \left(\frac{s_+}{\nu_+} - \frac{s_-}{\nu_-} \right) t_+^0 \right\} \chi_{\mathrm{ee}}^{\mathrm{m}} \, d\ln y \,. \tag{4.8}$$

Thus, the liquid-junction potential measured between the identical reference electrodes at either end of the concentration cell relates to the cation transference number and the thermodynamic factor of the salt.

4.1.2 Case II. The three-ion ionic liquid

The system of interest in this section is unique in that it is composed of ions entirely with no neutral solvent present. A three-ion ionic liquid may exist as a naturally occurring ternary salt in the liquid phase (at a given temperature and pressure), or it may be formed as a result of mixing two binary salts with a common ion. As demonstrated for the binary electrolyte, the molar content of at least one species must remain unchanged during the concentration-cell experiment. Since only neutral salts can be introduced, a feasible experiment for this system would involve preparing solutions of different concentrations by adding different amounts of a binary salt (constructed from two constitutive ions in the ionic liquid) to the reference three-ion-ionic-liquid composition. With this limitation in mind, two types of concentration-cell experiments are examined in the following subsections — one involving a mixture of two binary salts and the other involving an inherent ternary salt.

Adding (+2, −) to a mixture of (+1, −) and (+2, −)

First, consider a system made up of two binary salts $(+1,-)$ and $(+2,-)$ (as done by Pollard and Newman [168]) and assume the amount of $(+2,-)$ is actively altered to conduct the concentration-cell experiment. A general electrode reaction can be written

as

$$\sum_i A_i^{(\alpha)} + \sum_i B_i^{(\beta)} + s_{+1} M_{+1}^{z_{+1}(\delta)} + s_{+2} M_{+2}^{z_{+2}(\delta)} + s_- M_-^{z_-(\delta)} \rightleftharpoons n_{\mathrm{e}^-} \mathrm{e}^{-(\alpha)}. \tag{4.9}$$

The electrochemical potentials of the two salts are

$$\mu_{\mathrm{e1}} = \nu_{+1}\mu_{+1} + \nu_-^{\mathrm{e1}}\mu_- \qquad \mu_{\mathrm{e2}} = \nu_{+2}\mu_{+2} + \nu_-^{\mathrm{e2}}\mu_-, \tag{4.10}$$

where the scripts e1 and e2 denote the salts $(+1,-)$ and $(+2,-)$, respectively, and ν_i is the number of ion i a salt dissociates into. The superscript j on ν_-^j indicates the type of salt the coefficient is concerned with. Since both salts are electroneutral, they must obey

$$\begin{aligned} z_{+1}\nu_{+1} + z_-\nu_-^{\mathrm{e1}} = 0 \qquad & z_{+2}\nu_{+2} + z_-\nu_-^{\mathrm{e2}} = 0 \\ z_{+1}y_{+1} + z_-y_-^{\mathrm{e1}} = 0 \qquad & z_{+2}y_{+2} + z_-y_-^{\mathrm{e2}} = 0 \end{aligned}, \tag{4.11}$$

where y_-^{e1} and y_-^{e2} are the particle fractions of the anion released from salts $(+1,-)$ and $(+2,-)$, respectively. The total anion particle fraction is given by the sum of the two, i.e., $y_- = y_-^{\mathrm{e1}} + y_-^{\mathrm{e2}}$. The phase rule can be written with the salt particle fractions $y_{\mathrm{e1}} = y_{+1}/\nu_{+1} = y_-^{\mathrm{e1}}/\nu_-^{\mathrm{e1}}$ and $y_{\mathrm{e2}} = y_{+2}/\nu_{+2} = y_-^{\mathrm{e2}}/\nu_-^{\mathrm{e2}}$, so that

$$1 = \nu_{\mathrm{e1}}y_{\mathrm{e1}} + \nu_{\mathrm{e2}}y_{\mathrm{e2}}. \tag{4.12}$$

The two stoichiometric coefficients $\nu_{\mathrm{e1}} = \nu_{+1} + \nu_-^{\mathrm{e1}}$ and $\nu_{\mathrm{e2}} = \nu_{+2} + \nu_-^{\mathrm{e2}}$ designate the total number of ions after dissociation of each salt. The electrochemical-potential differential for the actively added salt $(+2,-)$ can be expressed as

$$d\mu_{\mathrm{e2}} = \nu_{\mathrm{e2}} RT \chi_{\mathrm{ee}}^{\mathrm{m}} d\ln y_{\mathrm{e2}}, \tag{4.13}$$

where the thermodynamic factor has to be defined slightly differently compared to the one for the binary electrolyte for eq.(4.13) to hold. This is because the particle fraction of the anion is not only controlled by the amount of added salt, but also by the amount

of the other salt already present in the system. It is given by

$$\chi_{\mathrm{ee}}^{\mathrm{m}} = K + \left(\frac{\partial \ln \lambda_{\mathrm{e}2}}{\partial \ln y_{\mathrm{e}2}}\right)_{T,p} \quad \text{with} \quad K(y_{\mathrm{e}2}) = \frac{\nu_{+2}}{\nu_{\mathrm{e}2}} + \frac{\nu_{-}^{\mathrm{e}2}}{\nu_{\mathrm{e}2}} \times \frac{\frac{\nu_{-}^{\mathrm{e}2}}{\nu_{-}^{\mathrm{e}1}} - \frac{\nu_{\mathrm{e}2}}{\nu_{\mathrm{e}1}}}{\frac{1}{\nu_{\mathrm{e}1} y_{\mathrm{e}2}} + \frac{\nu_{-}^{\mathrm{e}2}}{\nu_{-}^{\mathrm{e}1}} - \frac{\nu_{\mathrm{e}2}}{\nu_{\mathrm{e}1}}}, \tag{4.14}$$

where $\lambda_{\mathrm{e}2} = \lambda_{\mathrm{e}2}(y_{\mathrm{e}2})$ is the activity coefficient associated with the particle fraction of $(+2,-)$, which is defined as $\lambda_{\mathrm{e}2}^{\nu_{\mathrm{e}2}} = \lambda_{+2}^{\nu_{+2}} \lambda_{-}^{\nu_{-}^{\mathrm{e}2}}$ in terms of the activity coefficients of the individual ions. $K(y_{\mathrm{e}2})$ reduces to 1 when $\nu_{-}^{\mathrm{e}1} = 0$, as expected, but it approaches $\nu_{+2}/\nu_{\mathrm{e}2}$ when $y_{\mathrm{e}2} \to 0$, so that $d\mu_{\mathrm{e}2} \to RT\nu_{+2}\, d\ln y_{+2}$. That is, when an infinitesimal amount of $(+2,-)$ is added to pure $(+1,-)$, the change in the electrochemical potential of the added salt is solely controlled by the particle fraction of the added cation $+2$. This is not immediately intuitive but makes sense because the anion is already present in the system; therefore, dy_{-}/y_{-} is negligible in this case.

As in the binary-electrolyte case, one thermodynamic factor suffices to parameterise the system. Now, combining eq.(4.13), the phase rule in eq.(4.12), electroneutrality conditions in eq.(4.11), as well as the current–electrochemical-potential relation in eq.(4.7), a relationship between the measured liquid-junction potential and $\chi_{\mathrm{ee}}^{\mathrm{m}}$ can be derived.

$$-\frac{F z_{\mathrm{e}^-} n_{\mathrm{e}^-}}{RT}\left(\frac{d\Delta U}{d\ln y_{\mathrm{e}2}}\right)_{T,p} = \frac{\nu_{\mathrm{e}2}}{\nu_{-}^{\mathrm{e}2}}\left[s_{-} - \frac{\nu_{-}^{\mathrm{e}2}}{\nu_{+1}}\left\{\frac{\nu_{-}^{\mathrm{e}1}}{\nu_{-}^{\mathrm{e}2}} + \frac{y_{\mathrm{e}2}}{y_{\mathrm{e}1}}\right\} s_{+1} - \frac{n_{\mathrm{e}^-} z_{\mathrm{e}^-}}{z_{-}} t_{-}^{+1}\right] \chi_{\mathrm{ee}}^{\mathrm{m}} \tag{4.15}$$

Still, only one transference number appears in the above equation because the species that sets the reference frame always has zero transference number regardless of their charge state.

Adding $(+2, -)$ to $(+1, +2, -)$

Now, consider another concentration-cell measurement scheme where $(+2,-)$ is added to the ternary salt $(+1,+2,-)$. The phase rule is the same as in the experiment with two binary salts, hence eq.(4.12) applies, but the stoichiometric coefficients and salt

particle fractions need redefinitions.

$$\begin{gathered} y_{\mathrm{e}1}=\frac{y_{+1}^{\mathrm{e}1}}{\nu_{+1}^{\mathrm{e}1}}=\frac{y_{+2}^{\mathrm{e}1}}{\nu_{+2}^{\mathrm{e}1}}=\frac{y_{-}^{\mathrm{e}1}}{\nu_{-}^{\mathrm{e}1}} \qquad y_{\mathrm{e}2}=\frac{y_{+2}^{\mathrm{e}2}}{\nu_{+2}^{\mathrm{e}2}}=\frac{y_{-}^{\mathrm{e}2}}{\nu_{-}^{\mathrm{e}2}} \\ \nu_{\mathrm{e}1}=\nu_{+1}^{\mathrm{e}1}+\nu_{+2}^{\mathrm{e}1}+\nu_{-}^{\mathrm{e}1} \qquad \nu_{\mathrm{e}2}=\nu_{+2}^{\mathrm{e}2}+\nu_{-}^{\mathrm{e}2} \end{gathered} \tag{4.16}$$

The scripts e1 and e2 now denote the salts $(+1,+2,-)$ and $(+2,-)$, respectively. The individual ion particle fractions are:

$$\begin{gathered} y_{+1}=y_{+1}^{\mathrm{e}1} \\ y_{+2}=y_{+2}^{\mathrm{e}1}+y_{+2}^{\mathrm{e}2}=\nu_{+2}^{\mathrm{e}1}y_{\mathrm{e}1}+\nu_{+2}^{\mathrm{e}2}y_{\mathrm{e}2}\ . \\ y_{-}=y_{-}^{\mathrm{e}1}+y_{-}^{\mathrm{e}2}=\nu_{-}^{\mathrm{e}1}y_{\mathrm{e}1}+\nu_{-}^{\mathrm{e}2}y_{\mathrm{e}2} \end{gathered} \tag{4.17}$$

The electrochemical-potential differential of the salt $(+2,-)$ takes the same form as in the two-binary-salt-mixture case, i.e., eq.(4.13), but the activity coefficient $\lambda_{\mathrm{e}2}=\lambda_{\mathrm{e}2}(y_{\mathrm{e}2})$ is defined instead as $\lambda_{\mathrm{e}2}^{\nu_{\mathrm{e}2}}=\lambda_{+2}^{\nu_{+2}^{\mathrm{e}2}}\lambda_{-}^{\nu_{-}^{\mathrm{e}2}}$ and K in $\chi_{\mathrm{ee}}^{\mathrm{m}}$ becomes

$$K(y_{\mathrm{e}2})=\frac{\nu_{+2}^{\mathrm{e}2}}{\nu_{\mathrm{e}2}}\times\frac{\frac{\nu_{+2}^{\mathrm{e}2}}{\nu_{+2}^{\mathrm{e}1}}-\frac{\nu_{\mathrm{e}2}}{\nu_{\mathrm{e}1}}}{\frac{1}{\nu_{\mathrm{e}1}y_{\mathrm{e}2}}+\frac{\nu_{+2}^{\mathrm{e}2}}{\nu_{+2}^{\mathrm{e}1}}-\frac{\nu_{\mathrm{e}2}}{\nu_{\mathrm{e}1}}}+\frac{\nu_{-}^{\mathrm{e}2}}{\nu_{\mathrm{e}2}}\times\frac{\frac{\nu_{-}^{\mathrm{e}2}}{\nu_{-}^{\mathrm{e}1}}-\frac{\nu_{\mathrm{e}2}}{\nu_{\mathrm{e}1}}}{\frac{1}{\nu_{\mathrm{e}1}y_{\mathrm{e}2}}+\frac{\nu_{-}^{\mathrm{e}2}}{\nu_{-}^{\mathrm{e}1}}-\frac{\nu_{\mathrm{e}2}}{\nu_{\mathrm{e}1}}}. \tag{4.18}$$

Going through the same procedure as before finally generates the following expression.

$$\begin{aligned} -\frac{Fz_{\mathrm{e}^-}n_{\mathrm{e}^-}}{RT}\left(\frac{d\Delta U}{d\ln y_{\mathrm{e}2}}\right)_{T,p}= \\ \frac{\nu_{\mathrm{e}2}}{\nu_{-}^{\mathrm{e}2}}\left[s_{-}-\frac{\nu_{-}^{\mathrm{e}2}}{\nu_{+1}^{\mathrm{e}1}}\left\{\frac{\nu_{-}^{\mathrm{e}1}}{\nu_{-}^{\mathrm{e}2}}+\frac{\nu_{\mathrm{e}1}y_{\mathrm{e}2}}{1-\nu_{\mathrm{e}2}y_{\mathrm{e}2}}\right\}s_{+1}+\frac{n_{\mathrm{e}^-}z_{\mathrm{e}^-}\nu_{-}^{\mathrm{e}2}}{z_{+2}\nu_{+2}^{\mathrm{e}2}}t_{-}^{+1}\right]\chi_{\mathrm{ee}}^{\mathrm{m}} \end{aligned} \tag{4.19}$$

4.1.3 Case III. The binary salt in two neutral solvents

The salt considered in this section is made up of ν_{-} anions and ν_{+} cations, so μ_{e} in eq.(4.1) is still valid. Nonetheless, the presence of an extra solvent demands that there be two independent particle fractions upon which the electrochemical potentials depend. Choosing $\mu_{\mathrm{e}}=\mu_{\mathrm{e}}(y_{\mathrm{o}},y)$ and $\mu_{\mathrm{o}}=\mu_{\mathrm{o}}(y_{\mathrm{o}},y)$ under isothermal, isobaric condi-

tions, their differentials become

$$d\mu_{\mathrm{o}} = \frac{RT}{y_{\mathrm{o}}}\left[\chi^{\mathrm{m}}_{\mathrm{oo}}\, dy_{\mathrm{o}} + \chi^{\mathrm{m}}_{\mathrm{oe}}\, dy\right] \quad \text{and} \quad d\mu_{\mathrm{e}} = \frac{\nu RT}{y}\left[\chi^{\mathrm{m}}_{\mathrm{eo}}\, dy_{\mathrm{o}} + \chi^{\mathrm{m}}_{\mathrm{ee}}\, dy\right], \tag{4.20}$$

with thermodynamic factors defined as below[4].

$$\begin{aligned} \chi^{\mathrm{m}}_{\mathrm{oo}} &= 1 + \left(\frac{\partial \ln \lambda_{\mathrm{o}}}{\partial \ln y_{\mathrm{o}}}\right)_{T,p,y} & \chi^{\mathrm{m}}_{\mathrm{oe}} &= y_{\mathrm{o}}\left(\frac{\partial \ln \lambda_{\mathrm{o}}}{\partial y}\right)_{T,p,y_{\mathrm{o}}} \\ \chi^{\mathrm{m}}_{\mathrm{eo}} &= y\left(\frac{\partial \ln \lambda_{+-}}{\partial y_{\mathrm{o}}}\right)_{T,p,y} & \chi^{\mathrm{m}}_{\mathrm{ee}} &= 1 + \left(\frac{\partial \ln \lambda_{+-}}{\partial \ln y}\right)_{T,p,y_{\mathrm{o}}} \end{aligned} \tag{4.21}$$

Although four thermodynamic factors are presented, one is dependent on the other three. This dependence can be extracted by recognising the symmetry of the Hessian matrix of the Gibbs free energy *via* the core-potential theory, which was explored in section 3.4. The resulting relationship in eq.(3.108) is reproduced below after rearrangement.

$$\nu y_{\mathrm{o}}(1 - y_{\mathrm{o}})\chi^{\mathrm{m}}_{\mathrm{eo}} - y(1 - \nu y)\chi^{\mathrm{m}}_{\mathrm{oe}} = \nu y_{\mathrm{o}} y\left[\chi^{\mathrm{m}}_{\mathrm{ee}} - \chi^{\mathrm{m}}_{\mathrm{oo}}\right] \tag{4.22}$$

This equation suggests that $\chi^{\mathrm{m}}_{\mathrm{eo}} = O(y)$ or higher and $\chi^{\mathrm{m}}_{\mathrm{oe}} = O(y_{\mathrm{o}})$ or higher because $\chi^{\mathrm{m}}_{\mathrm{ee}}$ and $\chi^{\mathrm{m}}_{\mathrm{oo}}$ are finite in the dilute limits of y and y_{o}, respectively.

One can now proceed as in section 4.1.1 to derive a relationship relating thermodynamic factors and the liquid-junction potential. Writing out the electrode reactions involving the four species and recognising that the measured potential difference embodies the difference in the electrochemical potential of electrons in the two electrodes (submerged in the concentration cell), the liquid-junction potential can be expressed as

$$\begin{aligned} \frac{F z_{\mathrm{e}^-} n_{\mathrm{e}^-} \Delta U}{RT} &= \frac{1}{RT}\left[\int_{\delta}^{\delta'} \tau_{\mathrm{o}}\, d\mu_{\mathrm{o}} + \int_{\delta}^{\delta'} \tau_{\mathrm{e}}\, d\mu_{\mathrm{e}}\right] \\ &= \int_{y_{\mathrm{o}}^{(\delta)}}^{y_{\mathrm{o}}^{(\delta')}} \left(\frac{\tau_{\mathrm{o}}}{y_{\mathrm{o}}}\chi^{\mathrm{m}}_{\mathrm{oo}} + \frac{\nu\tau_{\mathrm{e}}}{y}\chi^{\mathrm{m}}_{\mathrm{eo}}\right) dy_{\mathrm{o}} + \int_{y^{(\delta)}}^{y^{(\delta')}} \left(\frac{\tau_{\mathrm{o}}}{y_{\mathrm{o}}}\chi^{\mathrm{m}}_{\mathrm{oe}} + \frac{\nu\tau_{\mathrm{e}}}{y}\chi^{\mathrm{m}}_{\mathrm{ee}}\right) dy, \end{aligned} \tag{4.23}$$

[4]As eq.(4.23) shows, the liquid-junction potential measurement is not sufficient to isolate the three independent thermodynamic factors. Nevertheless, the superscript m (which stands for measurable) is kept for consistency with the binary electrolyte and three-ion ionic liquid notations.

where

$$\begin{aligned}\tau_{\mathrm{o}} &= s_{\mathrm{o}} - \frac{s_0 y_{\mathrm{o}}}{1 - y_{\mathrm{o}} - \nu y} - z_+\nu_+\left(\frac{s_+}{\nu_+} - \frac{s_-}{\nu_-}\right)\frac{t_{\mathrm{o}}^0}{z_{\mathrm{o}}} \\ \tau_{\mathrm{e}} &= \frac{s_-}{\nu_-} - \frac{s_0 y}{1 - y_{\mathrm{o}} - \nu y} + \left(\frac{s_+}{\nu_+} - \frac{s_-}{\nu_-}\right) t_-^0\end{aligned} \quad . \tag{4.24}$$

It is reminded that although $z_{\mathrm{o}} = 0$, the ratio $t_{\mathrm{o}}^0/z_{\mathrm{o}}$ is well defined. In fact, it is related to the migration coefficient Ξ in the following way, where Ξ quantifies the amount of drag the solvent o experiences as a result of moving charged species [157].

$$\frac{t_{\mathrm{o}}^0}{z_{\mathrm{o}}} = -\frac{z_+ - z_-}{z_+ z_-}\Xi \tag{4.25}$$

Unless t_-^0 and Ξ are known, eq.(4.23) presents difficulty in probing the three independent thermodynamic factors individually. Even if either y or y_{o} was held constant at the reference composition to eliminate one of the integrals, it is not clear how the two interwoven thermodynamic factors in the remaining integral can be resolved further experimentally. This perhaps shows why solvent mixtures have been treated as a single species in the literature so far [161, 163, 164, 169, 170], albeit without formal justification.

Given the difficulty of dealing with two independent composition variables, we take a step back and check under which circumstances it is acceptable to group the two solvents together. To do so, one needs to define an equivalent single solvent in a thermodynamically consistent manner. An observation of the OSM equations suggests two possible approaches; one can either place a constraint on the velocities of the two solvents (constraint on the fluxes) or on their electrochemical-potential gradients (constraint on the forces).

Equivalent single solvent *via* constraint on the fluxes

To pursue the case where the fluxes are constrained, consider a system of three generic neutral species $\{A, B, C\}$. Constructing the OSM equations for the system gives the

following set of equations with the velocity of A as the reference velocity [49].

$$\begin{bmatrix} c_B \nabla \mu_B \\ c_C \nabla \mu_C \end{bmatrix} = \frac{RT}{c_\mathrm{T}} \begin{bmatrix} -\frac{c_A c_B}{\mathscr{D}_{AB}} - \frac{c_B c_C}{\mathscr{D}_{BC}} & \frac{c_B c_C}{\mathscr{D}_{BC}} \\ \frac{c_B c_C}{\mathscr{D}_{BC}} & -\frac{c_A c_C}{\mathscr{D}_{AC}} - \frac{c_B c_C}{\mathscr{D}_{BC}} \end{bmatrix} \begin{bmatrix} v_B - v_A \\ v_C - v_A \end{bmatrix} \tag{4.26}$$

To introduce the necessary constraint, one can assume that A and B move at the same velocity, i.e., $v_A = v_B$, independent of driving forces the system experiences. Then, the following relationship is established between the electrochemical-potential gradients of B and C.

$$y_C \nabla \mu_C = -\frac{y_B \mathscr{D}_{AC} + y_A \mathscr{D}_{BC}}{\mathscr{D}_{AC}} \nabla \mu_B \tag{4.27}$$

Using the isothermal, isobaric Gibbs–Duhem equation, this becomes

$$\frac{\mathscr{D}_{BC}}{\mathscr{D}_{AC}} = \frac{\nabla \mu_A}{\nabla \mu_B}. \tag{4.28}$$

One can see that this is a rather extraordinary condition to meet; this means that given a ternary solution of known concentrations, the Stefan–Maxwell diffusivities will change if it is subjected to different electrochemical-potential gradients. This is contrary to the common understanding that microscopic interactions between two species should be well defined when their concentrations are known.

Equivalent single solvent *via* constraint on the forces

The second approach to arriving at the equivalent single solvent involves constraining the electrochemical potentials, guided by thermodynamic principles. Consider mixing two neutral solvents 0 and o of known masses, so that the initial number of moles n_0 and n_o are known. A vacuum is pulled over the mixture and the system is sealed swiftly such that no molecules are lost during this process. It is then left to reach a vapour–liquid equilibrium, allowing some molecules to escape the liquid phase to the vapour phase. The conservation of mass consequently dictates that $n_i = n_i^L + n_i^V$, where the liquid and vapour phases are ascribed to the superscripts L and V, respectively.

To treat the two solvents as a single species, one can posit that a cluster equilibrium reaction takes place

$$\nu_0 M_0 + \nu_\mathrm{o} M_\mathrm{o} \rightarrow M_\odot, \tag{4.29}$$

where ν_i is the number of species i that congregates to form a cluster molecule $\odot$. It is assumed that the two solvents are distributed evenly across the solution volume at equilibrium so that there are no local variations in ν_i. Since this is a hypothetical reaction, it can always be taken to 100% completion. Furthermore, it is required that only one type of cluster $\odot$ is present in the system, which makes it possible to determine ν_0 and ν_o from the mole ratio of the two solvents. That is,

$$\frac{\nu_0}{\nu_\mathrm{o}} = \frac{n_0^L}{n_\mathrm{o}^L}, \tag{4.30}$$

where ν_0 and ν_o are selected such that they have no common factors[5], i.e., $\odot$ is the smallest-possible repeating unit. The number of clusters is then

$$n_\odot = \frac{n_0^L}{\nu_0} = \frac{n_\mathrm{o}^L}{\nu_\mathrm{o}} \tag{4.31}$$

and the solution can now be considered to be composed entirely of $\odot$.

Now, imagine adding a small amount of salt to this binary mixture (which is a pure $\odot$ in the liquid phase). The molar composition in the liquid phase is now $n_0^L, n_\mathrm{o}^L, n_+^L$, and n_-^L after reaching a vapour–liquid equilibrium. Assuming that the salt is involatile, the vapour phase is made up of the two solvents only, with n_0^V and n_o^V moles. It is fair to believe that the ions distribute themselves evenly across the solution volume at equilibrium. As a result, the presence of the salt should not promote variations in the concentrations of the two solvents in the length scale of interest. For the equivalent-

[5]In theory, choosing ν_0 and ν_o to have integer values is natural, but this might present some difficulties in practice. Likely, ν_0 and ν_o will be very large integers for an experimental system, so that any reasonable salt concentrations used for the measurement would be translated to concentrated regimes in the equivalent single solvent, with an extremely small spread. One possible circumvention is to choose $\nu_0 = 1$ and find a fractional value of ν_o to ensure a decent spread to conduct regression. This is not entirely satisfactory, since the cluster $\odot$ would contain a fraction of an o molecule, but it may not be of great concern because the concept of $\odot$ is already fictional, anyway.

single-solvent approach to be applicable, the clustering should remain independent of the salt content, n^L, i.e.,

$$\left(\frac{\partial(\nu_0/\nu_\mathrm{o})}{\partial n^L}\right)_{T,n_0,n_\mathrm{o}} = 0. \tag{4.32}$$

This mandates that n_0^L/n_o^L be a constant independent of the salt content, due to eq.(4.30).

To proceed further, one must now contemplate the meaning of an equivalent single species concerning the behaviour of the solvent activity coefficients as the salt content increases in the system. Section 4.1.1 showed that a binary electrolytic system (composed of a neutral solvent, a cation and an anion) has only one independent thermodynamic factor — this must apply to the system with an equivalent single solvent, too. Therefore, the two solvents' extent of deviation from thermodynamic ideality should be the same as a function of salt concentration, i.e.,

$$\left(\frac{\partial\lambda_0}{\partial n^L}\right)_{T,n_0,n_\mathrm{o}} = \left(\frac{\partial\lambda_\mathrm{o}}{\partial n^L}\right)_{T,n_0,n_\mathrm{o}}, \tag{4.33}$$

where λ_i is the particle-fraction activity coefficient of species i. This means that $\lambda_0 = \lambda_\mathrm{o} + \mathrm{const}$ at a fixed n_0^L/n_o^L ratio. However, in the dilute limit of salt, the two activity coefficients are both expected to approach 1, so the constant must be 0, or that $\lambda_0 = \lambda_\mathrm{o}$ must follow. This information leads to a statement about partial pressures at the vapour–liquid equilibrium. The electrochemical potentials and their differentials in the two phases are given by

$$\begin{aligned} \mu_i^L &= \mu_i^{\theta L} + RT\ln\lambda_i y_i^L \qquad \rightarrow \quad d\mu_i^L = RT\,d\ln\lambda_i y_i^L \\ \mu_i^V &= \mu_i^{\theta V} + RT\ln f_i/f_i^\theta \qquad \rightarrow \quad d\mu_i^V = RT\,d\ln P_i/P_i^{\mathrm{sat}} \end{aligned}, \tag{4.34}$$

where $\mu_i^{\theta L}$ is the electrochemical potential of pure species i in the liquid phase at a given temperature and pressure (i.e., the liquid-phase reference state), y_i^L is the particle fraction of i in the liquid phase, $\mu_i^{\theta V}$ is the electrochemical potential of saturated vapour of pure species i at a given temperature and pressure (i.e., the vapour-phase

reference state), f_i^θ is the corresponding fugacity, and f_i is the fugacity of species i in the mixture. Assuming that the vapour phase is an ideal gas mixture, the fugacity of each component is equal to its partial pressure, i.e., $f_i = P_i$ and $f_i^\theta = P_i^{\mathrm{sat}}$, where the superscript 'sat' denotes the saturated state. At a vapour–liquid equilibrium, the electrochemical-potential differentials in the two phases must equate, which provides a relationship between the partial pressure and the activity coefficient.

$$P_i = \lambda_i y_i^L P_i^{\mathrm{sat}} \tag{4.35}$$

Because $\lambda_0 = \lambda_{\mathrm{o}}$, the partial-pressure ratio must then be

$$\frac{P_0}{P_{\mathrm{o}}} = \frac{y_0^L P_0^{\mathrm{sat}}}{y_{\mathrm{o}}^L P_{\mathrm{o}}^{\mathrm{sat}}}. \tag{4.36}$$

It was asserted that $n_0^L/n_{\mathrm{o}}^L = y_0^L/y_{\mathrm{o}}^L$ is a constant, independent of the salt content due to eq.(4.32). Therefore, $P_0/P_{\mathrm{o}} = \text{constant}$ must follow.

To summarise, two conditions verify whether a mixture of two solvents can be treated as an equivalent single solvent: the diffusivity relation and the partial-pressure relation. The latter is less general than the former because it does not apply to involatile solvent species, but it provides a more convenient means to test the validity of the approximation for practical applications, e.g., for battery electrolytes.

Voltage–thermodynamic-factor relationship for a binary salt in an equivalent single solvent

A benefit of using an equivalent single solvent is that the voltage measured *via* the concentration-cell experiment can be processed in the same way as in the binary electrolyte. Employing the following notations, where $\odot$ denotes the equivalent single

solvent,

$$
\begin{gathered}
y_{\odot} = \frac{n_{\odot}}{n_{\mathrm{T}}^{L}} = \frac{y_{0}^{L}}{\nu_{0}} = \frac{y_{\mathrm{o}}^{L}}{\nu_{\mathrm{o}}} \qquad y = \frac{y_{+}^{L}}{\nu_{+}} = \frac{y_{-}^{L}}{\nu_{-}} \\
n_{\mathrm{T}}^{L} = n_{0}^{L} + n_{\mathrm{o}}^{L} + n_{+}^{L} + n_{-}^{L} \qquad \nu_{\odot} = \nu_{0} + \nu_{\mathrm{o}} \qquad \nu = \nu_{+} + \nu_{-} \\
\mu_{\odot} = \nu_{0}\mu_{0}^{L} + \nu_{\mathrm{o}}\mu_{\mathrm{o}}^{L} \qquad \mu_{\mathrm{e}} = \nu_{+}\mu_{+}^{L} + \nu_{-}\mu_{-}^{L}
\end{gathered}
\tag{4.37}
$$

the phase rule and the isothermal, isobaric Gibbs–Duhem relation become

$$1 = \nu_{\odot} y_{\odot} + \nu y \tag{4.38}$$

$$0 = y_{\odot} d\mu_{\odot} + y d\mu_{\mathrm{e}}. \tag{4.39}$$

In order to maintain the number of independent composition variables at one, the electrode reaction is assumed to involve units of $\odot$ so that the solvent ratio does not change. This is believed to be a reasonable assumption for many battery applications because solvents usually do not take part in common electrode reactions. Incorporating all the information leads to a relationship that is essentially identical to the one for the binary-salt system, as expected.

$$-\frac{F z_{\mathrm{e}^-} n_{\mathrm{e}^-}}{\nu RT}\left(\frac{d\Delta U}{d\ln y}\right)_{T,p} = \left\{\frac{s_{\odot}\nu_{\odot} y}{1-\nu y} - \frac{s_{+}}{\nu_{+}} + \left(\frac{s_{+}}{\nu_{+}} - \frac{s_{-}}{\nu_{-}}\right) t_{+}^{\odot}\right\} \chi_{\mathrm{ee}}^{\mathrm{m}\prime} \tag{4.40}$$

It is reminded that the thermodynamic factor in the above equation is defined as $\chi_{\mathrm{ee}}^{\mathrm{m}\prime} = 1 + (d\ln\lambda_{+-}/\,d\ln y)_{T,p}$ (the prime indicates that it is derived using an equivalent single solvent) and the transference number should be defined with respect to the velocity of $\odot$. When the concentration-cell measurements are carried out, the ratio of the two solvents r_i should be kept constant to ensure that the nature of $\odot$ does not change. Provided that the concentration dependence of the transference number is known, a functional form of $\chi_{\mathrm{ee}}^{\mathrm{m}\prime}(y)$ can be obtained *via* any regression technique for each ratio r_i.

4.2 Liquid-junction potential for EMC:EC:$LiPF_6$

To recapitulate, two solvents must at least satisfy one of the two criteria to be qualified as an equivalent single solvent; they must either move at the same velocity or have the same activity coefficients. The first criterion constrains Stefan–Maxwell diffusivities to be governed by the electrochemical-potential gradients. This is unusual since it forces Stefan–Maxwell diffusivities to vary depending on the magnitude of the diffusional driving forces. The second criterion, requiring the partial-pressure ratio of the two solvents to be fixed as more salt is added, is not going to hold for typical lithium-ion-battery solvent mixtures, because they are made up of solvents of different polarities, e.g., ethylene carbonate (EC) and ethyl-methyl carbonate (EMC). The more polar solvent is more strongly attached to the dissolved ions; hence, its vapour pressure is expected to be depressed more noticeably than the less-polar solvent in the presence of salt.

Despite this, almost all studies built on the popular physics-based pseudo-two-dimensional (P2D) battery model of Doyle et al. [171] have not addressed cosolvents as separate species [172–174]. As a result, many electrolyte characterisation efforts have also employed this 'single-solvent approximation' [161, 163, 164, 169, 170, 175]. Nonetheless, there is ample evidence that this may not be adequate. Firstly, solvent mobility has been shown to play an important role in controlling battery performance [176, 177]. When two solvents are present, they are likely to move at different rates during battery operation, necessiatating the consistent incorporation of the two mobilities in battery models. Other groups have also observed the bulk motion of both polymer and liquid electrolytes under applied currents, indicating that the migration effects must be taken into account to describe the flux of electrically uncharged solvent molecules accurately [178–181]. For the EMC:EC:lithium hexafluorophosphate ($LiPF_6$) ternary system —which is the system under study here—, Wang et al. [182] confirmed the two solvents migrate at noticeably different rates during Hittorf experiments. Therefore, one is obliged to question the single-solvent approximation when

studying Li-ion-battery electrolytes.

As evident from eq.(4.23), thermodynamic factors for a binary salt in two neutral solvents cannot be directly extracted from concentration-cell experiments, unless the composition dependences of the involved transport properties are known. Nevertheless, voltage measurements can be readily made using the same experimental procedure as in the one-solvent system. It is worth pointing out that not being able to isolate the thermodynamic factors is not an impediment to the practical purpose of acquiring the open-circuit voltage (OCV) of a given battery; it is immaterial how the overpotential in the liquid phase is obtained, as long as it accurately depicts the phenomenon. With one more solvent, however, the liquid-junction potential function lies above a two-dimensional composition space, so parameterisation is not as straightforward as it would be for a one-solvent system, as conveyed by Mistry and Srinivasan [183]. More specifically, the liquid-junction potential associated with differences in the solvent ratio is hard to predict *a priori*. Therefore, this section is presented as an exemplar to illustrate how a thermodynamically rigorous liquid-junction-potential ternary map can be constructed, through the concentration-cell measurements of $LiPF_6$ in EMC:EC mixtures. EMC, EC, and $LiPF_6$ are abbreviated as 0, o, and e, respectively. From now on, the superscript L on particle fractions is omitted because we are only concerned with the liquid-phase compositions.

4.2.1 Concentration-cell experiment

The method and apparatus outlined by Hou and Monroe [162] were used to carry out the concentration-cell experiment (Dr A. Wang performed the experiment). Ternary EMC:EC:$LiPF_6$ solutions were prepared gravimetrically within an argon glovebox (Inert Technologies) with a nominally 2 M $LiPF_6$ in EMC stock solution (battery grade, Sigma Aldrich), vacuum-dried $LiPF_6$ (99.99%, battery grade, Sigma Aldrich), EC (99%, Sigma Aldrich), and EMC (99.9%, Sigma Aldrich) solvents (appropriate amounts of pure components were added to the 2 M EMC:$LiPF_6$). The experiment was performed

within the glovebox, whose atmosphere was maintained at 25 °C by a thermostat. More detailed experimental conditions and procedures are provided in Jung et al. [5].

When EMC:EC:$LiPF_6$ solutions of different concentrations are introduced to a concentration cell, the following electrode reaction takes place at the lithium-metal electrodes submerged in the cell reservoirs.

$$\mathrm{Li} - \mathrm{Li}^+ \rightleftharpoons \mathrm{e}^- \tag{4.41}$$

The reaction is written with the electron on the right-hand side and the remaining species on the left-hand side to conform to the general form of the electrode reaction outlined in eq.(4.5). This is important to ensure that the coefficients s_i have the right sign. Thus, substitutions $z_{\mathrm{e}^-} = -1$, $n_{\mathrm{e}^-} = 1$, $\nu_+ = \nu_- = 1$, $s_0 = s_\mathrm{o} = s_- = 0$, and $s_+ = -1$ can be made, reducing τ's to be

$$\tau_\mathrm{o} = 2\Xi \qquad \text{and} \qquad \tau_\mathrm{e} = -t_-^0. \tag{4.42}$$

This also simplifies the liquid-junction potential in eq.(4.23) to be more simply written as

$$\frac{F\Delta U}{RT} = \int_{y_\mathrm{o}^{(\delta)}}^{y_\mathrm{o}^{(\delta')}} u_\mathrm{o}\, dy_\mathrm{o} + \int_{y_\mathrm{e}^{(\delta)}}^{y_\mathrm{e}^{(\delta')}} u_\mathrm{e}\, dy_\mathrm{e}, \tag{4.43}$$

where new parameters u_o and u_e arise, which will be called the 'junction coefficients' of EC and $LiPF_6$, respectively. They are defined as

$$\begin{aligned} u_\mathrm{o} &= -\left(\frac{2\Xi}{y_\mathrm{o}}\chi_{\mathrm{oo}}^\mathrm{m} - \frac{2t_-^0}{y_\mathrm{e}}\chi_{\mathrm{eo}}^\mathrm{m}\right) \\ u_\mathrm{e} &= -\left(\frac{2\Xi}{y_\mathrm{o}}\chi_{\mathrm{oe}}^\mathrm{m} - \frac{2t_-^0}{y_\mathrm{e}}\chi_{\mathrm{ee}}^\mathrm{m}\right) \end{aligned}. \tag{4.44}$$

Once the composition dependence of ΔU is available, the junction coefficients are

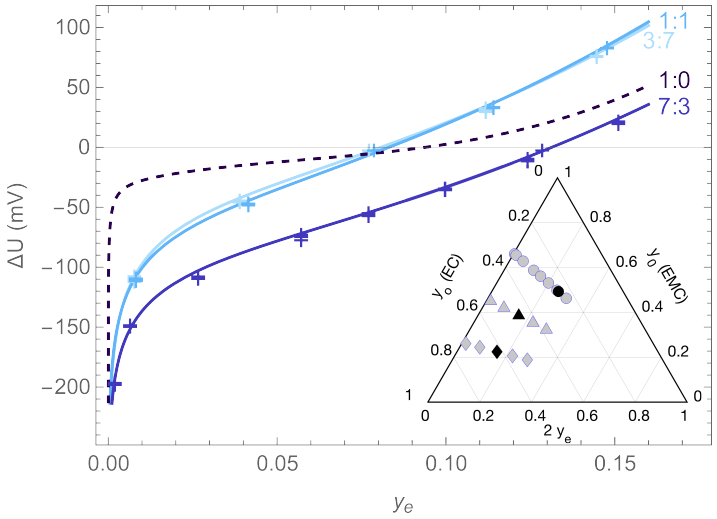

Figure 4.2: Liquid-junction potential measurements relative to the reference composition for 3:7, 1:1, and 7:3 solvent ratios (markers) are shown alongside the best-fit curves using eq.(4.46) (solid lines). The correlation measured by Wang et al. [4] for the EMC:LiPF$_6$ binary system (1:0 EMC:EC ratio) is shown for comparison (dashed line), referenced to the composition $(y_o, y_e) = (0, 0.09379)$, at which the binary solution exhibits an ideal thermodynamic factor. Inset: Ternary plot showing solution compositions of the test solutions (grey markers) and reference solutions (black markers) in concentration cells. Circles, triangles, and diamonds respectively indicate solutions prepared with EMC:EC ratios of 7:3, 1:1, and 3:7. Measurement data can be found in Jung et al. [5], which is summarised in Appendix B, as well.

attainable directly, by partially differentiating it.

$$
\begin{aligned}
u_o\left(y_o, y_e\right) &= \frac{F}{RT}\left(\frac{\partial \Delta U}{\partial y_o}\right)_{T,p,y_e} \\
u_e\left(y_o, y_e\right) &= \frac{F}{RT}\left(\frac{\partial \Delta U}{\partial y_e}\right)_{T,p,y_o}
\end{aligned}
\tag{4.45}
$$

Provided that enough voltage measurements are made across the composition space of interest, linear regression can be used to fit the data over a surface. To achieve this, the necessary voltage measurements were made first with fixed EMC:EC ratios, varying the salt content alone. Three ratios were prepared: 7:3, 1:1, and 3:7 of EMC:EC by weight, corresponding to the circular, triangular and diamond markers in the inset of Figure 4.2, respectively (see Jung et al. [5] or Appendix B for the actual data set). Black markers in the ternary map indicate the reference compositions used for the three ratios, which correspond to $(y_o, y_e) = (0.2498, 0.1286)$, $(y_o, y_e) = (0.4564, 0.07875)$, and

Table 4.1: Liquid-junction-potential fit parameters for the three solvent ratios.

EMC:EC	$a_{\ln}$	a_0	a_1	a_2
7:3	1.390	1.158	−8.955	164.7
1:1	1.491	3.007	−8.168	199.6
3:7	1.672	4.034	−14.57	207.6

$(y_o, y_e) = (0.6212, 0.07723)$ for 7:3, 1:1, and 3:7 ratios, respectively. As the salt fraction approaches its dilute limit ($y_e \to 0$), the voltage measurements increase rapidly in the negative direction for all three solvent ratios. This is not surprising, given the Nernstian behaviour at low salt concentration has been widely observed [4, 22, 23, 78, 184, 185]. Therefore, voltage measurements for each solvent ratio were curve-fitted with a logarithmic term and a second-order polynomial; the latter was included to correct any deviations from the logarithmic behaviour.

$$\Delta U(y_e) = \frac{RT}{F}\left(a_{\ln} \ln y_e + \sum_{k=0}^{2} a_k y_e^k\right) \tag{4.46}$$

The fit parameters $a_{\ln}$ and a_k, obtained by the method of least squares, are tabulated in Table 4.1 at the three solvent ratios. These values were used to plot the voltage curves in Figure 4.2.

To probe the effects of solvent-ratio changes on the liquid-junction potential, another set of experiments was performed with fixed salt contents. Eight solutions were prepared, labelled as A_1, B_1, C_1, D_1, A_2, B_2, C_2, and D_2 in Figure 4.3, whose compositions are tabulated in Table 4.2. Various pairwise combinations of the eight solutions were subjected to the concentration-cell experiment; six measurements were made for each pair. Average liquid-junction potentials with standard errors are presented in Table 4.3 (see Jung et al. [5] or Appendix B for the full data set).

Now, one needs to establish a relationship among the three EMC:EC-ratio voltage curves. This was achieved by the following three-step process.

1. Shift the reference compositions for 3:7, 1:1, and 7:3 measurement data sets to A_1, B_1, and C_1, respectively.

Table 4.2: Particle fractions used for constant-y_e concentration-cell measurements.

Position	y_o	y_e	Position	y_o	y_e
A_1	0.5985	0.09017	A_2	0.7191	0.01019
B_1	0.4438	0.08995	B_2	0.5265	0.01027
C_1	0.2753	0.08974	C_2	0.3273	0.01010
D_1	0	0.09009	D_2	0	0.01004

Table 4.3: Liquid-junction-potential measurements at constant y_e. See Jung et al. [5] or Appendix B for the full data set.

Ref – Test	ΔU (mV)	Ref – Test	ΔU (mV)
A_1 – B_1	8.4 ± 0.5	A_2 – B_2	14.9 ± 0.1
A_1 – C_1	22.3 ± 0.2	A_2 – C_2	40.0 ± 0.8
A_1 – D_1	57 ± 3	A_2 – D_2	132.6 ± 0.8
B_1 – C_1	13.6 ± 0.3	B_2 – C_2	23.86 ± 0.06
B_1 – D_1	49.7 ± 0.6	B_2 – D_2	116.3 ± 0.7
C_1 – D_1	35.26 ± 0.09	C_2 – D_2	91 ± 1

2. Add the voltage difference across A_1 – D_1, B_1 – D_1, and C_1 – D_1 to the three shifted data sets using the values provided in Table 4.3 so that they are anchored to the same reference composition, D_1.

3. Finally, add to the data sets the voltage difference between D_1 and the global reference composition 'ref' at $\mathbf{y}^{\mathrm{ref}} = (y_o, y_e) = (0, 0.09379)$. At this 'ref' composition, the EMC:$LiPF_6$ binary behaves ideally, according to Wang et al. [4].

To carry out the last step, the composition dependence of the liquid-junction potential in the EMC:$LiPF_6$ binary is required. The functional forms of the transference number t_+^0 and the thermodynamic factor χ_{ee}^{m}, provided by Wang et al. [4], can be used to obtain it through eq.(4.8). The resulting liquid-junction potential along the no-EC edge of the ternary space, $\Delta U_{1:0}$, is given by

$$\begin{aligned}\Delta U_{1:0}\,(y_e) = \frac{RT}{F}\Big[&7.167 - 43.16\; y_e^{0.5} + 185.4\; y_e - 402.4\; y_e^{1.5} + 236.9\; y_e^2 \\ &+ 253.7\; y_e^{2.5} - 408.1\; y_e^3 + 2509\; y_e^{3.5} - 2886\; y_e^{4.5} + 1.174\;\ln y_e\Big].\end{aligned} \tag{4.47}$$

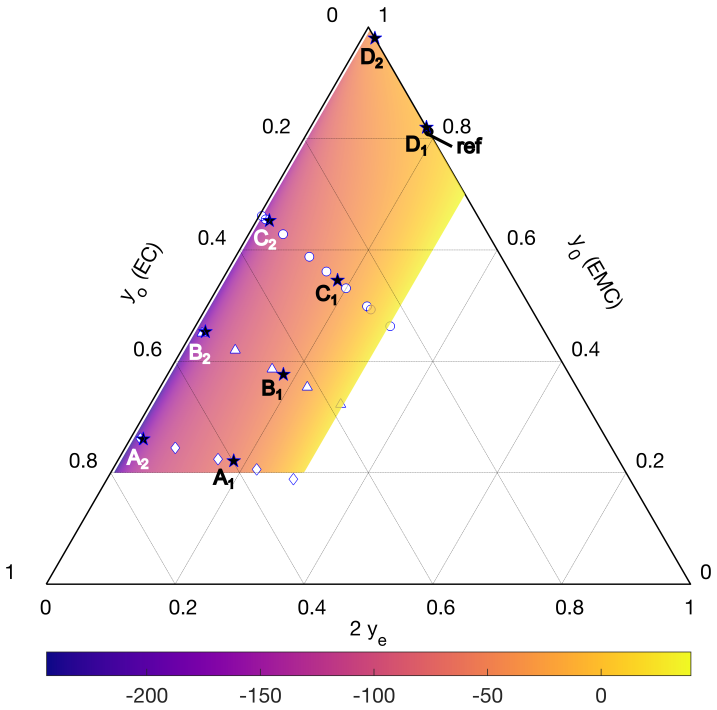

Figure 4.3: Ternary diagram showing all the compositions at which liquid-junction potentials were measured for EMC:EC:$LiPF_6$ mixtures (markers). The corresponding measurement data is provided in Jung et al. [5], as well as in Appendix B. The colour map shows the surface with the form of eq.(4.51) that best fits the liquid-junction potential data (in units of mV) after they are shifted to a common reference solution $\mathbf{y}^{\mathrm{ref}} = (0, 0.09379)$.

Thus, the final shift to 'ref' in step 3 amounts to adding $\Delta U_{1:0}(\mathrm{D}_1)$ to the adjusted measurement data sets in step 2. Compositions of all measurements are marked on a ternary map in Figure 4.3, as well as the reference composition.

4.2.2 Junction-potential correlation

To incorporate the concentration overpotentials in battery models, functional forms of the junction coefficients u_o and u_e must be known. Since they are partial derivatives of the state function $\Delta U(y_\mathrm{o}, y_\mathrm{e})$ with respect to the two compositions, cf. eq.(4.45), the curve-fitting of the experimental data must be done in a meaningful and consistent way for them to hold any significance. This can be ensured by adopting methods commonly used for fitting state functions in classical chemical thermodynamics [186].

Along the no-EC edge of the ternary composition space —where y_e varies but

$y_o = 0$—, it is logical to demand $\Delta U(y_o, y_e)$ returns the liquid-junction potential in the binary, as Wang et al. [4] presented. That is,

$$\Delta U\left(0, y_e\right) - \Delta U\left(0, y_e^{ref}\right) = \Delta U_{1:0}\left(y_e\right), \tag{4.48}$$

where $\Delta U_{1:0}(y_e)$ is given by eq.(4.47) relative to $y_e^{ref} = 0.09379$. Similarly, the liquid-junction potential along the no-EMC edge (which corresponds to $y_o = 1 - 2y_e$ because $y_0 = 0$) can be made to obey

$$\Delta U\left(1 - 2y_e, y_e\right) - \Delta U\left(1 - 2y_e^{ref}, y_e^{ref}\right) = \Delta U_{0:1}\left(y_e\right), \tag{4.49}$$

with a single composition dependence on y_e. Because EC is a solid at room temperature under atmospheric pressure, $\Delta U_{0:1}$ is not experimentally measurable. Nonetheless, the trend in the voltage curves in Figure 4.2 suggests that a Nernstian dependence for $\Delta U_{0:1}$ at low salt concentrations would be reasonable, too, similar to $\Delta U_{1:0}$. Therefore, a function in the same form of eq.(4.46) can describe $\Delta U_{0:1}$.

$$\Delta U_{0:1}\left(y_e\right) = \frac{RT}{F}\left(b_{\ln} \ln y_e + \sum_{k=0}^{2} b_k y_e^k\right) \tag{4.50}$$

To accommodate the binary-property correlations described by equations (4.48) and (4.50) in a consistent way, the liquid-junction-potential data were fit using the following general structure.

$$\Delta U\left(y_o, y_e\right) = \left(1 - \frac{y_o}{1 - 2y_e}\right)\Delta U_{1:0}\left(y_e\right) + \frac{y_o}{1 - 2y_e}\Delta U_{0:1}\left(y_e\right) + \Delta U_{ex}\left(y_o, y_e\right) \tag{4.51}$$

The prefactors of $\Delta U_{1:0}$ and $\Delta U_{0:1}$ guarantee the desired properties and derive from the facts that physical salt fractions lie within the range $0 \leq y_e \leq 1/2$ and EC fractions within $0 \leq y_o \leq 1 - 2y_e$. ΔU_{ex} is the excess liquid-junction potential that compensates for the deviation from the composition-weighted average of $\Delta U_{1:0}$ and $\Delta U_{0:1}$ at interior points within the ternary composition space. Inspired by the three-suffix Margules

correction for ternary solutions from thermodynamics, ΔU_{ex} can be expressed as a power-series expansion in particle fractions

$$\Delta U_{\mathrm{ex}}\left(y_{\mathrm{o}}, y_{\mathrm{e}}\right) = \frac{RTy_{\mathrm{o}}\left(1 - y_{\mathrm{o}} - 2y_{\mathrm{e}}\right)}{F}\left[p + qy_{\mathrm{o}} + r\left(1 - y_{\mathrm{o}} - 2y_{\mathrm{e}}\right)\right], \tag{4.52}$$

where p, q, and r are constants. It is important to point out that ΔU_{ex} should be nullified along the no-EC and no-EMC edges (i.e., $\Delta U_{\mathrm{ex}}(0, y_{\mathrm{e}}) = 0$ and $\Delta U_{\mathrm{ex}}(1 - 2y_{\mathrm{e}}, y_{\mathrm{e}}) = 0$), and the $y_{\mathrm{o}}(1 - y_{\mathrm{o}} - 2y_{\mathrm{e}})$ term assures this. The constants p, q, and r, as well as b_{ln}, b_0, b_1, and b_2 can be estimated by linearly regressing the (appropriately shifted) liquid-junction-potential measurement data, with the method of least squares. This yielded the parameter set in Table 4.4, which produces the best-fit surface shown in Figure 4.3 (as a ternary map) and Figure 4.4 (as a 3D plot). The residual voltages (the difference between the measured liquid-junction potentials and the best fit) in the bottom pane of Figure 4.4 illustrate that the fit is satisfactory; they are clustered densely near 0 mV and deviate at most 10 mV. Bear in mind that use of this correlation for $\Delta U(y_{\mathrm{o}}, y_{\mathrm{e}})$ should be restricted to the range $0 < y_{\mathrm{o}} < 0.75$ and $0.002 < y_{\mathrm{e}} < 0.15$ to avoid extrapolation.

Table 4.4: Fit parameters for the liquid-junction-potential correlation in equations (4.51), (4.50), and (4.52).

b_{ln}	b_0	b_1	b_2
3.024	8.233	−88.12	477.9

p	q	r
32.20	−37.99	−44.80

4.2.3 Discussion

A ternary map and a 3D plot of the liquid-junction potential over the tested compositions are illustrated in Figures 4.3 and 4.4, respectively. The most striking feature of the liquid-junction-potential surface is that appreciable voltage differences are registered

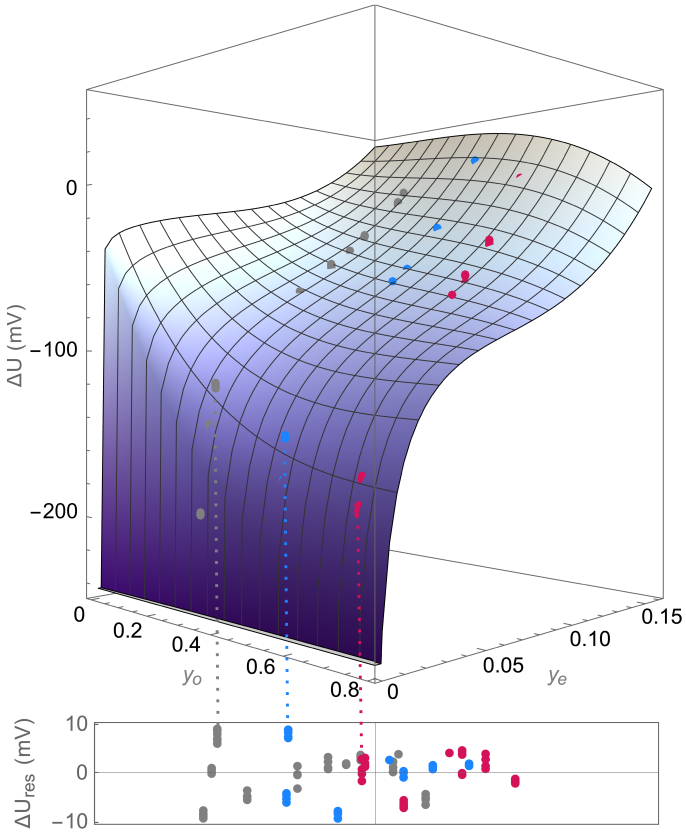

Figure 4.4: (Top) Liquid-junction-potential surface $\Delta U\,(y_\mathrm{o}, y_\mathrm{e})$ yielded by fitting eq.(4.51) to experimental data (marks). Data sets corresponding to different EMC:EC cosolvent ratios are distinguished with grey (7:3), blue (1:1), and red (3:7) markers. (Bottom) Scatter plot showing residual voltage difference between each experimental data point and the best-fit surface.

between different cosolvent fractions at constant salt content y_e, most clearly perceivable in Figure 4.4. Sizable variations of ΔU with cosolvent ratio, especially at low salt particle fractions, refute the electrical aspect of the single-solvent approximation for the EMC:EC:LiPF$_6$ electrolyte system.

The observed phenomenon carries practical significance in batteries only if applied currents induce cosolvent polarisation near the two electrodes; this is indeed the case. Solvent transport can be driven in two main ways. First, Faradaic convection occurs when the consumption and production of Li^+ at the electrodes bring changes in the local volume of the solutions, which in turn induces bulk flows [187]. Second, electro-osmotic solvent transport occurs when current-carrying ions exert a more diffusional drag on one solvent (EC, say) than the other (EMC) as they move. This is embodied

by the migration coefficient Ξ. Strong evidence of ion energetics influencing the solvent distribution exists in the literature. Raman spectroscopy by Jeong et al. [188] confirmed EC preference over dimethyl carbonate (DMC) and diethyl carbonate (DEC) —both structurally similar to EMC— in the Li^+ solvation shell, although the experiment was conducted at a fixed salt concentration with a single cosolvent ratio (1:1 by volume). Using the same technique, a more comprehensive study by Uchida and Kiyobayashi [189] indicated that EC is about twice as preferred in the solvation shell of Li^+ than DMC in low-EC mixtures and this preference decreases as the EC concentration is raised. More directly, Von Wald Cresce et al. [190], through the electrospray-ionization mass spectrometry, found that EC is much more strongly favoured in the solvation shell of Li^+ over EMC and again, this is especially pronounced in the lower range of EC particle fraction.

Ternary junction-potential correlations allow one to incorporate the effect of cosolvent polarisation to improve a battery's OCV estimation. Through the Hittorf measurements[6], Wang et al. [182] confirmed that the EMC:EC ratio near the surface of a cycling electrode can swing widely away from its bulk value. Their simulation indicated the EMC:EC mass ratio deviated from 1:1 (with $(c_0, c_o, c_e) = (5.27\text{M}, 6.24\text{M}, 1.00\text{M})$) to 1:1.6 at the cathode surface, which amounts to a 2 M rise in EC concentration and a drop of 0.8 M in salt concentration relative to the bulk. At the anode surface, the ratio changed to 1:0.6, with a 2 M drop in EC concentration and an increase of 0.9 M in salt concentration. The overpotential caused by salt polarisation is much larger in magnitude than that caused by EC polarisation; 53.4 mV/M vs. -5.85 mV/M, respectively, in the bulk solution of Wang et al.'s Hittorf cell [182]. However, because the solvent-concentration change is shown to be about twice as large as the salt-concentration change, the overpotential from the solvent polarisation cannot be ignored. The ΔU

[6]The experiment involved passing a constant current of 0.5 mA for 20 hours. Since this current is much smaller than what conventional Li-ion batteries sustain, one can use Sand's time from the Sand equation to predict the system dynamics under a higher current. Sand's time (t_{Sand}) corresponds to the time the reduced cation is depleted at the electrode-electrolyte interface when a metal is electrodepositied, which is what happens during the Hittorf experiment. The equation shows that $i\sqrt{t_{\text{Sand}}}$ = constant. Thus, the same experimental observation is expected to arise in less than one second when 1 A current is passed.

correlation established here shows that 8% and 10% of the overpotential at the cathode and anode surfaces, respectively, stem from the EC polarisation, relative to the bulk. Therefore, based on the size of observed current-induced changes in cosolvent ratio, accounting for the changes in solvent distribution is expected to be important, especially for high-fidelity battery models. For instance, the impact of consistently missing 10% of the overpotential is going to build up over multiple charge–discharge cycles, producing a noticeable discrepancy between the model output and the real battery behaviour the model aims to simulate. Such a model is likely to underestimate the effects of ageing, predicting a lower capacity loss over time, as a result. Other cascading effects of omitting the solvent-segregation overpotential in battery models may exist; actual numerical simulations will need to be implemented to confirm these.

Thermodynamic consistency of junction potentials

It should be reminded that the liquid-junction-potential surface-fitting exercise in the previous section is only valid if the voltage Φ in MacInnes equation in eq.(4.23) is a path-independent state function at open circuit. This was implicitly assumed when deriving eq.(4.43) to express ΔU as a thermodynamic path integral. This means that for the correlation $\Delta U(y_\mathrm{o}, y_\mathrm{e})$ in eq.(4.51) with the parameter set in Table 4.4 to attain utility, the amount of energy dissipated during concentration-cell experiments must be negligible. The liquid-junction-potential measurements reported here remained stable over time; however, this does not ensure the reversibility of the process being measured.

An intuitive method of testing the reversibility of the junction potential is to perform a series of concentration-cell experiments that traverse closed paths in the composition space. The net voltage change should add up to zero if irreversible losses are negligible. Six closed loops were drawn from concentration-cell experiments between the composition points listed in Table 4.2. The direct measurement values in Table 4.3 and the fixed-solvent-ratio liquid-junction-potential curves in eq.(4.46) —with the necessary parameters in Table 4.1— were used to calculate the net voltage around the loops. The accumulated voltage ($\sum \Delta U$) around each loop is provided in Table 4.5, as

Table 4.5: Liquid-junction potentials measured experimentally around six closed loops in the composition space.

	Path	$\sum \Delta U$ (mV)	$\sum \lvert\Delta U\rvert$ (mV)	$\lvert\sum \Delta U\rvert / \sum \lvert\Delta U\rvert$
Loop 1	A_1-A_2-B_2-B_1-A_1	7	237	0.030
Loop 2	B_1-B_2-C_2-C_1-B_1	−4	238	0.017
Loop 3	C_1-C_2-D_2-D_1-C_1	−11	246	0.045
Loop 4	A_1-A_2-C_2-C_1-A_1	5	262	0.019
Loop 5	B_1-B_2-D_2-D_1-B_1	−14	300	0.047
Loop 6	A_1-A_2-D_2-D_1-A_1	−5	322	0.016
	Average	−4	268	0.015

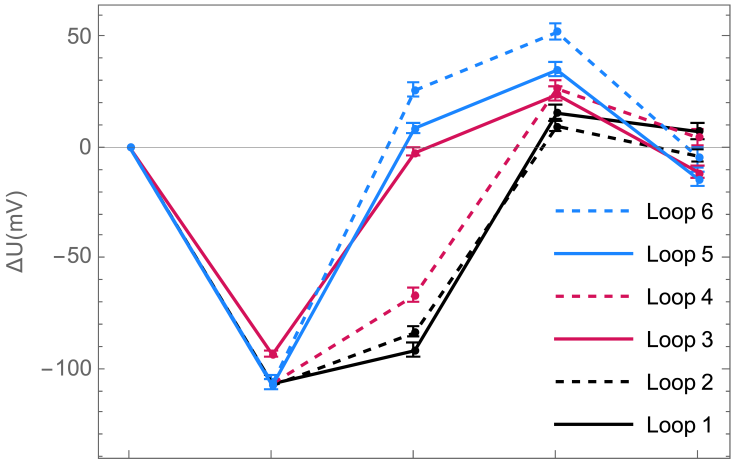

Figure 4.5: Net liquid-junction potential around the six loops in ternary composition space described in Table 4.5.

well as the total voltage traversed ($\sum |\Delta U|$). Figure 4.5 summarises this closing-the-loop exercise graphically. Clearly, it resulted in both voltage gains and losses around the loops, all of which closed within an average of 1.5% of the total voltage traversed. Notably, despite hundreds of miliovolts being traversed in each loop, as evident in Figure 4.5, the mismatch voltages are concentrated around 0 mV upon closing the loops (i.e., when returning to the starting composition of each loop). The biggest misalignment comes from Loop 5, whose mismatch was −14 mV, or 4.7 % of the total voltage traversed ($\sim$ 300 mV). This is about double the size of the residuals shown in Figure 4.4, and thus not far outside the range expected based on experimental error. Therefore, liquid-junction potentials appear to be reversible enough to justify the use

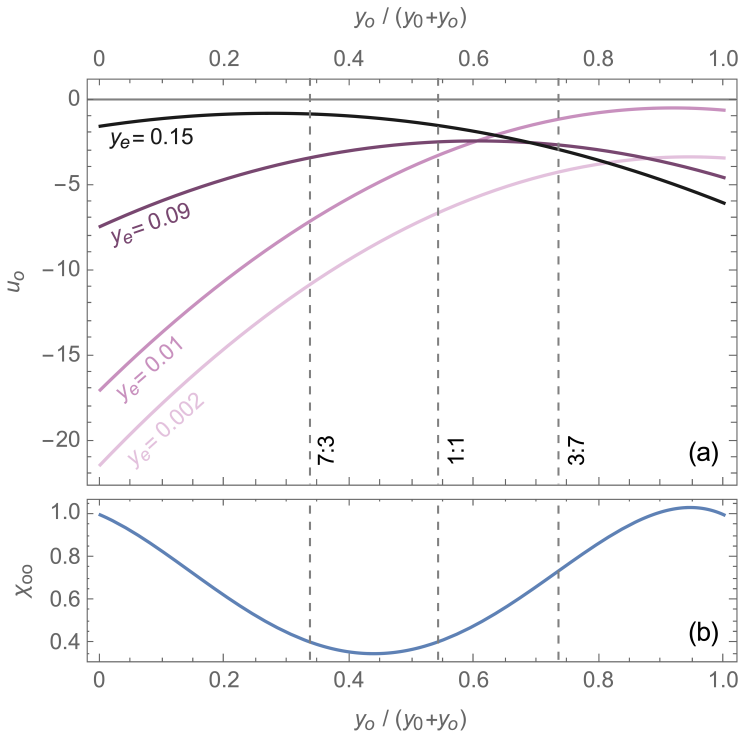

Figure 4.6: Plots against the EC particle fraction in neat cosolvent of (a) the junction coefficient u_o for four salt particle fractions y_e and (b) the thermodynamic factor χ^m_{oo} of a salt-free EMC:EC binary mixture derived from the correlation of Ding [6].

of experimental correlations in battery models.

Junction coefficients

What immediately follows from having a liquid-junction-potential parameterisation is the two junction coefficients u_o and u_e, *via* eq.(4.45). Figure 4.6(a) shows $u_o(y_o, y_e)$ for y_e = 0.002, 0.01, 0.09, and 0.15. The first and last of these values correspond to the boundaries of the experimental composition range; 0.01 and 0.09 correspond to y_e along the A_2-B_2-C_2-D_2 and A_1-B_1-C_1-D_1 paths (see Figure 4.3), respectively. Figure 4.7 presents the values of $y_e u_e(y_o, y_e)$, a more smoothly varying combination that does not diverge as the dilute limit of salt is approached, i.e., the leading-order $1/y_e$ dependence in u_e, expected from eq.(4.44)[7], is cancelled out by y_e. $y_e u_e$ for the three tested cosolvent

[7]Note, $\chi^m_{ee} \to 1$ and $\chi^m_{oe} \to 0$ as $y_e \to 0$. To model the expected Nernstian dependence of open-circuit potential on salt concentration more clearly, one can use the MacInnes equation of the form

$$\frac{\vec{i}}{\kappa} = -\nabla\Phi + \frac{RTu_o}{F}\nabla y_o + \frac{RTu_e y_e}{F}\nabla \ln y_e$$

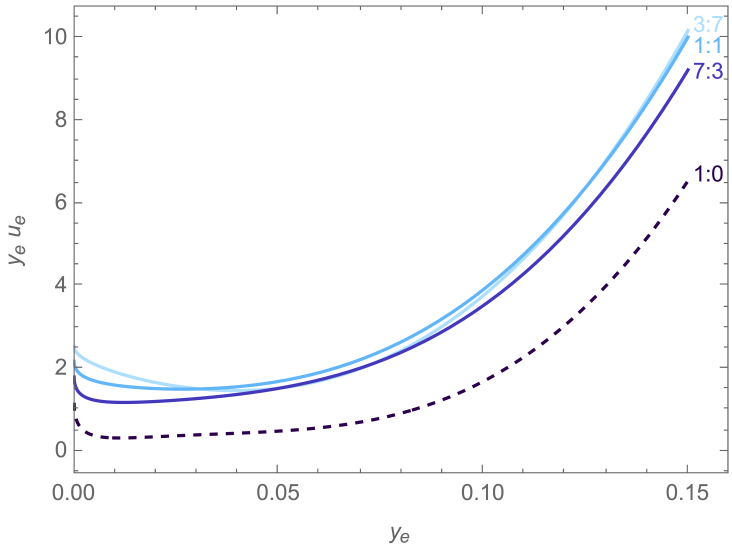

Figure 4.7: The junction coefficient u_e weighted by the salt particle fraction y_e at EMC:EC mole ratios of 3:7, 1:1, 7:3, and 1:0.

ratios are plotted, as well as for $LiPF_6$ in pure EMC (1:0) that Wang et al. [4] studied. The junction coefficients vary with both the salt and EC contents, but the salt content has a greater influence, especially for u_o when salt is dilute. This is in line with the expectation, given the Nernstian behaviour of concentration overpotential in the dilute regime. Significantly, in the moderately concentrated region where Li-ion batteries usually operate (NB: $y_e = 0.08902$ for 1 M $LiPF_6$ in EMC), u_o is sizable enough compared to $y_e u_e$, so that both junction coefficients are needed to describe the voltage accurately. This again supports the conclusion that the single-solvent approximation may not suffice for high-fidelity battery models.

The values of u_o in Figure 4.6(a), which relates to eq.(4.44), provide a gateway to infer about EC migration. It is observed that u_o declines substantially as the salt concentration decreases. This may come down either to the thermodynamic nature (i.e., χ^m_{oo} and χ^m_{eo}) or transport dynamics (i.e., Ξ and $t^0_- = 1 - t^0_+$) of the solution, as a function of composition. Their relative effects can be appraised at least in solutions of low salt content using the activity information in the EMC:EC binary [6]. By constructing a phase diagram of the system through calorimetry, Ding [6] obtained an

in the open-circuit condition to replace eq.(4.43). Then, the lumped quantity $y_e u_e$ can be recognised as a composition-dependent material parameter. Because $\Xi \propto y_o$, a similar transformation is not necessary for the coefficient of ∇y_o.

expression for the EC activity coefficient, which can be differentiated to produce the thermodynamic factor, $\chi^{\mathrm{m}}_{\mathrm{oo}}$. Its functional form at 25 °C is

$$\chi^{\mathrm{m}}_{\mathrm{oo}}\left(y_{\mathrm{o}},0\right)=1+2y_{\mathrm{o}}(1-y_{\mathrm{o}})\left[A_1-A_0+3(A_2-A_1)y_{\mathrm{o}}-6A_2y_{\mathrm{o}}^2\right], \tag{4.53}$$

where $A_0 = 1.0471$, $A_1 = 0.42506$, and $A_2 = -0.85568$. As shown in Figure 4.6(b), $\chi^{\mathrm{m}}_{\mathrm{oo}}$ lies between ~ 0.4 and ~ 1, with a minimum near $y_{\mathrm{o}} = 0.4$. The variation in $\chi^{\mathrm{m}}_{\mathrm{oo}}$ across the cosolvent composition range is about a factor of 2, whereas that in u_{o} is by a factor of ten or more. Also, in the solvent-ratio range between 0 and 0.4 where u_{o} is shown to rise, $\chi^{\mathrm{m}}_{\mathrm{oo}}$ decreases. Both these facts combine to conclude that cosolvent thermodynamics is an unlikely cause of the exhibited u_{o} behaviour —both in trend and magnitude— at high dilution.

In a prior model derived for lithium–oxygen-battery electrolytes, Monroe [157] derived an expression for the migration coefficient and showed that $\Xi \propto c_{\mathrm{o}}$. Hence, Ξ/y_{o} in eq.(4.44) remains finite even when y_{o} diminishes. To make this explicit, we define a new parameter $\tilde{\Xi}$, which relates to Ξ in the following way.

$$-\tilde{\Xi}=-\frac{2\Xi}{y_{\mathrm{o}}}=\frac{\mathscr{D}_{\mathrm{o}}\left(t^{\mathrm{o}}_{+\emptyset}-t^{0}_{+\emptyset}\right)}{y_0\mathscr{D}_{\mathrm{eo}}+y_{\mathrm{o}}\mathscr{D}_{\mathrm{e0}}} \tag{4.54}$$

Here, $\mathscr{D}_{\mathrm{eo}}$ and $\mathscr{D}_{\mathrm{e0}}$ are the respective thermodynamic diffusivities of salt in EC and EMC, dependent only on Stefan–Maxwell coefficients, and $t^{\mathrm{o}}_{+\emptyset}$ and $t^{0}_{+\emptyset}$ are respectively the (Hittorf) cation transference numbers relative to pure EC and pure EMC. The negative value of u_{o} across the composition range suggests that lithium transference in EMC is greater than that in EC. This is in line with the results in the literature; although no measurement data is available for the Li^+ transference number in EC (which is a solid at room temperature under atmospheric pressure), EMC exhibits a higher Li^+ transference number [4] than PC [162] —a cyclic carbonate similar to EC— up to moderate dilution. Given $\left|t^{\mathrm{o}}_{+\emptyset}-t^{0}_{+\emptyset}\right|<1$, the most feasible cause for the large magnitudes of u_{o} across the composition range (for low salt-content solutions)

seems to be the difference in the magnitudes of diffusivities in eq.(4.54). It must be the case that the thermodynamic diffusivities of salt in both solvents ($\mathscr{D}_{\mathrm{eo}}$ and $\mathscr{D}_{\mathrm{e0}}$) are substantially lower than EC's component diffusivity in the solution ($\mathscr{D}_{\mathrm{o}}$). A better understanding of u_{o} would be gained from more in-depth composition-dependent diffusion and transference characterisation studies across the ternary space.

Of course, $\chi^{\mathrm{m}}_{\mathrm{oo}}$ in eq.(4.53) is only valid in the absence of salt and its magnitude may become sufficiently large to influence u_{o} more strongly when salt is present (if $\chi^{\mathrm{m}}_{\mathrm{eo}}$ is relatively small, u_{o} would be proportional to $\chi^{\mathrm{m}}_{\mathrm{oo}}$). Still, activity coefficients of species in solution tend to depend most strongly on their own concentration. Hence, amplification of $\chi^{\mathrm{m}}_{\mathrm{oo}}$ due to the addition of salt may not be so dramatic.

An estimate for the migration coefficient of 1 M $LiPF_6$ in 1:1 mass-ratio EMC:EC is available from Wang et al., who processed Hittorf measurements for the ternary system with a Gaussian-process regression technique [182]. The quantity they reported (which is equal to $-y_{\mathrm{o}}\tilde{\Xi}$ in the present notation[8]) suggests that $\tilde{\Xi} = 3.0 \pm 0.2$. Making use of the binary correlation of Ding [6] for $\chi^{\mathrm{m}}_{\mathrm{oo}}$ in eq.(4.53) and assuming $\chi^{\mathrm{m}}_{\mathrm{eo}} \approx 0$, our u_{o} measurement at the corresponding composition produces $\tilde{\Xi} = 3.2$ through eq.(4.44). The fair agreement between these values indicates that $\tilde{\Xi}$ can be estimated from junction-coefficient measurements with the thermodynamic simplifications, without incurring large inaccuracy. Notably, junction coefficients are far easier to measure across the composition space than Hittorf transference numbers, so this route for property estimation has substantial practical utility.

Last, another possibility producing the observed trends in u_{o} is the composition dependence of $\chi^{\mathrm{m}}_{\mathrm{eo}}$. The Maxwell relation in eq.(4.22) suggests $\chi^{\mathrm{m}}_{\mathrm{eo}} = O\left(y_{\mathrm{e}}\right)$ or higher, but any dependence of order ${y_{\mathrm{e}}}^{\alpha}$, where $0 < \alpha < 1$, could induce the observed trend. This would be counterintuitive since thermodynamic stability demands that the salt activity coefficient approach a constant value at infinite dilution. Nonetheless, there could be a small window of low salt concentrations where such unusual concentration dependence

[8] Wang et al. [182] defined the migration flux of EC to be negative in the direction of the conventional current, whereas the opposite convention was used here, resulting in the sign switch between their value and our $\tilde{\Xi}$.

arises. To verify this statement, more extensive thermodynamic experiments in the ternary space will be needed. For example, vapour–liquid equilibrium may be studied to derive activity correlations of the EMC:EC:$LiPF_6$ electrolyte directly.

4.3 Deriving thermodynamic factors from partial pressures for the binary salt in two neutral solvents

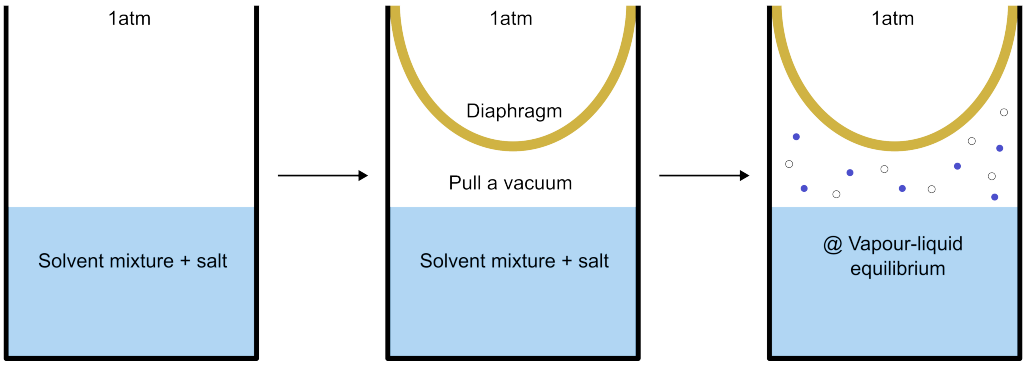

Figure 4.8: Partial-pressure measurement setup. The solution mixture is sealed with a diaphragm and a vacuum is pulled over its headspace, after which is left to reach a vapour–liquid equilibrium.

The amalgamation of thermodynamic and transport properties in the liquid-junction potential measured by the concentration cell prevents thermodynamic factors to be accessed directly. Manipulating the relationship between the fugacity (non-ideality in the gas phase) and activity (non-ideality in the liquid phase) is an alternative strategy that can circumvent this difficulty. Under a vapour–liquid equilibrium, partial pressures are a gateway to activity coefficients, as illustrated in eq.(4.35). A rearrangement of this equation leads to

$$\lambda_i = \frac{P_i}{P_i^{\text{sat}}} y_i^L, \tag{4.55}$$

where λ_i is the activity coefficient of species i on the particle fraction basis, P_i is its

partial pressure, P_i^{sat} is its saturated vapour pressure (at a vapour–liquid equilibrium of pure species i), and y_i^L denotes its particle fraction in the liquid phase, indicated by the superscript L. Consequently, if a system contains two volatile solvents, partial-pressure measurements can directly gauge all three thermodynamic factors.

When partial pressures are measured, the total pressure must be kept constant at the expected operating pressure of the system. For example, if the electrolytic solution inside a battery is to function under the atmospheric pressure (1 atm), then the headspace above the solution must maintain this level of pressure throughout the experiment. This may be achieved by using a tall container that can hold the solution at the bottom and whose opening at the top is sealed with a flexible diaphragm, as shown in Figure 4.8. When a vacuum is pulled over the solution and the system is allowed to reach an equilibrium, the external environment at 1 atm would push the diaphragm in so as to ensure that the solution's vapour phase is also at the same pressure. After measuring partial pressures for a suite of mixtures, a table like below can be constructed, with the last column calculated from eq.(4.55) (r_i indicates a fixed ratio of the two solvents 0 and o).

y	y_{o}^L	P_0	P_{o}	$\ln \lambda_{\text{o}}$	
⋮	⋮	⋮	⋮	⋮	} ratio r_1
⋮	⋮	⋮	⋮	⋮	} ratio r_2
⋮	⋮	⋮	⋮	⋮	⋮

From this, a functional form of $\ln \lambda_{\text{o}} = \ln \lambda_{\text{o}}(y_{\text{o}}^L, y)$ can be obtained by a multivariable regression. Differentiating it with respect to y and $\ln y_{\text{o}}^L$ produces χ_{oe} and $\chi_{\text{oo}} - 1$, respectively, according to eq.(4.21). A functional form of the activity coefficient of the second solvent, $\ln \lambda_0 = \ln \lambda_0(y_{\text{o}}^L, y)$, can be calculated in the same way. Because the salt particle fraction has been employed as an independent composition variable, thermodynamic factors relating to the salt are more desirable. They can indeed be

expressed as

$$\begin{aligned}\chi_{\mathrm{eo}}(y_{\mathrm{o}}^{L}, y) =& -\frac{1}{\nu}\left[\chi_{\mathrm{oo}} - 1 + \left(1 - y_{\mathrm{o}}^{L} - \nu y\right)\left(\frac{\partial \ln \lambda_0}{\partial y_{\mathrm{o}}^{L}}\right)_{T,p,y}\right] \\ \chi_{\mathrm{ee}}(y_{\mathrm{o}}^{L}, y) =& 1 - \frac{1}{\nu}\left[\chi_{\mathrm{oe}} + \left(1 - y_{\mathrm{o}}^{L} - \nu y\right)\left(\frac{\partial \ln \lambda_0}{\partial y}\right)_{T,p,y_{\mathrm{o}}^{L}}\right]\end{aligned}, \tag{4.56}$$

after introducing the isothermal, isobaric Gibbs–Duhem equation. A side benefit of this approach is that it allows one to check whether the assumption of symmetric core-potential Hessian is valid by comparing the $\chi_{\mathrm{eo}}(y_{\mathrm{o}}^{L}, y)$ above and the one obtained from eq.(4.22).

4.4 Summary and outlook

Parameterisation of thermodynamic factors was the focal point of this chapter. The liquid-junction-potential measurement *via* the concentration cell was investigated extensively, while the partial-pressure measurement was lightly touched on, as an alternative method. The main outcomes of this chapter are as follows.

1. In section 4.1.2, the salt thermodynamic factor in the three-ion ionic liquid case was found to be more complicated than the ones involving neutral solvents. The offset term K in $\chi_{\mathrm{ee}}^{\mathrm{m}} = K + \left(\frac{\partial \ln \lambda_{\mathrm{e}2}}{\partial \ln y_{\mathrm{e}2}}\right)_{T,p}$ is not just 1, but is a composition and stoichiometry (ν_i's) dependent quantity. For example, K reduces to $1/2$ in the dilute limit for a system made up of two symmetric binary salts containing single valency ions. This is due to the presence of the shared ion between the two salts.

2. The relationship between the liquid-junction potential and thermodynamic and transport properties was established for the binary salt in two neutral solvents in section 4.1.3. To the best of the author's knowledge, this is the first time such an exposition has been made for the system, despite the common use of cosolvent electrolytes in conventional Li-ion batteries.

3. The liquid-junction-potential measurement of EMC:EC:$LiPF_6$ in section 4.2 confirmed that the ubiquitous single-solvent approximation is not sufficient for high-fidelity Li-ion battery models.

Now, we are sufficiently equipped to extract functional forms of thermodynamic factors from experiments to employ $d\mu_i$'s in section 3.4 for numerical simulations. However, there are some aspects this chapter has not fully covered and the following is suggested for future work.

1. Salt thermodynamic-factor characterisation for three-ion ionic liquids based on experimental liquid-junction-potential data would be an interesting exercise to confirm the theory developed in section 4.1.2.

2. More liquid-junction potential data for EMC:EC:$LiPF_6$ would improve the accuracy of the ΔU functional form. The parameterisation of the cation transference number t_+^0 and the migration coefficient $\tilde{\Xi}$ over the ternary composition space will enable thermodynamic factors to be extracted from the ΔU obtained. Alternatively, partial pressures can be measured to extract transport properties from the parameterised ΔU.

3. Incorporating the ΔU in battery models would portray the effects of solvent polarisation more concretely and highlight the shortcomings of the current ones.

In the next chapter, techniques in Chapters 3 and 4 are applied to study membrane systems.

Chapter 5

Charged-membrane transport model and properties

Membranes in electrochemical energy systems serve not only to prevent the anolyte and catholyte from mixing but also to allow an ionic pathway, enabling redox reactions to proceed and electrical energy to be delivered or stored. In this chapter, we focus on Nafion, a widely used membrane for various energy systems —such as fuel cells and redox flow batteries— that acts as a selective barrier to regulate the flow of charged species. The semi-permeability of Nafion is imparted by negatively charged sulfonate end-groups (SO_3^-) that are attached to the hydrophobic backbones [89]. The backbones give the membrane integrity, while the embedded end-groups suppress the anion movement and promote the cation flow across the membrane.

One way of modelling charged membranes like Nafion is to treat its end-groups as a discrete species that can conceptually move within its volume [113, 114]. In reality, they are bound to the backbone chains and attain zero average velocity relative to the lab frame. In order to reflect this physical constraint, the charged end-group can be chosen as the species that sets the reference velocity of the system. Some take this even further and set its flux to zero to facilitate the inversion from the force-explicit OSM equations to the flux-explicit form [113, 114]. But this is not necessary for the inversion procedure put forward by Van-Brunt et al. [56]; their method can

deliver flux equations relative to any reference frame. Using their method to derive flux equations for a charged membrane submerged in a binary electrolyte is one of the two main objectives of this chapter. By comparing the acquired flux expressions to experimentally measured species fluxes across Nafion 117 [2], the Stefan–Maxwell diffusivity between the bisulfate ion ($-$) and the sulfonate end-group (M) (i.e., $\mathscr{D}_{-\mathrm{M}}$) can be extracted. This is the second objective of this chapter.

Although Stefan–Maxwell diffusivities are essential for the simulation of species movement in and across membranes, $\mathscr{D}_{i\mathrm{M}}$ (where i represents species other than M) have not been investigated extensively, yet. Delacourt and Newman [114] and Weber and Delacourt [113] extracted the desired parameters using the existing literature data but they were treated as constants, not concentration-dependent quantities. Sijabat et al. [191] estimated $\mathscr{D}_{ij}$ inside membranes using tortuosity and concentration-dependent $\mathscr{D}_{ij}$ in membrane-free solutions, based on Wesselingh et al.'s assertion [192]. However, $\mathscr{D}_{ij}$'s embody molecular interactions and it is unclear whether the porous structure of membranes —whose length scale must be well beyond the length scale at which species–species interactions take place— influences the diffusivities as proposed. More elaborately, Crothers et al. [131, 132] calculated $\mathscr{D}_{i\mathrm{M}}$ by considering its connection to a friction coefficient —a parameter that arises when the membrane is treated as a cluster of microchannels— so that it is a function of the membrane-pore radius, dry-membrane domain spacing, and the degree of swelling when submerged in water. This may well be a reasonable and accurate method of attack, but the complexity of their procedure would likely mean non-experts are hindered from applying it flexibly and even correctly. This approach may be undesirable for the sake of consistency, as well, if one wishes to treat the system macroscopically, which is the viewpoint this thesis takes. Moreover, the level of confidence one can have in theoretically derived quantities is intrinsically lower than the values obtained from measurements. Therefore, a direct parameterisation of $\mathscr{D}_{i\mathrm{M}}$ (as a function of concentration) would be of immense value for those wishing to carry out diffusion simulations across membranes without being

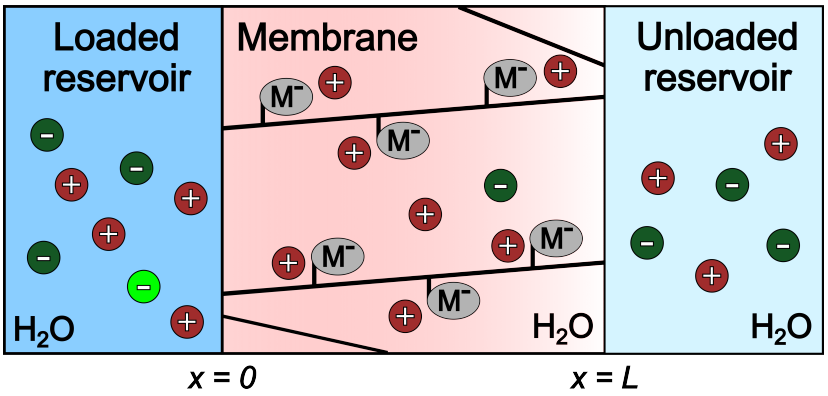

Figure 5.1: Diagram of Verbrugge and Hill's first experiment [2]. (+), (−), and M^- designate H^+, $HSO_4{}^-$, and the embedded sulfonate end-group, respectively. Radioactive H_2SO_4 is added to the loaded reservoir at $t = 0$. The bright green (−) shows a radioactive $HSO_4{}^-$.

concerned about their microscopic details. We revisit Verbrugge and Hill's work [2, 3] to achieve this.

5.1 Summary of Verbrugge and Hill's work

Two experiments were conducted by Verbrugge and Hill [2] using a radio-tracing technique. In both experiments, a piece of Nafion 117 was placed between two reservoirs of equal volume containing sulfuric acid and water, as shown in Figure 5.1. A small amount ($\sim 10^{-9}$ M) of radioactive sulfuric acid (unstable ^{35}S was used to distinguish it from the most common isotope ^{32}S) was added to one reservoir (called the loaded reservoir) at the start of the experiment. The amount of radioactive sulfur in the other reservoir (called the unloaded reservoir) was then recorded at various time steps using a liquid-scintillation spectrometer to measure the rate of diffusion across the membrane. The ratio of the radioactive sulfur in the two reservoirs was reported, which contains the diffusivity information.

Although Verbrugge and Hill [2] used the identical setup for the two experiments, the relative amount of sulfuric acid in the two reservoirs differentiates the two. While both reservoirs were filled with sulfuric acid of the same concentration in the first experiment, the loaded and unloaded reservoirs were filled with 1 M and 0.1 M sulfuric acid

solutions, respectively, in the second experiment. The analysis of the second experiment is rather tricky because all mobile species can move, driven by two independent concentration gradients (∇c_0 and ∇c_e). The contribution from each concentration gradient to each species flux is difficult to ascertain from this experiment alone, inhibiting further analysis. In contrast, the first experiment is performed very close to an equilibrium and many driving forces can be effectively turned off, simplifying the flux equations considerably. Thus, only the first experiment is re-analysed to find a Stefan–Maxwell diffusivity, assuming the binary interactions between water, proton, and bisulfate ion in membrane-free aqueous sulfuric acid remain unaffected inside Nafion.

Before embarking on the analysis, a few more simplifying assumptions are highlighted. Firstly, it is assumed that HSO_4^- is the only mobile anion in the system, i.e., the dissociation $HSO_4^- \rightarrow H^+ + SO_4^{2-}$ is not favoured. This is reasonable because the total proton concentration in the membrane is much higher than that of free anions, due to the attraction emanating from the negatively charged sulfonate end-groups in Nafion. Secondly, the molar concentration of the end-group is assumed to be constant at $c_M = 1.2$ M, as Verbrugge and Hill [2] assumed. This is justifiable because the membrane is not expected to swell actively during the experiment, having gone through appropriate pretreatments. Lastly, the entire membrane is treated as an electroneutral phase. Although non-electroneutral double layer regions are present near the membrane–solution interfaces, they are so thin (in the nm range) compared to the membrane thickness (in the hundreds of μm range) that they are often ignored in membrane models; this is the approach we adopt for the Stefan–Maxwell diffusivity characterisation, too.

5.2 Flux equations in membrane

Van-Brunt et al. [56] constructed a streamlined methodology to derive flux expressions under electroneutrality from the force-explicit OSM equations. Their approach is flexible in that not only does it allow a flux equation for each species to be written, but

also for each neutral cluster of species (which they referred to as component). For the simplest case of Nafion imbued with an aqueous sulfuric acid, four species are present; water, sulfonate group ($SO_3{}^-$), bisulfate ion ($HSO_4{}^-$), and proton (H^+), which are denoted by 0, M, −, and +, respectively. This can be translated to a three-component system composed of water, sulfuric acid (H_2SO_4), and sulfonic acid ($R{-}HSO_3$), denoted by 0, e, and $\overline{\mathrm{M}}$, respectively. Recognising that the transference number for the species that sets the reference-frame velocity is zero, the fluxes $\vec{N}_i$ for component $i \in \{0, \mathrm{e}, \overline{\mathrm{M}}\}$ relative to the sulfonate-group velocity $\vec{v}_\mathrm{M}$ can be written as

$$\begin{aligned}
\vec{N}_0 &= -\mathcal{D}_0 \frac{c_\mathrm{T} c_0 \nabla \mu_0}{2 c_{\overline{\mathrm{M}}} RT} - \mathcal{D}_\times \frac{c_0 c_\mathrm{e} \nabla \mu_\mathrm{e}}{2 c_{\overline{\mathrm{M}}} RT} + \frac{\tilde{\Xi} c_0}{c_\mathrm{T}} \frac{\vec{i}}{F} + c_0 \vec{v}_\mathrm{M} \\
\vec{N}_\mathrm{e} &= -\mathcal{D}_\times \frac{c_0 c_\mathrm{e} \nabla \mu_0}{2 c_{\overline{\mathrm{M}}} RT} - \mathcal{D}_\mathrm{e} \frac{c_\mathrm{T} c_\mathrm{e} \nabla \mu_\mathrm{e}}{4 c_{\overline{\mathrm{M}}} RT} + \left(\frac{1}{3} - t_-^\mathrm{M} \right) \frac{\vec{i}}{F} + c_\mathrm{e} \vec{v}_\mathrm{M} \,, \\
\vec{N}_{\overline{\mathrm{M}}} &= \frac{\vec{i}}{3F} + c_{\overline{\mathrm{M}}} \vec{v}_\mathrm{M}
\end{aligned} \tag{5.1}$$

where μ_i is the electrochemical potential of component i, $c_\mathrm{T} = c_0 + 2c_\mathrm{e} + 2c_{\overline{\mathrm{M}}}$ is the total concentration, F is the Faraday constant, t_-^M is the bisulfate-ion transference number (relative to the sulfonate-group velocity), and $\vec{i}$ is the current density. The appearance of 2 and 4 in eq.(5.1) is due to the fact that both sulfonic and sulfuric acids have the total stoichimetry of 2. Note that because the frame of reference follows the sulfonate end-group ($SO_3{}^-$), the sulfonic-acid flux $\vec{N}_{\overline{\mathrm{M}}}$ is not zero when an electric current flows through the system, due to the flow of protons. The three thermodynamic diffusivities in eq.(5.1), namely $\mathcal{D}_0$, $\mathcal{D}_\times$, and $\mathcal{D}_\mathrm{e}$, relate to the Stefan–Maxwell diffusivities and can be written succinctly if we introduce the following macroscopic binary diffusivities, first.

$$\begin{aligned}
D_{0\mathrm{e}} &= \frac{(z_+ - z_-)\mathscr{D}_{0-}\mathscr{D}_{0+}}{z_+ \mathscr{D}_{0+} - z_- \mathscr{D}_{0-}} \\
D_{0\overline{\mathrm{M}}} &= \frac{(z_+ - z_\mathrm{M})\mathscr{D}_{0\mathrm{M}}\mathscr{D}_{0+}}{z_+ \mathscr{D}_{0+} - z_\mathrm{M} \mathscr{D}_{0\mathrm{M}}} \\
\frac{1}{D_{\mathrm{e}\overline{\mathrm{M}}}} &= \frac{z_+^2}{(z_+ - z_-)(z_+ - z_\mathrm{M})\mathscr{D}_{-\mathrm{M}}} - \frac{c_0 z_- z_\mathrm{M}}{c_+ (z_+ - z_-)(z_+ - z_\mathrm{M})\mathscr{D}_{0+}} \\
&\quad - \frac{z_-(c_- z_- + c_+ z_+)}{c_+ (z_+ - z_-)(z_+ - z_\mathrm{M})\mathscr{D}_{+-}} - \frac{z_-(c_\mathrm{M} z_\mathrm{M} + c_+ z_+)}{c_+ (z_+ - z_-)(z_+ - z_\mathrm{M})\mathscr{D}_{+\mathrm{M}}}
\end{aligned} \tag{5.2}$$

z_j is the equivalent charge of species j and $z_+ = -z_- = -z_{\mathrm{M}} = 1$ for this system. The $\mathcal{D}_i$'s can then be expressed as[1]

$$\begin{aligned}
\mathcal{D}_0 &= \frac{D_{0\overline{\mathrm{M}}}(2c_{\overline{\mathrm{M}}}D_{0\mathrm{e}} + c_0 D_{\mathrm{e}\overline{\mathrm{M}}})}{2c_{\overline{\mathrm{M}}}D_{0\mathrm{e}} + 2c_{\mathrm{e}}D_{0\overline{\mathrm{M}}} + c_0 D_{\mathrm{e}\overline{\mathrm{M}}}} \\
\mathcal{D}_\times &= \frac{c_{\mathrm{T}} D_{0\overline{\mathrm{M}}} D_{\mathrm{e}\overline{\mathrm{M}}}}{2c_{\overline{\mathrm{M}}}D_{0\mathrm{e}} + 2c_{\mathrm{e}}D_{0\overline{\mathrm{M}}} + c_0 D_{\mathrm{e}\overline{\mathrm{M}}}}. \\
\mathcal{D}_{\mathrm{e}} &= \frac{2D_{\mathrm{e}\overline{\mathrm{M}}}(c_{\overline{\mathrm{M}}}D_{0\mathrm{e}} + c_{\mathrm{e}}D_{0\overline{\mathrm{M}}})}{2c_{\overline{\mathrm{M}}}D_{0\mathrm{e}} + 2c_{\mathrm{e}}D_{0\overline{\mathrm{M}}} + c_0 D_{\mathrm{e}\overline{\mathrm{M}}}}
\end{aligned} \tag{5.3}$$

After incorporating the Gibbs–Duhem relation, the MacInnes equation becomes

$$\frac{\vec{i}}{\kappa} = -\nabla\Phi_z - \frac{1}{3F}\left[\left(\frac{3\overline{\Xi}}{c_{\mathrm{T}}} - \frac{1}{c_{\overline{\mathrm{M}}}}\right) c_0 \nabla\mu_0 + \left(1 - 3t_-^{\mathrm{M}} - \frac{c_{\mathrm{e}}}{c_{\overline{\mathrm{M}}}}\right)\nabla\mu_{\mathrm{e}}\right], \tag{5.4}$$

where κ is the ionic conductivity and Φ_z is the electric potential. The flux and MacInnes equations contain electrochemical-potential gradients, which can be more intuitively written with concentration gradients and thermodynamic factors.

Before analysing thermodynamic factors for membrane systems, we first investigate to write the remaining macroscopic transport properties in terms of the Stefan–Maxwell diffusivities. The inversion process of Van-Brunt et al. [56] delivers κ to be

$$\kappa = \frac{c_{\mathrm{T}} F^2 A}{RTB}, \tag{5.5}$$

where

$$\begin{aligned}
A &= c_0\left(\frac{c_{\mathrm{M}} z_{\mathrm{M}}^2}{\mathscr{D}_{0-}\mathscr{D}_{0+}} + \frac{c_+ z_+^2}{\mathscr{D}_{0-}\mathscr{D}_{0\mathrm{M}}} + \frac{c_- z_-^2}{\mathscr{D}_{0+}\mathscr{D}_{0\mathrm{M}}}\right) + \left(\frac{c_-}{\mathscr{D}_{0-}} + \frac{c_{\mathrm{M}}}{\mathscr{D}_{0\mathrm{M}}} + \frac{c_+}{\mathscr{D}_{0+}}\right) A_{\emptyset} \\
B &= \frac{c_0}{\mathscr{D}_{0-}\mathscr{D}_{0+}}\left(\frac{c_-}{\mathscr{D}_{-\mathrm{M}}} + \frac{c_+}{\mathscr{D}_{+\mathrm{M}}}\right) + \left(\frac{c_-}{\mathscr{D}_{0-}} + \frac{c_{\mathrm{M}}}{\mathscr{D}_{0\mathrm{M}}} + \frac{c_+}{\mathscr{D}_{0+}}\right) B_{\emptyset} \\
&\quad + \frac{c_0}{\mathscr{D}_{0\mathrm{M}}}\left[\frac{c_{\mathrm{M}}}{\mathscr{D}_{0+}\mathscr{D}_{-\mathrm{M}}} + \frac{c_{\mathrm{M}}}{\mathscr{D}_{0-}\mathscr{D}_{+\mathrm{M}}} - \frac{c_{\mathrm{T}} F^2 z_+ z_-}{RT\kappa_{\not{\mathrm{M}}}}\left(\frac{c_-}{\mathscr{D}_{0-}} + \frac{c_+}{\mathscr{D}_{0+}}\right)\right]
\end{aligned} . \tag{5.6}$$

[1] $\mathscr{L}_i$'s that Van-Brunt et al. [56] used are connected to $\mathcal{D}_i$'s in the following way.

$$\mathscr{L}_o = \frac{c_0}{2c_{\overline{\mathrm{M}}}}\mathcal{D}_0 \qquad \mathscr{L}_\times = \frac{c_0 c_{\mathrm{e}}}{2c_{\mathrm{T}}c_{\overline{\mathrm{M}}}}\mathcal{D}_\times \qquad \mathscr{L}_{\mathrm{e}} = \frac{c_{\mathrm{e}}}{4c_{\overline{\mathrm{M}}}}\mathcal{D}_{\mathrm{e}}$$

$\kappa_{\not M}$ in B is the familiar ionic conductivity for the binary electrolyte, i.e.,

$$\frac{1}{\kappa_{\not M}} = -\frac{RT}{c_{\mathrm{T}}F^2 z_+ z_-}\left[\frac{1}{\mathscr{D}_{+-}} + \frac{c_0}{c_-\mathscr{D}_{0+} + c_+\mathscr{D}_{0-}}\right] \tag{5.7}$$

and $A_{\not\emptyset}$ and $B_{\not\emptyset}$ come from the $\kappa_{\not\emptyset}$ for the three-ion ionic liquid, cf. eq.(3.30). That is,

$$\kappa_{\not\emptyset} = \frac{c_{\mathrm{T}}F^2 A_{\not\emptyset}}{RTB_{\not\emptyset}} \tag{5.8}$$

such that

$$\begin{aligned} A_{\not\emptyset} &= \frac{c_- z_-^2}{\mathscr{D}_{+\mathrm{M}}} + \frac{c_{\mathrm{M}} z_{\mathrm{M}}^2}{\mathscr{D}_{+-}} + \frac{c_+ z_+^2}{\mathscr{D}_{-\mathrm{M}}} \\ B_{\not\emptyset} &= \frac{c_-}{\mathscr{D}_{-\mathrm{M}}\mathscr{D}_{+-}} + \frac{c_{\mathrm{M}}}{\mathscr{D}_{-\mathrm{M}}\mathscr{D}_{+\mathrm{M}}} + \frac{c_+}{\mathscr{D}_{+\mathrm{M}}\mathscr{D}_{+-}} \end{aligned} . \tag{5.9}$$

κ behaves correctly in the limit; $\kappa \to \kappa_{\not\emptyset}$ when $c_0 \to 0$ and $\kappa \to \kappa_{\not M}$ when $c_{\mathrm{M}} \to 0$, as well as $\mathscr{D}_{-\mathrm{M}} \to \infty$ and $\mathscr{D}_{+\mathrm{M}} \to \infty$ ($\mathscr{D}_{0\mathrm{M}}$ dependence cancels out in this limit, so setting $\mathscr{D}_{0\mathrm{M}} \to \infty$ is not necessary). The migration coefficient $\tilde{\Xi}$ is expressed as

$$\frac{\tilde{\Xi}c_0}{c_{\mathrm{T}}}A = -\frac{c_0 z_{\mathrm{M}}}{\mathscr{D}_{+-}}\left(\frac{c_-}{\mathscr{D}_{0-}} + \frac{c_+}{\mathscr{D}_{0+}}\right) + c_0\left(-\frac{c_0 z_{\mathrm{M}}}{\mathscr{D}_{0-}\mathscr{D}_{0+}} + \frac{c_+ z_+}{\mathscr{D}_{0+}\mathscr{D}_{-\mathrm{M}}} + \frac{c_- z_-}{\mathscr{D}_{0-}\mathscr{D}_{+\mathrm{M}}}\right), \tag{5.10}$$

where A is defined in eq.(5.6). The anion transference number t_-^{M} is

$$\frac{t_-^{\mathrm{M}}}{c_- z_-}A = \frac{c_0}{\mathscr{D}_{0+}}\left(-\frac{z_{\mathrm{M}}}{\mathscr{D}_{0-}} + \frac{z_-}{\mathscr{D}_{0\mathrm{M}}}\right) + \left(\frac{c_-}{\mathscr{D}_{0-}} + \frac{c_{\mathrm{M}}}{\mathscr{D}_{0\mathrm{M}}} + \frac{c_+}{\mathscr{D}_{0+}}\right)\left(-\frac{z_{\mathrm{M}}}{\mathscr{D}_{+-}} + \frac{z_-}{\mathscr{D}_{+\mathrm{M}}}\right). \tag{5.11}$$

5.3 Thermodynamic factors in membranes

Species in membranes are expected to behave thermodynamically differently than those in membrane-free solutions, due to their interactions with the embedded charged end-groups. It is easy to imagine that a voltage difference would be registered across two membranes (of the same type) in contact if the solution imbued in each membrane is at different concentrations. Therefore, the liquid-junction potential remains to be a feasible experimental quantity for gauging the thermodynamic characteristics of membrane

systems.

Again, the case considered in this section is the simplest one, where the system comprises a charged membrane end-group, a neutral solvent, and a binary electrolyte. We limit our attention to Nafion in a protonated form, i.e., the negatively charged sulfonate end-groups are paired up with protons to remain electroneutral in its dry state. Hence, proton is the only cation in the system under study. Assuming the membrane is thick enough to admit an electrode, the following procedure may be proposed for the thermodynamic-factor measurement.

1. Prepare two electrolytic solutions of different concentrations.

2. Place a block of the same (pretreated) membrane in each solution and let them equilibrate.

3. Take the membranes out of the solutions and insert an electrode to each membrane block.

4. Bring the two membranes together to establish an ionic contact. A light clamping may be necessary to hold them together in place. Because electrolytic solutions are imbued in polymer structures, a porous frit required in the conventional concentration cell may not be necessary.

5. Measure the voltage difference across the two membrane blocks using a galvanostat.

6. Work out the amount of solvent and salt in each membrane after the measurement. It should be possible to calculate the concentrations of all species, if the concentration of the membrane end-group (i.e., the sulfonate end-group) is known.

   (a) After performing the necessary pretreatment on the membrane, dry the membrane completely to remove any liquid in the system. Then, measure the membrane mass in its dry state: m_{trm}.

(b) Measure the mass of the membrane after submerging it in the electrolytic solution and reaching an equilibrium: m_{wet}.

(c) Measure the mass of the same equilibrated membrane after completely drying it: m_{dry}. Then, the mass of the solvent m_0 that was present in the membrane during the voltage measurement is

$$m_0 = m_{\text{wet}} - m_{\text{dry}}. \tag{5.12}$$

The mass of the electrolyte m_{e} that was present in the membrane during the voltage measurement is

$$m_{\text{e}} = m_{\text{dry}} - m_{\text{trm}}. \tag{5.13}$$

Note that eq.(5.13) would not hold if the solution the membrane was immersed in contained cations other than proton; other cations would replace some of the protons initially attached to the charged membrane end-groups, producing different neutral clusters in the system. This would result in having to calculate multiple electrolyte masses, e.g., m_{e1}, m_{e2}..., etc., which are cumbersome to extract experimentally.

Off-the-shelf Nafion might be too thin to perform this experiment on. Nonetheless, it is helpful to write this process out fully so that the diffusion driving forces can be expressed clearly using the concentration gradients.

Although there are four species in the membrane under study, only two composition variables are independent; this is because electroneutrality has to be imposed, since we are dealing with an experimental system. The fact that m_0 and m_{e} can be measured separately in the above thought experiment suggests that their particle fractions are a natural choice for independent composition variables. This choice allows the electrochemical-potential differential ($d\mu_i$) for the solvent (0) and electrolyte (e) to

be written as follows.

$$d\mu_0 = \frac{\partial \mu_0}{\partial y_0} dy_0 + \frac{\partial \mu_0}{\partial y} dy_\mathrm{e} \tag{5.14}$$

$$d\mu_\mathrm{e} = \frac{\partial \mu_\mathrm{e}}{\partial y_0} dy_0 + \frac{\partial \mu_\mathrm{e}}{\partial y} dy_\mathrm{e} \tag{5.15}$$

Here, y_0 and y_e denote the particle fraction of the solvent and electrolyte, respectively. The meaning of y_e can be more clearly articulated if the cation (proton) particle fraction is decomposed into two parts: $y_+ = y_+^{\overline{\mathrm{M}}} + y_+^\mathrm{e}$, where the superscripts $\overline{\mathrm{M}}$ and e indicate the proportion of y_+ paired with the sulfonate end-group and the bisulfate ion, respectively, to form electroneutral entities. The phase rule then becomes

$$1 = y_\mathrm{M} + y_0 + y_- + y_+ = y_0 + \nu^{\overline{\mathrm{M}}} y_{\overline{\mathrm{M}}} + \nu^\mathrm{e} y_\mathrm{e}, \tag{5.16}$$

where

$$\begin{aligned} y_{\overline{\mathrm{M}}} &= \frac{y_\mathrm{M}}{\nu_\mathrm{M}} = \frac{y_+^{\overline{\mathrm{M}}}}{\nu_+^{\overline{\mathrm{M}}}} \qquad & y_\mathrm{e} &= \frac{y_-}{\nu_-} = \frac{y_+^\mathrm{e}}{\nu_+^\mathrm{e}} \\ \nu^{\overline{\mathrm{M}}} &= \nu_\mathrm{M} + \nu_+^{\overline{\mathrm{M}}} \qquad & \nu^\mathrm{e} &= \nu_- + \nu_+^\mathrm{e} \end{aligned} . \tag{5.17}$$

Here, ν_i is the stoichiometric coefficient of a negatively charged species $i \in \{\mathrm{M}, -\}$ and ν_+^j is that of the proton associated with the electroneutral cluster $j \in \{\mathrm{e}, \overline{\mathrm{M}}\}$. It is assumed that the charged membrane end-groups are always matched with the exactly necessary number of protons so as to remain electroneutral, and any non-electroneutrality is brought by the imbalance between y_- and y_+^e. If one expresses $d\mu_0 = RTd\ln\lambda_0 y_0$, where $\lambda_0 = \lambda_0(y_0, y_\mathrm{e})$ is the activity coefficient of the solvent 0 with its functional dependence on y_0 and y_e, $d\mu_0$ can be expressed with two concentration gradients

$$\begin{gathered} d\mu_0 = \frac{RT}{y_0}\left[\chi_{00}^\mathrm{m} dy_0 + \chi_{0\mathrm{e}}^\mathrm{m} dy_\mathrm{e}\right], \\ \text{where} \qquad \chi_{00}^\mathrm{m} = \left(1 + \frac{\partial \ln \lambda_0}{\partial \ln y_0}\right)_{T,p,y_\mathrm{e}} \qquad \text{and} \qquad \chi_{0\mathrm{e}}^\mathrm{m} = \left(y_0 \frac{\partial \ln \lambda_0}{\partial y_\mathrm{e}}\right)_{T,p,y_0}. \end{gathered} \tag{5.18}$$

The electrochemical-potential differential of the salt can be derived by starting with $d\mu_i = RTd\ln\lambda_i y_i$ for $i = -$ and $+$, and invoking $d\mu_\mathrm{e} = \nu_- d\mu_- + \nu_+^\mathrm{e} d\mu_+$. Realising $y_+ = \nu_+^{\overline{\mathrm{M}}} y_{\overline{\mathrm{M}}} + \nu_+^\mathrm{e} y_\mathrm{e}$ and $y_{\overline{\mathrm{M}}} = (1 - y_0 - \nu^\mathrm{e} y_\mathrm{e})/\nu^{\overline{\mathrm{M}}}$, and letting $\ln\lambda_{+-}^{\nu_+^\mathrm{e}} = \ln\lambda_-^{\nu_-}\lambda_+^{\nu_+^\mathrm{e}}$ and representing a group of stoichiometric coefficients as $N = \nu_+^\mathrm{e}\nu^{\overline{\mathrm{M}}} - \nu_+^{\overline{\mathrm{M}}}\nu^\mathrm{e}$ (N for capital ν; note that $N = 0$ for sulfonic and sulfuric acids), $d\mu_\mathrm{e}$ becomes

$$\frac{d\mu_\mathrm{e}}{RT} = \nu^\mathrm{e} d\ln\lambda_{+-} + \left[\frac{\nu_-}{y_\mathrm{e}} + \frac{N\nu_+^\mathrm{e}}{\nu_+^{\overline{\mathrm{M}}}(1-y_0) + Ny_\mathrm{e}}\right] dy_\mathrm{e} - \frac{\nu_+^{\overline{\mathrm{M}}}\nu_+^\mathrm{e}}{\nu_+^{\overline{\mathrm{M}}}(1-y_0) + Ny_\mathrm{e}} dy_0. \tag{5.19}$$

If $d\mu_\mathrm{e}$ is to be written more simply as

$$d\mu_\mathrm{e} = \frac{\nu^\mathrm{e} RT}{y_\mathrm{e}}\left[\chi_{\mathrm{e}0}^\mathrm{m} dy_0 + \chi_\mathrm{ee}^\mathrm{m} dy_\mathrm{e}\right], \tag{5.20}$$

then the two thermodynamic factors must be defined as below.

$$\begin{aligned}
\chi_{\mathrm{e}0}^\mathrm{m} &= -\frac{\nu_+^{\overline{\mathrm{M}}}\nu_+^\mathrm{e} y_\mathrm{e}/\nu^\mathrm{e}}{\nu_+^{\overline{\mathrm{M}}}(1-y_0) + Ny_\mathrm{e}} + y_\mathrm{e}\left(\frac{\partial\ln\lambda_{+-}}{\partial y_0}\right)_{T,p,y_\mathrm{e}} \\
\chi_\mathrm{ee}^\mathrm{m} &= \frac{\nu_-}{\nu^\mathrm{e}} + \frac{\nu_+^\mathrm{e} N y_\mathrm{e}/\nu^\mathrm{e}}{\nu_+^{\overline{\mathrm{M}}}(1-y_0) + Ny_\mathrm{e}} + \left(\frac{\partial\ln\lambda_{+-}}{\partial\ln y_\mathrm{e}}\right)_{T,p,y_0}
\end{aligned} \tag{5.21}$$

The flux equations in eq.(5.1) written with concentration gradients using eq.(5.18) and eq.(5.20) give a sound footing to study species movement across Nafion immersed in a binary electrolyte. The flux equations simply become

$$\begin{aligned}
\vec{N}_\mathrm{M} &= c_\mathrm{M}\vec{v}_\mathrm{M} \\
\vec{N}_0 &= -D_{00}^0\nabla c_0 - D_{0\mathrm{e}}^0\nabla c_\mathrm{e} + \frac{\tilde{\Xi}c_0}{c_\mathrm{T}}\frac{\vec{i}}{F} + c_0\vec{v}_\mathrm{M} \\
\vec{N}_- &= -D_{\mathrm{e}0}^0\nabla c_0 - D_\mathrm{ee}^0\nabla c_\mathrm{e} + t_-^\mathrm{M}\frac{\vec{i}}{F} + c_-\vec{v}_\mathrm{M} \\
\vec{N}_+ &= -D_{\mathrm{e}0}^0\nabla c_0 - D_\mathrm{ee}^0\nabla c_\mathrm{e} + \left(1 - t_-^\mathrm{M}\right)\frac{\vec{i}}{F} + c_+\vec{v}_\mathrm{M}
\end{aligned}, \tag{5.22}$$

where D_{ij}^0 are Fickian diffusivities that relate to the component thermodynamic diffu-

sivities $\mathcal{D}_i$'s and thermodynamic factors *via* a matrix multiplication

$$\begin{bmatrix} D^0_{00} & D^0_{0\mathrm{e}} \\ D^0_{\mathrm{e}0} & D^0_{\mathrm{ee}} \end{bmatrix} = \boldsymbol{\mathcal{D}}\mathbf{X}\mathbf{C}, \tag{5.23}$$

where

$$\begin{aligned} \boldsymbol{\mathcal{D}} &= \begin{bmatrix} \mathcal{D}_0 & \frac{2c_0}{c_\mathrm{T}}\mathcal{D}_\times \\ \frac{c_\mathrm{e}}{c_\mathrm{T}}\mathcal{D}_\times & \mathcal{D}_\mathrm{e} \end{bmatrix}, \quad \mathbf{X} = \begin{bmatrix} \chi^\mathrm{m}_{00} & \chi^\mathrm{m}_{0\mathrm{e}} \\ \chi^\mathrm{m}_{\mathrm{e}0} & \chi^\mathrm{m}_{\mathrm{ee}} \end{bmatrix}, \\ \text{and} \quad \mathbf{C} &= \begin{bmatrix} \frac{1-\left(\overline{V}_\mathrm{e}-\overline{V}_{\overline{\mathrm{M}}}\right)c_\mathrm{e}}{c_{\overline{\mathrm{M}}}\overline{V}_{\overline{\mathrm{M}}}} & \frac{\left(\overline{V}_\mathrm{e}-\overline{V}_{\overline{\mathrm{M}}}\right)c_0}{c_{\overline{\mathrm{M}}}\overline{V}_{\overline{\mathrm{M}}}} \\ \frac{\left(2\overline{V}_0-\overline{V}_{\overline{\mathrm{M}}}\right)c_\mathrm{e}}{2c_{\overline{\mathrm{M}}}\overline{V}_{\overline{\mathrm{M}}}} & \frac{2-\left(2\overline{V}_0-\overline{V}_{\overline{\mathrm{M}}}\right)c_0}{2c_{\overline{\mathrm{M}}}\overline{V}_{\overline{\mathrm{M}}}} \end{bmatrix}. \end{aligned} \tag{5.24}$$

$\overline{V}_i$ is the partial molar volume of component i and $\mathbf{C}$ derives from the c_T–$\overline{V}_i$ relation. In particular, the particle-fraction gradients and the molar-concentration gradients are connected *via*

$$\begin{aligned} \nabla y_0 &= \frac{2-2\left(\overline{V}_\mathrm{e}-\overline{V}_{\overline{\mathrm{M}}}\right)c_\mathrm{e}}{c_\mathrm{T}^2\overline{V}_{\overline{\mathrm{M}}}}\nabla c_0 + \frac{2\left(\overline{V}_\mathrm{e}-\overline{V}_{\overline{\mathrm{M}}}\right)c_0}{c_\mathrm{T}^2\overline{V}_{\overline{\mathrm{M}}}}\nabla c_\mathrm{e} \\ \nabla y_\mathrm{e} &= \frac{\left(2\overline{V}_0-\overline{V}_{\overline{\mathrm{M}}}\right)c_\mathrm{e}}{c_\mathrm{T}^2\overline{V}_{\overline{\mathrm{M}}}}\nabla c_0 + \frac{2-\left(2\overline{V}_0-\overline{V}_{\overline{\mathrm{M}}}\right)c_0}{c_\mathrm{T}^2\overline{V}_{\overline{\mathrm{M}}}}\nabla c_\mathrm{e} \end{aligned}. \tag{5.25}$$

5.4 Describing Verbrugge and Hill's experiment

A small amount of radioactive sulfuric acid is introduced to track the movement of bisulfate ions in Verbrugge and Hill's experiment [2], so the flux equations in eq.(5.22) are not adequate; the radioactive bisulfate ion must be considered as a separate species. As done in section 5.2, flux equations for the five-species system $\{\mathrm{M}, 0, -, *, +\}$ can be derived using the method of Van-Brunt et al. [56], where $*$ and $-$ indicate the radioactive (tagged) and non-radioactive (untagged) bisulfate ions, respectively. This corresponds to four electroneutral clusters, namely, water, non-radioactive sulfuric acid, radioactive sulfuric acid, and sulfonic acid, denoted by 0, e, $\overline{\mathrm{e}}$, and $\overline{\mathrm{M}}$, respectively.

5.4.1 Fluxes across membrane

Because the added tagged sulfuric acid perturbs the equilibrium state of the membrane system only slightly, one can appeal that water and sulfonic acid do not induce any diffusion, i.e., $d\mu_0 = d\mu_{\overline{\mathrm{M}}} = 0$; their concentrations remain virtually the same across the membrane in this experiment. One can further assume species other than the tagged and untagged bisulfate ions are stationary, i.e., $\vec{N}_0 = \vec{N}_+ = 0$ relative to the sulfonate end-group. Since four oxygen atoms surround a sulfur atom tetrahedrally in the bisulfate ion, the extra neutrons in ^{35}S should not affect the effective radius of the ion greatly. Therefore, it is safe to set $\mathscr{D}_{*i} = \mathscr{D}_{-i}$ for $i = \mathrm{M}, 0, +$ and $1/\mathscr{D}_{-*} = 0$. The constraint $\vec{N}_+ = 0$ then enforces $\mathscr{D}_{0\mathrm{M}}$ to be

$$\mathscr{D}_{0\mathrm{M}} = -\frac{c_{\mathrm{M}}\mathscr{D}_{0-}\mathscr{D}_{0+}}{c_+\mathscr{D}_{0-} + (c_- + c_*)\mathscr{D}_{0+}}. \tag{5.26}$$

The Gibbs–Duhem relation also simplifies to

$$\begin{aligned} c_0 d\mu_0 + c_{\mathrm{e}} d\mu_{\mathrm{e}} + c_{\overline{\mathrm{e}}} d\mu_{\overline{\mathrm{e}}} + c_{\overline{\mathrm{M}}} d\mu_{\overline{\mathrm{M}}} &= 0 \\ \Rightarrow c_{\mathrm{e}} d\mu_{\mathrm{e}} + c_{\overline{\mathrm{e}}} d\mu_{\overline{\mathrm{e}}} &= 0 \\ \Rightarrow c_- d\mu_{\mathrm{e}} + c_* d\mu_{\overline{\mathrm{e}}} &= 0, \end{aligned} \tag{5.27}$$

where $c_{\mathrm{e}} = c_-$ and $c_{\overline{\mathrm{e}}} = c_*$ have been used to arrive at the last row because sulfuric acid is treated as a binary electrolyte. Then, the following set of flux equations is produced.

$$\begin{aligned} \vec{N}_* &= -\frac{c_-}{c_- + c_*} \times \frac{c_{\mathrm{T}}}{\frac{c_0}{\mathscr{D}_{0-}} + \frac{c_{\mathrm{M}}}{\mathscr{D}_{-\mathrm{M}}} + \frac{c_+}{\mathscr{D}_{+-}}} \times \frac{c_* \left(\nabla\mu_{\overline{\mathrm{e}}} - \nabla\mu_{\mathrm{e}}\right)}{RT} \\ \vec{N}_- &= -\vec{N}_* \end{aligned} \tag{5.28}$$

This agrees with intuition since Faraday's law enforces $\vec{N}_* + \vec{N}_- = 0$, where fluxes are measured relative to the sulfonate-ion velocity and no net current flows through the system. The Gibbs–Duhem relation in eq.(5.27) can reduce the difference in

electrochemical-potential gradients to be written as

$$\nabla\mu_{\bar{\mathrm{e}}} - \nabla\mu_{\mathrm{e}} = \left(1 + \frac{c_{\bar{\mathrm{e}}}}{c_{\mathrm{e}}}\right)\nabla\mu_{\bar{\mathrm{e}}} \approx \nabla\mu_{\bar{\mathrm{e}}}, \tag{5.29}$$

given $c_{\bar{\mathrm{e}}} \ll c_{\mathrm{e}}$. Thus, the tagged bisulfate-ion flux can be cast into Fick's formalism, once $\nabla\mu_{\bar{\mathrm{e}}}$ is expressed in terms of a concentration gradient.

5.4.2 Diffusion driving forces across membrane

Following the same procedure as in section 5.3, the electrochemical-potential gradients in the five-species membrane system can be expressed with concentration gradients using thermodynamic factors. If concentration-dependent thermodynamic nonidealities were to be examined experimentally in this system, one would control the concentration of the solvent, untagged (e) and tagged ($\bar{\mathrm{e}}$) sulfuric acids, i.e., $\{0, \mathrm{e}, \bar{\mathrm{e}}\}$ is a parsimonious set of independent composition variables after applying the phase rule and electroneutrality. Given only protonated Nafion is considered in this thesis, the proton particle fraction can be split into three parts, $y_+ = y_+^{\overline{\mathrm{M}}} + y_+^{\mathrm{e}} + y_+^{\bar{\mathrm{e}}}$, where the superscripts denote the electroneutral cluster each proton particle fraction is associated with (the superscript $\overline{\mathrm{M}}$ indicates the sulfonic acid that forms between the proton and the sulfonate end-group). The particle fractions of the three electroneutral clusters relate to the particle fractions of constituent ions such that

$$y_{\overline{\mathrm{M}}} = \frac{y_{\mathrm{M}}}{\nu_{\mathrm{M}}} = \frac{y_+^{\overline{\mathrm{M}}}}{\nu_+^{\overline{\mathrm{M}}}}, \qquad y_{\mathrm{e}} = \frac{y_-}{\nu_-} = \frac{y_+^{\mathrm{e}}}{\nu_+^{\mathrm{e}}}, \qquad y_{\bar{\mathrm{e}}} = \frac{y_*}{\nu_*} = \frac{y_+^{\bar{\mathrm{e}}}}{\nu_+^{\bar{\mathrm{e}}}}. \tag{5.30}$$

Again, ν_i is the stoichiometric coefficient of a negatively charged species $i \in \{\mathrm{M}, -, *\}$ and ν_+^j is that of the proton associated with the electroneutral cluster $j \in \{\overline{\mathrm{M}}, \mathrm{e}, \bar{\mathrm{e}}\}$. ν^j denotes the total number of ions the cluster j dissociates into, i.e., $\nu^{\overline{\mathrm{M}}} = \nu_{\mathrm{M}} + \nu_+^{\overline{\mathrm{M}}}$, $\nu^{\mathrm{e}} = \nu_- + \nu_+^{\mathrm{e}}$, and $\nu^{\bar{\mathrm{e}}} = \nu_* + \nu_+^{\bar{\mathrm{e}}}$. Thermodynamic factors for the tagged sulfuric acid can be acquired by recognising that $\mu_{\bar{\mathrm{e}}} = \nu_*\mu_* + \nu_+^{\bar{\mathrm{e}}}\mu_+$. Assuming the activity coefficients

λ_i combine such that $\lambda_*^{\nu_*}\lambda_+^{\nu_+^{\bar{e}}} = \lambda_{\bar{e}}^{\nu^{\bar{e}}}$, its electrochemical-potential differential becomes

$$d\mu_{\bar{e}} = \frac{\nu^{\bar{e}}RT}{y_{\bar{e}}}\left[\chi_{\bar{e}0}dy_0 + \chi_{\bar{e}e}dy_e + \chi_{\bar{e}\bar{e}}dy_{\bar{e}}\right], \tag{5.31}$$

where the thermodynamic factors are defined as

$$\begin{aligned}
\chi_{\bar{e}0} &= -\frac{\nu_+^{\bar{e}}\nu_+^{\overline{M}}y_{\bar{e}}/\nu^{\bar{e}}}{\nu_+^{\overline{M}}(1-y_0) + N^e y_e + N^{\bar{e}}y_{\bar{e}}} + y_{\bar{e}}\left(\frac{\partial \ln \lambda_{\bar{e}}}{\partial y_0}\right)_{T,p,y_{k\neq 0}} \\
\chi_{\bar{e}e} &= \frac{\nu_+^{\bar{e}}N^e y_{\bar{e}}/\nu^{\bar{e}}}{\nu_+^{\overline{M}}(1-y_0) + N^e y_e + N^{\bar{e}}y_{\bar{e}}} + y_{\bar{e}}\left(\frac{\partial \ln \lambda_{\bar{e}}}{\partial y_e}\right)_{T,p,y_{k\neq e}} \\
\chi_{\bar{e}\bar{e}} &= \frac{\nu_*}{\nu^{\bar{e}}} + \frac{\nu_+^{\bar{e}}N^{\bar{e}}y_{\bar{e}}/\nu^{\bar{e}}}{\nu_+^{\overline{M}}(1-y_0) + N^e y_e + N^{\bar{e}}y_{\bar{e}}} + \left(\frac{\partial \ln \lambda_{\bar{e}}}{\partial \ln y_{\bar{e}}}\right)_{T,p,y_{k\neq \bar{e}}}
\end{aligned} . \tag{5.32}$$

Note that recurring groups of stoichiometric coefficients have been combined to be represented as $N^e = \nu_+^e\nu^{\overline{M}} - \nu^e\nu_+^{\overline{M}}$ and $N^{\bar{e}} = \nu_+^{\bar{e}}\nu^{\overline{M}} - \nu^{\bar{e}}\nu_+^{\overline{M}}$ (where N stands for capital ν and both N^e and $N^{\bar{e}}$ are equal to 0 in this case because sulfonate and sulfuric acids are treated as symmetric binary electrolytes).

Because the radioactive sulfuric-acid concentration is very low, ideal thermodynamic behaviours can be assumed, in which case $d\mu_{\bar{e}}$ reduces to

$$\nabla\mu_{\bar{e}} = \frac{RT}{c_*}\nabla c_*, \tag{5.33}$$

after applying $\chi_{\bar{e}0} \to 0$, $\chi_{\bar{e}e} \to 0$, and $\chi_{\bar{e}\bar{e}} \to 1/2$ in the limit of $y_{\bar{e}} = y_*/\nu_* \to 0$. For the radio-tracing experiment, it is expected that ∇c_T is negligible, thus $\nabla y_*/y_* = \nabla c_*/c_*$ was used to arrive at eq.(5.33). Incorporating equations (5.28), (5.29), and (5.33), as well as $c_- \gg c_*$ gives the following Fickian flux expression for the radioactive bisulfate ion.

$$\vec{N}_* \approx -D\nabla c_* = -DK\frac{c_*^{\mathrm{uld}} - c_*^{\mathrm{ld}}}{L} \tag{5.34}$$

Here, K is the partition coefficient of the bisulfate ion evaluated at the bulk sulfuric-acid concentration in the reservoirs, L is the width of the membrane, c_*^{ld} and c_*^{uld} denote the tagged bisulfate-ion concentrations in the loaded and unloaded reservoirs,

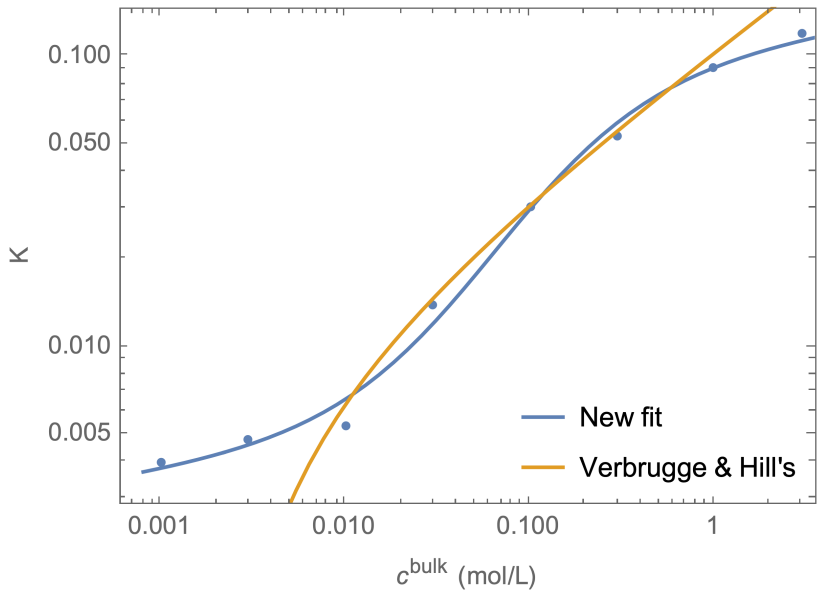

Figure 5.2: The partition coefficient K of sulfuric acid in Nafion 117. The blue line is the new fit in eq.(5.37) and the orange line is the fit from Verbrugge and Hill [7], accurate only between 0.01 M and 1 M. The circles show the measurement data in [8].

respectively, and

$$D = \frac{c_{\mathrm{T}}}{\frac{c_{\mathrm{M}}}{\mathscr{D}_{-\mathrm{M}}} + \frac{c_0}{\mathscr{D}_{-0}} + \frac{c_+}{\mathscr{D}_{+-}}} \tag{5.35}$$

is the Fickian diffusivity, which is reported by Verbrugge and Hill [2].

The partition coefficient K is a key parameter that quantifies the equilibrium intake of a solute for a given membrane submerged in a solution. It is defined as the ratio of the solute concentration in the membrane and that in the bulk reservoir (in which the membrane sits under an equilibrium). Verbrugge and Hill [8] verified the sulfuric-acid partition coefficient for Nafion 117 by the same radio-tracing technique[2] involving ^{35}S. Therefore, the bisulfate-ion concentration in Nafion can be simply calculated by employing

$$c_- = c^{\mathrm{bulk}} \times K\left(c^{\mathrm{bulk}}\right), \tag{5.36}$$

where c^{bulk} is the bulk sulfuric-acid concentration in the reservoir the membrane is in

[2]The experiment goes as follows. The membrane is submerged in a sulfuric-acid solution of known concentration that also contains a known amount of radioactive sulfuric acid. After sufficient soaking, the membrane is placed in a new vial with fresh non-radioactive sulfuric acid to extract all the radioactive sulfur that penetrated the membrane pores. A thorough extraction is ensured by placing the vial in a water bath at 50°C for 3 hours. The amount of extracted radioactive sulfur is then compared to the solution the membrane was initially equilibrated.

contact with. While the experimental data Verbrugge and Hill [8] collected ranged from 0.001 M to 10 M, the functional form provided by Verbrugge and Hill [7] was a fit valid in the 0.01 – 1 M range only. This is not adequate for the present purpose because the experiment under investigation includes measurements at 0.003 M and 3 M. Therefore, a new functional form accurate in the range 0.001 M $\leq c^{\mathrm{bulk}} \leq$ 3 M is rederived using the data from Verbrugge and Hill [8] and is provided below.

$$K\left(c^{\mathrm{bulk}}\right) = \left(c^{\mathrm{bulk}}\right)^{0.09820} \exp\left[-4.934 + \frac{5560}{2057 + 133.4/c^{\mathrm{bulk}}}\right] \tag{5.37}$$

This functional form was obtained by recognising that K is of sigmoidal form when plotted against the bulk concentration in the log–log format, evident in Figure 5.2.

Verbrugge and Hill [2] calculated the Fickian D by incorporating the partition coefficient and asserting that the system quickly reached a quasi-steady state, such that the flux of the tagged bisulfate ion was effectively constant, i.e., the concentration of the tagged bisulfate ion in the unloaded reservoir increased linearly with time. As Griffith [193] showed, this assumption is not entirely accurate at the beginning of the experiment because it overlooks the onset time — the delay between the moment the tagged sulfuric acid is added to the loaded reservoir and when an appreciable (or detectable) amount of it penetrates the membrane to leach into the unloaded reservoir. The validity of this assumption can be assessed formally by analysing the experiment using the methodology Barnes [194] put forward.

5.5 Finding $\mathscr{D}_{-\mathrm{M}}$ using the Barnes solution

Barnes [194] examined a diffusion problem across a membrane sandwiched between two well-stirred reservoirs, with the experiment initiated by adding a diffusing species to one reservoir — an analogous setup to Verbrugge and Hill's experiment [2]. Naturally, three separate regions arise: the loaded and unloaded reservoirs and the membrane. While the tagged bisulfate-ion concentration inside the membrane (c_*^{M}) depends on time

and the position along the width of the membrane, concentrations in the loaded and unloaded reservoirs (c_*^{ld} and c_*^{uld}, respectively) have no position dependence because the reservoirs are thoroughly mixed continuously. Since the particle number of the diffusing species must be conserved in this membrane–reservoir system, the following relationships arise.

$$V\frac{dc_*^{\mathrm{ld}}}{dt} = -AN_*(t,0) \qquad V\frac{dc_*^{\mathrm{uld}}}{dt} = AN_*(t,L) \tag{5.38}$$

Here, $N_*(t,x)$ is the flux of the tagged bisulfate ion at time t and position x inside the membrane, where $x = 0$ and L mark the interfaces between the membrane and the loaded and unloaded reservoirs, respectively. A is the cross-sectional area of the membrane and V is the reservoir volume. Inside the membrane, the continuity equation dictates that

$$\frac{\partial c_*^{\mathrm{M}}}{\partial t} = -\frac{\partial N_*}{\partial x}. \tag{5.39}$$

The flux is defined under the Fickian formalism such that

$$N_* = -D\frac{\partial c_*^{\mathrm{M}}}{\partial x}, \tag{5.40}$$

where D is the Fickian diffusivity of the tagged bisulfate ion in the membrane. Making use of the partition coefficient K in eq.(5.37), the boundary conditions are

$$c_*^{\mathrm{M}}(t,0) = Kc_*^{\mathrm{ld}}(t), \qquad c_*^{\mathrm{M}}(t,L) = Kc_*^{\mathrm{uld}}(t), \tag{5.41}$$

and K is evaluated at the bulk-reservoir concentration (it is reminded that the added amount of radioactive sulfuric acid is so small that the two reservoirs are essentially at the same concentration). Since the radioactive sulfuric acid is introduced to the loaded reservoir at $t = 0$, the initial conditions are

$$c_*^{\mathrm{ld}}(0) = c_*^{\mathrm{init}}, \qquad c_*^{\mathrm{uld}}(0) = 0, \qquad c_*^{\mathrm{M}}(0,x) = 0. \tag{5.42}$$

Non-dimensionalisation enables a more succinct description of the problem. Letting

$$\begin{gathered} \xi = \frac{x}{L} \qquad \tau = \frac{Dt}{L^2} \qquad \gamma = \frac{ALK}{V} \\ \theta^{\mathrm{ld}} = \frac{c_*^{\mathrm{ld}}}{c_*^{\mathrm{init}}} \qquad \theta^{\mathrm{uld}} = \frac{c_*^{\mathrm{uld}}}{c_*^{\mathrm{init}}} \qquad \theta^{\mathrm{M}} = \frac{c_*^{\mathrm{M}}}{K c_*^{\mathrm{init}}} \end{gathered} \quad , \tag{5.43}$$

the governing equations turn into

$$\frac{d\theta^{\mathrm{ld}}}{d\tau} = \gamma \frac{\partial \theta^{\mathrm{M}}}{\partial \xi}\bigg|_{(\tau,0)} \qquad \frac{d\theta^{\mathrm{uld}}}{d\tau} = -\gamma \frac{\partial \theta^{\mathrm{M}}}{\partial \xi}\bigg|_{(\tau,1)} \qquad \frac{\partial \theta^{\mathrm{M}}}{\partial \tau} = \frac{\partial^2 \theta^{\mathrm{M}}}{\partial \xi^2} \tag{5.44}$$

with the following initial and boundary conditions.

$$\begin{gathered} \theta^{\mathrm{ld}}(0) = 1 \qquad \theta^{\mathrm{uld}}(0) = 0 \qquad \theta^{\mathrm{M}}(0,\xi) = 0 \\ \theta^{\mathrm{ld}}(\tau) = \theta^{\mathrm{M}}(\tau,0) \qquad \theta^{\mathrm{uld}}(\tau) = \theta^{\mathrm{M}}(\tau,1) \end{gathered} \tag{5.45}$$

Analytic expressions for the dimensionless reservoir concentrations can be formulated by proceeding in the frequency domain *via* the Laplace transform. Denoting the frequency by s and the transformed variables with an overbar, the governing equations in eq.(5.44) become

$$\begin{gathered} s\overline{\theta}^{\mathrm{ld}}(s) - \theta^{\mathrm{ld}}(0) = \gamma \frac{\partial \overline{\theta}^{\mathrm{M}}}{\partial \xi}\bigg|_{(s,0)} \qquad s\overline{\theta}^{\mathrm{uld}}(s) - \theta^{\mathrm{uld}}(0) = -\gamma \frac{\partial \overline{\theta}^{\mathrm{M}}}{\partial \xi}\bigg|_{(s,1)} \\ s\overline{\theta}^{\mathrm{M}}(s) - \theta^{\mathrm{M}}(0,\xi) = \frac{\partial^2 \overline{\theta}^{\mathrm{M}}}{\partial \xi^2} \end{gathered} \tag{5.46}$$

and the initial and boundary conditions in eq.(5.45) become

$$\begin{gathered} \theta^{\mathrm{ld}}(0) = 1 \qquad \theta^{\mathrm{uld}}(0) = 0 \qquad \theta^{\mathrm{M}}(0,\xi) = 0 \\ \overline{\theta}^{\mathrm{ld}}(s) = \overline{\theta}^{\mathrm{M}}(s,0) \qquad \overline{\theta}^{\mathrm{uld}}(s) = \theta^{\mathrm{M}}(s,1) \end{gathered} \quad . \tag{5.47}$$

Substituting the initial conditions into the governing equations and applying the boundary conditions, the equations for the two reservoir concentrations (top row in eq.(5.46))

can be written in terms of the membrane concentration $\overline{\theta}^{\mathrm{M}}$ only (at the appropriate boundaries).

$$\begin{aligned}\overline{\theta}^{\mathrm{M}}(s,0) &= \frac{1}{s} + \frac{\gamma}{s}\frac{\partial\overline{\theta}^{\mathrm{M}}}{\partial\xi}\bigg|_{(s,0)} \\ \overline{\theta}^{\mathrm{M}}(s,1) &= -\frac{\gamma}{s}\frac{\partial\overline{\theta}^{\mathrm{M}}}{\partial\xi}\bigg|_{(s,1)}\end{aligned} \tag{5.48}$$

Assuming $\overline{\theta}^{\mathrm{M}}$ has a general form (which satisfies the bottom line of eq.(5.46)) of

$$\overline{\theta}^{\mathrm{M}}(s,\xi) = A\, e^{\xi\sqrt{s}} + B\, e^{-\xi\sqrt{s}}, \tag{5.49}$$

the coefficients A and B can be determined by substituting it into eq.(5.48) and simultaneously solving the two equations. The resulting non-dimensional tagged bisulfate-ion concentration in the membrane is

$$\overline{\theta}^{\mathrm{M}}(s,\xi) = \frac{1}{\Gamma(s)\sqrt{s}}\left[\left(\gamma+\sqrt{s}\right)e^{(1-\xi)\sqrt{s}} + \left(\gamma-\sqrt{s}\right)e^{-(1-\xi)\sqrt{s}}\right] \tag{5.50}$$

in the frequency domain, where

$$\Gamma(s) = \left(\gamma+\sqrt{s}\right)^2 e^{\sqrt{s}} - \left(\gamma-\sqrt{s}\right)^2 e^{-\sqrt{s}} \tag{5.51}$$

is chosen for notational compactness. This illustrates that the partition coefficient K in γ ultimately determines the tagged-anion concentration in the membrane, which agrees with intuition. Due to the chosen boundary conditions, the non-dimensional reservoir concentrations are equal to that at either end of the membrane.

$$\begin{aligned}\overline{\theta}^{\mathrm{ld}}(s) = \overline{\theta}^{\mathrm{M}}(s,0) &= \frac{1}{\Gamma(s)\sqrt{s}}\left[\left(\gamma+\sqrt{s}\right)e^{\sqrt{s}} + \left(\gamma-\sqrt{s}\right)e^{-\sqrt{s}}\right] \\ \overline{\theta}^{\mathrm{uld}}(s) = \overline{\theta}^{\mathrm{M}}(s,1) &= \frac{2\gamma}{\Gamma(s)\sqrt{s}}\end{aligned} \tag{5.52}$$

Evidently, both expressions contain isolated singularities (i.e., they blow up to infinity) when $\Gamma(s) = 0$ and $s = 0$ and the method of residues[3] can be employed to convert them back to the time domain [195].

$$\begin{aligned}\theta^{\mathrm{ld}}(\tau) &= \frac{1}{2+\gamma} + 2\gamma \sum_{j=1}^{\infty} \frac{\gamma^2 + \lambda_j^2}{\left[\gamma(1+\gamma) + \lambda_j^2\right]^2 - \gamma^2} e^{-\lambda_j^2 \tau} \\ \theta^{\mathrm{uld}}(\tau) &= \frac{1}{2+\gamma} + 2\gamma \sum_{j=1}^{\infty} \frac{\left(\gamma^2 - \lambda_j^2\right) \sec \lambda_j}{\left[\gamma(1+\gamma) + \lambda_j^2\right]^2 - \gamma^2} e^{-\lambda_j^2 \tau}\end{aligned} \tag{5.53}$$

Here, λ_j are real positive values that satisfy

$$\tan \lambda_j = \frac{2\gamma\lambda_j}{\lambda_j^2 - \gamma^2}. \tag{5.54}$$

θ^{ld} and θ^{uld} for Verbrugge and Hill's radio-tracing experiment [2] are plotted in Figures 5.3a and 5.3b, respectively, the latter illustrating lags associated with the onset times. Figure 5.3c is the ratio of the two reservoir concentrations in the τ range that approximately corresponds to the duration of the experiment. After sufficient time is elapsed, the ratio reaches 1 as expected and is illustrated in Figure 5.3d.

Figures 5.3b and 5.3c clearly exhibit that the onset times are very short in comparison to the total durations of the experiment for all six concentrations studied. The exact onset time can be calculated by drawing a tangent line to the θ^{uld} curve at the inflection point, as shown in Figure 5.3b for the 3 M system, following Griffith's analysis [193]. The concentration evolution must possess an inflection point because the initial rapid increase in concentration in the unloaded reservoir eventually slows down to approach an equilibrium limit. The time at which the system reaches the inflec-

[3] If a Laplace transform $\overline{f}(s)$ contains isolated singularities at s_n for $n = 1, ..., \infty$, i.e., $\overline{f}(s_n) = \infty$, then its inverse is simply [195]

$$f(t) = \mathscr{L}^{-1}\left\{\overline{f}(s)\right\} = \sum_{n=1}^{\infty} e^{s_n t} \lim_{s \to s_n} (s - s_n)\overline{f}(s).$$

For the present case, the equilibrium behaviour $1/(2+\gamma)$ comes from the pole s = 0 and the transient behaviour that depends on $e^{-\lambda_j^2 \tau}$ comes from the poles that satisfy $\Gamma(s) = 0$. The location of the poles is obtained by solving eq.(5.54), where $\lambda_j^2 = -s_j$.

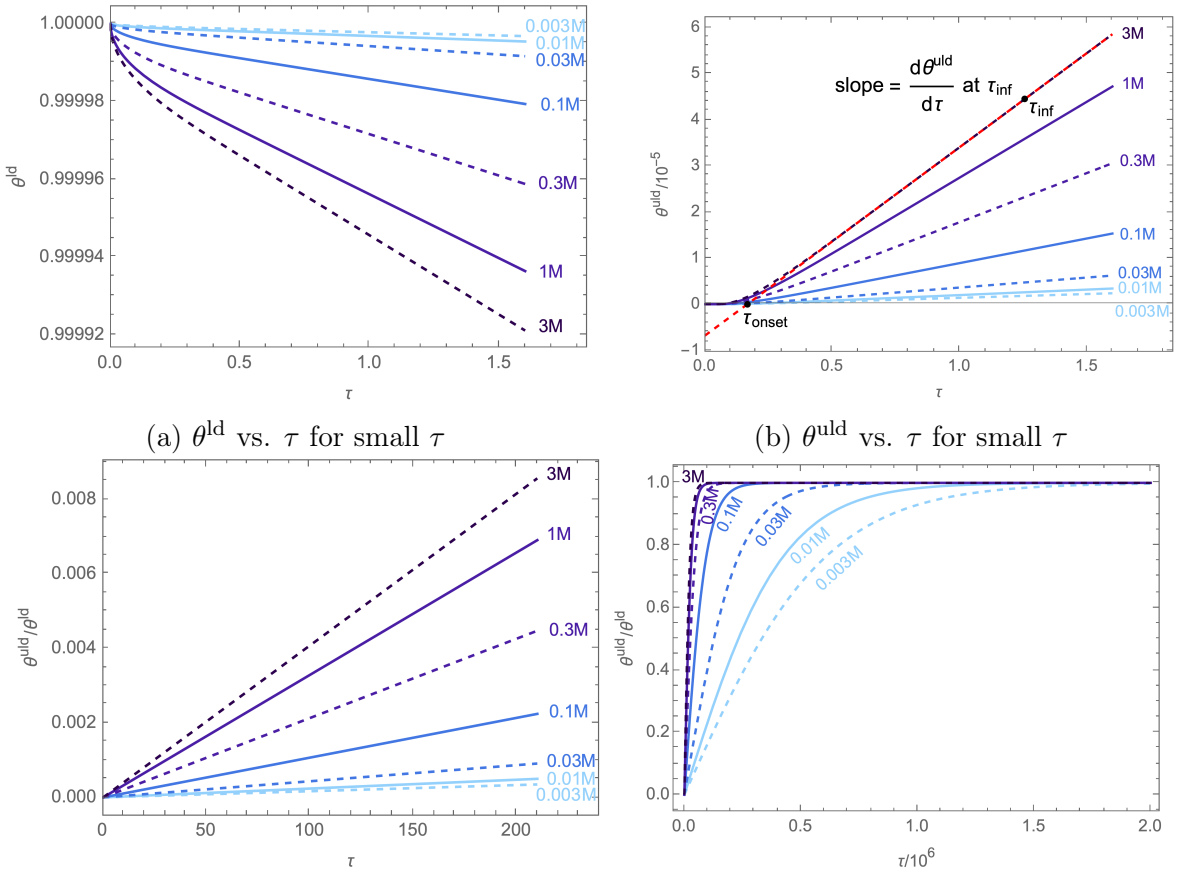

(a) θ^{ld} vs. τ for small τ

(b) θ^{uld} vs. τ for small τ

(c) $\theta^{\mathrm{uld}}/\theta^{\mathrm{ld}}$ vs. τ for moderate τ

(d) $\theta^{\mathrm{uld}}/\theta^{\mathrm{ld}}$ vs. τ for large τ

Figure 5.3: Non-dimensional tagged bisulfate-ion concentrations in the loaded and unloaded reservoirs, plotted against the non-dimensional time, corresponding to Verbrugge and Hill's first experiment [2]. Different lines represent different untagged sulfuric-acid concentrations in the reservoirs. The summations in eq.(5.53) were terminated at $j = 100$.

tion point (τ_{inf}) is tabulated in Table 5.1. The onset time (τ_{onset}) is then defined as the τ-intercept of the tangent line to θ^{uld} at τ_{inf} [193]. The seven concentrations Verbrugge and Hill [2] studied give $\tau_{\mathrm{onset}} = 0.16664 \pm 0.00002$, which indicates that τ_{onset} is a concentration-independent, inherent property of the tested membrane. This seems reasonable because τ_{onset} characterises the time it takes for an appreciable *normalised* amount of a diffusing species to traverse across the membrane.

The solution in eq.(5.53) simplifies in the asymptotic regime where $\gamma \ll 1$, which is usually the case for practical membrane systems, since the membrane volume is only a fraction of the reservoir volume. Using the small-angle approximation, $\lambda_1 \approx \sqrt{2\gamma}$ (where λ_1 is the smallest real positive value that satisfies eq.(5.54)) and this reduces

Table 5.1: The dimensionless time at which the system crosses the inflection point (τ_{inf}), the slope of θ^{uld} at the corresponding time, the smallest real positive λ_j that satisfies eq.(5.54), and the resulting Fickian diffusivity (D) in 10^{-6} cm^2/s are tabulated. Because $\theta^{\mathrm{ld}} \approx 1$ at early times, $\frac{d\theta^{\mathrm{uld}}}{d\tau}\big|_{\tau_{\mathrm{inf}}} = \frac{d(\theta^{\mathrm{uld}}/\theta^{\mathrm{ld}})}{d\tau}\big|_{\tau_{\mathrm{inf}}}$ (up to three significant digits).

c^{bulk} (M)	0.003	0.01	0.03	0.1	0.3	1	3
τ_{inf}	1.58	1.54	1.48	1.39	1.32	1.28	1.26
$\frac{d\theta^{\mathrm{uld}}}{d\tau}\big\|_{\tau_{\mathrm{inf}}}$	0.166	0.237	0.433	1.07	2.13	3.29	4.08
$\lambda_1 \times 10^3$	1.82	2.18	2.94	4.62	6.53	8.11	9.03
D	0.878	1.71	1.62	1.81	1.62	1.04	0.431

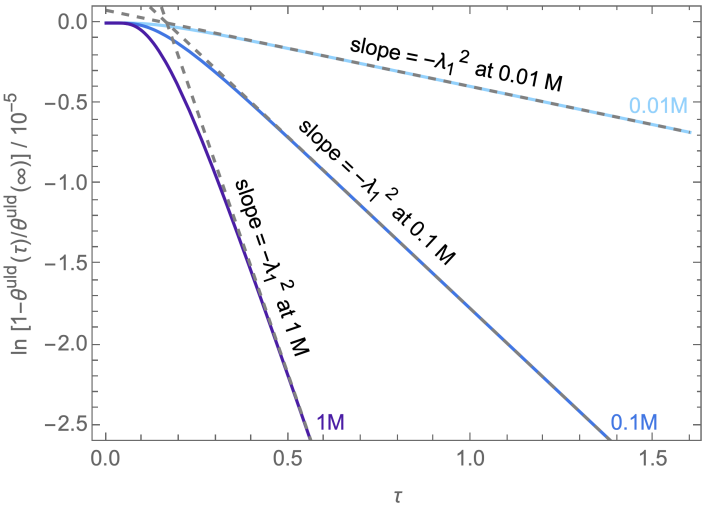

Figure 5.4: The transient behaviour of θ^{uld} is exponential in nature and is dominated by the smallest real positive λ, λ_1.

the dimensionless concentrations to be

$$\theta^{\mathrm{ld}}(\tau) \approx \frac{1}{2}\left(1 + e^{-2\gamma\tau}\right) \qquad \theta^{\mathrm{uld}}(\tau) \approx \frac{1}{2}\left(1 - e^{-2\gamma\tau}\right) \tag{5.55}$$

for large enough τ. This shows that the transient term decays exponentially, which can be more clearly enunciated by plotting $\ln\left(1 - \theta^{\mathrm{uld}}(\tau)/\theta^{\mathrm{uld}}(\infty)\right)$ vs. τ, as in Figure 5.4. It is evident that the transient behaviour quickly converges to a line with the slope $-\lambda_1^2 = -2\gamma$, i.e., λ_1 essentially determines how the concentration of the diffusing species progresses across the membrane for $\tau > \tau_{\mathrm{onset}}$. Taking the ratio of the two functions in eq.(5.55) produces $\theta^{\mathrm{uld}}/\theta^{\mathrm{ld}} \approx \tanh \lambda\tau$, which captures the behaviour in

Figure 5.3d well. Therefore, Verbrugge and Hill's linearity assumption in constructing the $c_*^{\mathrm{uld}}/c_*^{\mathrm{ld}}$ vs.time plot [2] is not strictly correct, but is still a fair approximation since λ_1 is very small.

Because $\theta^{\mathrm{uld}}/\theta^{\mathrm{ld}} = c_*^{\mathrm{uld}}/c_*^{\mathrm{ld}}$, the Fickian diffusivity D can be obtained by comparing the Barnes-solution slopes at τ_{inf} to the slopes Verbrugge and Hill [2] reported (in their Figures 4 and 5), which we denote as m_{VH}, i.e., $m_{\mathrm{VH}} = d\left(c_*^{\mathrm{uld}}/c_*^{\mathrm{ld}}\right)/dt$.

$$D = m_{\mathrm{VH}} L^2 \div \left.\frac{d\left(\theta^{\mathrm{uld}}/\theta^{\mathrm{ld}}\right)}{d\tau}\right|_{\tau_{\mathrm{inf}}} \tag{5.56}$$

This allows D at different reservoir concentrations to be calculated, which are provided in Table 5.1.

5.5.1 Evaluation of $\mathscr{D}_{-\mathrm{M}}$

Estimation for water concentration in membrane

$\mathscr{D}_{-\mathrm{M}}$ can be calculated from the Fickian D using eq.(5.35), as long as all the concentrations and $\mathscr{D}_{-0}$ and $\mathscr{D}_{+-}$ in the membrane are known. Unfortunately, there is insuccieint information to calculate the water concentration in the membrane Verbrugge and Hill [2] used exactly; thus, a reasonable approximation needs to be made to proceed forward. Provided the membrane is well hydrated, i.e., all pores are filled with the solution, water concentration in the membrane can be approximated as

$$c_0 = c_0^{\mathrm{pure}} \times \text{porosity} = 55.4\ \text{mol/L} \times 0.28 = 15.5\ \text{mol/L}, \tag{5.57}$$

where $c_0^{\mathrm{pure}} = 55.4$ mol/L is the molar concentration of pure water at 20°C (calculated from the density of water, tabulated by Tanaka et al. [196]) and the porosity of 0.28 can be taken for the membrane [8] used[4]. The concentration of the bisulfate ion can be calculated from the partition coefficient K using eq.(5.36). The proton concentration

[4]Although the Nafion porosity reported by Verbrugge and Hill [8] is concentration dependent, a constant value of 0.28 was taken to simplify the calculation. Their data suggest that this is a reasonable approximation for most of the concentration range dealt with in this chapter.

can then be obtained by electroneutrality, i.e.,

$$c_+ = -\frac{1}{z_+}(z_- c_- + z_{\mathrm{M}} c_{\mathrm{M}}). \tag{5.58}$$

Since $c_{\mathrm{M}} = 1.2$ mol/L, the total concentration can now be calculated by summing all species concentrations, i.e., $c_{\mathrm{T}} = c_0 + c_{\mathrm{M}} + c_- + c_+$.

Estimations for $\mathscr{D}_{-0}$, $\mathscr{D}_{+0}$, and $\mathscr{D}_{+-}$

To calculate $\mathscr{D}_{-\mathrm{M}}$, one should also ensure appropriate Stefan–Maxwell diffusivity values are substituted into eq.(5.35). A good starting point is the work of Umino and Newman [9], where the functional forms of $\mathscr{D}_{-0}$, $\mathscr{D}_{+0}$, and $\mathscr{D}_{+-}$ for sulfuric acid in water at 25°C are provided. Because Verbrugge and Hill's experiment was conducted at 20°C [2], some adjustments are required. Conveniently, Umino and Newman [197] showed that the temperature dependence of the diffusivities in aqueous sulfuric acid is well captured by the Arrhenius equation. Therefore, the three Stefan–Maxwell diffusivities at the desired temperature T and concentration can be obtained by

$$\mathscr{D}_{ij}(r, T) = \mathscr{D}_{ij}^{T_{\mathrm{ref}}}(r) \times \exp\left[\frac{E_{ij}}{R}\left(\frac{1}{T_{\mathrm{ref}}} - \frac{1}{T}\right)\right], \tag{5.59}$$

where $r = c_{\mathrm{e}}/c_0$ is the ratio of the sulfuric acid and water concentrations, $T_{\mathrm{ref}} = 298.15\ \mathrm{K} = 25\,^{\circ}\mathrm{C}$, and E_{ij} is the activation energy associated with diffusion for each pair of species $\{i, j\}$; $E_{+0} = 13.6$ kJ/mol, $E_{-0} = 18.4$ kJ/mol, and $E_{+-} = 12.2$ kJ/mol, according to Umino and Newman [197]. $\mathscr{D}_{ij}^{T_{\mathrm{ref}}}$ given by Umino and Newman [9] are functions of the sulfuric-acid concentration in the absence of membrane, which must be translated to functions of r in order to be employed in membrane systems. This can be easily achieved by substituting $c_{\mathrm{e}} = c_0 r$ into the Umino and Newman's general expression [9]:

$$F(r) = \exp\left[f_1 + \frac{f_2\sqrt{c_0 r}}{1 + \sqrt{c_0 r}} + f_3 c_0 r + f_4 (c_0 r)^{3/2} + f_5 (c_0 r)^2\right] \tag{5.60}$$

Table 5.2: The fitting parameters f_i for $\mathscr{D}_{+0}$, $\mathscr{D}_{-0}$, and $\mathscr{D}_{+-}$ from Umino and Newman [9] are presented again for convenience.

	f_1	f_2	f_3	f_4	f_5
$\mathscr{D}_{+0}$	−9.282	0.3139	−0.4583	0.1375	−0.03996
$\mathscr{D}_{-0}$	−11.45	0.1604	−0.3309	0.1211	−0.03275
$\mathscr{D}_{+-}$	−14.09	0.5634	1.456	−0.9512	0.1535

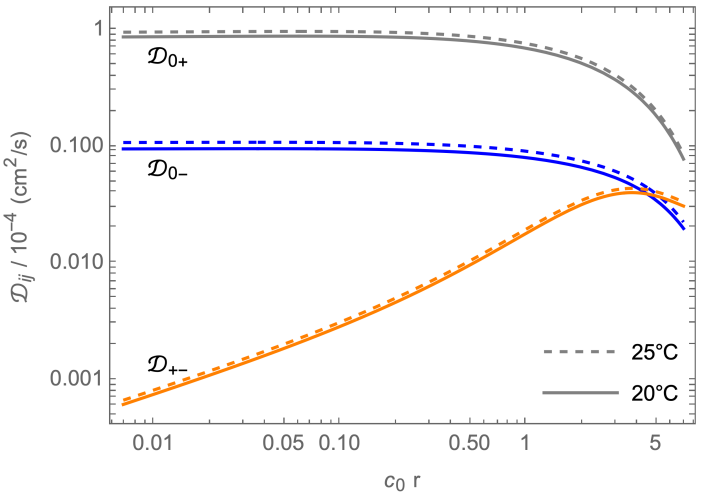

Figure 5.5: $\mathscr{D}_{+0}$, $\mathscr{D}_{-0}$, and $\mathscr{D}_{+-}$ are plotted against the sulfuric-acid/water concentration ratio, r, at 20°C and 25°C.

for $F = \mathscr{D}_{+0}^{T_{\mathrm{ref}}}$, $\mathscr{D}_{-0}^{T_{\mathrm{ref}}}$, and $\mathscr{D}_{+-}^{T_{\mathrm{ref}}}/\sqrt{c_0 r}$. The fitting coefficients f_i are listed in Umino and Newman [9], which are tabulated in Table 5.2 again for easy reference. $\mathscr{D}_{+0}$, $\mathscr{D}_{-0}$, and $\mathscr{D}_{+-}$ are plotted in Figure 5.5 at 20°C and 25°C. The exponential correction term ensures that $\mathscr{D}_{ij}$ at 20°C is lower than at the reference temperature.

Because the cation and anion concentrations differ inside Nafion, the evaluation of Stefan–Maxwell-diffusivity functions is not immediately straightforward. Remembering that the Stefan–Maxwell diffusivity $\mathscr{D}_{ij}$ captures microscopic interactions between species i and j, it is fair to say that $\mathscr{D}_{-0} = \mathscr{D}_{-0}(c_-/c_0)$ and $\mathscr{D}_{+0} = \mathscr{D}_{+0}(c_+/c_0)$. More attention has to be paid when calculating $\mathscr{D}_{+-}$ because it is not sufficient to evaluate it at a single concentration anymore. Given the anions encounter c_+ of cations during the diffusion process while the cations encounter c_- of anions, a reasonable approximation

of $\mathscr{D}_{+-}$ may be

$$\mathscr{D}_{+-}^{\mathrm{eff}} = \frac{c_- \mathscr{D}_{+-}(c_+/c_0) + c_+ \mathscr{D}_{+-}(c_-/c_0)}{c_- + c_+}, \tag{5.61}$$

i.e., it is the weighted average of $\mathscr{D}_{+-}$ at the two ion concentrations. It is noted that eq.(5.61) is a *choice* we make; there is no guarantee that this indeed describes the actual dynamics between the two ions. Nonetheless, eq.(5.61) seems to make sense at least qualitatively since $\mathscr{D}_{+-}$ is expected to be more strongly influenced by c_-. This is because most of the protons would be (loosely) bound to the charged membrane end-groups anyway, so it is the remaining small number of freely floating protons (which is equal to c_- in the membrane bulk) that would be more responsible for interfering with the bisulfate-ion movement. One can see eq.(5.61) boils down to $\mathscr{D}_{+-}^{\mathrm{eff}} \approx \mathscr{D}_{+-}(c_-/c_0)$ when $c_+ \gg c_-$, which is the case here because $c_{\mathrm{M}} \gg c_-$.

Functional form of $\mathscr{D}_{-\mathrm{M}}$

Now, all information is available to isolate $\mathscr{D}_{-\mathrm{M}}$ from eq.(5.35). The resulting $\mathscr{D}_{-\mathrm{M}}$ from Verbrugge and Hill's data set [2] is illustrated in Figure 5.6a. Due to its seemingly divergent nature as it approaches 0.5 M and the sign change, it is more sensible to look at the inverse of $\mathscr{D}_{-\mathrm{M}}$, which is plotted in Figure 5.6b. Evidently, it varies smoothly and its best fit, obtained *via* the method of least squares, is given by

$$\frac{10^{-7}}{\mathscr{D}_{-\mathrm{M}}\left(c^{\mathrm{bulk}}\right)} = 0.877 + 1.16 \ln c^{\mathrm{bulk}} + 0.724 \left(\ln c^{\mathrm{bulk}}\right)^2 + 0.281 \left(\ln c^{\mathrm{bulk}}\right)^3 \tag{5.62}$$

in $\mathrm{s/cm^2}$, valid at 20 °C. Since $1/\mathscr{D}_{ij}$ reflects the frictional force between the species i and j (*via* the Nernst–Einsten relation), this indicates that the interplay between the bisulfate and sulfonate ions is only truly nullified at $c^{\mathrm{bulk}} = 0.284$ M where $\mathscr{D}_{-\mathrm{M}} \to \infty$. This refutes the common assumption of ignoring such interactions by setting $1/\mathscr{D}_{-\mathrm{M}} = 0$ for all reservoir concentrations. This critical concentration marks the transition of the membrane behaviour from hindering anion diffusion to promoting it as the bulk-reservoir concentration increases.

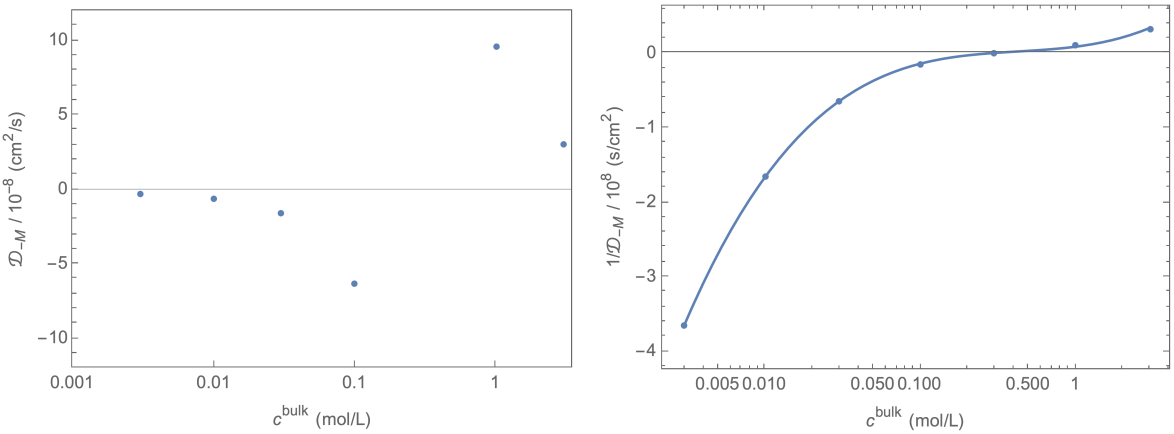

(a) $\mathscr{D}_{-\mathrm{M}}$ calculated from experimental data.

(b) Best fit of $1/\mathscr{D}_{-\mathrm{M}}$.

Figure 5.6: $\mathscr{D}_{-\mathrm{M}}$ extracted from Verbrugge and Hill's first experiment [2]. The circles show their measurement data.

Table 5.3: Literature $\mathscr{D}_{0\mathrm{M}}$ values.

Reference	$\mathscr{D}_{0\mathrm{M}}$ (cm^2/s)	Comment	Pretreatment
Delacourt and Newman [114]	10.5×10^{-6}	Using the data of Okada et al. [198] for Nafion 115 and 117 at 25°C	Boiled in H_2O_2 (2 hrs) and HCl (24 hrs) then rinsed in water
Zawodzinski, Jr. et al. [199]	5.5×10^{-6}	PGSE-NMR of Nafion 117 at 40°C	Boiled in H_2O_2 (1 hr), water (1 hr), H_2SO_4 (1 hr), and water (1 hr)
Roy et al. [200]	2×10^{-6}	PGSE-NMR of Nafion 112 at 30°C	Boiled in H_2SO_4 (2 hrs) and water (2 hrs)

5.6 Macroscopic transport-property estimation

Now, four out of six independent Stefan–Maxwell diffusivities are available for Nafion 117 immersed in aqueous sulfuric-acid solutions of concentrations up to 3 M. The remaining two, namely, $\mathscr{D}_{0\mathrm{M}}$ and $\mathscr{D}_{+\mathrm{M}}$, can be estimated from the existing literature data and the ionic-conductivity measurement of Verbrugge and Hill [3].

5.6.1 $\mathscr{D}_{0\mathrm{M}}$ values in the literature

Although the exact $\mathscr{D}_{0\mathrm{M}}$ for Nafion 117 Verbrugge and Hill [2] used (i.e., treated with the same pretreatment process) is not accessible, there is abundant data elucidating Nafion–water interactions in the literature. Relevant studies are summarised in Table 5.3 and a reasonable estimate can be made.

Using the ionic conductivity, electro-osmotic coefficient, and the water permeability measurements of Okada et al. [198] on Nafion 115 and 117 at 25°C, Delacourt and Newman [114] calculated $\mathscr{D}_{0\mathrm{M}}$ to be 10.5×10^{-6} cm^2/s. This may be the most relevant estimate in line with Newman's concentrated-solution theory.

Measurements by pulsed field-gradient spin-echo nuclear magnetic resonance (PGSE-NMR) are also useful in gauging the magnitude of $\mathscr{D}_{0\mathrm{M}}$. PGSE-NMR is a technique that can detect the drifting of a species (it has to have an intrinsic nuclear magnetic moment, though) due to random fluctuations it experiences as a result of interactions with its surrounding environment, i.e., it can measure diffusivity associated with the Brownian motion, which is often termed self-diffusivity. Since the Stefan–Maxwell diffusivity encapsulates the drag force between two species at the molecular level, the self-diffusivity is expected to capture at least the dominant first-order dynamics of what the Stefan–Maxwell diffusivity represents.

Numerous studies have reported water self-diffusivity in Nafion with this technique, usually at low to moderate water contents (a pretreated membrane is dried and then equilibrated in water vapour to control the water content) for the PEM fuel-cell application, e.g., see references [201–204]. However, only the results of studies on fully hydrated Nafion (i.e., submerged in liquid water) are admissible for the current investigation; therefore, Zawodzinski's result [199] is of high relevance. Combining the PGSE-NMR with an imaging technique of Neeman et al. [205], they reported water self-diffusivity of 5.5×10^{-6} cm^2/s for Nafion 117 of water content $\lambda = 12.9$ (which is the water content of Verbrugge and Hill's system) at 30°C . Their Arrhenius plot of membrane conductivity shows convergence for temperatures below 40°C. Thus, Za-

wodzinski's self-diffusivity value may be extended down to 20°C without incurring too much error, based on the Nernst–Einstein relation (which states that the conductivity and diffusivity are proportional).

Roy et al. [200], on the other hand, reported 2×10^{-6} cm^2/s for fully hydrated Nafion 112 at 30°C, measured by PGSE-NMR (Nafions 112 and 117 are made of the identical material, except the former is thinner; 0.002 and 0.007 inch for Nafion 112 and 117, respectively). A range of $\mathscr{D}_{0\mathrm{M}}$ found in the literature is likely attributed to the difference in pretreatment procedures; Zawodzinski, Jr. et al. [199], Okada et al. [198], and Roy et al. [200] used different combinations of acids and treatment durations, as summarised in Table 5.3. Given Verbrugge and Hill's pretreatment involved boiling in nitric acid —which none of the three papers employed— followed by boiling in H_2SO_4 [2], the true value of $\mathscr{D}_{0\mathrm{M}}$ in their experiment may deviate from the values discussed, but the average of their values —6.0×10^{-6} cm^2/s— is used to calculate $\mathscr{D}_{+\mathrm{M}}$ in the next subsection.

5.6.2 $\mathscr{D}_{+\mathrm{M}}$ from ionic conductivity

Only one Stefan–Maxwell diffusivity $\mathscr{D}_{+\mathrm{M}}$ remains to be determined and the ionic conductivity κ data of Verbrugge and Hill [3] can be utilised to verify this. $\mathscr{D}_{+\mathrm{M}}$ can be expressed in terms of the other Stefan–Maxwell diffusivities and κ by rearranging eq.(5.5). Substituting Verbrugge and Hill's κ [3] (which was measured at three bulk-reservoir concentrations), the desired $\mathscr{D}_{+\mathrm{M}}$ can be calculated and is tabulated in Table 5.4. The other four Stefan–Maxwell diffusivities at the corresponding concentrations are also presented. One can observe that $\mathscr{D}_{+\mathrm{M}}$ remains relatively constant, unlike $\mathscr{D}_{-\mathrm{M}}$ that varies by two orders of magnitude in the 0.3 – 3 M range. Given the inverse diffusivity relates to resistivity (*via* the Nernst–Einstein relation), $1/\mathscr{D}_{+\mathrm{M}}$ tells us that Nafion 117 is the least resistive to protons when submerged in a 1 M solution, which agrees with the measured ionic-conductivity trend that peaks at 1 M.

Table 5.4: $\mathscr{D}_{+\mathrm{M}}$ calculated from Verbrugge and Hill's κ data (in mS/cm) [3], as well as $\mathscr{D}_{ij}$'s estimated in the preceding sections. Note a concentration-independent value of $\mathscr{D}_{0\mathrm{M}} = 6.0 \times 10^{-6}$ cm^2/s was used. All $\mathscr{D}_{ij}$ are reported in units 10^{-6} cm^2/s.

c^{bulk}	κ	$\mathscr{D}_{0-}$	$\mathscr{D}_{0+}$	$\mathscr{D}_{+-}$	$\mathscr{D}_{-\mathrm{M}}$	$\mathscr{D}_{+\mathrm{M}}$
0.3 M	73	9.51	64.8	0.131	2.74	1.4
1 M	87	9.48	63.5	0.398	0.114	2.0
3 M	84	9.08	58.9	1.04	0.0294	1.6

Table 5.5: Macroscopic transport properties calculated using $\mathscr{D}_{ij}$'s in Table 5.4. Diffusivities are reported in units 10^{-6} cm^2/s.

c^{bulk}	t_-^{M}	$\tilde{\Xi}$	$\mathcal{D}_0$	$\mathcal{D}_{\mathrm{e}}$	$\mathcal{D}_\times$
0.3 M	−0.011	1.4	11	0.43	2.1
1 M	−0.011	1.3	10	0.32	1.5
3 M	−0.0018	1.2	9	0.11	0.50

5.6.3 Macroscopic transport properties

Once all the independent Stefan–Maxwell diffusivities are available, macroscopic transport properties can be easily acquired using equations (5.3), (5.10), and (5.11); the calculated values are provided in Table 5.5. Interestingly, the bisulfate ion has a negative transference number, which means that $t_+^{\mathrm{M}} = 1 - t_-^{\mathrm{M}} > 1$. Thus, the proton and the bisulfate ion form a neutral cluster to move in the same direction and the total current is smaller than the sum of the magnitude of the two ionic currents. Nonetheless, t_-^{M} is very small and it confirms the widely accepted notion that the proton transference number is unity for protonated Nafion (when no other cations are present in the system).

Furthermore, $\tilde{\Xi}$ values illustrate that proton drags water strongly as it migrates; e.g., a proton carries with it on average 1.4 water molecules in current-carrying systems when Nafion is submerged in a 0.3 M aqueous sulfuric-acid solution. The calculated $\tilde{\Xi}$ is well within the range previously reported in the literature. Fuller and Newman

[206] (Nafion equilibrated in saturated water vapour) and Luo et al. [207] (Nafion 117 at $\lambda = 13$ in contact with water) obtained $\tilde{\Xi} = 1.4$, which is very close to the $\tilde{\Xi}$ values in this work. Both larger and smaller $\tilde{\Xi}$ have been reported; $\tilde{\Xi} = 2.8$, 1.9, and 1.1 were obtained by Okada et al. [208], Ise et al. [209], and Ye and Wang [210], respectively. Again, the exact $\tilde{\Xi}$ value is expected to be strongly affected by pretreatment.

The comparison of component thermodynamic diffusivities reveals the nature of Nafion 117 as a diffusion medium. The fact that $\mathcal{D}_\times > \mathcal{D}_\mathrm{e}$ corroborates again that the proton is well solvated by water molecules and thus its movement induces a sizable water flow, and vice versa. $\mathcal{D}_0$ is significantly larger than $\mathcal{D}_\mathrm{e}$, indicating that water transport is favourable across the membrane. This is in line with the observed Nafion characteristics; it is known to admit water well and prone to swelling [89, 204]. An extensive list compilated by Kusoglu and Weber [211] shows that the effective water diffusivity in Nafion is in general $\sim 10^{-6}$ cm^2/s, which is slightly lower than $\mathcal{D}_0$ in Table 5.5. Since $\mathcal{D}_0$ does not contain any thermodynamic information, this suggests that the water thermodynamic factor in Nafion is smaller than 1, provided off-diagonal entries of $\mathbf{X}$ in eq.(5.24) are negligible. A more accurate functional form of the water thermodynamic factor for the pretreated membrane Verbrugge and Hill [2] used may be derived when a consistent concentration-dependent set of the effective water diffusivity is available.

5.7 Non-electroneutral membrane–reservoir interfaces

The Gibbs–Donnan effect is a well-known phenomenon observed in charged membranes in contact with electrolytic solutions. The Donnan potential arises at the membrane–reservoir interface and a finite-width non-electroneutral region must appear to sustain it, nonetheless very thin. For example, the thickness of Nafion used by Verbrugge and Hill [2] ($L = 230\,\mu$m $= 2.3 \times 10^5$ nm) in comparison to the Debye length (5.6

nm in a membrane-free 0.003 M sulfuric acid solution) demonstrates the scale of non-electroneutral regions. However, precisely because of its small length scale, the electric-potential gradient is expected to be large and it may be beneficial to understand its dynamics separately from the concentration gradients. This is especially more pertinent in situations where ion movement across membranes has a considerable effect on the system performance, e.g., in vanadium redox flow battery. To do so, corrected electrochemical-potential differentials are derived based on the core-potential theory and Boltzmann distribution.

5.7.1 Corrections for electrochemical-potential differentials

The procedure in section 3.3 can be employed to derive the electrochemical-potential differentials with appropriate corrections for the four-species membrane system in non-electroneutral regions. However, unlike conventional membrane-free solutions, one of the charged species is bound to polymer chains and thus immobile relative to the lab frame. Consequently, it is more appropriate to assume the embedded charged end-group is uniformly distributed, rather than Boltzmann distributed. This means that the excess charge density should be rewritten as

$$\overline{\mathrm{P}} = F z_{\mathrm{M}} y_{\mathrm{M}}^{0} + F \sum z_k y_k^{0} \exp(-z_k \phi), \tag{5.63}$$

with the ionic strength of

$$\overline{I}^{\mathrm{B}} = \frac{1}{2} z_{\mathrm{M}}^{2} y_{\mathrm{M}}^{0} + \frac{1}{2} \sum z_k^{2} y_k^{0} \exp(-z_k \phi). \tag{5.64}$$

$\phi = F\Phi^{\mathrm{P}}/RT$ is a dimensionless Poisson–Boltzmann overpotential, as before. The new $\overline{\mathrm{P}}$ expression also mandates a redefinition of some entries of the core-potential thermodynamic-factor matrix that correspond to the charging ion. By partially differ-

entiating $\overline{\mathrm{P}}$ with respect to composition variables, one gets

$$\begin{aligned}\overline{X}^{\mathrm{B}}_{(n-1)j} =& \frac{RT}{2\overline{I}^{\mathrm{B}} - z_{\mathrm{M}}^2 y_{\mathrm{M}}^0}\Big[\left(z_n - z_{n-1}\right)^2 \delta_{(n-1)j} - z_{\mathrm{M}}\left(z_n - z_{n-1}\right)\delta_{\mathrm{M}j} \\ &+ z_n z_j \left\{e^{-z_n\phi} - \left(1-\delta_{\mathrm{M}j}\right)e^{-z_j\phi}\right\} + z_n z_{n-1}\left(e^{-z_{n-1}\phi} - e^{-z_n\phi}\right) \\ &+ z_{n-1}z_j\left\{\left(1-\delta_{\mathrm{M}j}\right)e^{-z_j\phi} - e^{-z_{n-1}\phi}\right\}\Big].\end{aligned} \tag{5.65}$$

Now, one can apply the procedure in section 3.3. The electroneutral reference composition for the system $\{\mathrm{M}, 0, -, +\}$ is

$$\begin{aligned}&\{y_{\mathrm{M}}^0, y_0^0, y_-^0, y_+^0\} \\ &\qquad = \left\{y_{\mathrm{M}}, y_0, \frac{z_+(1-y_0-y_{\mathrm{M}}) + z_{\mathrm{M}}y_{\mathrm{M}}}{z_+ - z_-}, -\frac{z_-(1-y_0-y_{\mathrm{M}}) + z_{\mathrm{M}}y_{\mathrm{M}}}{z_+ - z_-}\right\}.\end{aligned} \tag{5.66}$$

Near the interface where the membrane meets the membrane-free solution, an excess charge density appears and eq.(5.63) becomes

$$\begin{aligned}\overline{\mathrm{P}} =& \frac{Fz_-z_+}{z_+ - z_-}(1-y_0-y_{\mathrm{M}})\left(e^{-z_-\phi} - e^{-z_+\phi}\right) \\ &+ \frac{Fy_{\mathrm{M}}z_{\mathrm{M}}}{z_+ - z_-}\left\{z_+\left(1-e^{-z_+\phi}\right) - z_-\left(1-e^{-z_-\phi}\right)\right\}.\end{aligned} \tag{5.67}$$

The ionic strength in eq.(5.64) becomes

$$\begin{aligned}\overline{I}^{\mathrm{B}} =& \frac{z_{\mathrm{M}}^2 y_{\mathrm{M}}}{2} + \frac{z_{\mathrm{M}}y_{\mathrm{M}}}{2(z_+ - z_-)}\left(z_-^2 e^{-z_-\phi} - z_+^2 e^{-z_+\phi}\right) \\ &+ \frac{z_+z_-}{2(z_+ - z_-)}(1-y_0-y_{\mathrm{M}})\left(z_- e^{-z_-\phi} - z_+ e^{-z_+\phi}\right).\end{aligned} \tag{5.68}$$

Defining

$$\begin{aligned}\delta_1 &= \frac{z_+z_-}{(z_+ - z_-)^2}\left(e^{-z_-\phi} - e^{-z_+\phi}\right) \\ \delta_2 &= \frac{z_{\mathrm{M}}}{(z_+ - z_-)^2}\left[\left(1-e^{-z_-\phi}\right)z_- - \left(1-e^{-z_+\phi}\right)z_+\right]\end{aligned} \tag{5.69}$$

for notational convenience, eq.(5.65) produces the following core-potential thermody-

namic factors.

$$\begin{gathered}\overline{X}^{\mathrm{B}}_{-\mathrm{M}} = \frac{RT(z_+ - z_-)^2}{2\overline{I}^{\mathrm{B}} - z_{\mathrm{M}}^2 y_{\mathrm{M}}^0}\,(\delta_1 + \delta_2) \\ \overline{X}^{\mathrm{B}}_{-0} = \frac{RT(z_+ - z_-)^2}{2\overline{I}^{\mathrm{B}} - z_{\mathrm{M}}^2 y_{\mathrm{M}}^0}\delta_1 \qquad \overline{X}^{\mathrm{B}}_{--} = \frac{RT(z_+ - z_-)^2}{2\overline{I}^{\mathrm{B}} - z_{\mathrm{M}}^2 y_{\mathrm{M}}^0}\end{gathered} \tag{5.70}$$

This leads to the following Newman's electroneutral thermodynamic-factor matrix using eq.(3.68).

$$\begin{aligned}\boldsymbol{\chi}_- &= \begin{bmatrix} \chi_{\mathrm{MM}} & \chi_{\mathrm{M0}} \\ \chi_{0\mathrm{M}} & \chi_{00} \\ \chi_{-\mathrm{M}} & \chi_{-0} \\ \chi_{+\mathrm{M}} & \chi_{+0} \end{bmatrix} \\ &= \frac{1}{RT}\begin{bmatrix} y_{\mathrm{M}}\left((1-y_{\mathrm{M}})\overline{X}^{\mathrm{B}}_{\mathrm{MM}} - y_0\overline{X}^{\mathrm{B}}_{0\mathrm{M}}\right) & y_{\mathrm{M}}\left((1-y_{\mathrm{M}})\overline{X}^{\mathrm{B}}_{\mathrm{M0}} - y_0\overline{X}^{\mathrm{B}}_{00}\right) \\ y_0\left((1-y_0)\overline{X}^{\mathrm{B}}_{0\mathrm{M}} - y_{\mathrm{M}}\overline{X}^{\mathrm{B}}_{\mathrm{MM}}\right) & y_0\left((1-y_0)\overline{X}^{\mathrm{B}}_{00} - y_{\mathrm{M}}\overline{X}^{\mathrm{B}}_{\mathrm{M0}}\right) \\ -y_-^0\left(y_{\mathrm{M}}\overline{X}^{\mathrm{B}}_{\mathrm{MM}} + y_0\overline{X}^{\mathrm{B}}_{0\mathrm{M}}\right) & -y_-^0\left(y_{\mathrm{M}}\overline{X}^{\mathrm{B}}_{\mathrm{M0}} + y_0\overline{X}^{\mathrm{B}}_{00}\right) \\ -y_+^0\left(y_{\mathrm{M}}\overline{X}^{\mathrm{B}}_{\mathrm{MM}} + y_0\overline{X}^{\mathrm{B}}_{0\mathrm{M}}\right) & -y_+^0\left(y_{\mathrm{M}}\overline{X}^{\mathrm{B}}_{\mathrm{M0}} + y_0\overline{X}^{\mathrm{B}}_{00}\right) \end{bmatrix}\Bigg|_{\overline{\mathrm{P}}=0}\end{aligned} \tag{5.71}$$

Comparing $d\mu_0$ and $d\mu_{\mathrm{e}}$ constructed from eq.(3.68) with the elements of $\boldsymbol{\chi}_-$ and equations (5.18) and (5.20) involving χ^{m}_{ij}, one can work out the relationships between the measurable and Newman's electroneutral thermodynamic factors. Because equations (5.18) and (5.20) are written with dy_0 and dy_{e}, dy_{M} in eq.(3.68) can be equivalently expressed as $dy_{\mathrm{M}} = -\frac{\nu_{\mathrm{M}}}{\nu^{\overline{\mathrm{M}}}}(dy_0 + \nu^{\mathrm{e}}dy_{\mathrm{e}})$ —*via* the phase rule and electroneutrality— for a more straightforward comparison. After identifying the relationships among the elements of $\boldsymbol{\chi}_-$ and χ^{m}_{ij}, any appearance of y_{e} can be replaced with $y_{\mathrm{e}} = (1 - y_0 - \nu^{\overline{\mathrm{M}}}y_{\mathrm{M}}/\nu_{\mathrm{M}})/\nu^{\mathrm{e}}$ to avoid having three composition variables. If the identified relationships are extended to non-electroneutral systems with the same

functionalities, then Newman's non-electroneutral thermodynamic factors χ^*_{ij} can be expressed as

$$\chi^*_{00} = \chi_{00} - \frac{\nu_{\mathrm{M}}}{\nu^{\overline{\mathrm{M}}}}\chi_{0\mathrm{M}} = \chi^{\mathrm{m}}_{00} + \chi^{\mathrm{el}}_{00}$$

$$\chi^*_{0\mathrm{e}} = -\frac{\nu_{\mathrm{M}}\nu^{\mathrm{e}}}{\nu^{\overline{\mathrm{M}}}}\chi_{0\mathrm{M}} = \chi^{\mathrm{m}}_{0\mathrm{e}} + \chi^{\mathrm{el}}_{0\mathrm{e}}$$

$$\begin{aligned}\chi^*_{\mathrm{e}0} &= \frac{1 - y_0 - \frac{\nu^{\overline{\mathrm{M}}}}{\nu_{\mathrm{M}}}y_{\mathrm{M}}}{\nu^{\mathrm{e}}}\left[\frac{\nu^{\mathrm{e}}_+}{y^0_+}\left(\chi_{+0} - \frac{\nu_{\mathrm{M}}}{\nu^{\overline{\mathrm{M}}}}\chi_{+\mathrm{M}}\right) + \frac{\nu_-}{y^0_-}\left(\chi_{-0} - \frac{\nu_{\mathrm{M}}}{\nu^{\overline{\mathrm{M}}}}\chi_{-\mathrm{M}}\right)\right] \\ &= \chi^{\mathrm{m}}_{\mathrm{e}0} + \chi^{\mathrm{el}}_{\mathrm{e}0}\end{aligned} \tag{5.72}$$

$$\chi^*_{\mathrm{ee}} = -\frac{1 - y_0 - \frac{\nu^{\overline{\mathrm{M}}}}{\nu_{\mathrm{M}}}y_{\mathrm{M}}}{\nu^{\mathrm{e}}\nu^{\overline{\mathrm{M}}}/\nu_{\mathrm{M}}}\left(\frac{\nu^{\mathrm{e}}_+}{y^0_+}\chi_{+\mathrm{M}} + \frac{\nu_-}{y^0_-}\chi_{-\mathrm{M}}\right) = \chi^{\mathrm{m}}_{\mathrm{ee}} + \chi^{\mathrm{el}}_{\mathrm{ee}},$$

where χ^{el}_{ij} captures the electrical dependence. To find χ^{el}_{ij}, one needs to look at the electrochemical-potential differentials of neutral species, i.e., $d\mu_0$ and $d\mu_{\mathrm{e}}$ in this case, and require that they are independent of electric potential. This leads to the following χ^{el}_{ij}.

$$\chi^{\mathrm{el}}_{00} = \frac{y_0(z_+ - z_-)}{F\left(2\overline{I}^{\mathrm{B}} - z^2_{\mathrm{M}}y^0_{\mathrm{M}}\right)}\left[\left(1 - \frac{\nu_{\mathrm{M}}}{\nu^{\overline{\mathrm{M}}}}\right)\delta_1 - \frac{\nu_{\mathrm{M}}}{\nu^{\overline{\mathrm{M}}}}\delta_2\right]\overline{\mathrm{P}}$$

$$\chi^{\mathrm{el}}_{0\mathrm{e}} = -\frac{\nu^{\mathrm{e}}\nu_{\mathrm{M}}y_0(z_+ - z_-)}{F\nu^{\overline{\mathrm{M}}}\left(2\overline{I}^{\mathrm{B}} - z^2_{\mathrm{M}}y^0_{\mathrm{M}}\right)}(\delta_1 + \delta_2)\overline{\mathrm{P}}$$

$$\begin{aligned}\chi^{\mathrm{el}}_{\mathrm{e}0} = \frac{\left(1 - y_0 - \frac{\nu^{\overline{\mathrm{M}}}}{\nu_{\mathrm{M}}}y_{\mathrm{M}}\right)(z_+ - z_-)^2}{\nu^{\mathrm{e}}\left(2\overline{I}^{\mathrm{B}} - z^2_{\mathrm{M}}y^0_{\mathrm{M}}\right)}&\left[\left(1 - \frac{\nu_{\mathrm{M}}}{\nu^{\overline{\mathrm{M}}}}\right)\delta_1 - \frac{\nu_{\mathrm{M}}}{\nu^{\overline{\mathrm{M}}}}\delta_2\right] \\ &\times\left[\frac{\overline{\mathrm{P}}}{F(z_+ - z_-)} + \frac{\left(e^{-z_+\phi} - e^{-z_-\phi}\right)z_+z_-}{(z_+ - z_-)^2}\right]\end{aligned} \tag{5.73}$$

$$\begin{aligned}\chi^{\mathrm{el}}_{\mathrm{ee}} = &-\frac{\nu_{\mathrm{M}}\left(1 - y_0 - \frac{\nu^{\overline{\mathrm{M}}}}{\nu_{\mathrm{M}}}y_{\mathrm{M}}\right)(z_+ - z_-)^2}{\nu^{\overline{\mathrm{M}}}\left(2\overline{I}^{\mathrm{B}} - z^2_{\mathrm{M}}y^0_{\mathrm{M}}\right)}(\delta_1 + \delta_2) \\ &\times\left[\frac{\overline{\mathrm{P}}}{F(z_+ - z_-)} + \frac{\left(e^{-z_+\phi} - e^{-z_-\phi}\right)z_+z_-}{(z_+ - z_-)^2}\right]\end{aligned}$$

With these values, $d\mu_i$ that are consistent in non-electroneutral regions can finally be

obtained.

$$
\begin{aligned}
d\mu_{\mathrm{M}} = & -\frac{RT}{y_{\mathrm{M}}}\left[\left\{\chi^{\mathrm{m}}_{0\mathrm{e}}+\frac{(1-y_0-y_{\mathrm{M}})\nu^{\mathrm{e}}}{1-y_0-\frac{\nu^{\overline{\mathrm{M}}}}{\nu_{\mathrm{M}}}y_{\mathrm{M}}}\chi^{\mathrm{m}}_{\mathrm{ee}}\right\} d\left(\frac{1-y_0-\frac{\nu^{\overline{\mathrm{M}}}}{\nu_{\mathrm{M}}}y_{\mathrm{M}}}{\nu^{\mathrm{e}}}\right)\right.\\
& \left.+\left\{\chi^{\mathrm{m}}_{00}+\frac{(1-y_0-y_{\mathrm{M}})\nu^{\mathrm{e}}}{1-y_0-\frac{\nu^{\overline{\mathrm{M}}}}{\nu_{\mathrm{M}}}y_{\mathrm{M}}}\chi^{\mathrm{m}}_{\mathrm{e}0}\right\} dy_0\right]\\
& +\frac{Fz_{\mathrm{M}}}{z_+-z_-}\left[z_+\exp\left(\frac{Fz_+\Phi}{RT}\right)-z_-\exp\left(\frac{Fz_-\Phi}{RT}\right)\right]d\Phi\\
d\mu_0 = & \frac{RT}{y_0}\left[\chi^{\mathrm{m}}_{0\mathrm{e}}\,d\left(\frac{1-y_0-\frac{\nu^{\overline{\mathrm{M}}}}{\nu_{\mathrm{M}}}y_{\mathrm{M}}}{\nu^{\mathrm{e}}}\right)+\chi^{\mathrm{m}}_{00}\,dy_0\right]\\
d\mu_- = & \frac{\nu^{\mathrm{e}}RT}{1-y_0-\frac{\nu^{\overline{\mathrm{M}}}}{\nu_{\mathrm{M}}}y_{\mathrm{M}}}\left[\chi^{\mathrm{m}}_{\mathrm{ee}}\,d\left(\frac{1-y_0-\frac{\nu^{\overline{\mathrm{M}}}}{\nu_{\mathrm{M}}}y_{\mathrm{M}}}{\nu^{\mathrm{e}}}\right)+\chi^{\mathrm{m}}_{\mathrm{e}0}\,dy_0\right]\\
& +Fz_-\left[1+\frac{z_+}{z_+-z_-}\left\{\exp\left(\frac{Fz_+\Phi}{RT}\right)-\exp\left(\frac{Fz_-\Phi}{RT}\right)\right\}\right]d\Phi\\
d\mu_+ = & \frac{\nu^{\mathrm{e}}RT}{1-y_0-\frac{\nu^{\overline{\mathrm{M}}}}{\nu_{\mathrm{M}}}y_{\mathrm{M}}}\left[\chi^{\mathrm{m}}_{\mathrm{ee}}\,d\left(\frac{1-y_0-\frac{\nu^{\overline{\mathrm{M}}}}{\nu_{\mathrm{M}}}y_{\mathrm{M}}}{\nu^{\mathrm{e}}}\right)+\chi^{\mathrm{m}}_{\mathrm{e}0}\,dy_0\right]\\
& +Fz_+\left[1+\frac{z_-}{z_+-z_-}\left\{\exp\left(\frac{Fz_+\Phi}{RT}\right)-\exp\left(\frac{Fz_-\Phi}{RT}\right)\right\}\right]d\Phi
\end{aligned}
\tag{5.74}
$$

Since the core-potential thermodynamic-factor matrix is the Hessian of the Gibbs free energy, it must be symmetric. This dictates there be three independent thermodynamic factors, and one of the four thermodynamic factors in equations (5.18) and (5.20) can be written in terms of the other three. For example, using the symmetry constraint, one can derive

$$
\chi^{\mathrm{m}}_{\mathrm{e}0}=\frac{1-y_0-\frac{\nu^{\overline{\mathrm{M}}}}{\nu_{\mathrm{M}}}y_{\mathrm{M}}}{(1-y_0)\nu^{\mathrm{e}}}\left[\chi^{\mathrm{m}}_{\mathrm{ee}}-\chi^{\mathrm{m}}_{00}+\left(1+\frac{\nu^{\overline{\mathrm{M}}}y_{\mathrm{M}}}{\nu_{\mathrm{M}}y_0}\right)\frac{\chi^{\mathrm{m}}_{0\mathrm{e}}}{\nu^{\mathrm{e}}}\right]. \tag{5.75}
$$

5.7.2 Interfacial electric potential

A rigorous simulation of a membrane system requires knowledge of the electric-potential distribution across the system domain. The electric potential internal to the membrane

can be obtained by solving the Poisson–Boltzmann equation, but this still demands the boundary values (i.e., where the membrane and the membrane-free solution meet) to be fixed. Fortunately, one can follow the approach of Mauro [90] to calculate this. However, his analytical solution cannot be directly applied in this thesis, due to the difference in the reference composition the electric potential is measured against; Mauro's Poisson–Boltzmann electric potential is referenced to the electroneutral composition in the bulk reservoir, while Goyal and Monroe's Poisson–Boltzmann electric overpotential is defined relative to the bulk of the membrane. In this section, a workaround is presented so that the desired interfacial electric potential consistent with Goyal and Monroe's framework can be calculated.

The starting point of this analysis is the Poisson–Boltzmann equation

$$\frac{d^2\phi}{dx^2} = -\frac{F}{RT\epsilon}\rho_{\mathrm{e}}, \tag{5.76}$$

where x denotes the spatial domain across the membrane width, $\phi = F\Phi_{\mathrm{P}}/RT$ is the dimensionless Poisson–Boltzmann overpotential as before, ϵ is the permittivity of the medium, and ρ_{e} is the excess charge, which relates to the molar excess charge by $\rho_{\mathrm{e}} = c_{\mathrm{T}}\overline{\mathrm{P}}$. Let $x = 0$ be the membrane–reservoir interface, with the membrane on the left and the reservoir on the right. The electric potential in the core-potential theory is referenced to the electroneutral part of the system, so the potentials in both phases should be treated separately. The two potentials must tend to zero far away from the interface when each phase is investigated in isolation; a connection between the two can be made later by incorporating Mauro's result [90]. Denoting ϕ and ϕ_{R} as the electric potential in the membrane and the reservoir, respectively, the Poisson–Boltzmann equation can be written as

$$\begin{aligned} \frac{d^2\phi_{\mathrm{R}}}{dx^2} &= -\frac{2F^2 z_+ z_- \nu^{\mathrm{e}} c^{\mathrm{bulk}}}{RT\epsilon(z_- - z_+)} \times \frac{e^{-z_+\phi_{\mathrm{R}}} - e^{-z_-\phi_{\mathrm{R}}}}{2} && \text{reservoir} \\ \frac{d^2\phi}{dx^2} &= -\frac{F^2}{RT\epsilon}\left[z_{\mathrm{M}}c_{\mathrm{M}} + z_- c_{\mathrm{T}} y_-^0 e^{-z_-\phi} + z_+ c_{\mathrm{T}} y_+^0 e^{-z_+\phi}\right] && \text{membrane} \end{aligned}, \tag{5.77}$$

after making use of eq.(3.70) for $\overline{\mathrm{P}}$ in the reservoir. The exact expressions for the electroneutral compositions y_i^0 in the membrane phase can be found in eq.(5.66). It is assumed that the permittivity remains the same across the two phases. The Debye length in the reservoir can be identified as

$$\lambda_{\mathrm{D}}^2 = \frac{RT\epsilon(z_- - z_+)}{2F^2 z_+ z_- \nu^{\mathrm{e}} c^{\mathrm{bulk}}}, \tag{5.78}$$

which can be used to non-dimensionalise the spatial variable x to get $\xi_{\mathrm{D}} = x/\lambda_{\mathrm{D}}$.

The two electric potentials can be related by considering the limiting behaviours. It is reasonable to expect ϕ —defined with respect to the electroneutral part of the membrane— to converge to a constant value (say, ϕ_∞) when approaching the bulk of the reservoir, while $\phi_{\mathrm{R}} \to 0$ in the same limit. This, along with the fact that the electric-potential difference should be independent of the choice of the reference point, suggest that ϕ_{R} can be written as a simple translation, i.e., $\phi_{\mathrm{R}} = \phi - \phi_\infty$. Hence, the Poisson–Botlzmann equations simplify further to

$$\begin{aligned}
\frac{d^2\phi_{\mathrm{R}}}{d\xi_{\mathrm{D}}^2} = \frac{d^2\phi}{d\xi_{\mathrm{D}}^2} &= \frac{e^{-z_-(\phi-\phi_\infty)} - e^{-z_+(\phi-\phi_\infty)}}{2} && \text{reservoir} \\
\frac{d^2\phi}{d\xi_{\mathrm{D}}^2} &= -\frac{z_- - z_+}{2z_+ z_- \nu^{\mathrm{e}} c^{\mathrm{bulk}}} && \\
&\quad \times \left[z_{\mathrm{M}} c_{\mathrm{M}} + z_- c_{\mathrm{T}} y_-^0 e^{-z_-\phi} + z_+ c_{\mathrm{T}} y_+^0 e^{-z_+\phi}\right] && \text{membrane}
\end{aligned} \quad . \tag{5.79}$$

Employing the integrating-factor method as Mauro [90] did, expressions for the gradient of ϕ can be obtained,

$$\begin{aligned}
\left(\frac{d\phi}{d\xi_{\mathrm{D}}}\right)^2 &= -z_- e^{-z_-(\phi-\phi_\infty)} + z_+ e^{-z_+(\phi-\phi_\infty)} + C_{\mathrm{R}} && \text{reservoir} \\
\left(\frac{d\phi}{d\xi_{\mathrm{D}}}\right)^2 &= \frac{z_- - z_+}{z_+ z_- \nu^{\mathrm{e}} c^{\mathrm{bulk}}} \times && \\
&\quad \left[-z_{\mathrm{M}} c_{\mathrm{M}} \phi + z_-^2 c_{\mathrm{T}} y_-^0 e^{-z_-\phi} + z_+^2 c_{\mathrm{T}} y_+^0 e^{-z_+\phi} + C_{\mathrm{M}}\right] && \text{membrane}
\end{aligned} \quad , \tag{5.80}$$

where C_{R} and C_{M} are constants of integration. Requiring $\phi \to \phi_\infty$ and $\frac{d\phi}{d\xi_{\mathrm{D}}} \to 0$ as

$x \to \infty$, it must be the case that

$$C_{\mathrm{R}} = z_- - z_+. \tag{5.81}$$

Similarly, $\phi \to 0$ and $\frac{d\phi}{d\xi_{\mathrm{D}}} \to 0$ as x approaches the middle of the membrane produce

$$C_{\mathrm{M}} = -z_-^2 c_{\mathrm{T}} y_-^0 - z_+^2 c_{\mathrm{T}} y_+^0. \tag{5.82}$$

The interfacial electric potential ϕ_{int} can be obtained by requiring both ϕ and its derivative to be continuous at the interface, i.e., replace ϕ by ϕ_{int} and equate the two equations in eq.(5.80) to solve for ϕ_{int}. For aqueous sulfuric acid in Nafion, this amounts to solving

$$z_{\mathrm{M}} c_{\mathrm{M}} \phi_{\mathrm{int}} + c_{\mathrm{T}} y_-^0 \left(1 - e^{\phi_{\mathrm{int}}}\right) + c_{\mathrm{T}} y_+^0 \left(1 - e^{-\phi_{\mathrm{int}}}\right) = -2c^{\mathrm{bulk}} \left[\cosh(\phi_{\mathrm{int}} - \phi_\infty) - 1\right]. \tag{5.83}$$

Further progress is hindered with the core-potential formalism because the exact value of ϕ_∞ cannot be verified. At this point, we strategically go back to Mauro's framework [90] and argue again that the electric-potential difference must be independent of the choice of the reference composition. Mauro [90] acquired the value of the electric potential in the membrane relative to the bulk solution (by solving the Poisson–Botlzmann equation in the limit of approaching the electroneutral part of the membrane, where $\frac{d^2\phi}{d\xi_{\mathrm{D}}^2} \to 0$). Because this potential is referenced to the reservoir bulk solution, $z_{\mathrm{M}} c_{\mathrm{M}}$ term forces ϕ to be non-zero in the membrane. In fact, the electric potential in the membrane ϕ_{M} remote from the interface satisfies

$$\sinh \phi_{\mathrm{M}} = \frac{z_{\mathrm{M}} c_{\mathrm{M}}}{2c^{\mathrm{bulk}}} \tag{5.84}$$

if the electrolyte in the system satisfies $z_+ = -z_- = 1$, which is the case here. For membranes with negatively charged end-groups, as in Nafion, this means that the potential in the membrane is lower than in the bulk reservoir, i.e., $\phi_{\mathrm{M}} < 0$. From the

Table 5.6: The dimensionless Poisson–Boltzmann over-potentials in the bulk of the reservoir containing aqueous sulfuric acid (ϕ_∞) and at the membrane–reservoir interface (ϕ_{int}). The values are relative to the middle of the membrane, where the excess charge density is zero.

c^{bulk} (M)	0.003	0.01	0.03	0.1	0.3	1	3
ϕ_∞	5.99	4.79	3.69	2.49	1.44	0.569	0.199
ϕ_{int}	0.995	0.983	0.952	0.851	0.637	0.317	0.128

core-potential point of view, ϕ in the reservoir must be a positive number because the zero potential now sits in the middle of the membrane and the relative positions of potential should remain unaffected by the choice of the reference point. Therefore, it follows that $\phi_\infty = -\phi_{\text{M}}$. With this, eq.(5.83) can be solved numerically for ϕ_{int}.

Table 5.6 shows ϕ_∞ and ϕ_{int} for concentrations tested by Verbrugge and Hill [2], illustrating that they decrease as the reservoir bulk concentration increases. To understand this trend, one should look at the concentration difference across the membrane–reservoir interface. Although the counter-ion (cation) concentration in the membrane rises as more salt is added to the reservoir, the rate at which this concentration changes is smaller than that in the bulk concentration. This is due to two reasons; (1) the partition coefficient K suppresses the ion intake and (2) the counter-ion concentration in the membrane is already high to satisfy electroneutrality in the middle of the membrane. These effects contribute to the reduction of the counter-ion concentration gradient across the interface as the bulk-reservoir concentration increases. Since the interfacial potential —emanating from the charged membrane end-groups— counteracts this diffusion driving force at equilibrium, the observed trend in Table 5.6 makes sense.

5.8 Summary and outlook

In this chapter, techniques employed in Chapters 3 and 4 were applied to study a simple membrane system: Nafion in aqueous sulfuric acid. The focus of this investigation evolved around characterising Stefan–Maxwell diffusivities for the system, instead of

performing numerical simulations. This was because simulations demand the knowledge of all independent transport properties, which, unfortunately, the currently available literature insufficiently provides, especially when it comes to the Stefan–Maxwell diffusivities. Thus, this chapter is expected to serve as a useful case study for filling in this gap. The main outcomes of this chapter are summarised below.

1. Flux equations for a charged membrane imbued with a binary electrolyte were derived and used to identify the relationships between macroscopic transport properties and Stefan–Maxwell diffusivities in sections 5.2 and 5.3.

2. Section 5.3 showed that thermodynamic factors in membrane systems resemble those in the three-ion ionic liquid; they approach stoichiometry-dependent values in the dilute limit, not simply 1.

3. Two previously unknown Stefan–Maxwell diffusivities for Nafion in aqueous sulfuric acid —$\mathscr{D}_{-\mathrm{M}}$ and $\mathscr{D}_{+\mathrm{M}}$— were extracted by re-analysing the experimental data of Verbrugge and Hill [2, 3] in sections 5.5 and 5.6.2. The Barnes method [194] played an important role. The resulting $\mathscr{D}_{-\mathrm{M}}$ showed that the common assumption of nullifying $1/\mathscr{D}_{-\mathrm{M}}$ is not valid in general, since this is only true at a particular reservoir concentration. In contrast, $\mathscr{D}_{+\mathrm{M}}$ remained positive in the concentration range tested and peaked at 1 M, coinciding with the reported ionic conductivity [3].

4. Thus acquired $\mathscr{D}_{-\mathrm{M}}$ and $\mathscr{D}_{+\mathrm{M}}$ were then used to calculate the macroscopic transport properties in section 5.6.3, which were in good agreement with the literature values.

5. In addition, section 5.7 established the basis for membrane simulations encompassing non-electroneutral regions. The core-potential informed electrochemical-potential differentials were derived and a method to find the boundary electric potential (which is necessary for solving the Poisson–Boltzmann equation) was outlined, based on the idea of Mauro [90].

Despite having all the necessary information, solving the continuity and Poisson–Boltzmann equations is not straightforward in membrane systems when non-electroneutral regions are to be included within the system boundary. This is because the distance over which the electric potential varies is minuscule compared to the total membrane width, making it numerically challenging to solve. Some numerical ingenuity will be required to achieve robust and trustworthy solutions with sufficient computational efficiency. If this can be achieved, it may be possible to simulate a vanadium redox flow battery with its non-electroneutral boundary regions. Diffusion driving forces augmented by the core-potential correction terms will be essential in carrying this out correctly. Whether the correction terms contribute to an improved prediction of species crossover in comparison to the less-rigorous model would be an interesting aspect of future investigation. Nonetheless, some simplifications would still be necessary to reduce the number of independent transport properties. For example, all vanadium species may be assumed to have the same interactions with other species.

Chapter 6

Conclusions

This thesis attempted to apply the core-potential theory within the context of concentrated solution theory so that diffusion in non-dilute solutions in non-electroneutral regions can be modelled consistently. In particular, three simple electrolytic solutions —(1) the binary electrolyte, (2) the three-ion ionic liquid, and (3) the binary salt in two neutral solvents— and Nafion 117 in aqueous sulfuric acid were examined in detail.

After a brief introduction in Chapter 1 and a literature review in Chapter 2, transport and MacInnes equations were written directly using core-potential gradients in Chapter 3. Accompanying transport properties were also derived. This exercise demonstrated that the core-potential theory, despite its intrinsic thermodynamic consistency in non-electroneutral regions, produced convoluted expressions that did not permit easy utility. In response, the Boltzmann distribution was incorporated to arrive at correction terms for the electrical parts of the electrochemical-potential gradients $d\mu_i$. It was evident that the corrected $d\mu_i$'s are preferable because they can be directly substituted in place of the standard Guggenheim $d\mu_i$. Although no structural changes or improvements to the core-potential theory were advocated (nonetheless, an extension was made to generalise the procedure of finding the correction terms), the value of Chapter 3 is found in consolidating the abstract treatment Goyal and Monroe [1] provided by applying it to three concrete systems step by step. This also helped establish a solid basis upon which more complicated charged-membrane systems can be

analysed.

In Chapter 4, thermodynamic factors were introduced to translate the chemical parts of $d\mu_i$ in terms of concentration gradients. The liquid-junction potential measured *via* the concentration cell —as a means of characterising thermodynamic factors— was the focal point of this chapter. As an illustrative example, the liquid-junction potential for EMC:EC:$LiPF_6$ was parameterised and the corresponding ternary map was created. Surprisingly, a voltage difference was observed across two solutions of the same $LiPF_6$ concentration but of different EMC:EC ratios, a direct indication that dismisses the conventional single-solvent approximation. Because commercial lithium-ion-battery electrolytes usually incorporate a blend of a polar solvent (to facilitate the dissociation of the lithium salt) and a non-polar solvent (to lower solution viscosity), the implication of this exercise was wide and clear; the solvent-polarisation overpotential is expected to influence the outcomes of high-fidelity battery models, most noticeably in battery-capacity-loss prediction after long-term use, as well as ageing/degradation effects. To the best of the author's knowledge, the impact of the cosolvent segregation on the liquid-junction potential (and ultimately on the battery OCV) has not been elucidated before and is the most noteworthy contribution of this thesis to the battery community. A fruitful follow-up of this work would involve verifying how significantly battery-model simulation results are affected when the obtained ΔU functional form is implemented. Another interesting future work would be to characterise thermodynamic factors using partial-pressure measurements instead and map out the transference number and migration coefficient from the liquid-junction-potential data.

Many tools of analysis introduced in Chapters 3 and 4 were employed again to study membrane systems in Chapter 5. Specifically, Nafion —a proton exchange membrane with negatively charged sulfonate end-groups— took centre stage in this chapter. Verbrugge and Hill's radio-tracing experiment [2] was revisited to derive the Stefan–Maxwell diffusivity between the bisulfate ion and sulfonate end-group $\mathscr{D}_{-\mathrm{M}}$. The method of Barnes [194] was critical in obtaining the Fickian diffusivity accurately,

from which $\mathscr{D}_{-\mathrm{M}}$ was extracted. Also, the Stefan–Maxwell diffusivity between the proton and sulfonate end-group $\mathscr{D}_{+\mathrm{M}}$ was estimated from Verbrugge and Hill's ionic-conductivity measurement [3]. Having a full suite of independent Stefan–Maxwell diffusivities gave us the flexibility to estimate concentration-dependent macroscopic transport properties, revealing interesting information about transport in Nafion, e.g., the anion transference number is small and negative, indicating the proton and bisulfate ion form a neutral cluster to move together. Finally, the core-potential-guided electrochemical-potential differential expressions were provided to facilitate the simulation of non-electroneutral regions close to the membrane–reservoir interfaces. A method to calculate the interfacial electric potential was also outlined, based on the work of Mauro [90].

Stefan–Maxwell diffusivities are critical parameters in concentrated-solution theory, but their functional forms are unknown more often than not in membrane systems. The knowledge of the Stefan–Maxwell diffusivities is particularly pertinent when modelling vanadium redox flow batteries (VRFBs), because the electrolytes are far from dilute [151] and the crossover of active species across the membrane adversely affects the system efficiency [212–214]. Although the resulting capacity loss is not permanent, i.e., the imbalances can be resolved simply by regenerating the electrolytes [215], it is critical for models to predict the associated losses correctly to evaluate the device long-term behaviours and economics more accurately. Thus, concentration-dependent functional forms of $\mathscr{D}_{-\mathrm{M}}$ and $\mathscr{D}_{+\mathrm{M}}$ —which have not been known so far— are expected to be useful references for the VRFB modelling community.

Various experimental works confirm that vanadium crossover does take place during battery operation and it is driven by both electric-potential and concentration gradients [213, 214, 216–219]. Moreover, Lei et al. [150] showed that the concentration profiles of species in the membrane change considerably as a result of the interfacial space-charge regions evaluated under the Gibbs–Donnan framework, compared to the model outputs that disregard this effect. Therefore, one can see the benefit of embracing dynamics

in the non-electroneutral interfacial regions consistently for the accurate depiction of VRFB behaviours, especially over multiple charge–discharge cycles. Nonetheless, implementing this under the core-potential framework would be a formidable exercise, given there are eight species in the system (four vanadium oxidation states, proton, sulfate ion, water, and sulfonate end-group). Deriving the correction terms for $d\mu_i$ alone is anticipated to be very complicated because all species in the system are charged except the solvent (water). Another hurdle is the sheer number of transport properties needed for proper modelling of the system; 28 in this case. It would be possible to extract some of the necessary Stefan–Maxwell diffusivities using the radio-tracing experiment Verbrugge and Hill [2] conducted and following the analysis explored in Chapter 5. Still, some approximations would be unavoidable to construct a tractable VRFB model, such as designating all vanadium species to have the same interactions with other species. Simulation of Verbrugge and Hill's second radio-tracing experiment [2] —where Nafion is sandwiched between a 1 M reservoir and a 0.1 M reservoir of aqueous sulfuric acid— might be a good system to model first before attempting to simulate a full-scale VRFB model.

A short literature review on VRFB models is provided in Appendix A.

Appendix A

Literature review on VRFB models

A redox flow battery is a type of electrochemical energy-storage technology, characterised by the pumping of electrolytes through porous electrodes to sustain redox reactions. It was developed by NASA in the 1970s in response to the energy crisis [220]. Redox flow batteries have desirable features such as simple electrode reactions, room-temperature operation, deep discharge without damage [215], and decoupled power and energy capacities [12]. While the size of electrolyte reservoirs dictates the amount of energy storage, the concentration of reacting species and the stack size determine the power (a stack contains two electrodes, separated by an ion-exchange membrane, on whose surface electrochemical reactions take place).

Many active materials have been employed for redox flow batteries, such as iron/chromium and bromine/polysulfide (both of which are aqueous systems, see references [12, 215] for a summary of different chemistries), but the aqueous all-vanadium has received the most attention in recent years. Developed by Skyllas-Kazacos et al. [221] at the University of New South Wales, Australia, its main benefit is that the same element at different oxidation states are used so that cross-contamination is eliminated; crossover of active species across the membrane only represents a loss of efficiency and does not lead to irreversible consumption of active material [12]. Vanadium redox flow batteries (VRFBs) also have low maintenance and waste-disposal costs (as a result of the long shelf life of electrolytes), as well as easy state-of-charge determination [222].

Nonetheless, the system is still prohibitively expensive for widespread deployment, mainly due to the high stack cost and the cost of vanadium itself per kWh [215, 220].

Various alternative redox-flow-battery chemistries have also been demonstrated on the bench scale, including non-aqueous vanadium [223, 224] and even all-organic systems [225, 226]. But it remains difficult to evaluate whether these systems have the potential to beat the costs of other chemistries or even other storage paradigms such as Li-ion batteries, pumped hydro, or flywheels. In order to compare different systems objectively and to design more economical redox flow batteries, mathematical modelling holds the key to success since accurate yet inexpensive, fast, and flexible evaluation methods are essential. To aid a redox-flow-battery model development, a brief summary of the progress in VRFB modelling is presented in the rest of this section. The focus on the vanadium system is a mere reflection of the popularity of the chemistry.

A.1 Zero-dimensional VRFB models

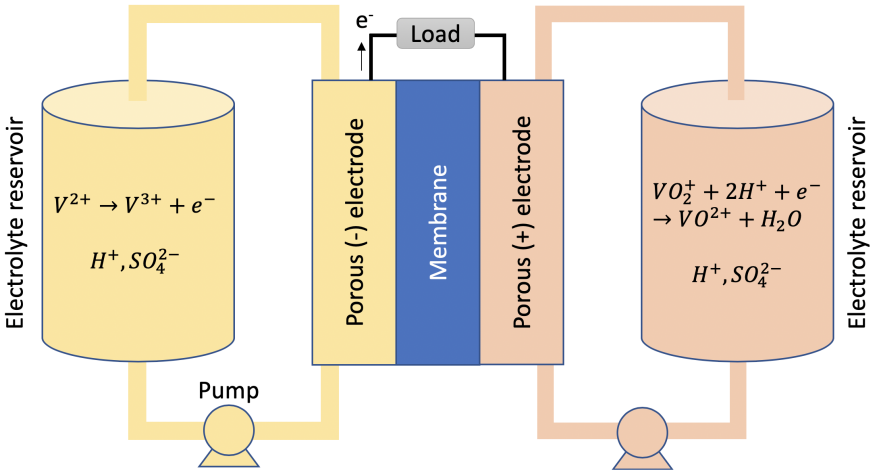

Figure A.1: Schematic of a VRFB during discharge.

A schematic of a typical aqueous all-vanadium redox flow battery is provided in Figure A.1. The anolyte and catholyte are stored separately and are pumped to a reaction chamber (known as the stack) containing porous electrodes, between which a

membrane is placed. At the two electrodes, the following reactions take place.

$$\begin{aligned} &(-)\text{ electrode: } \mathrm{V^{3+} + e^- \underset{\text{discharge}}{\overset{\text{charge}}{\rightleftharpoons}} V^{2+}} \\ &(+)\text{ electrode: } \mathrm{VO^{2+} + H_2O \underset{\text{discharge}}{\overset{\text{charge}}{\rightleftharpoons}} VO_2{}^{+} + 2\,H^{+} + e^-} \end{aligned} \tag{A.1}$$

The ion-exchange membrane allows the transport of protons to complete the circuit but may also permit a small amount of undesired active-species crossover [212–214]. To characterise and better understand the system, models at different length scales have been devised. Early modelling efforts were relatively simple, e.g., an equivalent-circuit model was constructed by Enomoto et al. [227]. Li and Hikihara's work [228] was similar but a transient model was also included, considering mechanical pumping and chemical kinetics. Tang et al. [229] and Skyllas-Kazacos and Goh [230] presented a model that predicted capacity loss due to the vanadium-ion crossover based on species mass balances. These 'zero-dimensional' models are suitable for control purposes but insufficient to enhance understanding of the underlying physical processes, a need which has become more prominent since the optimisation of performance metrics is required for the commercialisation of VRFBs.

A.2 VRFB models with the dilute-solution approximation

A great leap in VRFB modelling was made in 2008 when Shah et al. [231] proposed a more comprehensive physics-oriented two-dimensional, transient model. Their approach was adopted from well-established fuel-cell models, with which redox flow batteries share many structural similarities. This was the first physics-based model for the VRFB system that detailed electrochemical kinetics, as well as transport across each component of the stack. It was able to capture many aspects of the system well without being a complete black box, hence was well received by the VRFB research community. However, its limitations were also clear; vanadium crossover —an im-

portant phenomenon that dictates self-discharge of VRFBs— was not considered and isothermal and dilute-solution assumptions (with the Nernst–Planck flux equation) meant reduced flexibility. Following the success of the model, Shah and colleagues incorporated more physical phenomena and realistic operating conditions. Al-Fetlawi et al. [232] relaxed the isothermal assumption and included the heat generated by activation losses, electrochemical reactions, and ohmic resistance, and concluded that a thermal management scheme is necessary to minimise hotspots and membrane degradation (this was later extended to 3D by Wang and Cho [233]). Hydrogen evolution at the negative electrode was investigated by Shah et al. [234] and oxygen evolution at the positive electrode by Al-Fetlawi et al. [235].

In the meantime, attempts were made to reduce the complexity of Shah's model without compromising its rigour to serve as an optimisation tool. You et al.'s 2D steady-state model [236] was one of the popular such models, although they went so far as to ignore the migration contribution in their Nernst–Planck flux equations. An extension of this model to 3D was made by Ma et al. [237]. More fluid-mechanical considerations were also given within You et al.'s framework; now taking migration forces into account, the effect of the flow layout [238] and viscosity of the electrolyte [239] were investigated. In contrast, Vynnycky [240] took a more mathematical approach by asymptotically reducing Shah's model, using dimensional analysis to remove physically insignificant terms.

The next major improvement was delivered by Kumbur's group at Drexel University, USA, by accounting for the crossover of vanadium ions in their 2D transient model [149]. The following chemical reactions are known to occur in VRFBs due to crossover

[213, 229].

$$\begin{aligned}
&(-)\text{ electrode:} \quad \begin{cases} \mathrm{VO^{2+}} + \mathrm{V^{2+}} + 2\,\mathrm{H^{+}} \longrightarrow 2\,\mathrm{V^{3+}} + \mathrm{H_2O} \\ \mathrm{VO^{2+}} + 2\,\mathrm{V^{2+}} + 4\,\mathrm{H^{+}} \longrightarrow 3\,\mathrm{V^{3+}} + 2\,\mathrm{H_2O} \end{cases} \\
&(+)\text{ electrode:} \quad \begin{cases} \mathrm{V^{2+}} + 2\,\mathrm{VO_2^{+}} + 2\,\mathrm{H^{+}} \longrightarrow 3\,\mathrm{VO^{2+}} + \mathrm{H_2O} \\ \mathrm{V^{3+}} + \mathrm{VO_2^{+}} \longrightarrow 2\,\mathrm{VO^{2+}} \end{cases}
\end{aligned} \tag{A.2}$$

Knehr et al. [149] assumed that these reactions are instantaneous, i.e., species that cross over are consumed immediately upon entry to the other electrode. Although the dilute approximation was still made, they also managed to rectify the inaccurate open-circuit-voltage (OCV) curve in Shah et al's model [231][1]. Knehr et al.'s model was fairly successful and was used as a basis for several subsequent models; e.g., for optimisation and comparison studies by Knehr and Kumbur [241] and Agar et al. [242] and for a reduced-order model appropriate for long-term performance simulations by Boettcher et al. [243]. Ju's group at Inha University, Republic of Korea, similarly strove to include the crossover effects in 3D, along with temperature variations, but the side reactions in eq.(A.2) were handled volumetrically rather than as instantaneous boundary effects [244–246]. Water crossover due to electro-osmosis —produced by moving vanadium ions and protons— was also studied by the group [247].

A.3 VRFB models and the Gibbs–Donnan effect

Currently, there are only a handful of VRFB models in the literature that take into account the Gibbs–Donnan effect. Knehr et al.'s work [149] was one of the first models to consider it but their description was not entirely satisfactory, since electroneutrality was forced across the entire model domain. In doing so, they had to admit discontinuous

[1]This was achieved by (1) employing a more complete Nernst equation, (2) by taking into account the presence of protons at the positive electrode, and (3) by considering the Donnan potential across the membrane, according to Knehr and Kumbur [84].

co-ion (HSO_4^-) concentration and electric potential profiles at the membrane–electrode interfaces. A more elegant approach was implemented by Yang et al. [248] a few years later; utilising the so-called single-domain approach, the Gibbs–Donnan potential jump and continuous fluxes were automatically captured at the membrane–electrode interfaces. This eliminated the need to match the interfacial fluxes specifically as boundary conditions, as Knehr et al. [149] had done, while keeping the electroneutrality assumption.

Shortly after, Lei et al. [150] delivered a VRFB model that explicitly included space-charge regions. They concluded that the Gibbs–Donnan effect promoted vanadium crossover and led to a greater imbalance of vanadium species between the two reservoirs at the end of a charge–discharge cycle, illustrating the importance of the phenomenon in improving the accuracy of the model prediction.

A.4 VRFB models and concentrated-solution theory

The models discussed so far are all based on dilute-solution theory, in which species fluxes are described by the Nernst–Planck equation. This is relatively straightforward to implement since only the solute–solvent interactions are considered. However, VRFBs typically operate with 1 – 2 mol/L vanadium solutions and 3 – 6 mol/L supporting electrolyte (sulfuric acid) [151], calling the dilute approximation into question. Given that the counter-ion concentration is even higher in charged membranes than in the bulk solution [249], it is expected that interactions between solute species are not insignificant. Furthermore, dilute-solution theory neglects water transport, which is particularly important for aqueous VRFBs; the positive-electrode reaction in eq.(A.1) and the side reactions in eq.(A.2) both involve water. Concentrated solution theory that accounts for interactions between every pair of species in the system is therefore a more suitable framework to elucidate the coupled transport in VRFBs. In fact, Psaltis and Farrell [58] demonstrated that significant differences can arise in the concentration profiles from the two theories, especially during the transient periods.

Despite this, only a few models have utilised concentrated-solution theory to study VRFBs, the main impediment being the excessive number of transport properties required to fully describe the system. Given that eight chemical species are present in all-vanadium redox flow batteries, proper modelling demands 28 transport properties, almost all of which have not been verified experimentally. As such, there seems to be only one rigorous VRFB membrane model available in the literature that has successfully incorporated concentrated-solution effects: that of Crothers et al. [132]. Their model construction involved estimating the necessary Stefan–Maxwell diffusivities using hydrodynamic theory [131][2]. The model indeed showed that solute–solute interactions are not negligible, confirming the inadequacy of dilute-solution approximations.

[2]Hydrodynamic theory demands the knowledge of the equilibrium contents of water and ionic species in the membrane, which can be calculated according to Crothers et al. [130].

Appendix B

Liquid-Junction-Potential Measurement Data for EMC:EC:$LiPF_6$

B.1 Raw liquid-junction-potential measurement data

Table B.1: EMC:EC = 7:3 mass ratio with $y_o^{ref} = 0.249805$ and $y_e^{ref} = 0.128585$.

y_o^{test}	y_e^{test}	ΔU (mV)			
		Run 1	Run 2	Run 3	Run 4
0.334936	0.00201116	-193.9	-195.51	-194.55	-195.0
0.331892	0.00653695	-147.05	-145.91	-146.16	-146.5
0.318331	0.0266993	-106.39	-107.04	-105.13	-106.3
0.297815	0.0572036	-74.95	-72.04	-70.34	-72.14
0.284403	0.0771436	-53.27	-52.31	-54.73	-54.47
0.269155	0.0998158	-32.18	-32.34	-31.88	-32.98
0.252723	0.124247	-6.93	-8.93	-9.06	-8.035
0.249805	0.128585	0			
0.234636	0.151139	22.08	23.51	24.26	23.16

Table B.2: EMC:EC = 1:1 mass ratio with $y_{\mathrm{o}}^{\mathrm{ref}} = 0.456376$ and $y_{\mathrm{e}}^{\mathrm{ref}} = 0.0787517$.

$y_{\mathrm{o}}^{\mathrm{test}}$	$y_{\mathrm{e}}^{\mathrm{test}}$	ΔU (mV)			
		Run 1	Run 2	Run 3	Run 4
0.532733	0.00827132	-107.2	-108.0	-106.9	-108.8
0.496650	0.0415770	-45.8	-44.8	-44.3	-44.7
0.456376	0.0787517	0			
0.418035	0.114142	35.85	36.12	35.3	36.0
0.381605	0.147768	85.17	85.33	85.27	85.63

Table B.3: EMC:EC = 3:7 mass ratio with $y_{\mathrm{o}}^{\mathrm{ref}} = 0.621185$ and $y_{\mathrm{e}}^{\mathrm{ref}} = 0.0772349$.

$y_{\mathrm{o}}^{\mathrm{test}}$	$y_{\mathrm{e}}^{\mathrm{test}}$	ΔU (mV)			
		Run 1	Run 2	Run 3	Run 4
0.723204	0.00780305	-105.0	-109.5	-107.1	-108.0
0.677397	0.0389784	-42.39	-43.32	-42.88	-41.74
0.621185	0.0772349	0			
0.570355	0.111829	35.17	32.1	32.66	34.05
0.522070	0.144690	77.94	78.43	78.25	78.85

Table B.4: Liquid-junction potentials along A_1–B_1–C_1–D_1 and A_2–B_2–C_2–D_2. See Table 4.2 for the probed solution compositions.

Ref	Test	ΔU (mV)					
		Run 1	Run 2	Run 3	Run 4	Run 5	Run 6
A_1	B_1	8.52	8.10	8.86	8.00	8.945	7.90
A_1	C_1	22.25	22.55	22.20	22.45	22.25	22.15
A_1	D_1	55.20	54.35	54.54	59.02	59.36	59.33
B_1	C_1	14.02	13.93	13.86	13.43	13.33	13.26
B_1	D_1	50.20	50.20	50.21	48.93	49.20	49.17
C_1	D_1	35.22	35.42	35.15	35.31	35.22	35.22
A_2	B_2	15.16	14.98	14.94	14.79	14.87	14.9
A_2	C_2	39.62	39.3	39.02	40.66	40.64	40.64
A_2	D_2	133.45	133.6	132.9	131.8	131.85	131.84
B_2	C_2	23.93	23.85	23.78	23.93	23.88	23.81
B_2	D_2	115.35	115.84	115.94	116.84	116.9	117.07
C_2	D_2	90.75	90.05	89.7	91.7	92.06	92.73

B.2 Liquid-junction potentials relative to a common reference composition: $y_{\mathbf{o}}^{\mathbf{ref}} = 0$ and $y_{\mathbf{e}}^{\mathbf{ref}} = 0.09379$

Table B.5: EMC:EC = 7:3 mass ratio.

y_o^{test}	y_e^{test}	ΔU (mV)			
		Run 1	Run 2	Run 3	Run 4
0.249805	0.128585	6.33			
0.334936	0.002011	-187.57	-189.18	-188.22	-188.67
0.331892	0.006537	-140.72	-139.58	-139.83	-140.17
0.318331	0.026699	-100.06	-100.71	-98.80	-99.97
0.297815	0.057204	-68.62	-65.71	-64.01	-65.81
0.284403	0.077144	-46.94	-45.98	-48.40	-48.14
0.269155	0.099816	-25.85	-26.01	-25.55	-26.65
0.252723	0.124247	-0.60	-2.60	-2.73	-1.71
0.234636	0.151139	28.41	29.84	30.59	29.49

Table B.6: EMC:EC = 1:1 mass ratio.

y_o^{test}	y_e^{test}	ΔU (mV)			
		Run 1	Run 2	Run 3	Run 4
0.456376	0.078752	-58.63			
0.532733	0.008271	-165.83	-166.63	-165.53	-167.43
0.496650	0.041577	-104.43	-103.43	-102.93	-103.33
0.418035	0.114142	-22.78	-22.51	-23.33	-22.63
0.381605	0.147768	26.54	26.70	26.64	27.00

Table B.7: EMC:EC = 3:7 mass ratio.

$y_{\mathrm{o}}^{\mathrm{test}}$	$y_{\mathrm{e}}^{\mathrm{test}}$	ΔU (mV)			
		Run 1	Run 2	Run 3	Run 4
0.621185	0.077235	-68.22			
0.723204	0.007803	-173.22	-177.72	-175.32	-176.22
0.677397	0.038978	-110.61	-111.54	-111.10	-109.96
0.570355	0.111829	-33.05	-36.12	-35.56	-34.17
0.522070	0.144690	9.72	10.21	10.03	10.63

Table B.8: Across A_1–ref, B_1–ref, and C_1–ref.

$y_{\mathrm{o}}^{\mathrm{test}}$	$y_{\mathrm{e}}^{\mathrm{test}}$	ΔU (mV)					
		Run 1	Run 2	Run 3	Run 4	Run 5	Run 6
0.598516	0.0901736	-56.56	-55.71	-55.90	-60.38	-60.72	-60.69
0.443758	0.0899525	-51.56	-51.56	-51.57	-50.29	-50.56	-50.53
0.275268	0.0897390	-36.58	-36.78	-36.51	-36.67	-36.58	-36.58

Table B.9: Across A_2–ref, B_2–ref, and C_2–ref.

$y_{\mathrm{o}}^{\mathrm{test}}$	$y_{\mathrm{e}}^{\mathrm{test}}$	ΔU (mV)					
		Run 1	Run 2	Run 3	Run 4	Run 5	Run 6
0.719059	0.0101935	-161.10	-161.25	-160.55	-159.45	-159.50	-159.49
0.526531	0.0102671	-143.00	-143.49	-143.59	-144.49	-144.55	-144.72
0.327312	0.0100977	-118.40	-117.70	-117.35	-119.35	-119.71	-120.38

Bibliography

[1] Goyal, P.; Monroe, C. W. Thermodynamic factors for locally non-neutral, concentrated electrolytic fluids. *Electrochimica Acta* **2021**, *371*, 137638.

[2] Verbrugge, M. W.; Hill, R. F. Ion and Solvent Transport in Ion-Exchange Membranes: II. A Radiotracer Study of the Sulfuric-Acid, Nation-117 System. *Journal of The Electrochemical Society* **1990**, *137*, 893–899.

[3] Verbrugge, M. W.; Hill, R. F. Analysis of Promising Perfluorosulfonic Acid Membranes for Fuel-Cell Electrolytes. *Journal of The Electrochemical Society* **1990**, *137*, 3770.

[4] Wang, A. A.; Hou, T.; Karanjavala, M.; Monroe, C. W. Shifting-reference concentration cells to refine composition-dependent transport characterization of binary lithium-ion electrolytes. *Electrochimica Acta* **2020**, *358*, 136688.

[5] Jung, T.; Wang, A. A.; Monroe, C. W. Overpotential from Cosolvent Imbalance in Battery Electrolytes: LiPF6 in EMC:EC. *ACS Omega* **2023**, *8*, 21133–21144.

[6] Ding, M. S. Excess Gibbs Energy of Mixing for Organic Carbonates from Fitting of Their Binary Phase Diagrams with Nonideal Solution Models. *Journal of Solution Chemistry 2005 34:3* **2005**, *34*, 343–359.

[7] Verbrugge, M. W.; Hill, R. F. Ion and Solvent Transport in Ion-Exchange Membranes: I. A Macrohomogeneous Mathematical Model. *Journal of The Electrochemical Society* **1990**, *137*, 886.

[8] Verbrugge, M. W.; Hill, R. F. Experimental and Theoretical Investigation of Perfluorosulfonic Acid Membranes Equilibrated with Aqueous Sulfuric Acid Solutions. *Journal of Physical Chemistry* **1988**, *92*, 6778–6783.

[9] Umino, S.; Newman, J. Diffusion of Sulfuric Acid in Concentrated Solutions. *Journal of The Electrochemical Society* **1993**, *140*, 2217–2221.

[10] United Nations Climate Change, The Paris Agreement. 2015; https://unfccc.int/process-and-meetings/the-paris-agreement.

[11] Chowdhury, J. I.; Balta-Ozkan, N.; Goglio, P.; Hu, Y.; Varga, L.; McCabe, L. Techno-environmental analysis of battery storage for grid level energy services. *Renewable and Sustainable Energy Reviews* **2020**, *131*, 110018.

[12] Weber, A. Z.; Mench, M. M.; Meyers, J. P.; Ross, P. N.; Gostick, J. T.; Liu, Q. Redox flow batteries: a review. *Journal of Applied Electrochemistry* **2011**, *41*, 1137–1164.

[13] Usiskin, R.; Lu, Y.; Popovic, J.; Law, M.; Balaya, P.; Hu, Y.-S.; Maier, J. Fundamentals, status and promise of sodium-based batteries. *Nature Reviews Materials* **2021**, *6*, 1020–1035.

[14] Ritchie, H.; Roser, M.; Rosado, P. CO_2 and Greenhouse Gas Emissions. *Our World in Data* **2020**,

[15] Manthiram, A. An Outlook on Lithium Ion Battery Technology. *ACS Central Science* **2017**, *3*, 1063–1069.

[16] Hsieh, I.-Y. L.; Pan, M. S.; Chiang, Y.-M.; Green, W. H. Learning only buys you so much: Practical limits on battery price reduction. *Applied Energy* **2019**, *239*, 218–224.

[17] Zuo, X.; Zhu, J.; Müller-Buschbaum, P.; Cheng, Y.-J. Silicon based lithium-ion battery anodes: A chronicle perspective review. *Nano Energy* **2017**, *31*, 113–143.

[18] Cheng, X.-B.; Zhang, R.; Zhao, C.-Z.; Zhang, Q. Toward Safe Lithium Metal Anode in Rechargeable Batteries: A Review. *Chemical Reviews* **2017**, *117*, 10403–10473.

[19] Kwak, W.-J.; Rosy,; Sharon, D.; Xia, C.; Kim, H.; Johnson, L. R.; Bruce, P. G.; Nazar, L. F.; Sun, Y.-K.; Frimer, A. A.; Noked, M.; Freunberger, S. A.; Aurbach, D. Lithium–Oxygen Batteries and Related Systems: Potential, Status, and Future. *Chemical Reviews* **2020**, *120*, 6626–6683.

[20] Eriksson, E.; Gray, E. Optimization and integration of hybrid renewable energy hydrogen fuel cell energy systems – A critical review. *Applied Energy* **2017**, *202*, 348–364.

[21] Manoharan, Y.; Hosseini, S. E.; Butler, B.; Alzhahrani, H.; Senior, B. T. F.; Ashuri, T.; Krohn, J. Hydrogen Fuel Cell Vehicles; Current Status and Future Prospect. *Applied Sciences* **2019**, *9*.

[22] Newman, J.; Thomas-Alyea, K. E. *Electrochemical systems*, 3rd ed.; John Wiley & Sons, Inc.: Hoboken, New Jersey, 2004.

[23] Guggenheim, E. The conceptions of electrical potential difference between two phases and the individual activities of ions. *Journal of Physical Chemistry* **1929**, *33*, 842–849.

[24] Fick, A. Ueber Diffusion. *Annalen der Physik* **1855**, *170*, 59–86.

[25] Graham, T. On the Diffusion of Liquids. *Philosophical Transactions of the Royal Society of London* **1850**, *140*, 1–46.

[26] Fick, A. V. On liquid diffusion. *The London, Edinburgh, and Dublin Philosophical Magazine and Journal of Science* **1855**, *10*, 30–39.

[27] Patzek, T. W. Fick's Diffusion Experiments Revisited —Part I. *Advances in Historical Studies* **2014**, *3*, 194–206.

[28] Patzek, T. W. Fick's Diffusion Experiments Revisited —Part II (English Translation of Fick's Orginal Thinking). *Advances in Historical Studies* **2014**, *3*, 207–220.

[29] Cussler, E. L. *Multicomponent Diffusion*; Chemical engineering monographs ; v. 3; Elsevier Scientific Pub. Co.: Amsterdam; New York, 1976.

[30] Maxwell, J. C. Illustrations of the Dynamical Theory of Gases. *Philosophical Magazine* **1860**,

[31] Maxwell, J. C. IV. On the Dynamical Theory of Gases. *Philosophical transactions of the Royal Society of London* **1867**, 49–88.

[32] Stefan, J. Über das Gleichgewicht und die Bewegung, insbesondere die Diffusion von Gasgemengen. *Sitzungsberichte der Kaiserlichen Akademie der Wissenschaften Wien 63* **1871**, 63 – 124.

[33] Planck, M. Ueber die erregung von electricität und wärme in electrolyten. *Annalen der Physik* **1890**, *275*, 161–186.

[34] Planck, M. Ueber die Potentialdifferenz zwischen zwei verdünnten Lösungen binärer Electrolyte. *Annalen der Physik* **1890**, *276*, 561–576.

[35] Onsager, L. Theories and Problems of Liquid Diffusion. *Annals of the New York Academy of Sciences* **1945**, *46*, 241–265.

[36] Onsager, L. Reciprocal Relations in Irreversible Processes. I. *Phys. Rev.* **1931**, *37*, 405–426.

[37] Onsager, L. Reciprocal Relations in Irreversible Processes. II. *Phys. Rev.* **1931**, *38*, 2265–2279.

[38] Kondepudi, D.; Prigogine, I. *Modern thermodynamics: from heat engines to dissipative structures*, 2nd ed.; 2015.

[39] Goyal, P.; Monroe, C. W. New Foundations of Newman's Theory for Solid Electrolytes: Thermodynamics and Transient Balances. *Journal of The Electrochemical Society* **2017**, *164*, E3647–E3660.

[40] Hirschfelder, J. O.; Bird, R. B.; Curtiss, C. F. *Molecular Theory of Gases and Liquids*, 1st ed.; Wiley, 1954.

[41] Kirkwood, J. G. The Statistical Mechanical Theory of Transport Processes I. General Theory. *The Journal of Chemical Physics* **1946**, *14*, 180–201.

[42] Kirkwood, J. G. The Statistical Mechanical Theory of Transport Processes: II. Transport in Gases. *The Journal of Chemical Physics* **1947**, *15*, 72–76.

[43] Kirkwood, J. G.; Buff, F. P.; Green, M. S. The Statistical Mechanical Theory of Transport Processes. III. The Coefficients of Shear and Bulk Viscosity of Liquids. *The Journal of Chemical Physics* **1949**, *17*, 988–994.

[44] Irving, J. H.; Kirkwood, J. G. The Statistical Mechanical Theory of Transport Processes. IV. The Equations of Hydrodynamics. *The Journal of Chemical Physics* **1950**, *18*, 817–829.

[45] Lightfoot, E. N.; Cussler, E. L.; Rettig, R. L. Applicability of the Stefan-Maxwell equations to multicomponent diffusion in liquids. *AIChE Journal* **1962**, *8*, 708–710.

[46] Taylor, R.; Krishna, R. *Multicomponent Mass Transfer*; Wiley series in chemical engineering; Wiley: New York ; Chichester, 1993.

[47] Fong, K. D.; Bergstrom, H. K.; McCloskey, B. D.; Mandadapu, K. K. Transport phenomena in electrolyte solutions: Nonequilibrium thermodynamics and statistical mechanics. *AIChE Journal* **2020**, *66*, e17091.

[48] Newman, J.; Bennion, D.; Tobias, C. W. Mass Transfer in Concentrated Binary

Electrolytes. *Berichte der Bunsengesellschaft für physikalische Chemie* **1965**, *69*, 608–612.

[49] Monroe, C. W.; Delacourt, C. Continuum transport laws for locally non-neutral concentrated electrolytes. *Electrochimica Acta* **2013**, *114*, 649–657.

[50] Smyrl, W. H.; Newman, J. Potentials of cells with liquid junctions. *The Journal of Physical Chemistry* **1968**, *72*, 4660–4671.

[51] Graham, E. E.; Dranoff, J. S. Application of the Stefan-Maxwell Equations to Diffusion in Ion Exchangers. 1. Theory. *Industrial and Engineering Chemistry Fundamentals* **1982**, *21*, 360–365.

[52] Pinto, N. D.; Graham, E. E. Evaluation of Diffusivities in Electrolyte Solutions using Stefan-Maxwell Equations. *AIChE Journal* **1986**, *32*, 291–296.

[53] Lightfoot, E. N.; Scattergood, E. M. Suitability of the Nernst-Planck equations for Describing Electrokinetic Phenomena. *AIChE Journal* **1965**, *11*, 175–192.

[54] Bearman, R. J.; Kirkwood, J. G. Statistical Mechanics of Transport Processes. XI. Equations of Transport in Multicomponent Systems. *The Journal of Chemical Physics* **1958**, *28*, 136–145.

[55] Helfand, E. On Inversion of the Linear Laws of Irreversible Thermodynamics. *The Journal of Chemical Physics* **1960**, *33*, 319–322.

[56] Van-Brunt, A.; Farrell, P. E.; Monroe, C. W. Structural electroneutrality in Onsager–Stefan–Maxwell transport with charged species. *Electrochimica Acta* **2023**, *441*, 141769.

[57] Datta, R.; Vilekar, S. A. The continuum mechanical theory of multicomponent diffusion in fluid mixtures. *Chemical Engineering Science* **2010**, *65*, 5976–5989.

[58] Psaltis, S. T.; Farrell, T. W. Comparing charge transport predictions for a ternary electrolyte using the Maxwell-Stefan and Nernst-Planck equations. *Journal of the Electrochemical Society* **2011**, *158*.

[59] Bird, R. B.; Klingenberg, D. J. Multicomponent diffusion—A brief review. *Advances in Water Resources* **2013**, *62*, 238–242.

[60] Johnson, M. H. Diffusion as Hydrodynamic Motion. *Physical Review* **1951**, *84*, 566–568.

[61] Truesdell, C. Mechanical Basis of Diffusion. *The Journal of Chemical Physics* **1962**, *37*, 2336–2344.

[62] Lamm, O. The Force and Friction Conception in the Diffusion of Multicomponent Systems. *Acta Chemica Scandinavica* **1957**, *11*, 362–364.

[63] Miller, D. G. Application of Irreversible Thermodynamics to Electrolyte Solutions. I. Determination of Ionic Transport Coefficients lij for Isothermal Vector Transport Processes in Binary Electrolyte Systems. *Journal of Physical Chemistry* **1966**, *70*, 2639–2659.

[64] Coleman, B. D.; Truesdell, C. On the reciprocal relations of Onsager. *The Journal of Chemical Physics* **1960**, *33*, 28–31.

[65] Monroe, C. W.; Wheeler, D. R.; Newman, J. Nonequilibrium linear response theory: Application to Onsager-Stefan-Maxwell diffusion. *Industrial and Engineering Chemistry Research* **2015**, *54*, 4460–4467.

[66] Tolman, R. C. The Principle of Microscopic Reversibility. *Proceedings of the National Academy of Sciences of the United States of America* **1925**, *11*, 436–439.

[67] Casimir, H. B. G. On Onsager's principle of microscopic reversibility. *Reviews of Modern Physics* **1945**, *17*, 343.

[68] Bearman, R. J. The Onsager Thermodynamics of Galvanic Cells with Liquid-Liquid Junctions. *The Journal of Chemical Physics* **1954**, *22*, 585–587.

[69] Monroe, C. W.; Newman, J. Onsager's shortcut to proper forces and fluxes. *Chemical Engineering Science* **2009**, *64*, 4804–4809.

[70] Monroe, C. W.; Newman, J. An introduction to the onsager reciprocal relations. *Chemical Engineering Education* **2007**, *41*, 233 – 238.

[71] Miller, D. G. Thermodynamics of Irreversible Processes: The Experimental Verification of the Onsager Reciprocal Relations. *Chemical Reviews* **1960**, *60*, 15–37.

[72] Miller, D. G. Ternary isothermal diffusion and the validity of the Onsager reciprocity relations. *Journal of Physical Chemistry* **1959**, *63*, 570–578.

[73] Wheeler, D. R.; Newman, J. Molecular dynamics simulations of multicomponent diffusion. 1. Equilibrium method. *The Journal of Physical Chemistry B* **2004**, *108*, 18353–18361.

[74] Darken, L. S. Diffusion, mobility and their interrelation through free energy in binary metallic systems. *Trans. AIME* **1948**, *175*, 184–201.

[75] Pethica, B. A. Are electrostatic potentials between regions of different chemical composition measurable? The Gibbs–Guggenheim principle reconsidered, extended and its consequences revisited. *Physical Chemistry Chemical Physics* **2007**, *9*, 6253–6262.

[76] Guggenheim, E. On the Conception of Electrical Potential Difference between two Phases. II. *The Journal of Physical Chemistry* **1930**, *34*, 1540–1543.

[77] Debye, P. J. W.; Hückel, E. On the theory of electrolytes. I. Freezing point depression and related phenomena. *Physikalische Zeitschrift* **1923**, *24*, 185–206.

[78] Guggenheim, E. A. *Thermodynamics: an advanced treatment for chemists and physicists*, 3rd ed.; Series in physics; North-Holland Pub. Co. ; Interscience Publishers: Amsterdam : New York, 1957.

[79] Garrido, J.; Manzanares, J. A. Observable Electric Potential and Electrostatic Potential in Electrochemical Systems. *The Journal of Physical Chemistry B* **2000**, *104*, 658–662.

[80] Bizeray, A. M.; Howey, D. A.; Monroe, C. W. Resolving a discrepancy in diffusion potentials, with a case study for Li-Ion batteries. *Journal of the Electrochemical Society* **2016**, *163*, E223–E229.

[81] Kokotov, Y. A. Electrochemical and Twin Chemical Potentials as Thermodynamic Driving Forces. *Solvent Extraction and Ion Exchange* **1999**, *17*, 1083–1131.

[82] Donnan, F. G. The Theory of Membrane Equilibria. *Chemical Reviews* **1924**, *1*, 73–90.

[83] Zenyuk, I. V.; Litster, S. Modeling ion conduction and electrochemical reactions in water films on thin-film metal electrodes with application to low temperature fuel cells. *Electrochimica Acta* **2014**, *146*, 194–206.

[84] Knehr, K. W.; Kumbur, E. C. Open circuit voltage of vanadium redox flow batteries: Discrepancy between models and experiments. *Electrochemistry Communications* **2011**, *13*, 342–345.

[85] Qasem, N. A. A.; Qureshi, B. A.; Zubair, S. M. Improvement in design of electrodialysis desalination plants by considering the Donnan potential. *Desalination* **2018**, *441*, 62–76.

[86] Chen, H.; Rose, M.; Fleming, M.; Souizi, S.; Shashvatt, U.; Blaney, L. Recent advances in Donnan dialysis processes for water/wastewater treatment and resource recovery: A critical review. *Chemical Engineering Journal* **2023**, *455*, 140522.

[87] Ohshima, H.; Ohki, S. Donnan Potential and Surface Potential of a Charged Membrane. *Biophysical Journal* **1985**, *47*, 673–678.

[88] Luo, T.; Abdu, S.; Wessling, M. Selectivity of Ion Exchange Membranes: A Review. *Journal of Membrane Science* **2018**, *555*, 429–454.

[89] Kusoglu, A.; Weber, A. Z. New Insights into Perfluorinated Sulfonic-Acid Ionomers. *Chemical Reviews* **2017**, *117*, 987–1104.

[90] Mauro, A. Space Charge Regions in Fixed Charge Membranes and the Associated Property of Capacitance. *Biophysical Journal* **1962**, *2*, 179–198.

[91] Anderson, J. L.; Koh, W.-H. Electrokinetic Parameters for Capillaries of Different Geometries. *Journal of Colloid and Interface Science* **1977**, *59*, 149–158.

[92] Gebel, G. Structural evolution of water swollen perfluorosulfonated ionomers from dry membrane to solution. *Polymer* **2000**, *41*, 5829–5838.

[93] Haubold, H. G.; Vad, T.; Jungbluth, H.; Hiller, P. Nano structure of NAFION: a SAXS study. *Electrochimica Acta* **2001**, *46*, 1559–1563.

[94] Kim, M.-H.; Glinka, C. J.; Grot, S. A.; Grot, W. G. SANS Study of the Effects of Water Vapor Sorption on the Nanoscale Structure of Perfluorinated Sulfonic Acid (NAFION) Membranes. *Macromolecules* **2006**, *39*, 4775–4787.

[95] Schmidt-Rohr, K.; Chen, Q. Parallel cylindrical water nanochannels in Nafion fuel-cell membranes. *Nature Materials* **2008**, *7*, 75–83.

[96] Rubatat, L.; Rollet, A. L.; Gebel, G.; Diat, O. Evidence of Elongated Polymeric Aggregates in Nafion. *Macromolecules* **2002**, *35*, 4050–4055.

[97] Rollet, A.-L.; Diat, O.; Gebel, G. A New Insight into Nafion Structure. *Journal of Physical Chemistry B* **2002**, *106*, 3033–3036.

[98] Rubatat, L.; Gebel, G.; Diat, O. Fibrillar Structure of Nafion: Matching Fourier and Real Space Studies of Corresponding Films and Solutions. *Macromolecules* **2004**, *37*, 7772–7783.

[99] Traube, M. Experimente zur Theorie der Zellenbildung und Endosmose. *Arch. Anat. Physiol. Wiss. Med* **1867**, *87*, 129.

[100] Kramer, P. J.; Boyer, J. S. *Water relations of plants and soils*; Academic press, 1995; p 4.

[101] Teorell, T. Transport Phenomena in Membranes Eighth Spiers Memorial Lecture. *Discussions of the Faraday Society* **1956**, *21*, 9–26.

[102] Teorell, T. Studies on the "Diffusion Effect" upon Ionic Distribution. I. Some Theoretical Considerations. *Proceedings of the National Academy of Sciences of the United States of America* **1935**, *21*, 152.

[103] Michaelis, L. Contribution to the Theory of Permeability of Membranes for Electrolytes. *Journal of General Physiology* **1925**, *8*, 33–59.

[104] Teorell, T. An attempt to formulate a quantitative theory of membrane permeability. *Proceedings of the Society for Experimental Biology and Medicine* **1935**, *33*, 282.

[105] Meyer, K. H.; Sievers, J. F. The permeability of membranes Ithe theory of ionic permeability I. *Helv. Chim. Acta* **1936**, *19*, 649–664.

[106] Meyer, K. H. Part II.—Artificial membranes. Introductory paper. Artificial membranes: their structure and permeability. *Transactions of the Faraday Society* **1937**, *33*, 1073–1081.

[107] Bard, A. J.; Faulkner, L. R. *Electrochemical Methods: Fundamentals and Applications*, 2nd ed.; John Wiley and Sons Inc, 2000; p 72.

[108] Yasuda, H.; Lamaze, C. E.; Ikenberry, L. D. Permeability of Solutes through Hydrated Polymer Membranes Part I. Diffusion of Sodium Chloride. *Die Makromolekulare Chemie* **1968**, *118*, 19–35.

[109] Wijmans, J. G.; Baker, R. W. The solution-diffusion model: a review. *Journal of Membrane Science* **1995**, *107*, 1–21.

[110] Geise, G. M.; Falcon, L. P.; Freeman, B. D.; Paul, D. R. Sodium chloride sorption in sulfonated polymers for membrane applications. *Journal of Membrane Science* **2012**, *423-424*, 195–208.

[111] Geise, G. M.; Paul, D. R.; Freeman, B. D. Fundamental water and salt transport properties of polymeric materials. *Progress in Polymer Science* **2014**, *39*, 1–42.

[112] Merten, U. Flow relationships in reverse osmosis. *Industrial & Engineering Chemistry Fundamentals* **1963**, *2*, 229–232.

[113] Weber, A. Z.; Delacourt, C. Mathematical Modelling of Cation Contamination in a Proton-exchange Membrane. *Fuel Cells* **2008**, *8*, 459–465.

[114] Delacourt, C.; Newman, J. Mathematical Modeling of a Cation-Exchange Membrane Containing Two Cations. *Journal of The Electrochemical Society* **2008**, *155*, B1210.

[115] Fetcher, J., E.S. A Criticism of the Teorell–Meyer–Sievers Theory of Membrane Permeability. *The Journal of Physical Chemistry* **1942**, *46*, 570–574.

[116] Sollner, K.; Carr, C. W. The structure of the collodion membrane and its electrical behavior. X. An experimental test of some aspects of the Teorell and Meyer-Sievers theories of electrical membrane behavior. *Journal of General Physiology* **1944**, *28*, 1–15.

[117] Scatchard, G. Ion Exchanger Electrodes. *Journal of the American Chemical Society* **1953**, *75*, 2883–2887.

[118] Paul, D. R. Reformulation of the solution-diffusion theory of reverse osmosis. *Journal of Membrane Science* **2004**, *241*, 371–386.

[119] Lorenz, P. B. The phenomenology of electro-osmosis and streaming potential. *The Journal of Physical Chemistry* **1952**, *56*, 775–778.

[120] Muskat, M. *The flow of homogeneous fluids through porous media*, 1st ed.; McGraw-Hill: New York; London, 1937.

[121] Nagasawa, M.; Kobatake, Y. The Theory of Membrane Potential. *Journal of Physical Chemistry* **1952**, *56*, 1017–1024.

[122] Kobatake, Y. Irreversible Electrochemical Processes of Membranes. *The Journal of Chemical Physics* **1958**, *28*, 146.

[123] Kobatake, Y.; Fujita, H. Flows Through Charged Membranes. I. Flip-Flop Current vs Voltage Relation. *The Journal of Chemical Physics* **1964**, *40*, 2212.

[124] Dresner, L. Electrokinetic Phenomena in Charged Microcapillaries. *The Journal of Physical Chemistry* **1963**, *67*, 1635–1641.

[125] Morrison, F. A.; Osterle, J. F. Electrokinetic Energy Conversion in Ultrafine Capillaries. *The Journal of Chemical Physics* **1965**, *43*, 2111.

[126] Gross, R. J.; Osterle, J. F. Membrane Transport Characteristics of Ultrafine Capillaries. *The Journal of Chemical Physics* **1968**, *49*, 228.

[127] Fair, J. C.; Osterle, J. F. Reverse Electrodialysis in Charged Capillary Membranes. *The Journal of Chemical Physics* **1971**, *54*, 3307.

[128] Pintauro, P. N.; Verbrugge, M. W. The electric-potential profile in ion-exchange membrane pores. *Journal of Membrane Science* **1989**, *44*, 197–212.

[129] Guzmán-Garcia, A. G.; Pintauro, P. N.; Verbrugge, M. W.; Hill, R. F. Development of a Space-Charge Transport Model for Ion-Exchange Membranes. *AIChE Journal* **1990**, *36*, 1061–1074.

[130] Crothers, A. R.; Darling, R. M.; Kusoglu, A.; Radke, C. J.; Weber, A. Z. Theory of Multicomponent Phenomena in Cation-Exchange Membranes: Part I. Thermodynamic Model and Validation. *Journal of The Electrochemical Society* **2020**, *167*, 013547.

[131] Crothers, A. R.; Darling, R. M.; Kusoglu, A.; Radke, C. J.; Weber, A. Z. Theory of Multicomponent Phenomena in Cation-Exchange Membranes: Part II. Transport Model and Validation. *Journal of The Electrochemical Society* **2020**, *167*, 013548.

[132] Crothers, A. R.; Darling, R. M.; Kushner, D. I.; Perry, M. L.; Weber, A. Z. Theory of Multicomponent Phenomena in Cation-Exchange Membranes: Part III. Transport in Vanadium Redox-Flow-Battery Separators. *Journal of The Electrochemical Society* **2020**, *167*, 013549.

[133] Teorell, T. 9 - Transport Processes and Electrical Phenomena in Ionic Membranes. *Progress in Biophysics and Biophysical Chemistry* **1953**, *3*, 305–369.

[134] Sonin, A. A.; Probstein, R. F. A hydrodynamic theory of desalination by electrodialysis. *Desalination* **1968**, *5*, 293–329.

[135] Higa, M.; Tanioka, A.; Miyasaka, K. Simulation of the transport of ions against their concentration gradient across charged membranes. *Journal of Membrane Science* **1988**, *37*, 251–266.

[136] Higa, M.; Tanioka, A.; Miyasaka, K. A study of ion permeation across a charged membrane in multicomponent ion systems as a function of membrane charge density. *Journal of Membrane Science* **1990**, *49*, 145–169.

[137] Fíla, V.; Bouzek, K. A mathematical model of multiple ion transport across an ion-selective membrane under current load conditions. *Journal of Applied Electrochemistry* **2003**, *33*, 675–684.

[138] Fidaleo, M.; Moresi, M. Optimal strategy to model the electrodialytic recovery of a strong electrolyte. *Journal of Membrane Science* **2005**, *260*, 90–111.

[139] Volgin, V. M.; Davydov, A. D. Ionic transport through ion-exchange and bipolar membranes. *Journal of Membrane Science* **2005**, *259*, 110–121.

[140] Tedesco, M.; Hamelers, H. V.; Biesheuvel, P. M. Nernst-Planck transport theory for (reverse) electrodialysis: I. Effect of co-ion transport through the membranes. *Journal of Membrane Science* **2016**, *510*, 370–381.

[141] Pintauro, P. N.; Bennion, D. N. Mass Transport of Electrolytes in Membranes. 1. Development of Mathematical Transport Model. *Industrial and Engineering Chemistry Fundamentals* **1984**, *23*, 230–234.

[142] Pintauro, P. N.; Bennion, D. N. Mass Transport of Electrolytes in Membranes. 2. Determination of NaCI Equilibrium and Transport Parameters for Nafion. *Industrial and Engineering Chemistry Fundamentals* **1984**, *23*, 234–243.

[143] Kraaijeveld, G.; Sumberova, V.; Kuindersma, S.; Wesselingh, H. Modelling electrodialysis using the Maxwell-Stefan description. *The Chemical Engineering Journal* **1995**, *57*, 163–176.

[144] Staverman, A. J. Non-equilibrium thermodynamics of membrane processes. *Transactions of the Faraday Society* **1952**, *48*, 176–185.

[145] Koh, W.-H.; Anderson, J. L. Electroosmosis and Electrolyte Conductance in Charged Microcapillaries. *AIChE Journal* **1975**, *21*, 1176–1188.

[146] Levine, S.; Marriott, J. R.; Neale, G.; Epstein, N. Theory of Electrokinetic Flow in Fine Cylindrical Capillaries at High Zeta-Potentials. *Journal of Colloid and Interface Science* **1975**, *52*, 136–149.

[147] Oren, Y. S.; Biesheuvel, P. M. Theory of Ion and Water Transport in Reverse-Osmosis Membranes. *Physical Review Applied* **2018**, *9*, 024034.

[148] Dresner, L.; Kraus, K. A. Ion Exclusion and Salt Filtering with Porous Ion-Exchange Materials. *Journal of Physical Chemistry* **1963**, *67*, 990–996.

[149] Knehr, K. W.; Agar, E.; Dennison, C. R.; Kalidindi, A. R.; Kumbur, E. C. A Transient Vanadium Flow Battery Model Incorporating Vanadium Crossover and Water Transport through the Membrane. *Journal of The Electrochemical Society* **2012**, *159*, A1446–A1459.

[150] Lei, Y.; Zhang, B. W.; Bai, B. F.; Zhao, T. S. A transient Electrochemical Model Incorporating the Donnan Effect for All-Vanadium Redox Flow Batteries. *Journal of Power Sources* **2015**, *299*, 202–211.

[151] Ashraf Gandomi, Y.; Zawodzinski, T. A.; Mench, M. M. Concentrated Solution Model of Transport in All Vanadium Redox Flow Battery Membrane Separator. *ECS Transactions* **2014**, *61*, 23–32.

[152] Fukunaga, A.; Nohira, T.; Kozawa, Y.; Hagiwara, R.; Sakai, S.; Nitta, K.; Inazawa, S. Intermediate-temperature ionic liquid NaFSA-KFSA and its application to sodium secondary batteries. *Journal of Power Sources* **2012**, *209*, 52–56.

[153] Fiore, M.; Wheeler, S.; Hurlbutt, K.; Capone, I.; Fawdon, J.; Ruffo, R.; Pasta, M. Paving the Way toward Highly Efficient, High-Energy Potassium-Ion Batteries with Ionic Liquid Electrolytes. *Chemistry of Materials* **2020**, *32*, 7653–7661.

[154] Fawdon, J.; Rees, G. J.; La Mantia, F.; Pasta, M. Insights into the Transport and Thermodynamic Properties of a Bis(fluorosulfonyl)imide-Based Ionic Liquid Electrolyte for Battery Applications. *The Journal of Physical Chemistry Letters* **2022**, *13*, 1734–1741.

[155] Tang, X.; Lv, S.; Jiang, K.; Zhou, G.; Liu, X. Recent development of ionic liquid-based electrolytes in lithium-ion batteries. *Journal of Power Sources* **2022**, *542*, 231792.

[156] von Cresce, A.; Xu, K. Preferential Solvation of Li+ Directs Formation of Interphase on Graphitic Anode. *Electrochemical and Solid-State Letters* **2011**, *14*, A154.

[157] Monroe, C. W. Does oxygen transport affect the cell voltages of metal/air batteries? *Journal of the Electrochemical Society* **2017**, *164*, E3547–E3551.

[158] Ma, Y.; Doyle, M.; Fuller, T. F.; Doeff, M. M.; De Jonghe, L. C.; Newman, J. The Measurement of a Complete Set of Transport Properties for a Concentrated Solid Polymer Electrolyte Solution. *Journal of The Electrochemical Society* **1995**, *142*, 1859–1868.

[159] Georén, P.; Lindbergh, G. Characterisation and modelling of the transport properties in lithium battery polymer electrolytes. *Electrochimica Acta* **2001**, *47*, 577–587.

[160] Georén, P.; Lindbergh, G. Characterisation and modelling of the transport properties in lithium battery gel electrolytes: Part I. The binary electrolyte PC/LiClO4. *Electrochimica Acta* **2004**, *49*, 3497–3505.

[161] Nyman, A.; Behm, M.; Lindbergh, G. Electrochemical characterisation and modelling of the mass transport phenomena in LiPF6–EC–EMC electrolyte. *Electrochimica Acta* **2008**, *53*, 6356–6365.

[162] Hou, T.; Monroe, C. W. Composition-dependent thermodynamic and mass-transport characterization of lithium hexafluorophosphate in propylene carbonate. *Electrochimica Acta* **2019**, 135085.

[163] Stewart, S.; Newman, J. Measuring the Salt Activity Coefficient in Lithium-Battery Electrolytes. *Journal of The Electrochemical Society* **2008**, *155*, A458.

[164] Lundgren, H.; Behm, M.; Lindbergh, G. Electrochemical Characterization and Temperature Dependency of Mass-Transport Properties of LiPF6 in EC:DEC. *Journal of The Electrochemical Society* **2015**, *162*, A413–A420.

[165] Lundgren, H.; Scheers, J.; Behm, M.; Lindbergh, G. Characterization of the Mass-Transport Phenomena in a Superconcentrated LiTFSI:Acetonitrile Electrolyte. *Journal of The Electrochemical Society* **2015**, *162*, A1334–A1340.

[166] Dickinson, E. J. F.; Freitag, L.; Compton, R. G. Dynamic Theory of Liquid Junction Potentials. *The Journal of Physical Chemistry B* **2010**, *114*, 187–197.

[167] Liu, J.; Monroe, C. W. On the characterization of battery electrolytes with polarization cells. *Electrochimica Acta* **2015**, *167*, 357–363.

[168] Pollard, R.; Newman, J. Transport Equations for a Mixture of Two Binary Molten Salts in a Porous Electrode. *Journal of The Electrochemical Society* **1979**, *126*, 1713.

[169] Valøen, L. O.; Reimers, J. N. Transport Properties of LiPF6-Based Li-Ion Battery Electrolytes. *Journal of The Electrochemical Society* **2005**, *152*, A882.

[170] Landesfeind, J.; Gasteiger, H. A. Temperature and Concentration Dependence of the Ionic Transport Properties of Lithium-Ion Battery Electrolytes. *Journal of The Electrochemical Society* **2019**, *166*, A3079–A3097.

[171] Doyle, M.; Fuller, T. F.; Newman, J. Modeling of Galvanostatic Charge and Discharge of the Lithium/Polymer/Insertion Cell. *Journal of The Electrochemical Society* **1993**, *140*, 1526–1533.

[172] Dees, D. W.; Kawauchi, S.; Abraham, D. P.; Prakash, J. Analysis of the Galvanostatic Intermittent Titration Technique (GITT) as applied to a lithium-ion porous electrode. *Journal of Power Sources* **2009**, *189*, 263–268.

[173] Krachkovskiy, S. A.; Foster, J. M.; Bazak, J. D.; Balcom, B. J.; Goward, G. R. Operando Mapping of Li Concentration Profiles and Phase Transformations in Graphite Electrodes by Magnetic Resonance Imaging and Nuclear Magnetic Resonance Spectroscopy. *The Journal of Physical Chemistry C* **2018**, *122*, 21784–21791.

[174] Castle, M.; Richardson, G.; Foster, J. M. Understanding rapid charge and discharge in nano-structured lithium iron phosphate cathodes. *European Journal of Applied Mathematics* **2022**, *33*, 328–368.

[175] Bergstrom, H. K.; Fong, K. D.; McCloskey, B. D. Interfacial Effects on Transport Coefficient Measurements in Li-ion Battery Electrolytes. *Journal of The Electrochemical Society* **2021**, *168*, 60543.

[176] Farkhondeh, M.; Pritzker, M.; Delacourt, C.; Liu, S. S.-W.; Fowler, M. Method of the Four-Electrode Electrochemical Cell for the Characterization of Concentrated Binary Electrolytes: Theory and Application. *The Journal of Physical Chemistry C* **2017**, *121*, 4112–4129.

[177] Mistry, A.; Grundy, L. S.; Halat, D. M.; Newman, J.; Balsara, N. P.; Srinivasan, V. Effect of Solvent Motion on Ion Transport in Electrolytes. *Journal of The Electrochemical Society* **2022**, *169*, 40524.

[178] Steinrück, H.-G. et al. Concentration and velocity profiles in a polymeric lithium-ion battery electrolyte. *Energy & Environmental Science* **2020**, *13*, 4312–4321.

[179] Schmidt, F.; Schönhoff, M. Solvate Cation Migration and Ion Correlations in Solvate Ionic Liquids. *The Journal of Physical Chemistry B* **2020**, *124*, 1245–1252.

[180] Halat, D. M.; Fang, C.; Hickson, D.; Mistry, A.; Reimer, J. A.; Balsara, N. P.; Wang, R. Electric-Field-Induced Spatially Dynamic Heterogeneity of Solvent Motion and Cation Transference in Electrolytes. *Physical Review Letters* **2022**, *128*, 198002.

[181] Mistry, A.; Srinivasan, V.; Steinrück, H.-G. Characterizing Ion Transport in Electrolytes via Concentration and Velocity Profiles. *Advanced Energy Materials* **2023**, *13*, 2203690.

[182] Wang, A. A.; Greenbank, S.; Li, G.; Howey, D. A.; Monroe, C. W. Current-driven solvent segregation in lithium-ion electrolytes. *Cell Reports Physical Science* **2022**, *3*, 101047.

[183] Mistry, A.; Srinivasan, V. Do we need an accurate understanding of transport in electrolytes? *Joule* **2021**, *5*, 2773–2776.

[184] Taylor, P. B. Electromotive Force of the Cell with Transference and Theory of Interdiffusion of Electrolytes. *The Journal of Physical Chemistry* **1927**, *31*, 1478–1500.

[185] Hartley, G. S. XLI. Theory of the velocity of diffusion of strong electrolytes in dilute solution. *The London, Edinburgh, and Dublin Philosophical Magazine and Journal of Science* **1931**, *12*, 473–488.

[186] Newman, J.; Battaglia, V. *The Newman Lectures on Thermodynamics*; Pan Stanford Publishing, 2019; p 328.

[187] Liu, J.; Monroe, C. W. Solute-volume effects in electrolyte transport. *Electrochimica Acta* **2014**, *135*, 447–460.

[188] Jeong, S.-K.; Inaba, M.; Iriyama, Y.; Abe, T.; Ogumi, Z. Surface film formation on a graphite negative electrode in lithium-ion batteries: AFM study on the effects of co-solvents in ethylene carbonate-based solutions. *Electrochimica Acta* **2002**, *47*, 1975–1982.

[189] Uchida, S.; Kiyobayashi, T. How does the solvent composition influence the transport properties of electrolyte solutions? LiPF6 and LiFSA in EC and DMC binary solvent. *Physical Chemistry Chemical Physics* **2021**, *23*, 10875–10887.

[190] Von Wald Cresce, A.; Borodin, O.; Xu, K. Correlating Li+ Solvation Sheath Structure with Interphasial Chemistry on Graphite. *Journal of Physical Chemistry C* **2012**, *116*, 26111–26117.

[191] Sijabat, R. R.; de Groot, M. T.; Moshtarikhah, S.; van der Schaaf, J. Maxwell–Stefan model of multicomponent ion transport inside a monolayer Nafion membrane for intensified chlor-alkali electrolysis. *Journal of Applied Electrochemistry* **2019**, *49*, 353–368.

[192] Wesselingh, J. A.; Vonk, P.; Kraaijeveld, G. Exploring the Maxwell-Stefan description of ion exchange. *The Chemical Engineering Journal* **1995**, *57*, 75–89.

[193] Griffith, L. D. Multi-Component Transport in Next-Generation Batteries. Ph.D. thesis, 2016.

[194] Barnes, C. Diffusion Through a Membrane. *Physics* **1934**, *5*, 4–8.

[195] Newman, J.; Battaglia, V. *The Newman Lectures on Mathematics*; Pan Stanford Publishing, 2018.

[196] Tanaka, M.; Girard, G.; Davis, R.; Peuto, A.; Bignell, N. Recommended table for the density of water between 0 °C and 40 °C based on recent experimental reports. *Metrologia* **2001**, *38*, 301.

[197] Umino, S.; Newman, J. Temperature Dependence of the Diffusion Coefficient of Sulfuric Acid in Water. *Journal of The Electrochemical Society* **1997**, *144*, 1302.

[198] Okada, T.; Satou, H.; Okuno, M.; Yuasa, M. Ion and water transport characteristics of perfluorosulfonated ionomer membranes with H+ and alkali metal cations. *Journal of Physical Chemistry B* **2002**, *106*, 1267–1273.

[199] Zawodzinski, Jr., T. A.; Derouin, C.; Radzinski, S.; Sherman, R. J.; Smith, V. T.; Springer, T. E.; Gottesfeld, S. Water Uptake by and Transport Through Nafion® 117 Membranes. *Journal of The Electrochemical Society* **1993**, *140*, 1041–1047.

[200] Roy, A.; Hickner, M. A.; Yu, X.; Li, Y.; Glass, T. E.; McGrath, J. E. Influence of chemical composition and sequence length on the transport properties of pro-

ton exchange membranes. *Journal of Polymer Science Part B: Polymer Physics* **2006**, *44*, 2226–2239.

[201] Zawodzinski, Jr., T. A.; Neeman, M.; Sillerud, L. O.; Gottesfeld, S. Determination of water diffusion coefficients in perfluorosulfonate ionomeric membranes. *The Journal of Physical Chemistry* **1991**, *95*, 6040–6044.

[202] Gong, X.; Bandis, A.; Tao, A.; Meresi, G.; Wang, Y.; Inglefield, P. T.; Jones, A. A.; Wen, W.-Y. Self-diffusion of water, ethanol and decafluropentane in perfluorosulfonate ionomer by pulse field gradient NMR. *Polymer* **2001**, *42*, 6485–6492.

[203] Ochi, S.; Kamishima, O.; Mizusaki, J.; Kawamura, J. Investigation of proton diffusion in Nafion®117 membrane by electrical conductivity and NMR. *Solid State Ionics* **2009**, *180*, 580–584.

[204] Zhao, Q.; Majsztrik, P.; Benziger, J. Diffusion and interfacial transport of water in Nafion. *Journal of Physical Chemistry B* **2011**, *115*, 2717–2727.

[205] Neeman, M.; Jarrett, K. A.; Sillerud, L. O.; Freyer, J. P. Self-Diffusion of Water in Multicellular Spheroids Measured by Magnetic Resonance Microimaging1. *Cancer Research* **1991**, *51*, 4072–4079.

[206] Fuller, T. F.; Newman, J. Experimental Determination of the Transport Number of Water in Nafion 117 Membrane. *Journal of The Electrochemical Society* **1992**, *139*, 1332–1337.

[207] Luo, Z.; Chang, Z.; Zhang, Y.; Liu, Z.; Li, J. Electro-osmotic drag coefficient and proton conductivity in Nafion® membrane for PEMFC. *International Journal of Hydrogen Energy* **2010**, *35*, 3120–3124.

[208] Okada, T.; Møller-Holst, S.; Gorseth, O.; Kjelstrup, S. Transport and equilibrium properties of Nafion® membranes with H+ and Na+ ions. *Journal of Electroanalytical Chemistry* **1998**, *442*, 137–145.

[209] Ise, M.; Kreuer, K. D.; Maier, J. Electroosmotic drag in polymer electrolyte membranes: an electrophoretic NMR study. *Solid State Ionics* **1999**, *125*, 213–223.

[210] Ye, X.; Wang, C.-Y. Measurement of Water Transport Properties Through Membrane-Electrode Assemblies: I. Membranes. *Journal of The Electrochemical Society* **2007**, *154*, B676.

[211] Kusoglu, A.; Weber, A. Z. *Polymers for Energy Storage and Delivery: Polyelectrolytes for Batteries and Fuel Cells*; ACS Symposium Series; American Chemical Society, 2012; Vol. 1096; pp 11–175.

[212] Schwenzer, B.; Zhang, J.; Kim, S.; Li, L.; Liu, J.; Yang, Z. Membrane Development for Vanadium Redox Flow Batteries. *ChemSusChem* **2011**, *4*, 1388–1406.

[213] Sun, C.; Chen, J.; Zhang, H.; Han, X.; Luo, Q. Investigations on Transfer of Water and Vanadium Ions across Nafion Membrane in an Operating Vanadium Redox Flow Battery. *Journal of Power Sources* **2010**, *195*, 890–897.

[214] Wiedemann, E.; Heintz, A.; Lichtenthaler, R. N. Transport Properties of Vanadium Ions in Cation Exchange Membranes: Determination of Diffusion Coefficients Using a Dialysis Cell. *Journal of Membrane Science* **1998**, *141*, 215–221.

[215] Ponce de León, C.; Frías-Ferrer, A.; González-García, J.; Szánto, D. A.; Walsh, F. C. Redox flow cells for energy conversion. *Journal of Power Sources* **2006**, *160*, 716–732.

[216] Luo, Q.; Li, L.; Nie, Z.; Wang, W.; Wei, X.; Li, B.; Chen, B.; Yang, Z. In-situ Investigation of Vanadium Ion Transport in Redox Flow Battery. *Journal of Power Sources* **2012**, *218*, 15–20.

[217] Sing, D. C.; Meyers, J. P. Direct Measurement of Vanadium Crossover in an Operating Vanadium Redox Flow Battery. *ECS Transactions* **2013**, *50*, 61–72.

[218] Ashraf Gandomi, Y.; Aaron, D. S.; Mench, M. M. Coupled Membrane Transport Parameters for Ionic Species in All-Vanadium Redox Flow Batteries. *Electrochimica Acta* **2016**, *218*, 174–190.

[219] Darling, R. M.; Weber, A. Z.; Tucker, M. C.; Perry, M. L. The Influence of Electric Field on Crossover in Redox-Flow Batteries. *Journal of The Electrochemical Society* **2016**, *163*, A5014–A5022.

[220] Perry, M. L.; Weber, A. Z. Advanced Redox-Flow Batteries: A Perspective. *Journal of The Electrochemical Society* **2016**, *163*, A5064–A5067.

[221] Skyllas-Kazacos, M.; Rychick, M.; Robins, R. All-vanadium redox battery. 1988; US Patent 4,786,567.

[222] Skyllas-Kazacos, M.; Menictas, C. Vanadium redox battery for emergency back-up applications. INTELEC, International Telecommunications Energy Conference (Proceedings). 1997; pp 463–471.

[223] Fang, B.; Iwasa, S.; Wei, Y.; Arai, T.; Kumagai, M. A study of the Ce(III)/Ce(IV) redox couple for redox flow battery application. *Electrochimica Acta* **2002**, *47*, 3971–3976.

[224] Liu, Q.; Sleightholme, A. E.; Shinkle, A. A.; Li, Y.; Thompson, L. T. Non-aqueous vanadium acetylacetonate electrolyte for redox flow batteries. *Electrochemistry Communications* **2009**, *11*, 2312–2315.

[225] Li, Z.; Li, S.; Liu, S.; Huang, K.; Fang, D.; Wang, F.; Peng, S. Electrochemical Properties of an All-Organic Redox Flow Battery Using 2,2,6,6-Tetramethyl-1-Piperidinyloxy and N-Methylphthalimide. *Electrochemical and Solid-State Letters* **2011**, *14*, A171 – A173.

[226] Wei, X.; Xu, W.; Huang, J.; Zhang, L.; Walter, E.; Lawrence, C.; Vijayakumar, M.; Henderson, W. A.; Liu, T.; Cosimbescu, L.; Li, B.; Sprenkle, V.;

Wang, W. Radical Compatibility with Nonaqueous Electrolytes and Its Impact on an All-Organic Redox Flow Battery. *Angewandte Chemie - International Edition* **2015**, *54*, 8684–8687.

[227] Enomoto, K.; Sasaki, T.; Shigematsu, T.; Deguchi, H. Evaluation study about Redox flow battery response and its modeling. *IEICE Transactions B (Journal of Electric Power and Energy)* **2002**, *122*, 554–560.

[228] Li, M.; Hikihara, T. A Coupled Dynamical Model of Redox Flow Battery Based on Chemical Reaction, Fluid Flow, and Electrical Circuit. *IEICE TRANSACTIONS on Fundamentals of Electronics, Communications and Computer Sciences* **2008**, *E91-A*, 1741–1747.

[229] Tang, A.; Bao, J.; Skyllas-Kazacos, M. Dynamic modelling of the effects of ion diffusion and side reactions on the capacity loss for vanadium redox flow battery. *Journal of Power Sources* **2011**, *196*, 10737–10747.

[230] Skyllas-Kazacos, M.; Goh, L. Modeling of vanadium ion diffusion across the ion exchange membrane in the vanadium redox battery. *Journal of Membrane Science* **2012**, *399-400*, 43–48.

[231] Shah, A. A.; Watt-Smith, M. J.; Walsh, F. C. A dynamic performance model for redox-flow batteries involving soluble species. *Electrochimica Acta* **2008**, *53*, 8087–8100.

[232] Al-Fetlawi, H.; Shah, A. A.; Walsh, F. C. Non-isothermal modelling of the all-vanadium redox flow battery. *Electrochimica Acta* **2009**, *55*, 78–89.

[233] Wang, Y.; Cho, S. C. Analysis and Three-Dimensional Modeling of Vanadium Flow Batteries. *Journal of The Electrochemical Society* **2014**, *161*, A1200–A1212.

[234] Shah, A. A.; Al-Fetlawi, H.; Walsh, F. C. Dynamic modelling of hydrogen evolution effects in the all-vanadium redox flow battery. *Electrochimica Acta* **2010**, *55*, 1125–1139.

[235] Al-Fetlawi, H.; Shah, A. A.; Walsh, F. C. Modelling the effects of oxygen evolution in the all-vanadium redox flow battery. *Electrochimica Acta* **2010**, *55*, 3192–3205.

[236] You, D.; Zhang, H.; Chen, J. A simple model for the vanadium redox battery. *Electrochimica Acta* **2009**, *54*, 6827–6836.

[237] Ma, X.; Zhang, H.; Xing, F. A Three-dimensional Model for Negative Half Cell of the Vanadium Redox Flow Battery. *Electrochimica Acta* **2011**, *58*, 238–246.

[238] Xu, Q.; Zhao, T. S.; Leung, P. K. Numerical Investigations of Flow Field Designs for Vanadium Redox Flow Batteries. *Applied Energy* **2013**, *105*, 47–56.

[239] Xu, Q.; Zhao, T. S.; Zhang, C. Effects of SOC-dependent Electrolyte Viscosity on Performance of Vanadium Redox Flow Batteries. *Applied Energy* **2014**, *130*, 139–147.

[240] Vynnycky, M. Analysis of a model for the operation of a vanadium redox battery. *Energy* **2011**, *36*, 2242–2256.

[241] Knehr, K. W.; Kumbur, E. C. Role of convection and related effects on species crossover and capacity loss in vanadium redox flow batteries. *Electrochemistry Communications* **2012**, *23*, 76–79.

[242] Agar, E.; Knehr, K. W.; Chen, D.; Hickner, M. A.; Kumbur, E. C. Species Transport Mechanisms Governing Capacity Loss in Vanadium Flow Batteries: Comparing Nafion® and Sulfonated Radel Membranes. *Electrochimica Acta* **2013**, *98*, 66–74.

[243] Boettcher, P. A.; Agar, E.; Dennison, C. R.; Kumbur, E. C. Modeling of Ion Crossover in Vanadium Redox Flow Batteries: A Computationally-Efficient Lumped Parameter Approach for Extended Cycling. *Journal of The Electrochemical Society* **2016**, *163*, A5244–A5252.

[244] Oh, K.; Yoo, H.; Ko, J.; Won, S.; Ju, H. Three-dimensional, Transient, Non-isothermal Model of All-Vanadium Redox Flow Batteries. *Energy* **2015**, *81*, 3–14.

[245] Oh, K.; Won, S.; Ju, H. A Comparative Study of Species Migration and Diffusion Mechanisms in All-Vanadium Redox Flow Batteries. *Electrochimica Acta* **2015**, *181*, 238–247.

[246] Won, S.; Oh, K.; Ju, H. Numerical Analysis of Vanadium Crossover Effects in All-Vanadium Redox Flow Batteries. *Electrochimica Acta* **2015**, *177*, 310–320.

[247] Oh, K.; Moazzam, M.; Gwak, G.; Ju, H. Water Crossover Phenomena in All-Vanadium Redox Flow Batteries. *Electrochimica Acta* **2019**, *297*, 101–111.

[248] Yang, X.-G.; Ye, Q.; Cheng, P.; Zhao, T. S. Effects of the Electric Field on Ion Crossover in Vanadium Redox Flow Batteries. *Applied Energy* **2015**, *145*, 306–319.

[249] Wiedemann, E.; Heintz, A.; Lichtenthaler, R. N. Sorption Isotherms of Vanadium with H3O+ Ions in Cation Exchange Membranes. *Journal of Membrane Science* **1998**, *141*, 207–213.